Spin-density-wave antiferromagnetism in chromium alloys

E. Fawcett

Department of Physics, University of Toronto, Toronto, Canada M5S 1A7

H. L. Alberts

Department of Physics, Rand Afrikaans University, Johannesburg 2000, South Africa

V. Yu. Galkin

Bardin Central Research Institute of Ferrous Metallurgy, 107005 Moscow, Russia

D. R. Noakes

Superconducting Materials Research Program, Virginia State University, Petersburg, Virginia 23806

J. V. Yakhmi

Chemistry Division, Bhabha Atomic Research Centre, Trombay, Bombay 400085, India

The account given here of the macroscopic and microscopic physical properties of antiferromagnetic (AFM) chromium alloys supplements the previous review of spin-density-wave (SDW) antiferromagnetism in pure Cr. The existence of an incommensurate spin-density wave results from Fermi-surface nesting, which changes with electron concentration as atoms of different valence are introduced into Cr. This gives rise for most impurities to a prototypical composition-temperature (x-T) magnetic phase diagram, which is described quite well by a model of nesting electron-hole octahedra and electron reservoir, with changes in the amplitude of the spin-density wave and its wave vector corresponding to the changes with impurity concentration of the Néel temperature. There are, however, numerous cases of idiosyncratic behavior in the x-T phase diagram, some of which appear to correspond to unusual features in the pressure-temperature (p-T) phase diagram, e.g., in the CrFe, CrAl, and CrSi alloy systems. With these exceptions and a few others, the effect of impurities in the same group of the periodic table is fairly similar, so that this classification is used for the description of both the x-T and p-T phase diagrams. The properties of the alloy systems for each group of impurities are first summarized in the context of the x-T phase diagram. The general features of the various physical properties are then considered: (1) magnetic susceptibility, whose temperature dependence signals the existence of local moments in some cases; (2) transport properties, in particular, electrical resistivity and thermopower, which show characteristic temperature dependence corresponding to the occurrence of spin fluctuations around the Néel temperature T_N, and in some cases well into the paramagnetic phase, followed below T_N by effects due to the electron-hole condensation in the ordered AFM phase, and in some cases at lower temperatures to the formation of local impurity states; and (3) magnetoelastic properties, which show large effects associated with the spin-density wave and with SDW fluctuations in Cr alloys just as in pure Cr. Analysis of magnetic anomalies in the thermal expansion and bulk modulus in terms of magnetic Grüneisen parameters is employed for some Cr alloy systems to describe the large body of experimental data. The empirical correspondence between increasing volume and increasing electron concentration is illustrated for several systems. The study of dilute Cr alloys provides insight into the reason for pure Cr having a weak first-order Néel transition, and provides examples of other phase transitions, including the incommensurate-commensurate SDW, the spin-glass, and AFM-superconducting phase transitions. The similarities between the incommensurate SDW fluctuations in Cr and Cr alloys and in the high-temperature superconducting cuprates strongly motivates, in particular, the examination of the inelastic neutron-scattering results. Optical properties provide an interesting picture of the relation between the magnitude of the energy gap at the Fermi surface and the Néel temperature, which is quite different in the incommensurate and commensurate SDW alloys. Local probes providing microscopic information about the environment of an impurity are clearly of great potential value in Cr alloy systems. The Mössbauer effect has, however, yielded disappointingly little information, but other probes such as perturbed angular correlation and nuclear magnetic resonance have provided interesting results.

CONTENTS

 0034-6861/94/66(1)/25(103)/$15.30

I. INTRODUCTION

Chromium alloy systems exhibit antiferromagnetic (AFM) properties, which excite the interest of the experimentalist because of their great variety; and of the theorist because they constitute a special case, accessible to experiment, of a general class of model systems that undergo electric or magnetic phase transitions associated with nesting of the Fermi surface. These transitions include the metal-insulator, ferroelectric, and ferromagnetic, as referenced by Kulikov and Tugushev (1984) and Tugushev (1992), as well as the spin-density-wave (SDW) AFM transition seen in Cr alloy systems. These review papers also discuss and reference the many other physical systems that exhibit SDW antiferromagnetism: $TiBe_2$, CrB_2, vanadium chalcogenides V_mX_n with $X=$S or Se, NiS, MnSi, Magnel phases V_nO_{2n+1} (Kulikov and Tugushev, 1984), FeRh, MnSi, and Pt_3Fe (Tugushev, 1992).

Incommensurate SDW fluctuations in the high-temperature superconducting cuprates, in particular in $La_{1-x}Sr_xCuO_4$ (Mason *et al.*, 1992), are very similar to those seen in the paramagnetic phase of chromium close to the Néel transition (Noakes, Holden, and Fawcett, 1990; Noakes, Holden, Fawcett, and de Camargo, 1990). This result encourages speculation about the physical similarities (and differences) between the two systems and should help us understand both all the better. The origin of the incommensurate spin-density wave in Cr was recognized by Overhauser (1962) to be the nesting electron and hole Fermi surfaces, and the first conclusion from the similarity in the dynamic susceptibility is that nesting Fermi surfaces, perhaps associated with their superconductivity, occur also in the cuprates. Furthermore, the magnetic stiffness of the spin fluctuations shows that the quasiparticle mass in both systems is of the same order as the free-electron mass.

The analogy may be pursued by comparing the spin waves in AFM La_2CuO_4 (Hayden *et al.*, 1991) with those seen in the commensurate SDW (i.e., simple AFM) alloy, Cr+5 at. % Mn (Sinha *et al.*, 1977), which are found to have similar high velocity of the same order as that of electrons at the Fermi surface. Thus we might regard CrMn (a metal) and La_2CuO_4 (an insulator) as being simple antiferromagnetics, which by suitable doping with V (or otherwise reducing the electron concentration by removing Mn) and Sr, respectively, develop similar incommensurate spin fluctuations associated with imperfectly nested Fermi surfaces.

The two doped systems are, nevertheless, physically quite different in that, in the ordered phase, one becomes an incommensurate spin-density wave and the other a superconductor. We might seek an explanation for this difference in the dimensionality of the two systems, which is reflected in the dimensionality of their magnetic fluctuations: the interactions in the cuprates reside in the copper oxide planes, whereas Cr alloys constitute a three-dimensional magnetic system. Perhaps the

difference lies in the fact that the nesting parts of the Fermi surface in the former case are in the same energy band, while in the latter they are different electron and hole bands. Or perhaps the difference is due to the fact that the high-temperature superconducting cuprates are a strong-coupling system, with an energy gap of order 2 eV as in La_2CuO_4 (Uchida *et al.*, 1991), whereas the coupling in the Cr alloy system is weak, with a gap of about 0.4 eV (see Sec. VIII.A).

These considerations, in view of the great current interest in high-temperature superconductors (the relevant neutron-scattering work has been reviewed recently by Aeppli *et al.*, 1993 and Hayden, Mason, *et al.*, 1993), motivates renewed efforts to understand the Cr alloy system. We shall, in particular, take up this interesting parallelism between the two systems in our considerations in Sec. VI.E of superconductivity (where the approach to commensurate antiferromagnetism suppresses the superconducting state) and in Sec. VII.B of inelastic neutron scattering in Cr alloys.

There has been no previous review of experimental and theoretical work on SDW antiferromagnetism in Cr alloy systems. Arrott (1966, 1972) discussed the general principles of SDW antiferromagnetism, with special reference to neutron scattering, in Cr and Mn and their alloys, as well as in rare earths and γ-Fe. Landolt-Börnstein (1986) presented a considerable body of data on AFM Cr alloys with transition metals, but without any theoretical treatment. Kulikov and Tugushev (1984) were mainly interested in giving a theoretical review of Cr alloys. Fawcett (1988a) reviewed both experimental and theoretical work on SDW antiferromagnetism in Cr, but discussed work on Cr alloys only insofar as it illuminated the behavior of the pure metal.

The historical development of our understanding of SDW antiferromagnetism and its connection with nesting of the Fermi surface relied heavily on studies of Cr alloys. These started with de Vries (1959), whose discovery that the Néel temperature T_N, in Cr alloys with 1 at. % each of V, Mn, Fe, Co, and Ni, is strongly dependent on the nature and concentration of the impurity, first indicated the electronic nature of the transition.

Butylenko and Gridnev (1964, 1965) extended this work with a comprehensive, but little known, study of alloys of Cr with the 4*d* and 5*d* metals, Ta, W, Re, Ru, and Os, and the rare earth metals, Lu and Hf, as well as the 3*d* alloys CrV and CrMn. They measured the temperature dependence of the resistivity and the thermal expansion, for temperatures from 77 K to above 600 K, for alloys having a wide range of compositions, and constructed phase diagrams from the anomalies seen at the Néel transition.

The variation of the wave vector **Q** and the rms moment $\langle \mu \rangle$, which is a measure of the amplitude of the SDW, in dilute alloys of Cr with other transition metals, was first studied systematically by Koehler *et al.* (1966) and Komura *et al.* (1967a, 1967b).

We present here an account of the extensive literature on experimental and theoretical studies of SDW antiferromagnetism in Cr alloys. The main body of experimental work has been concerned with the temperature dependence of various physical properties for different alloy concentrations or pressures, with a view to determining the magnetic composition-temperature or pressure-temperature phase diagram, respectively, and the nature of the transition between the paramagnetic (*P*), the incommensurate SDW (ISDW or *I*), and commensurate SDW (CSDW or *C*) phases. The incommensurate phase may be polarized transverse to the wave vector **Q** (the transverse SDW or AF_1 phase) or parallel to **Q** (the longitudinal SDW or AF_2 phase). In this "AF notation" the commensurate SDW phase is referred to as the "AF_0 phase."

We discuss first, in Sec. II.A, theoretical models to account for some of the magnetic composition-temperature phase diagrams observed in real Cr alloy systems, as described in Secs. II.B, II.C, and II.D. Since the literature on such models is extensive, we do not attempt to describe them in detail. We restrict our attention to the dependence of the Néel temperature on the concentration of the different solute atoms and to the various forms the magnetic phase diagram can take when the commensurate SDW phase is encountered. The two main aspects of the theory are, on the one hand, the change of nesting of electron and hole sheets of the Fermi surface, due to the different valence of the solute atom from Cr, and, on the other, the effect of impurity scattering.

The experimental data on the magnetic phase diagrams of binary (and in some cases ternary) Cr alloys, which can relatively easily be measured by the singular behavior usually seen at the phase transitions, are summarized in Sec. II.B. We present there also the available data for the initial dependence on alloy concentration of the wave vector and rms moment of the SDW. In Sec. II.C we present phase diagrams for individual binary-alloy systems and bring together for each system the results, which are discussed according to physical properties in the later sections. Whenever possible the experimental data are related to the theoretical results presented in Sec. II.A and in later theoretical sections. Finally, in Sec. II.D, we discuss ternary alloy systems, though in those cases where the third element is introduced as a dopant to modify the properties of the binary-alloy system, the results are presented in Sec. II.C.

The magnetic susceptibility and transport properties are considered in Sec. III and Sec. IV, respectively. The latter is the major topic, partly because the anomaly in the resistivity has often been used as an indicator of the Néel transition, but mainly for the more important fundamental reason that the transport properties not only reflect the changing electronic structure as the SDW develops with decreasing temperature, but also manifest the dramatic effects of conduction-electron scattering at the impurity states. Different theoretical aspects of transport properties are discussed in five subsections of Sec. IV.A, but the experimental work in Sec. IV.B cannot so con-

veniently be classified.

The effect of pressure on Cr alloy systems has been studied for a number of solutes, since the atomic volume is a fundamental parameter whose effect on the magnetic properties should give considerable physical insight. The variation of the Néel temperature T_N with volume V, which provides an estimate of a magnetic Grüneisen parameter, $\Gamma_N = -d \ln T_N / d \ln V$, can be determined with relatively modest pressures, since Γ_N is usually much larger than unity (and negative) as in pure Cr, for which $\Gamma_N \simeq -30$.

For several alloy systems in which the solute element, in sufficient concentration, induces a transition to the commensurate SDW phase, quite low pressures may be enough to move the alloy back past its triple point to the incommensurate SDW phase. In several cases the similarity between the general form of the phase diagrams in the pressure-temperature and composition-temperature planes, with pressure being equivalent to reproducing the electron concentration, is quite striking.

The change of volume with temperature and pressure, namely, the thermal expansivity β and the isothermal compressibility κ (or its reciprocal, the bulk modulus B) are physical properties clearly related to the effect of pressure, which are commonly referred to as magnetoelastic properties. They have been measured in many magnetic Cr alloys from well above T_N down to low temperature. A knowledge of the magnetic contributions to both β and B provides an estimate of magnetic Grüneisen parameters Γ_i, which are usually different above and below T_N (and in the limit of zero temperature) and can be compared with Γ_N determined directly from the pressure dependence of T_N.

Very little has been done to explain these pressure and magnetoelastic effects in the Cr alloy systems in terms of microscopic theory. In Sec. V.A we show how the pressure dependence of the Neél temperature T_N can, in principle, be related to the theoretical models discussed in Sec. II.A. The magnetoelastic coupling constant relating the magnetovolume to the square of the SDW amplitude, i.e., the mean-square moment, is expressed there in terms of band-structure parameters. In Sec. V.B, a methodology based on thermodynamic considerations is developed, which enables us to employ the magnetic contributions to the magnetoelastic properties of an alloy to calculate several different magnetic Grüneisen parameters. The magnetoelastic properties and the pressure-temperature phase diagram of the individual alloy systems are presented in Sec. V.C, and the remarkable similarity between the effects of pressure and the decrease in electron concentration seen in many Cr alloy systems is discussed in Sec. V.D.

The various phase transitions in Cr alloy systems are discussed in Sec. VI as a function of both temperature and composition, including the spin-glass transition in the CrFe alloy system and the transition to the superconducting phase in CrRe and CrRu. Neutron scattering has been a powerful tool in the study of Cr alloy systems, and its findings are used throughout the review. In Sec. VII we present work mostly on magnetic excitations studied by inelastic neutron scattering, including resonant lattice modes, but also on elastic neutron and x-ray scattering by the charge-density wave that accompanies the SDW in Cr alloy systems.

In Sec. VIII we present experimental material relating to the energy-band structure of Cr alloys. The optical reflectivity determines the size of the energy-band gap introduced by electron-hole condensation in the formation of the SDW, while the low-temperature electronic specific heat provides some information about the fraction of the Fermi surface that disappears due to the condensation. The few experiments on Cr alloys by the use of the quantum oscillations are also described.

There has been a considerable amount of work, with 70 or so references listed here, on the use of local probes to explore the microscopic properties of Cr alloys. These are discussed in Sec. IX, with a summary subsection to help point the way to future developments in this important field.

The concluding Sec. X provides an overview of SDW antiferromagnetism in Cr alloys, which highlights several areas that are clearly important, but that we still do not understand, in the hope of stimulating future research.

II. MAGNETIC PHASE DIAGRAMS

We shall deal in Sec. V with magnetic phase diagrams for Cr alloy systems in the pressure-temperature plane. There is a striking similarity in some cases to the phase diagram for the same system in the composition-temperature plane, which leads to some speculation in Sec. V.D about the fundamental nature of magnetoelastic coupling in Cr and Cr alloys.

In the present section we shall first describe briefly the well-known canonical model for SDW antiferromagnetism in the Cr alloy system, which comprises nesting electron and hole octahedra with a reservoir of electrons corresponding to the rest of the Fermi surface. This model provides a satisfactory picture of the magnetic phase diagram for many systems, but further development, which includes the effects of impurity scattering, is required to explain some unusual features. In particular, impurity scattering may explain why in some systems the commensurate AF_0 phase associated with higher electron concentration x occurs at lower temperatures than the incommensurate AF_1 phase for concentrations, $x < x_L$, below the triple point L.

Impurity scattering effects are, of course, much more important in relation to transport properties. We shall take up again in Sec. IV the story of resonant scattering at local impurity states in the energy gap in Cr alloy systems.

A. Theory

Four distinct phases are known to exist in Cr alloys: longitudinal SDW (AF_2), transverse SDW (AF_1), com-

mensurate SDW (AF_0), and paramagnetic (P). The region of the phase diagram in the neighborhood of the triple point between the P, AF_0, and AF_1 phases is of great physical interest, and there has been extensive analysis by use of model systems based in some cases on microscopic theories. The spin-flip transition, on the other hand, has proved thus far impossible to understand in a microscopic theory (Allen and Young, 1977), though it is readily modeled by use of a Landau-type free energy (Allen and Young, 1975).

The experimental parameters available in a study of the magnetic phase diagram are alloy composition and pressure. Magnetic field has not been used to study phase transitions in Cr alloys, since the coupling to the antiferromagnetism is very weak relative to the thermal energy at the high Néel temperature (Barak *et al.*, 1981). The canonical conjugate parameter of pressure is volume strain, whose effect we shall analyze in Sec. V. Alloy composition, which in a binary alloy $Cr_{1-x}A_x$ is described by the concentration x (at. %) of the solute atom A, may enter the theory in two ways. The most striking effect of alloying is due to the change of the electron concentration with x, when the solute atom has a number of conduction electrons different from Cr, which is normally represented by a composition-dependent chemical potential or Fermi level $E_F(x)$. The other effect, which is also seen in alloys of Cr with the isoelectronic metals Mo and W, occurs due to electron scattering by the solute atoms regarded as impurities in the solvent.

In our theoretical treatment of the magnetic phase diagram, we shall follow the recent review by Tugushev (1992) while employing wherever possible for consistency the notation of Fawcett (1988a). Since these two reviews provide an adequate introduction, with references, to the theory of SDW antiferromagnetism, we proceed at once to consider the phase diagrams shown in Figs. 1(a) and 1(b). The Fermi energy E_F is defined relative to the zero-temperature energy gap Δ_0, which provides a nesting parameter, or reduced energy,

$$h=\frac{E_F}{\Delta_0}\equiv\frac{H}{\delta_0}\ , \tag{1}$$

the latter being the notation of Fawcett (1988a). A reduced temperature is defined by reference to the Néel temperature T_{N0} for perfect nesting, when $E_F=0$,

$$t=\frac{T}{T_{N0}},\quad \text{with } t_N=\frac{T_N}{T_{N0}}\ . \tag{2}$$

The paramagnetic phase P, incommensurate SDW phase AF_1, and commensurate SDW phase AF_0 coexist at the triple point, which in this context is often referred to as the "Lifshitz point" and denoted L. In the various versions of the canonical model described below, Δ_0 and T_{N0} are related by the equation

$$\frac{T_{N0}}{\Delta_0}=\frac{e^{\gamma}}{\pi}=0.57,\quad \gamma=\text{Euler constant}\ . \tag{3}$$

The development of the canonical model for SDW antiferromagnetism in the Cr alloy system is described by Fawcett (1988a). The simplest model for a SDW, a one-dimensional gas of electrons (Overhauser, 1960a), was followed by the remarkable result (Overhauser, 1962) that for a three-dimensional gas the linearly polarized SDW would have lower energy than a helical SDW. Overhauser first identified AFM (antiferromagnetic) Cr as being a manifestation of a static SDW, while Lomer (1962) recognized that the large amplitude of the SDW is connected with peculiar geometric features of the Fermi surface of Cr, which permit nesting between electron and hole sheets having similar shape. These are connected by a nesting vector directed along a cube axis, which is roughly constant and equal in magnitude to the measured wave vector of the SDW in Cr. The band-structure calculation of Asano and Yamashita (1967) for pure Cr in the commensurate AFM state was frequently employed to discuss work on Cr alloy systems, which could be understood by an appropriate adjustment of the Fermi level.

The Rice (1970) model, illustrated in Fig. 1(a), has spherical electron and hole surfaces of different radii, while the model of Shibatani *et al.* (1969), illustrated in Fig. 1(b), uses octahedra of different sizes with planar nesting surfaces, with a reservoir of electrons correspond-

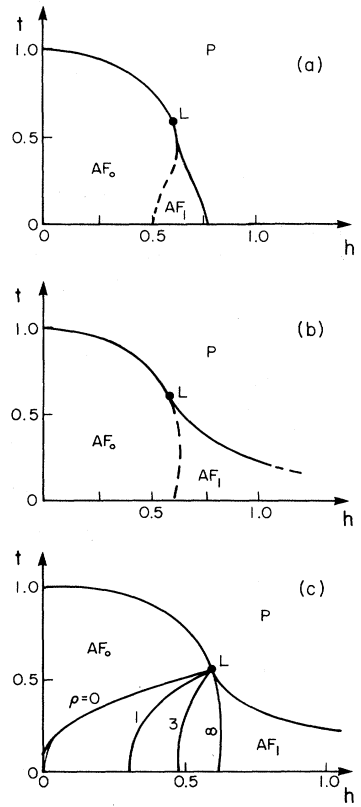

FIG. 1. Phase diagrams: (a) for the Rice model; (b) for the Shibatani model, with infinite reservoir; (c) for the canonical model for various values of the power ρ of the reservoir (from Machida and Fujita, 1984).

ing to the rest of the Fermi surface, which more closely approximates the situation in Cr. In both models the triple point occurs at the point, $h_L=0.61$, $t_L=0.56$; but the Néel transition line $t_N(h)$ to the incommensurate SDW phase AF_1 is significantly different. The $t_N(h)$ line in Fig. 1(a), ending at $h_N=0.76$, $t_N=0$, was found under the assumption that the P-AF_1 transition is second order, which is valid only for particular values of other parameters in the model. In Fig. 1(b), the $t_N(h)$ line approaches the abscissa asymptotically, so that formally t_N is never zero. The inclusion of impurity scattering leads, however, to behavior like that shown in Fig. 1(a); but in the Shibatani model, the P-AF_1 transition is always second order. Furthermore, the AF_1-AF_0 transition occurs in the Shibatani model, but not in the Rice model, so that the dashed line showing this transition in Fig. 1(a) is schematic.

While the Fermi energy corresponds directly to the experimental parameter x, the solute concentration, another parameter that determines the rate of change of band structure of the solvent metal Cr is available to the theorist. This is the reservoir density of states ρ_r, which is expressed relative to the sum of the electron ρ_e and hole ρ_h densities of state in the form

$$\rho=\frac{\rho_r}{\rho_e+\rho_h} . \tag{4}$$

When the power of the reservoir (the term used by Tugushev, 1992) is large, $\rho \gg 1$, the Fermi level is essentially fixed as x changes or, for given x, as the alloy enters the AFM phase, whereas when $\rho \leq 1$ it will change significantly.

The effect of the reservoir on the AF_1-AF_0 transition is shown in the phase diagram of Fig. 1(c). The Néel transition to the commensurate SDW phase AF_0 and to the incommensurate SDW phase AF_1, and the triple point L, are not affected by changes in the power ρ of the reservoir. All the phase transitions are second order. We call this the canonical model, since it was developed in different forms by several authors from the nesting-octahedra model of Shibatani *et al.* (1969), some of whom also took into account harmonics of the SDW (Windsor, 1972; Kotani, 1974a; Sato and Maki, 1974; Nakanishi and Kasuya, 1977; Kotani, 1978; Buzdin and Tugushev, 1983a, 1983b; Angelescu *et al.*, 1984; Machida and Fujita, 1984).

The experimental data for CrV and CrMn alloys superposed on plots showing the predictions of the canonical model were shown by Machida and Fujita (1984) and reproduced in Figs. 51, 52, and 53 of the review by Fawcett (1988a). The value, $\rho=3$, for the power of the reservoir gives the best overall fit for the phase diagram and the dependence of the wave vector **Q** and rms moment $\langle\mu\rangle$ on the nesting parameter h. The fit in the phase diagram is optimized by arbitrary scaling of h and the alloy concentration x.

Another quite different approach, based on band-structure calculations, has been used by Hirai (1993) to determine the dependence of **Q** and $\langle\mu\rangle$ on electron concentration, and is successful also in reproducing the observed variation in amplitude of the harmonics of the SDW.

Tugushev (1992) points out an effect that has not previously been included explicitly, namely, the spatial redistribution of electrons in the incommensurate SDW phase and the attendant loss of electrostatic energy. When $\rho \simeq 1$, so that the Fermi level is not locked by a large reservoir, but the incommensurate SDW phase is still relatively narrow, an incommensurate helicoidal structure may become more favorable. On the other hand, magnetic anisotropy may still favor the linearly polarized incommensurate SDW. An interesting feature of Tugushev's analysis is the existence of a first-order transition line corresponding to thermodynamic equilibrium between the phases, which is labeled t_{II} in Fig. 2 and lies between the lines t_{IC} and t_{CI}, these being the boundaries of the metastable AF_1 and AF_0 phases, respectively.

The other parameter that should be included in the theory is the impurity scattering, which, in general, lowers the Néel temperature and contracts the incommensurate SDW region of the phase diagram, by cutting off antiferromagnetism at a smaller value of h, while at the same time increasing its stability relative to that of the commensurate SDW (see Fig. 3). Zittartz (1967) showed that randomly distributed nonmagnetic impurities have a pair-breaking effect in an excitonic semimetal. This model of interacting electron and hole semiconductor bands is formally similar to the two-band model of Fedders and Martin (1966) for an AFM metal, and the results of the Zittartz theory may be applied to Cr alloys. The pair-breaking by nonmagnetic impurities in the AFM metal is analogous to the effect of magnetic impurities in a superconductor (Abrikosov and Gorkov, 1960) and, in both cases, results in a depression of the ordering temperature. A comparison of the experimental data with the prediction of the Zittartz theory is given in Sec. V.C.4. Behera and Viswanathan (1969) calculated, for a model of equal electron and hole spheres (Fedders and Martin, 1966), the depression of T_N for $3d$ paramagnetic impurities in Cr, using the Wolff-Clogson model in the Hartree-Fock approximation. They were thus able to ex-

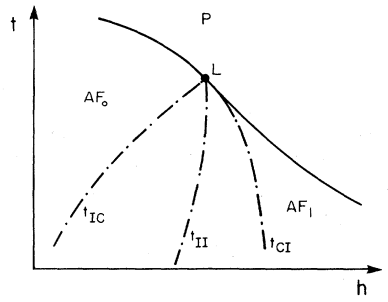

FIG. 2. Phase diagram for the Volkov-Tugushev model showing the line t_{II} of first-order transitions and the boundaries t_{IC} and t_{CI} of the metastable phases (after Tugushev, 1992).

plain the fact that T_N is only weakly depressed by Fe and Co impurities, because the increase of T_N in the rigid-band approximation due to the increase in electron concentration is compensated by a depression of T_N due to spin-dependent scattering by the local moments carried by these atoms in the paramagnetic phase (see Sec. III). There is a weak depression of T_N also by the isoelectronic impurities Mo and W, which is attributed to the change in the intra-atomic Coulomb potential at the impurity site. Behera and Viswanathan (1969) showed that with a reasonable choice of parameters their theory gave good agreement with the observed depression of the Néel temperature (see Table I) by the 3*d* metals, and Mo and W, introduced as dilute impurities in Cr.

It is interesting to note that Sato and Maki (1974) calculated in a similar fashion the effect of electron-phonon scattering on the Néel temperature of Cr, with the phonons being simulated by randomly distributed impurities. The scattering rate expressed in temperature units is $0.24\pi T$, and the Néel temperature is accordingly depressed by a factor, $T_N/T_{N0}=0.24\pi$.

The effect of impurity scattering on the phase diagram around the triple point was first discussed by Nakanishi and Kasuya (1977). This important paper distinguishes between scattering by normal impurities and by magnetic impurities, in an effort to understand the unusual feature of the phase diagram of the CrFe system that the commensurate SDW phase AF_0 occurs at lower temperature than the incommensurate SDW phase AF_1 (see Fig. 14). It turns out, however, that this behavior is associated with the length change at the strongly first-order phase transitions from the paramagnetic phase P to AF_0 (and also from AF_0 to AF_1), rather than from the magnetic scattering due to the local moments known to be associated with the Fe atoms in the SDW phase (see Sec. III). Nakanishi and Kasuya were able to reproduce this magnetostrictive behavior and to account for the unusual phase diagram of the CrFe system by postulating a magnetovolume term in the magnetic free energy.

Maki and Sakurai (1972) confirmed the result of Behera and Viswanathan (1969) that scattering due to

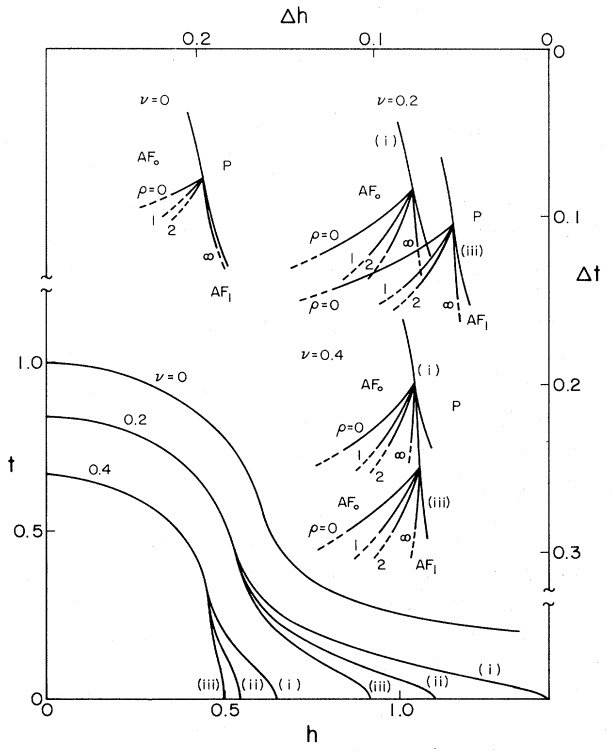

FIG. 3. Phase diagram for the canonical model with impurity scattering. The scattering rates are $\nu=0$, 0.2, and 0.4 (in units of T_{N0}), and the effect is shown of (i) potential intraband scattering, $\nu_i=\nu$; (ii) potential and exchange reservoir-nesting surface scattering, $\nu_r=2\nu$; and (iii) exchange interband scattering, $\nu_\sigma=3\nu$. For some of these cases, the *I-C* phase boundary is shown in the inset figures, with scales enlarged by a factor 5, for reservoir powers $\rho=0$, 1, 2, and ∞. For $\nu=0.2$, the inset figures for cases (i) and (iii) are displaced by $\Delta h=0.02$ for clarity (from Nakanishi and Kasuya, 1977).

TABLE I. Dependence of the Néel temperature T_N and spin-flip temperature T_{SF} on concentration x of the solute A (in the limit $x\rightarrow 0$) for chromium alloy systems $Cr_{1-x}A_x$.

Solute *A*	$\frac{dT_N}{dx}$ (K/at. %)	$\frac{dT_{SF}}{dx}$ (K/at. %)	Reference
Ti	−160	−220	Fig. 10
V	−80	−100	Fig. 11
Nb	−70		a
Ta	−100		a
Mo	−14		Fig. 10
W	−18	−35	Fig. 10
Mn	50	−30	Fig. 12
Re	80	−5	Fig. 13
Fe	−25	−70	Fig. 14
Co	−20		Fig. 10
Ni	−140		Fig. 10
Ru	80	−150	Fig. 15
Os	25		Fig. 10
Pd	−20		Fig. 10
Rh	50		Fig. 10
Ir	50		Fig. 10
Pt	0	0	Fig. 10
Au	−30		Fig. 10
Be	−30	−80	Fig. 9
Al	−80	−65	Fig. 16
Ga	−50		Fig. 9
Si	−60	−30	Fig. 17
Ge	−20	−50	Fig. 9
Sn	0	−30	Fig. 9
Sb	30		Fig. 9
Yb,Er	−5000		b
Gd	−7		c
Y,La	0		d
Tb,Dy,Ho,Lu	<40		d

[a]Koehler *et al.* (1966).
[b]Giurgiu *et al.* (1981).
[c]Hsu and Fu (1994).
[d]Butylenko *et al.* (1974).

both normal and magnetic impurities have a depairing effect and thus depress the Néel temperature. Antonoff (1977, 1978) later showed, however, that paramagnetic impurities in an itinerant electron antiferromagnet can be polarized by the SDW, leading to an exchange enhancement of the SDW, which tends to raise the Néel temperature and thus offset the effect of impurity scattering. By a suitable choice of the parameters describing the scattering rate per impurity and the exchange interaction, the nonmonotonic dependence of $T_N(x)$ in $Cr_{1-x}Co_x$ alloys (see Sec. II.C.5) can be reproduced. Gunther and Antonoff (1983; see also Antonoff, 1986, 1988) further developed this idea to determine the discontinuity in the wave vector at the AF_1-AF_0 transition, which they found to increase with impurity concentration.

Only intraband processes, for the case of perfect nesting, had, however, been considered by Maki and Sakurai. Nakanishi and Kasuya (1977) added the following scattering terms to the Hamiltonian of the system with impurities at $\mathbf{r}_j$:

$$\mathcal{H}=\sum_{j,\mathbf{k},\mathbf{k}',\mu,\nu}\exp[i(\mathbf{k}-\mathbf{k}')\cdot\mathbf{r}_j][(V_{ee})_{\mu\nu}a^*_{\mathbf{k}'\mu}a_{\mathbf{k}\nu}+(V_{hh})_{\mu\nu}b^*_{\mathbf{k}'\nu}b_{\mathbf{k}\nu}+(V_{rr})_{\mu\nu}c^*_{\mathbf{k}'\mu}c_{\mathbf{k}\nu}$$
$$+\{(V_{eh})_{\mu\nu}a^*_{\mathbf{k}'\mu}b_{\mathbf{k}\nu}+(V_{er})_{\mu\nu}a^*_{\mathbf{k}'\mu}c_{\mathbf{k}\nu}+(V_{hr})_{\mu\nu}b^*_{\mathbf{k}'\mu}c_{\mathbf{k}\nu}+(\text{Hermitian conjugate})\}], \quad (5)$$

where $a^*_{\mathbf{k}'\mu}, a_{\mathbf{k}\nu}$ are creation and annihilation operators for the nesting electron surface, $b^*_{\mathbf{k}'\mu}, b_{\mathbf{k}\nu}$ for the nesting hole surface, and $c^*_{\mathbf{k}'\mu}, c_{\mathbf{k}\nu}$ for the reservoir.

The matrix elements

$$(V_{ij})_{\mu\nu}=V_{ij}\delta_{\mu\nu}+J_{ij}(\mathbf{S}\sigma)_{\mu\nu} \quad (6)$$

correspond to a scattering of electrons between electron (e), hole (h), and reservoir (r) parts of the Fermi surface labeled by the indices i,j, having spin in directions labeled μ,ν. $\mathbf{S}$ is the spin corresponding to the local moment on the impurity and σ is the polarization of the SDW. The first term corresponds to potential impurity scattering, for which the spin direction of the scattered carrier is unchanged, i.e., $\mu=\nu$, and

$$V_{ee}=V_{hh},\quad V_{eh}=V_{he},\quad V_{er}=V_{re}=V_{hr}=V_{rh}\ . \quad (7a)$$

The second term in Eq. (6) corresponds to exchange impurity scattering, for which, in general, $\mu\neq\nu$, and

$$J_{ee}=J_{hh},\quad J_{er}=J_{re}=J_{hr}=J_{rh}\ ; \quad (7b)$$

but

$$J_{eh}=J_{he}=0\ , \quad (7c)$$

because in the CrFe system the SDW couples only weakly to the local moment (see Sec. III).

Nakanishi and Kasuya first checked their work by calculating the phase diagram of Cr doped with V or Mn, for which there is no magnetic moment and there is no magnetovolume term in the free energy, and obtained the following parameters for the canonical model: the energy gap is $2\Delta_0=0.30$ eV, giving $T_{N0}=972$ K; the Fermi energy in pure Cr is $h=82$ meV, well below the middle of the gap; the change of the Fermi level with doping is $dh/dx=20$ meV/at. % Mn, and the triple point occurs at $h_L=76$ meV and $T_L=370$ K. They also calculated the AF_0-AF_1 line of transitions and reproduced the result of Kotani (1974a) that, as the power ρ of the reservoir defined in Eq. (4) decreases, the commensurate SDW phase AF_0 becomes relatively more stable than the incommensurate SDW phase AF_1, as illustrated in Fig. 1(c).

For potential intraband scattering between the nesting parts of the Fermi surface and for impurity concentration x, the rate is

$$\nu_i=2\pi(\rho_e+\rho_h)x(V^2_{ee}+V^2_{eh})\ ; \quad (8a)$$

for exchange intraband scattering,

$$\nu_\sigma=2\pi(\rho_e+\rho_h)xS(S+1)J^2_{ee}\ ; \quad (8b)$$

and for potential and exchange interband scattering between the nesting surfaces and the reservoir,

$$\nu_r=2\pi\rho_r x[V^2_{er}+S(S+1)J^2_{er}]\ . \quad (8c)$$

The effect of scattering on the phase diagram is shown in Fig. 3, which is complicated but repays study. Nakanishi and Kasuya note the following features: (a) The three types of scattering described in Eqs. (8) all lower the Néel temperature, and, for the P-AF_0 transition, ν_i, $\frac{1}{2}\nu_r$, and $\frac{1}{3}\nu_\sigma$ have the same effect. (b) For the AF_1-AF_0 transition, the effect of the three types of scattering differs, with $\frac{1}{3}\nu_\sigma$ having the strongest depairing effect and ν_i the weakest; the same is true of the effect on the position of the triple point (for clarity, the curves for $\frac{1}{2}\nu_r$ are not shown in the insets to Fig. 3). (c) As already noted, the commensurate SDW phase becomes relatively more stable than the incommensurate SDW phase as the power ρ of the reservoir increases, but this effect becomes weaker as the scattering increases.

We note, in particular, that only for weak scattering and high reservoir power does the incommensurate SDW phase occur at higher temperature than the commensurate SDW phase, as shown, for example, in the extreme case by the AF_1-AF_0 transition line in the upper-left inset to Fig. 3 for $\nu=0$ and $\rho=\infty$. Thus in the CrFe system, where this effect is very pronounced, as shown in Figs. 14 and 57(b), we must look for another explanation, as, for example, the magnetostrictive effect discussed in Sec. VI.B.

Men'shov and Tugushev (1989) have described another situation that could give rise to an inversion of the AF_1-AF_0 line of phase transitions, thus making the commensurate SDW phase stable at lower temperatures. They

consider the special case of nonmagnetic scattering, for which $\rho_r \gg \rho_e, \rho_h$, but with scattering into the reservoir suppressed, due, say, to the symmetry of the wave function, so that $\nu_i \gg \nu_r$ ($\nu_\sigma = 0$) in Eqs. (8). The total scattering, $\nu = \nu_i + \nu_r$, is of course proportional to x, while the Fermi level remains essentially constant as x changes due to the essentially infinite power of the reservoir. Thus the plots in Fig. 4 showing the transition lines as a function of ν are effectively phase diagrams.

We see in Fig. 4 that, when the nesting parameter is between the values, $h \simeq 0.60$ to 0.63, the AF_0 phase lies below the AF_1 phase, with the triple point rapidly moving to lower values of ν with increasing h. For $h = 0.63$, the triple point disappears, and the sequence of phases, $P \rightarrow AF_1 \rightarrow AF_0$, with decreasing temperature, occurs even for zero scattering, since there is no triple point. The special case considered by Men'shov *et al.* is, however, not relevant to the CrFe case, since, when we compare Fig. 4(a) with Figs. 14 or 57(b), we see that along the line of AF_1-AF_0 transitions the sign of dT_{IC}/dx is opposite to that of $dT_{IC}/d\nu$.

It should be noted that there is no discontinuity in the concentration dependence dT_N/dx of the Néel temperature at the triple point in any of the theoretical models considered (see Figs. 1–4). This is in strong contrast with the observed behavior in most Cr alloy systems (see Figs. 9 and 10).

Fishman and Liu (1992, 1993a, 1993b) have recently embarked on a program of calculations designed mainly to understand the new experimental results discussed in Sec. VII.B for critical scattering in the paramagnetic phase of pure Cr and Cr alloys. These calculations were motivated initially (1992, 1993c) by the wish to understand the effect of impurities in dilute CrV and CrMn alloys on the nature of the Néel transition to the incommensurate SDW phase (see Sec. VI.A). They promise, however, to give new insight also into the phase diagrams in Cr alloy systems (1993d).

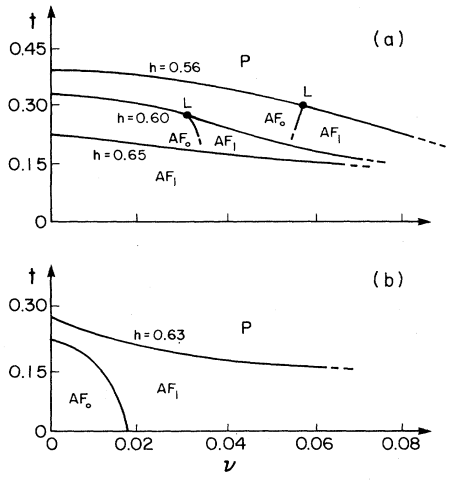

FIG. 4. Phase diagram for the Volkov-Tugushev model with potential intraband impurity scattering ν (in units of Δ_0) for various values of the nesting parameter h and infinite reservoir power (after Tugushev, 1992).

Young and Sokoloff (1974) had previously considered the three-band model used by Fishman and Liu, which comprised the two hole surfaces centered on the points H at $a^*(\pm 1,0,0)$ and the smaller electron surface at the origin Γ in reciprocal space (see Fig. 61 of Fawcett, 1988a). They showed that, while the Coulomb electron-hole interaction is responsible for the incommensurate SDW in Cr, the hole-hole repulsion will cause the appearance of a charge-density wave with twice the wave vector of the SDW (see Sec. VII.A). Young and Sokoloff were mainly interested in explaining the first-order nature of the Néel transition in pure Cr, while Fishman and Liu sought to go further and explain the observed effect of impurities in making the transition continuous.

Fishman and Liu discovered also that the SDW always has a wave vector closer to the commensurate value, $a^* = 2\pi/a$, than the nesting vector $\tilde{\mathbf{Q}}$; and when the nesting parameter h decreases due to doping, the SDW becomes commensurate with a continuous transition well before the condition, $\tilde{\mathbf{Q}} = 2\pi/a$, is reached. This has the effect that the triple point x_L occurs as observed (Table IV) at a somewhat lower value of the concentration x of elements A of groups 7 and 8 in alloys $Cr_{1-x}A_x$ than might be expected. Furthermore, the Néel temperature to the commensurate SDW phase continues to rise considerably, as observed (Secs. II.C.4 and II.C.6), as x increases beyond x_L and the nesting between the concentric electron and hole surfaces continues to improve. The analysis is, however, complicated by the fact that scattering by the impurities favors the incommensurate SDW phase and lowers the Néel temperature in both phases, so that there is a complex interplay of different effects that have not thus far been analyzed for lack of knowledge of the parameters involved in the calculation. It is not clear how the introduction of the electron reservoir representing the rest of the Fermi surface, which is such a prominent feature of the canonical model, will affect the calculation.

Comparison between the canonical model and the experimental data for the CrV and CrMn alloy systems was found to give an excellent fit, for appropriate and reasonable choice of the parameters of the theory. The success of this early experimental work (Loshmanov, 1964; Hamaguchi *et al.*, 1965; Komura and Kunitomi, 1965; Moller *et al.*, 1965; Koehler *et al.*, 1966; Komura *et al.*, 1967a) in validating the predictions of the theoretical work described in Sec. II.A provided great impetus to the study of the Cr alloy SDW system.

The fit to the canonical model in the case of CrV and CrMn is predicted on a rigid-band picture, with V and Mn having five and seven electrons per atom, respectively. In the case of other alloy systems, however, the model often provides little understanding of the observed behavior. For example, the numbers of electrons contributed to the nesting bands by each impurity atom depends on its electronic state, which is not known in particular

in the case of nontransition metals without additional information from microscopic measurements (see Sec. X). The formation of local moments, in particular for potentially magnetic atoms, such as Fe, Co, or Ni, might also strongly modify the behavior.

B. Experiment: general

We present in Figs. 9 and 10 the schematic composition-temperature phase diagrams for most Cr alloy systems $Cr_{1-x}A_x$ over the range up to $x=5$ at. %. The complete phase diagrams showing all the available data, in some cases obtained from the anomalies at the phase transitions observed in several different properties, are given in Figs. 11 to 17 of Sec. II.C only for the prototypical or more interesting systems. The phase diagrams for individual systems compiled from the literature, but not shown in these figures, are available on request from any of the authors.

In Table I are the observed values of the initial dependence on alloy composition of the Néel temperature T_N, and of the spin-flip temperature T_{SF}, in all the alloy systems for which they have been measured. Neutron-diffraction measurements, giving the initial dependence on alloy composition of the wave vector **Q** and the rms moment $\langle\mu\rangle$ of the SDW, have been performed on a good number of these alloy systems, with the results as given in Table II. We combine these data in Table III to show the interdependence between these characteristic physical properties of dilute chromium alloys.

The value of dQ/dx is roughly equal and opposite for CrV and CrMn alloys, as predicted by the canonical model. A calculation of the wave-vector-dependent susceptibility $X(\mathbf{q})$ gives a peak value at the nesting vector **Q** which has essentially the same behavior (Schwartzman *et al.*, 1989).

Referring first to Table I, we see the general result that transition metals of groups 4, 5, and 6 and most of the nontransition metals depress T_N, while, with the exception of the three ferromagnetic metals (and Pd for which the nature of the behavior is still in doubt), transition metals of groups 7 and 8 elevate T_N. Two of the rare-

TABLE II. Dependence of the wave vector Q (in units of $a^*=2\pi/a$, a being the lattice parameter) and the rms moment $\langle\mu\rangle$ of the SDW on concentration x of the solute A (in the limit $x\to 0$) for chromium alloy systems $Cr_{1-x}A_x$.

Solute A	$T\lesssim T_N$ $\frac{dQ}{dx}$	$T\gtrsim 77$ K $\frac{dQ}{dx}$	$T\gtrsim 77$ K $\frac{d\langle\mu\rangle}{dx}$ (μ_B)	$T\gtrsim 4$ K $\frac{dQ}{dx}$	$T\gtrsim 4$ K $\frac{d\langle\mu\rangle}{dx}$ (μ_B)	Reference
V	−4.1			−1.9	−12	a
		−1.7	−10			b
Ta					−20	a
Mo				−0.7	−1.6	a
					−1.7	c
W	−0.17			−0.6	−4.1	a
Mn					14	a
		1.7	10			b
Re	2.5			2.5	$\gtrsim 30$	a
	5	2.3				d
Fe	1.2			1.0	$\lesssim 0$	e
				0.7	20	f
Co	2.0			0.9	−1.1	g
Ni	−0.5			1.5	−14	g
Ru					$\gtrsim 30$	a
Pd		0			−6	h
Rh					$\gtrsim 40$	a
Pt		2.7			11	k
Be		−0.9	−15			l
Ga				0.5	10	m
Si				1.25	50	n
Ge				1.5	20	m,p
Sn				$\simeq 0$	$\simeq 0$	q
Sb				$\simeq 0$	$\simeq 0$	q

[a]Koehler *et al.* (1966).
[b]Komura *et al.* (1967b).
[c]Cywinski and Hicks (1986).
[d]Lebech and Mikke (1972).
[e]Ishikawa *et al.* (1967).
[f]Arrott *et al.* (1967).
[g]Endoh *et al.* (1968).
[h]Ziebeck and Chagnon (1977).
[k]Booth *et al.* (1978).
[l]Sano *et al.* (1981).
[m]Booth *et al.* (1983,1991).
[n]Cable (1977).
[p]Iida, Kawarazaki, and Kunitomi (1981).
[q]Okpalugo *et al.* (1985).

TABLE III. Variation of the Néel temperature T_N with the low-temperature values of the wave vector **Q** and the rms moment $\langle\mu\rangle$ of the SDW for chromium alloy systems $Cr_{1-x}A_x$.

Solute A	$\frac{dT_N}{d\langle\mu\rangle}$ [a] (10^2 K μ_B^{-1})	$\frac{d\mathbf{Q}}{d\langle\mu\rangle}$ [b] (μ_B^{-1})	$\frac{dT_N}{d\mathbf{Q}}$ [c] (10^2 K)
V	7	0.32	43
Ta	5		
Mo	8.5	0.4	20
W	4.5	0.15	30
Mn[d]	5	0.17	30
Re	2	$\lesssim 0.08$	30
Fe	−2.5	0.1	−30
Co	18	−0.8	−22
Ni	10	−0.11	−90
Ru	2		
Pd	3		large
Rh	1		
Pt	0		0
Be[d]	2	0.06	30
Ga	−5	0.05	−100
Si	−2.5	0.025	−50
Ge	−1	0.075	−13

[a] $dT_N/d\langle\mu\rangle = (dT_N/dx)(d\langle\mu\rangle/dx)^{-1}$, from Tables I and II.
[b] $d\mathbf{Q}/d\langle\mu\rangle = (d\mathbf{Q}/dx)(d\langle\mu\rangle/dx)^{-1}$, from Table II.
[c] $dT_N/d\mathbf{Q} = (dT_N/dx)(d\mathbf{Q}/dx)^{-1}$, from Tables I and II.
[d] Values for temperature $T \lesssim 77$ K.

earth alloy systems that have been studied show a remarkably large initial depression. In all cases T_{SF} is depressed by the introduction of impurities, though the initial depression may be zero, as for CrPt.

We shall resume later the discussion of the dependence of the Néel temperature on impurity concentration, in connection with the phase diagrams of Cr alloy systems. The various phase transitions represented in the phase diagram are determined from the anomalies seen at the transition in the temperature dependence of the various physical properties. The Néel temperature, both to the incommensurate SDW phase AF_1 and, in the case of systems that exhibit a triple point at a concentration of impurity x_L, to the commensurate SDW phase, which appears for $x > x_L$, is usually determined from the anomaly in the temperature dependence of the resistivity, which invariably accompanies the Néel transition.

The measurement of resistivity is relatively easy and can readily be performed under pressure for the determination of the pressure-temperature phase diagram. However, almost all physical properties have been put to this use, as may be seen by an inspection of the phase diagrams for individual elements given in Figs. 11 to 17.

The AF_0-AF_1 transition between the commensurate and incommensurate SDW phases at temperature T_{IC} does not normally exhibit an anomaly in the temperature dependence of the resistivity. T_{IC} has often been determined from anomalies in the temperature dependence of the magnetoelastic properties, namely, the thermal expansion and the sound velocities, though other physical properties may be used. Anderson *et al.* (1993) have found that elastic anomalies occur at T_{IC} in CrSi single crystals, though absent in polycrystalline samples (Alberts and Lourens, 1988a). The definitive measurement is, of course, neutron diffraction, which shows the onset of the AF_1 phase through the appearance of incommensurate Bragg peaks; but this experiment is much more laborious, not least because a single crystal is required. Neutron diffraction does, however, have the capability of demonstrating the coexistence of two phases over a temperature range around the transition. When a two-phase region occurs, the anomaly in the temperature dependence of the resistivity may be smeared out to such an extent that it is not observable, which may account for its absence in many cases at the AF_0-AF_1 and the AF_1-AF_2 phase transitions. This is clearly the case, for example, in the CrGe alloy system, where Booth *et al.* (1991) find extensive two-phase regions at both these transitions in careful neutron-diffraction experiments, which is the only technique that reveals the existence of the AF_1-AF_2 phase transition in these alloys.

The identification of the exact position of a phase transition from the anomaly in the temperature dependence of a physical property is a vexing problem. The temperature dependence of the electrical resistivity $\rho(T)$ may show a true minimum, or merely a shoulder on the side of a curve corresponding to ρ rising rapidly with temperature T; but in either case, the derivative $d\rho/dT$ is a minimum (i.e., the inflection on the low-T side of the minimum in $\rho(T)$ or in the middle of the shoulder) and provides a better estimate of the Néel temperature T_N than the minimum in $\rho(T)$ itself, or any other feature of the anomaly. We refer, for example, to Arajs, Moyer, and Abukay (1980), who compared values of T_N in the CrRe alloy system with values obtained by neutron diffraction (Lebech and Mikke, 1972) and by the anomaly in the magnetic susceptibility (Arajs *et al.*, 1976) and found quite good agreement. Arajs *et al.* (1973) summarized data obtained in this way for 15 Cr alloy systems.

Butylenko and Nevdacha (1980a, 1980b) published two papers giving a review of their experimental data for the phase diagram around the triple point obtained from the resistivity anomaly in CrCo, CrRu, CrRh, CrOs, and CrIr, and also in CrPd, where no triple point is observed. These data are of unusually high quality, and, in all cases except CrCo, the AF_0-AF_1 phase transition is observed. One can only suppose that, in the case of other work where this transition is not observed, the absence of the resistivity anomaly is due to inferior sample quality. Unfortunately, the curves showing the temperature dependence of the resistivity over a wide range are shown only for the CrRu alloys (Fig. 1 in Butylenko and Nevdacha, 1980a, 1980b; both references are given, since these journals may not easily be available).

The physical origin of the anomalies in the thermal expansivity $\beta(T)$ and the bulk modulus $B(T)$ is, however,

quite different from that of the anomaly in $\rho(T)$, and the choice of minimum or inflection point to identify T_N must be argued on its merits. Alberts and Lourens (1983) found in CrCo alloys that the minima in $\beta(T)$ and $B(T)$ agree better with the inflection point in $\rho(T)$ (minimum in $d\rho/dT$) than with the minimum in $\rho(T)$. When, however, the minima in either $\beta(T)$ or $B(T)$, at the Néel temperature T_N and the AF_0-AF_1 phase-transition temperature T_{IC}, are so close that they coalesce to form a single broad minimum, the inflection points on either side of this minimum give reasonably good estimates for T_N and T_{IC}. This behavior was first understood in CrGa (Alberts and Lourens, 1985), but it had been observed some years earlier by Munday (1971) in CrRe, CrRu, and CrRh, as illustrated in Fig. 47.

A comparison of the dependence on the impurity concentration x of the Néel temperature T_N and the rms moment $\langle\mu\rangle$ of the SDW for all the transition metals, except the ferromagnetic metals Co and Ni (the sign of $d\langle\mu\rangle/dx$ is still in doubt for Fe), shows that dT_N/dx and $d\langle\mu\rangle/dx$ have the same sign. Koehler *et al.* (1966) found a linear variation of $\langle\mu\rangle$ with T_N for incommensurate alloys with V, Mo, W, Mn, Re, and Ru, giving $dT_N/d\langle\mu\rangle = 312/0.43 \simeq 7.3(10^2\ \mathrm{K}\mu_B^{-1})$, with somewhat higher values of T_N for the same value of $\langle\mu\rangle$ in the commensurate relative to the incommensurate alloys. There is, however, considerable variation about this value of $dT_N/d\langle\mu\rangle$ for the nonferromagnetic transition-metal alloys in Table III. In particular, the values for the group-7 metals Re, and especially Mn, are much smaller.

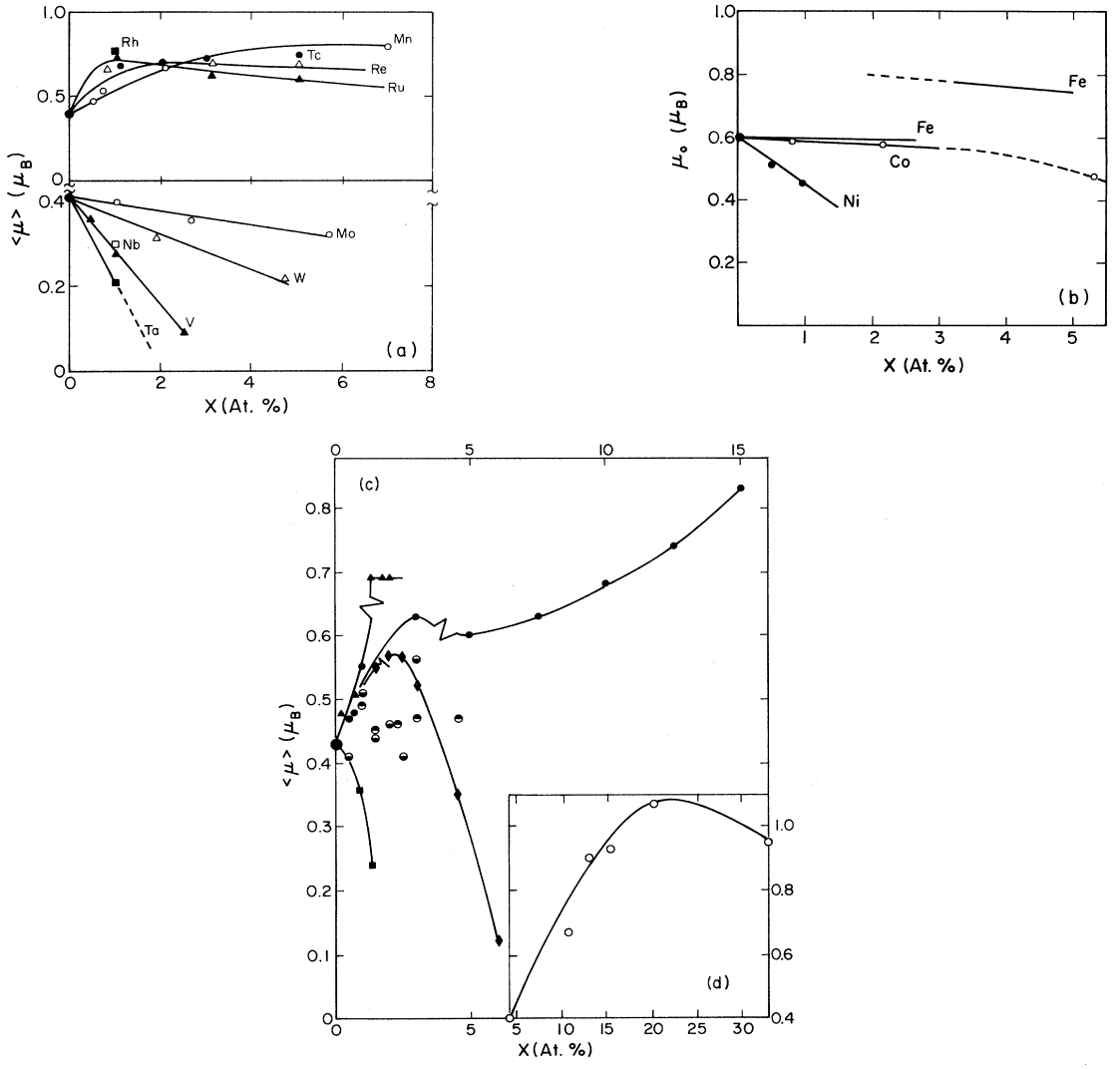

FIG. 5. Amplitude of the SDW at temperature 4.2 K, expressed in (a) and (c) as the rms moment $\langle\mu\rangle$, and in (b) and (d) as the peak moment μ_0 (with $\langle\mu\rangle = \mu_0$ for a commensurate SDW) in chromium alloy systems $Cr_{1-x}A_x$: (a) transition metals A=V, Mn, etc. (from Koehler *et al.*, 1966); (b) magnetic transition metals A=Fe, Co, and Ni (from Endoh *et al.*, 1968); (c) nontransition metals compiled from the references in Table II: CrBe (■) at 77 K; CrGa (●); CrSi (◆); CrGe (△); CrSn (◒); CrSb (◓) (the continuous lines are guides to the eye, and a break in a line shows that the *I-C* transition occurs between these two data points); (d) CrAl (○) (from Kallel and De Bergevin, 1967).

In contrast to the transition-metal alloys, the sign of $dT_N/d\langle\mu\rangle$ is negative for the three non-transition-metal alloys in Table III. On the other hand, $d\mathbf{Q}/d\langle\mu\rangle$ is positive for all alloys with nontransition and nonferromagnetic transition metals.

The variation of T_N and $\langle\mu\rangle$ with the incommensurablity parameter, $\delta=1-\mathbf{Q}$, provides physical quantities more meaningful than those listed in Table III. Thus we can write an equation for the logarithmic derivative,

$$\frac{d\ln\delta}{d\ln\langle\mu\rangle}=-\frac{\langle\mu\rangle}{\delta}\frac{d\mathbf{Q}}{d\langle\mu\rangle}\simeq-9\frac{d\mathbf{Q}}{d\langle\mu\rangle}\ , \tag{9}$$

where we have used the values for Cr at low temperature, $\delta=0.047$ and $\langle\mu\rangle=0.43\mu_B$. Figure 7 shows that for incommensurate SDW alloys $\langle\mu\rangle$ is roughly proportional to δ, so that Eq. (9) may be used to convert $d\mathbf{Q}/d\langle\mu\rangle$ for any alloy in Table III into the more useful logarithmic derivative, by using the same value, $\langle\mu\rangle/\delta=9\mu_B$, as for pure Cr. Similarly, we can obtain the logarithmic derivative

$$\frac{d\ln T_N}{d\ln\delta}=-\frac{\delta}{T_N}\frac{dT_N}{d\mathbf{Q}}\ ; \tag{10}$$

but in this case the specific values of δ and T_N for each individual alloy must be used, since these two quantities are, of course, not proportional and, indeed, vary in opposition (compare Figs. 51 and 52 of Fawcett, 1988a).

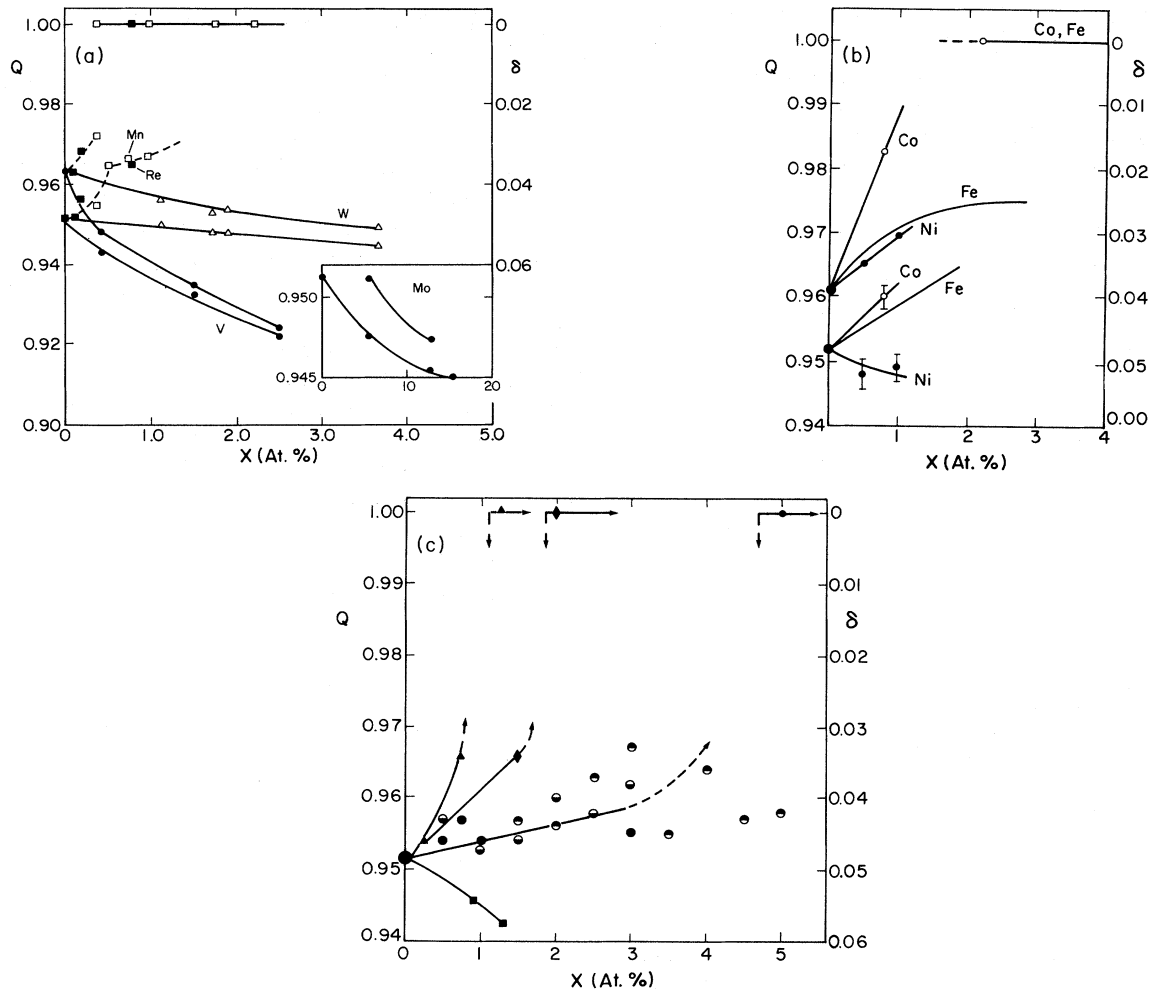

FIG. 6. Wave vector, $\mathbf{Q}=1-\delta$ (both in units of $a^*=2\pi/a$), of the SDW in chromium alloy systems $Cr_{1-x}A_x$, with $\mathbf{Q}=1$, $\delta=0$, corresponding to a commensurate SDW. For each solute metal A in (a) and (b), the upper curve corresponds to measurements near the Néel temperature, while the lower curve corresponds to low temperature: (a) transition metals A=V, Mn, etc. with data points for Mn and Re connected by dashed lines as guides to the eye (from Koehler *et al.*, 1966); (b) magnetic transition metals (from Endoh *et al.*, 1968); (c) nontransition metals, compiled from the references in Table II: pure Cr (●); CrBe (■) at 77 K; CrGa (●); CrSi (◆); CrGe (△); CrSn (◒) at 100 K; CrSb (◓) at 100 K. The continuous lines are guides to the eye, and the dashed lines with arrows connecting the data points corresponding to the incommensurate SDW and commensurate SDW phases are schematic, since the critical concentration and the order of the *I-C* transition are not known.

The data given in Tables II and III are illustrated in Figs. 5 and 6. While Table II shows that CrBe is the only alloy system of chromium with a nontransition metal for which the initial value of $d\langle\mu\rangle/dx$ is negative, Fig. 5(c) shows that CrSi has a remarkable reversal of sign of $d\langle\mu\rangle/dx$, with $\langle\mu\rangle$ decreasing rapidly for commensurate SDW alloys with $x > 2.5$ at. %. In most cases the amplitude of the SDW remains fairly constant with increasing x in the commensurate SDW phase, as seen in Figs. 5(a) and 5(b), except for CrGa, for which $\langle\mu\rangle$ is increasing rapidly for $x \gtrsim 5$ at. %. Figures 5(c) and 6(c) illustrate the remarkable feature of the CrSn and CrSb alloy systems that both the amplitude and the wave vector of the SDW vary only very slowly with x.

The proportionality between the amplitude of the SDW and Néel temperature for several Cr alloys with both transition and nontransition metals is noteworthy and was first remarked for transition metals by Koehler *et al.* (1966). They pointed out that this was to be expected from the Fedders-Martin (1966) theory of nesting electron and hole spheres, which gives a law of corresponding states relating the energy gap to the Néel temperature. A similar result is obtained for the canonical model of nesting octahedra with a reservoir (Machida and Fujita, 1984).

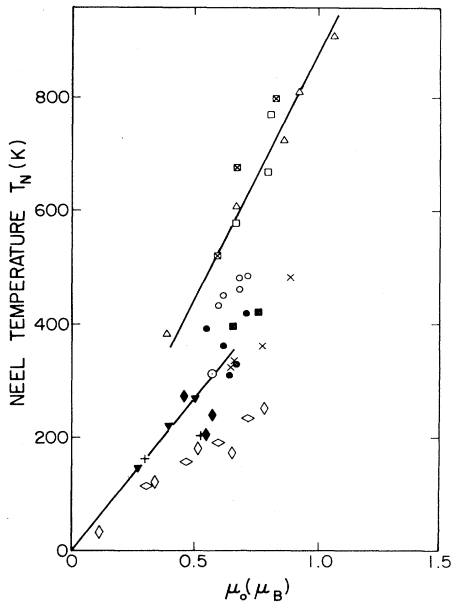

FIG. 7. The relation between the Néel temperature T_N and the amplitude μ_0 of the spin-density wave in chromium alloy systems. The open symbols are used for commensurate SDW data and the solid symbols (and +, ×) for incommensurate SDW data: pure Cr (⊙); CrMn (□ ■); CrV (▽); CrAl (△), CrBe (+); CrGe (○ ●) [Iida, Kawarazaki, and Kunitomi (1981); Booth *et al.*, 1983]; CrGa (⊠ ×) (Booth *et al.*, 1983); CrSi (◇ ◆) (Costa *et al.*, 1980); CrFe (◇) (Burke and Rainford, 1978). In most cases the amplitude is measured at 4.2 K, but the data for the two CrAl samples with $T_N > 800$ K were taken at room temperature, while the data of Iida *et al.* (1981) for CrGe were taken at temperatures of 77 K or 120 K, well below T_N (after Iida, Kawarazaki, and Kunitomi, 1981).

The constant of proportionality is $1.12\times10^{-3}\mu_B$ K^{-1} for the commensurate SDW alloys and is larger by a factor 1.64 than for the incommensurate SDW alloys, according to the linear fits shown in Fig. 7, which were suggested by Iida, Kawarazaki, and Kunitomi (1981). This agrees roughly with the factor $\sqrt{2}$ that one would expect as the ratio $\mu_0/\langle\mu\rangle$ for a sinusoidal SDW if the magnetic energy density were the same in two samples, in the commensurate and incommensurate SDW phases, having the same Néel temperature. The data points for commensurate alloys in the CrFe and CrSi systems, however, lie well below those for the other commensurate systems. The Néel temperature for one of these alloys having a given SDW amplitude is only about half as large as for another commensurate alloy having a SDW of the same amplitude. The CrFe and CrSi alloy systems are anomalous in other respects, as we shall see in Secs. V.C, and VI.A, and VI.B.

When we examine the relation between the amplitude of the SDW and the wave vector **Q** of the incommensurate SDW (see in Table III and Fig. 8), we find rough proportionality, with $d\mathbf{Q}/d\langle\mu\rangle \simeq 0.15$. There is, however, considerable variation with, for example, **Q** remaining essentially constant in CrGa as the amplitude μ_0 increases from $0.6\mu_B$ in pure Cr to $0.89\mu_B$ in Cr+3 at. % Ga (Booth *et al.*, 1983), while $d\mathbf{Q}/d\langle\mu\rangle$ is large and negative in CrCo (see Table III).

All the nontransition metals, in solution in Cr, initially decrease the Néel temperature, except for the group-5 metals As and Sb, and perhaps Sn, as seen in Fig. 9. The nontransition metals of groups 3 and 4 lead to a triple point at a concentration, $x_L \lesssim 1$ at. %, as shown in Table IV. The Néel temperature T_{NC} to the commensurate SDW phase, for $x \gtrsim x_L$, increases rather more rapidly with x than T_{NI} to the incommensurate SDW phase decreases, except for CrSi.

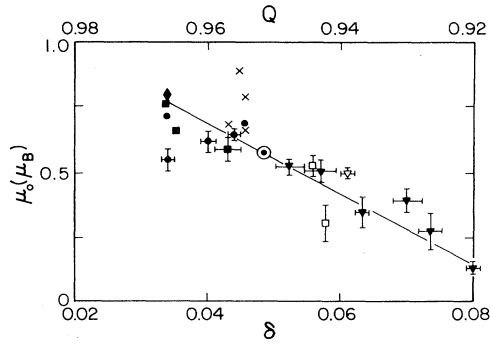

FIG. 8. The relation between the wave vector, $\mathbf{Q}=1-\delta$ (both in units of $a^*=2\pi/a$), and the amplitude μ_0 of the incommensurate SDW in chromium alloy systems: pure Cr (⊙); CrMn (■); CrV (▽); CrBe (□) at temperature 77 K; CrGe (●) (Booth *et al.*, 1983; Iida, Kawarazaki, and Kunitoni, 1981 at temperature 77 K); CrGa (×) (Booth *et al.*, 1983); CrSi (◇) (Costa *et al.*, 1980). The line is a guide to the eye (after Iida, Kawarazaki, and Kunitomi, 1981).

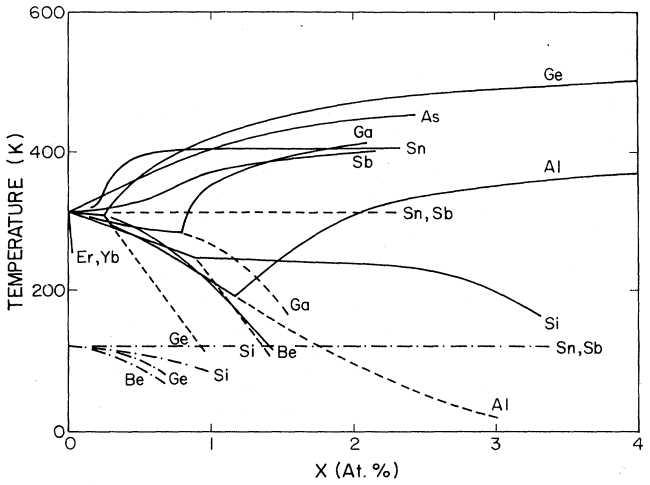

FIG. 9. Schematic phase diagrams for alloy systems $Cr_{1-x}A_x$ of chromium with nontransition metals. The Néel transition T_N, *I-C* transition T_{IC} between the AF_0 and AF_1 phases, and the spin-flip transition T_{SF} between the AF_1 and AF_2 phases are shown by solid, dashed, and dot-dashed curves, respectively. This figure has been developed from Fig. 6 of Iida, Kawarazaki, and Kunitomi (1981) by adding data for T_{IC} data for the CrAl and CrGa systems and by removing the T_{IC} data for CrSn and CrSb systems, about which there is some doubt, as discussed in Sec. II.C. It should be noted that the curve for CrAs is not given in Sec. II.C, since these data have not been published (see Ref. 9 of Iida, Kawarazaki, and Kunitomi, 1981).

The reason for this behavior is not understood. Experiments on proton channeling and propagation of induced x-ray emission in single crystals of CrAl and CrSi by Takahashi *et al.* (1980) show that the impurity atoms are substitutional and not interstitial, as previously suggested (Jayaraman *et al.*, 1976). In either case, the electronic state of the impurity atom is not known, and it is remarkable that elements of groups 3 and 4 produce such similar behavior.

None of the group 4, 5, and 6 transition metals give rise to a triple point when introduced into Cr; and with the depression of the Néel temperature by these metals, as seen in Table I and illustrated in Fig. 10, the prediction of the nesting Fermi-surface model, for decreasing electron concentration in a rigid-band picture, is qualitatively confirmed. By contrast, alloys of Cr with all the nonmagnetic transition metals of groups 7 and 8, with the sole exception of CrPd, exhibit a triple point. The Néel temperature T_{NI} to the incommensurate SDW phase slowly increases or, in the case of CrOs and CrPt, remains essentially constant, as seen in Table IV, up to the triple-point concentration, $x_L \simeq 0.1$ to 0.2 at. %. The Néel temperature T_{NC} to the commensurate SDW phase then rises rapidly for $x \gtrsim x_L$.

Thus the existence of a triple point and the sign of dT_{NI}/dx, in the nonmagnetic transition metals, are consistent qualitatively with the nesting Fermi-surface model in a rigid-band picture. There is, however, no quantitative correlation between the value of x_L, or the magnitude of the rates of change, dT_{NI}/dx and dT_{NC}/dx, of the Néel temperature with impurity concentration, and the electron concentration according to any systematic valence scheme (see Fig. 38).

The behavior of the Cr alloys with the magnetic metals is anomalous, in that CrNi does not have a triple point at all, while for CrFe and CrCo, dT_{NI}/dx is small and negative, dT_{NC}/dx is much smaller than for the alloys with nonmagnetic transition metals, and the triple-point concentration is about an order of magnitude larger, $x_L \simeq 2$ at. % (see Table IV).

The CrFe alloy system is unique in that the commensurate SDW phase AF_0 exists at low temperature for $x \lesssim x_L$, so that as temperature increases, a transition occurs from AF_0 to the incommensurate SDW phase

TABLE IV. Concentration dependence, near the triple-point temperature T_L and concentration x_L, of the Néel temperature of the transition from the paramagnetic phase to the incommensurate SDW phase (I), T_{NI}, and to the commensurate SDW phase (*C*), T_{NC}, and of the temperature T_{IC} of the incommensurate-commensurate SDW phase transition for chromium alloy systems $Cr_{1-x}A_x$.

Solute *A*	x_L (at. %)	T_L (K)	$\frac{dT_{NL}}{dx}$ (K/at. %)	$\frac{dT_{NC}}{dx}$ (K/at. %)	$\frac{dT_{IC}}{dx}$ (K/at. %)	Reference
Mn	0.3	325	50	350	−500	Fig. 12
Re	0.3	335	80	300	−300	Fig. 13
Fe	2.4	250	−40	0	10	Fig. 14
Co	1.3	280	−25	50	−5	a
Ru	0.16	330	80	800	−600	Fig. 15
Os	0.14	320	25	800	−400	a
Rh	0.11	320	50	800	−800	a
Ir	0.16	320	50	1200	−600	a
Pt	0.08	310	0	600	−350	a
Al	1.9	130	−300	300	−300	Fig. 16
Ga	0.6	280	−50	250	−80	a
Si	1.3	240	−30	10	10	Fig. 17
Ge	0.3	300	−20	350	−350	a

[a]Obtained from the phase diagram fit to the experimental data referenced in Sec. II.C, which is available on request from any of the authors.

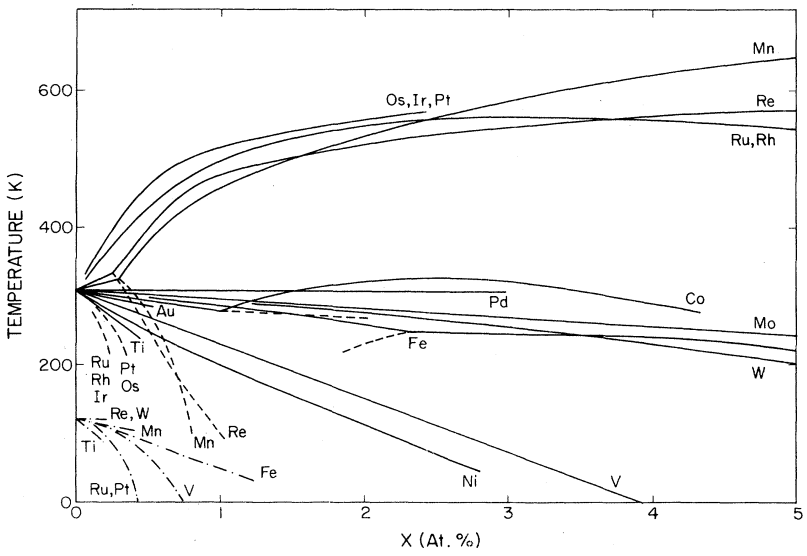

FIG. 10. Schematic phase diagrams for alloy systems $Cr_{1-x}A_x$ of chromium with transition metals. The systems CrTi, CrNb, CrTa, CrCo, CrOs, CrPd, and CrRh are not shown here. Some of these phase diagrams are plotted by Fawcett (1988a) with electron concentration per atom relative to Cr as abscissa, assuming the number of electrons per atom to correspond to the number of the group in the periodic table. This provides a better basis for comparison with the predictions of theoretical models, as, for example, in Figs. 5 and 51 of Fawcett (1988a).

AF_1, instead of the normal AF_1 to AF_0 phase transition. This contrast in the behavior of CrFe with all other Cr alloys is seen in Figs. 9 and 10, and the phase diagram for CrFe is shown in more detail in Fig. 14. We shall discuss the anomalous behavior of the CrFe alloy system and of ternary alloys based on CrFe in Sec. VI.B

C. Experiment: binary systems

In the case of Cr alloy systems for which the individual phase diagram is not given, reference to the literature is given in the relevant section with the physical property used to determine the phase transitions denoted according to the following rubric: C—specific heat; χ—magnetic susceptibility; ρ—electrical resistivity; **S**—thermopower; κ—thermal conductivity; β—thermal expansion; US—ultrasonic velocity and/or attenuation; ND—neutron diffraction; XRD—x-ray diffraction; TDPAC—time-differential perturbed angular correlation.

1. Cr alloys with group-4 transition metal Ti

The CrTi alloy system was used by Chiu *et al.* (1971) to study the temperature dependence of magnetic scattering around the Néel temperature and well into the paramagnetic phase, as described in Sec. IV.B and illustrated in Fig. 35. Both dT_N/dx and dT_{SF}/dx are about a factor 2 larger for $Cr_{1-x}Ti_x$ than for $Cr_{1-x}V_x$ alloys, in accordance with expectations for a rigid-band picture and the canonical model of nesting electron and hole Fermi surfaces (see Sec. II.A), with Ti differing in valence from Cr by two electrons per atom, as compared with a difference of one electron per atom for V.

2. Cr alloys with group-5 transition metals V, Nb, and Ta

The phase diagram of $Cr_{1-x}V_x$ is shown in Fig. 11. Arajs (1969—ρ) provides data for $Cr_{1-x}Nb_x$ and $Cr_{1-x}Ta_x$, and Butylenko and Gridnev (1964—ρ,β) also provide data for the latter.

V might be expected to be the ideal dopant to lower the electron concentration while otherwise causing the least perturbation to the pure Cr SDW. Both V and Cr are $3d$ transition metals, and they have roughly the same relatively high density of states. Being neighbors in the periodic table, they have about the same atomic mass, so that the effect of V doping on the phonon-dispersion relations should be minimal.

Thus V has been employed as a dopant, along with Mn, which for similar reasons is used to increase the elec-

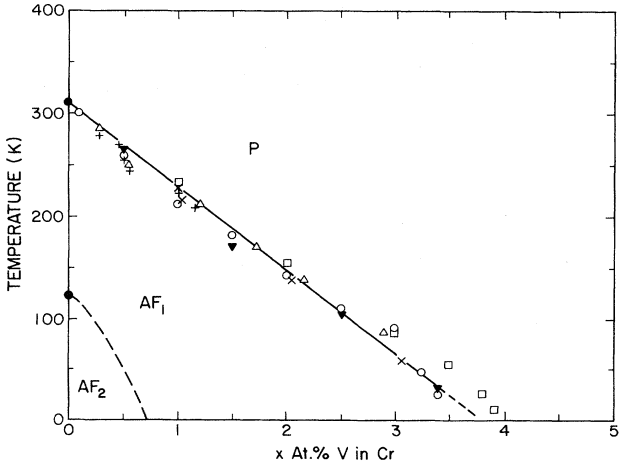

FIG. 11. Magnetic phase diagram of the $Cr_{1-x}V_x$ alloy system: △ (Barnes and Graham, 1965: NMR); + (Komura *et al.*, 1967a, 1967b: ND); — — — (Hamaguchi *et al.*, 1965: ND); ○ (Trego and Mackintosh, 1968: ρ); × (Arajs, 1969; ρ); □ (Takeuchi *et al.*, 1980: NMR); ▼ (White *et al*, 1986: β).

tron concentration, in several systematic studies of Cr alloy systems. These include, on a historical note, the first measurements by de Vries (1959), and other early work, with a review by Butylenko and Gridnev (1965), on the temperature dependence of the resistivity $\rho(T)$ in dilute Cr alloys and hence on the effect of the impurity on the Néel temperature identified by the anomaly in $\rho(T)$; the effect of changing the electron concentration, and hence the Fermi level, on the SDW wave vector and amplitude, and the Néel temperature, which served to confirm the essential features of the canonical model of nesting electron and hole octahedra, as described in Secs. II.A and II.B (see, for example, Machida and Fujita, 1984, Figs. 9, 10, and 11); the effect of tuning the Fermi level through impurity-state levels in Cr alloys (see Sec. IV.A.3 and, in particular, Fig. 30); the use of the paramagnetic alloy, Cr+5 at. % V, as a reference material, with which Cr and Cr alloys can be compared to determine the magnetic contributions to the thermal expansion and bulk modulus (see Sec. V.C and, in particular, Fig. 40); and the study of the phonon spectrum in Cr+10 at. % V (see Sec. VII.B).

It has become apparent, however, that V produces a strong effect on several physical properties around the Néel transition, and especially in the paramagnetic phase (Fawcett, 1992a). At low concentrations, where the effect of V in lowering the Néel temperature is still small, the V impurity appears to suppress spin fluctuations. We refer to Sec. IV.B and, in particular, to Fig. 22 and Table VI, which illustrate the remarkable effect of V doping in lowering the resistivity in the paramagnetic phase; to Figs. 2 and 3 in Fawcett (1992a) V.C.2, which show the effect on the magnetoelastic properties; and to Fig. 66 and Table XVI in Sec. VII.B, which illustrate the strong reduction in the inelastic neutron scattering in the paramagnetic phase close to the Néel transition. These effects are thought to be related to the existence of a moment on the V atom in dilute CrV alloys (see Sec. III).

There have been several studies of nuclear magnetic resonance in CrV alloys, as described in Sec. IX.D. Kontani and Masuda (1979, 1981, 1983) have measured the spin-lattice relaxation time and described its variation with V concentration in the paramagnetic phase by means of a theory of critical spin fluctuations.

When 0.5 at. % V is introduced into Cr, the hyperfine field, determined at room temperature by the Mössbauer effect in ^{119}Sn probe atoms (see Sec. IX.A), drops from the value 4 T in pure Cr to a value, $\mathbf{B} \lesssim 1$ T (Dubiel, 1988). This temperature is, however, about 20 K above the Néel transition of the Cr+0.5 at. % V sample (see Fig. 11); and Dubiel finds, remarkably, that further V doping reduces the hyperfine field only slightly, so that it still has the relatively large value, $\mathbf{B} \simeq 0.7$ T, at room temperature in a paramagnetic alloy containing more than 5 at. % V. Similar effects are seen in CrFe alloys, where $\mathbf{B} \gtrsim 1$ T in a sample containing 6 at. % Fe at room temperature, which is about 40 K above the Néel transition (see Fig. 14).

3. Cr alloys with group-6 transition metals Mo and W

Mo is the ideal dopant to reduce the strength of the exchange and correlation interactions responsible for establishing the SDW in Cr, since they are weaker in the 4*d* metal, because of the lower density of states, without change of the electron concentration. The same is true of W, which like Mo is isoelectronic with Cr; but the effects are stronger for W, since the 5*d* transition metals have a still lower density of states than the 4*d*. Furthermore, the atomic mass of W is nearly 4 times that of Cr, while that of Mo is only about twice as large, so that the effect of W on the lattice vibrations of Cr will be stronger.

The Néel temperature decreases linearly with x across the whole composition range in $Cr_{1-x}Mo_x$, with the AFM phase disappearing at $x \simeq 23$ at. % Mo [Heiniger *et al.* (1965)—ρ; Arajs (1968)—ρ; Schröder and Tomaschke (1968)—*S*; Trego and Mackintosh (1968)—*S* and ρ; Bender and Müller (1970)—χ; Meaden *et al.* (1970)—κ; Mitchell and Goff (1972)—ρ; Mamiya and Masuda (1976)—*C*; Ström-Olsen and Wilford (1980)—ρ; Venter *et al.* (1986)—US]. In $Cr_{1-x}W_x$, data are available only up to $x = 6$ at. % W [Butylenko and Gridnev 1964)—ρ,β; Arajs (1968)—ρ; Trego and Mackintosh (1968)—*S* and ρ; Bender and Müller (1970)—χ; Hedman *et al.* (1974, 1975)—χ].

The weakness of the effect of the Mo dopant on the SDW in Cr is evident from the small value of dT_N/dx, which is less than for any other transition metal and, in particular, about a factor 6 less than for V (see Table I). Mo (and also V) has been used as a dopant to make it possible, with the pressure available to the experimentalist, to suppress the SDW in Cr alloys and thus to determine the nature of the phase transition under pressure (see Sec. V.C.2 and Fig. 39). The temperature dependence of the resistivity in CrMo alloys, described in Sec. IV.B (see Fig. 24), was found to conform with a law of corresponding states. As the Mo concentration increases in CrMo alloys, there is a progressive decrease in the magnetic Grüneisen parameters around the Néel transition.

Mo has been used as a dopant in ternary alloys to study two interesting binary Cr alloy SDW systems. We see in Fig. 16 the remarkable effect that 5 at. % Mo has in suppressing the SDW in $Cr_{1-x}Al_x$ alloys in the range $2 < x < 5$ at. % Al, while Fig. 54 shows the effect of Mo on the phase diagram of the CrSi alloy system.

4. Cr alloys with group-7 transition metals Mn and Re

The phase diagrams of $Cr_{1-x}Mn_x$ and $Cr_{1-x}Re_x$ are shown in Figs. 12 and 13, respectively. Butylenko and Gridnev (1964—ρ,β) give additional data for CrRe. Sternlieb *et al.* (1994) find in CrMn that the spin-flip temperature T_{SF} decreases more slowly with Mn concentration x than shown in Fig. 12, with $T_{SF} = 87$ K for $x = 0.7$ at. %.

Mn and Re increase the electron concentration, which

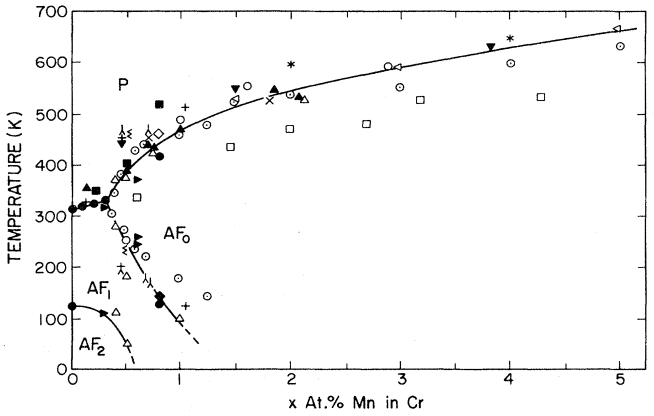

FIG. 12. Magnetic phase diagram of the $Cr_{1-x}Mn_x$ alloy system: + (Bastow, 1966: ND); □ (Suzuki, 1966: ρ); △ (Koehler *et al.*, 1966: ρ, ND); ⊙ (Butylenko and Nevdacha, 1980c; ρ); ■ (Ohno *et al.*, 1967: ρ); × (Jayaraman *et al.*, 1970: ρ); * (Iusan *et al.*, 1973: ND, XRD); ▼ (Fukamichi and Saito, 1974: β); ○ (Hausch *et al.*, 1976: β); ▷ (Kondorskii *et al.*, 1978: β); ◁ (Maki and Adachi, 1979: ρ, χ); ♦ (Peretto *et al.*, 1981: TDPAC); ⅄ (Geerken *et al.*, 1982; ρ, β, ND); Σ (Mizuki *et al.*, 1982: ND); ● (Yakhmi *et al.*, 1984: ρ).

brings the electron and hole octahedral Fermi surfaces closer in dimensions and thus moves the SDW system towards commensurability. The rate of increase of the Néel temperature T_N with concentration of the impurity is somewhat smaller in CrMn alloys than the rate of decrease in CrV alloys (see Table I and Fig. 43), because the depairing effect produced by scattering electrons at the impurity ion reduces T_N in both cases, as discussed in Sec. V.C.4 (see Eq. 85).

When, however, the $Cr_{1-x}Mn_x$ system reaches the triple point, at $x_L = 0.3$ at. % Mn, further increase of x gives a commensurate SDW, and T_N thereafter rises much more rapidly (compare dT_{NC}/dx with dT_{NI}/dx in Table IV). The same is true for CrRe, and this rapid increase of T_N beyond the triple point is in fact predicted by all the nesting models of the SDW in Cr alloys (see Figs. 1 to 4). We pointed out in Sec. II.B that there is, however, no discontinuity in the concentration dependence dT_N/dx of the Néel temperature at the triple point in any of these models.

This result is illustrated in Fig. 57(a), where Nakanishi and Kasuya (1977) adjust the parameters of their model to fit a triple point, $x_L = 0.35$ at. % Mn, $T_L = 370$ K, with values that are a little different from those observed, $x_L = 0.3$ at. % Mn, $T_L = 325$ K, as given in Table IV and Fig. 12. When we compare Fig. 57(a) with the observed phase diagram shown in Fig. 12, we see, however, that the AF_0-AF_1 line of phase transition can be fit quite well with a reservoir power, $\rho \simeq 1$. The three lines of phase transitions are tangential at the triple point only for infinite reservoir power, $\rho = \infty$, as seen also in Figs. 1(c) and 3.

Both CrMn and CrRe alloys exhibit a very pronounced resistivity maximum below the Néel temperature (see Fig. 23), with the magnitude of the hump, $(\Delta R/R_0)_{max}$, as defined in Eq. (15), being exceeded only in the CrFe alloy system (see Table VI). This maximum value of the hump occurs at a high value, $x \simeq 0.2$, in $Cr_{1-x}Mn_x$, and in fact this alloy system is antiferromagnetic across the whole phase diagram from pure Cr to Mn. The magnetic susceptibility of $Cr_{1-x}Mn_x$ alloys gives a Curie-Weiss law both below and above the Néel temperature (see Table V) for a wide range of compositions, above about $x = 0.1$ to 0.2, according to Maki and Adachi (1979), as discussed in Sec. III. Another manifestation of the magnetic character of Mn in $Cr_{1-x}Mn_x$ alloys, which occurs even at a concentration as low as $x \simeq 0.01$, is the low-temperature hump in the temperature dependence of the thermoelectric power due to magnon drag, as illustrated in Fig. 27.

CrRe alloys (as well as CrTi in Fig. 35 and CrOs in Fig. 36) are the prototypes providing evidence, in the temperature dependence of the resistivity, for spin fluctuations existing well above the Néel transition.

CrMn was employed as the prototype Cr alloy system to illustrate the connection between the opposite signs of the extrema, as seen in the temperature dependence of the thermal expansivity $\beta(T)$ in Fig. 45, at the Néel transition T_N and at the incommensurate-commensurate SDW phase transition T_{IC}, and the opposite signs of the pressure dependence of the transition temperatures dT_N/dp and dT_{IC}/dp, as seen in Fig. 44. Similar behavior of $\beta(T)$ is seen, as listed in Table IX, in CrMn, CrRu (Fig. 43), CrPt, CrGa, CrSi, and CrGe (Fig. 55),

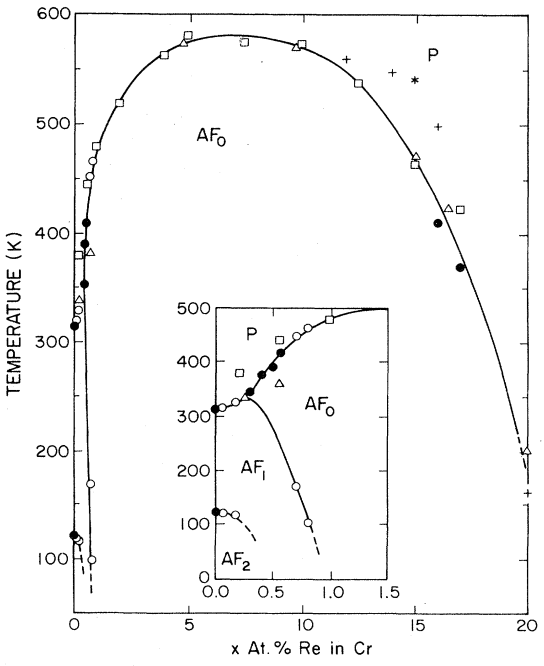

FIG. 13. Magnetic phase diagram of the $Cr_{1-x}Re_x$ alloy: * (Jayaraman *et al.*, 1970: ρ); ○ (Lebech and Mikke, 1972: ND); □ (Arajs *et al.*, 1976: ρ); △ (Kondorskii *et al.*, 1978: β); + (Nishihara *et al.*, 1985: ρ, χ, NMR); ● (Alberts, 1989: US).

TABLE V. Chromium alloy systems $Cr_{1-x}A_x$ classified according to whether or not they exhibit a Curie-Weiss (C-W) law for the temperature dependence of the magnetic susceptibility, corresponding to the formation of a local moment μ_A with a Curie-Weiss temperature θ.

Solute A	C-W law	Temperature range	x (at. %)	μ_A (μ_B)	θ (K)	Reference
Ti	no					a
V	yes	$T > T_N$	0.58	1.8	−10	b
			1.04	1.44	10	
			1.52	1.12	−3	
	no	$T < T_N$				b
	yes	$T > T_N$	0.2			c
			0.4			
	no	$T < T_N$				c
Mo	no					c
W	no					d
Mn	yes	all T	>20	~1.7	−150	e
		all T	2–16	see text		f
Re	see text					d,g
Fe	yes	$T > T_N$	2.3–5.7			h
	yes	$T < T_N$	2.3	2.8	−70	h
			3.0	2.8	−30	
			4.0	3.0	−20	
			4.7	3.2	0	
			5.7	3.3	30	
	yes	$T < T_N$	1.0	2.2	−20	k
			3.5	2.3	−10	
			4.7	2.3	0	
			6.0	3.0	10	
			9.0	4.2	60	
	yes	$T > T_N$	3.3	2.7	50	l
			3.7	2.7	50	
			4.5	2.8	80	
	yes	$T < T_N$	3.3	3.1	0	l
			3.7	3.2	−10	
			4.5	3.2	0	
	yes	$T > T_N$	1.2	2.4	−120	m
			2.2	2.4	−70	
			3.3	2.4	−25	
	yes	$T < T_N$	1.2	1.3	−40	m
			2.2	0.9	−15	
			3.3	1.1	−5	
Co	yes	$T > T_N$	1.0–5.1	2.9		h
	no	$T < T_N$				h
	yes	$T > T_N$	1.0	2.2	−20	n
			1.9	1.9	0	
			2.8	1.7	30	
			9.3	2.0	−90	
	no	$T < T_N$				n
	yes	$T > T_N$	0.4–10	2.2–3.5		p
	yes	$T > T_N$	1.7–6.2	2.9–3.6		q
Ni	no					b,n
Os	no					d,l
Rh	yes	$T > T_N$	>10	0.5		n
	no	$T < T_N$				n
Pd	no					r,s
Pt	no					t
Al	no					u,v
Si	see text					w
Ge	no					x

TABLE V. (*Continued*).

Solute *A*	*C-W* law	Temperature range	x (at. %)	μ_A (μ_B)	θ (K)	Reference
Yb	yes	$T > T_N$	0.11			y
	no	$T < T_N$				
Er	yes	$T > T_N$	0.4			y
	no	$T < T_N$				

[a]Chiu *et al.* (1971); see Fig. 11 in Landolt-Börnstein (1986).
[b]Kondorskii *et al.* (1979).
[c]de Camargo *et al.* (1993).
[d]Bender and Muller (1970). See Figs. 22 (Cr Mo), 23 (CrW), and 26 (CrRe) in Landolt-Börnstein (1986).
[e]Maki and Adachi (1979).
[f]Aidun *et al.* (1985).
[g]Arajs *et al.* (1976).
[h]Suzuki and Takaki (1964); Suzuki (1966).
[k]Ishikawa *et al.* (1965).
[l]Hedgcock *et al.* (1977).
[m]Friedel and Hedman (1978); Hedman *et al.* (1978).
[n]Booth (1966).
[p]Kondorskii, Kostina, Trubitsina, and L'vova (1983).
[q]Arajs *et al.* (1974).
[r]Abdul-Noor and Booth (1973).
[s]Yakhmi, Gopalakrishnan, Iyer, and Gupta (1985).
[t]Abdul-Noor and Booth (1975).
[u]Pop *et al.* (1981).
[v]Sousa *et al.* (1980).
[w]Dadarlat *et al.* (1980).
[x]Dadarlat *et al.* (1982).
[y]Giurgiu *et al.* (1981).

and we shall discuss in the appropriate sections the connection with the pressure data. We note in Fig. 43 and Table VII that, in $Cr_{1-x}Mn_x$, $|dT_{NC}/dp| \gg |dT_{NI}/dp|$; and this discontinuity in the pressure dependence of T_N at the triple point parallels the discontinuity in dT_N/dx (see Table IV).

The incommensurate-commensurate SDW phase transition in CrMn alloys is interesting in that it shows a large degree of hysteresis while being quite sharp in a sample of uniform composition (Geerken *et al.*, 1982). There is some evidence, based on hysteresis of the ultrasonic attenuation, that cooling a sample through this phase transition in a large magnetic field applied along a cube axis may result in a single-**Q** state in the incommensurate SDW phase (Fawcett, 1979). This method is analogous to field cooling through the Néel transition, which is used to produce a single-**Q** sample of pure Cr (Fawcett, 1988a; Fawcett, Muir, *et al.*, 1988). The only other case in a Cr alloy system where field cooling appeared to produce a predominantly single-**Q** state was in a sample, Cr+0.5 at. % V, with an applied magnetic field, $\mathbf{B}=12$ T, the evidence here being based on the resultant anisotropy of the ultrasonic attenuation (de Camargo *et al.*, 1990).

Inelastic neutron-scattering measurements were performed on CrMn alloys in the commensurate SDW phase in an effort to resolve the spin waves, as described by Fawcett (1988a, Table I). The most interesting feature of this work is, however, the unusual temperature dependence of the integrated intensity of the inelastic scattering below the Néel transition, which is quite different from that seen in other Cr alloy systems, as illustrated in Fig. 64. The interesting fact that a dilute CrRe alloy has a weak first-order transition to the incommensurate SDW phase like pure Cr, but unlike dilute CrV, is discussed in Sec. VI.A.

Both the local probes PAC (Sec. IX.C) and NMR (Sec. IX.D) have been used to study the microscopic properties of CrMn alloys. The existence of a zero-field spin echo of ^{185}Re and ^{187}Re in CrRe alloys in the range of concentrations where superconductivity appears (see Sec. VI.E) is related to the question of coexistence of the SDW and superconducting states.

5. Cr alloys with group-8 magnetic transition metals Fe, Co, and Ni

The phase diagrams for these systems are shown schematically in Fig. 10 and are quite different one from another. The simplest is CrNi [Booth (1966)—χ; Endoh *et al.* (1968)—β, ND; Schröder and Baum (1968)—ρ, S; Arajs (1970c)—ρ; Butylenko and Nevdacha (1993)—ρ], which does not develop a commensurate SDW phase like CrFe and CrCo. In $Cr_{1-x}Ni_x$, the Néel temperature T_N decreases rapidly with increasing x, the value of dT_N/dx

being twice as large as it is for CrV, as seen in Table I. This result is rather surprising, since one might expect a group-8 metal to *increase* T_N through increase in the electron concentration (see Sec. II.C.6), or perhaps to show an initial slow decrease similar to that seen in CrFe (Fig. 14) and CrCo due to impurity depairing by the magnetic ions (see Sec. II.A and especially Nakanisha and Kasuya, 1977). This feature, and the anomalous temperature dependence of the resistivity (Arajs, 1970c) and the thermoelectric power in the paramagnetic phase (Schröder and Baum, 1968), are discussed in Sec. IV.B.

The phase diagram for CrCo beyond the triple point, $x_L = 1.3$ at. % Co, is rather poorly determined, with a wide range of values for T_N determined through different physical properties [Arajs *et al.* (1967)—ρ; Endoh *et al.* (1968)—β, ND; Arajs *et al.* (1974)—χ; Hedgcock *et al.* (1977)—χ; Mikke and Jankowska (1978a)—ND; Butylenko and Nevdacha (1980a)—ρ; De Koning *et al.* (1980)—ρ; Katano *et al.* (1980)—ρ; Alberts and Lourens (1983)—US; Kondorskii, Kostina, and Trubitsina (1983a)—ρ].

The phase diagram of $Cr_{1-x}Fe_x$ is extraordinary in that the line of transitions from the incommensurate AF_I to the commensurate AF_0 phase corresponds to a positive value of dT_{IC}/dx, so that the AF_0 phase lies at *lower* temperatures than the AF_I phase, as seen in Fig. 14. There have been considerable efforts to understand this singular behavior, as discussed in Sec. II.A [see Fig. 4(a)] and in Sec. VI.B. The model of Nakanishi and Kasuya (1977) was the most successful, as illustrated in Fig. 57(b), but it relies upon a rather arbitrary magnetostrictive term, given in Eq. (86), to produce this unusual feature of the AF_I-AF_0 branch of the CrFe phase diagram.

Ternary alloys of Cr with 0.5 and 1.5 at. % Fe, doped with up to 1 at. % Mn, give a similar phase diagram close to the triple point, as shown in Fig. 59, but have the bizarre feature of a *re-entrant* AF_0 phase (Fawcett and Galkin, 1992, 1993). Only the CrSi alloy system seems to exhibit similar behavior, as we shall see in Sec. II.C.10.

The phase transition to the commensurate SDW phase in binary Cr alloys, from both the paramagnetic phase and from the incommensurate SDW phase, exhibits hysteresis (see, for example, the pressure-temperature phase diagram shown in Fig. 58), and the former has a remarkably large latent heat (see Table XV). There is also a very large change at the Néel transition to the AF_0 phase in the resistivity and in the thermoelectric power, as illustrated in Fig. 26.

Another remarkable feature, illustrated in Fig. 7, of the behavior of both the CrFe and CrSi systems is that commensurate SDW alloys have a much lower value of the Néel temperature T_N than is found in alloys with other metals having the same magnetic moment μ. One might suppose that in CrFe this follows from the depairing and the resultant depression of T_N associated with scattering at magnetic Fe ions, whose occurrence is demonstrated by the Curie-Weiss law, as seen in the magnetic susceptibility (see Figs. 18 and 19 and Table V). This does not, however, explain the low value of the T_N at the transition to the commensurate SDW phase in CrSi alloys, since in this case there is no sign of a magnetic moment in the form of a Curie-Weiss law at low temperatures.

Ternary alloys of CrFe with (V,Mn) and with Mo have been used to study the impurity resonance scattering seen in the residual resistivity, as shown in Fig. 30 and discussed in Sec. IV.B. Remarkable effects are seen in the temperature dependence (Fig. 31), in the magnetic-field dependence (Fig. 32), and in the pressure dependence (Fig. 33) of the resistivity of these ternary alloys, which are discussed in Sec. IV.A.3 and Sec. IV.B; these effects are believed to be manifestations of scattering at the local

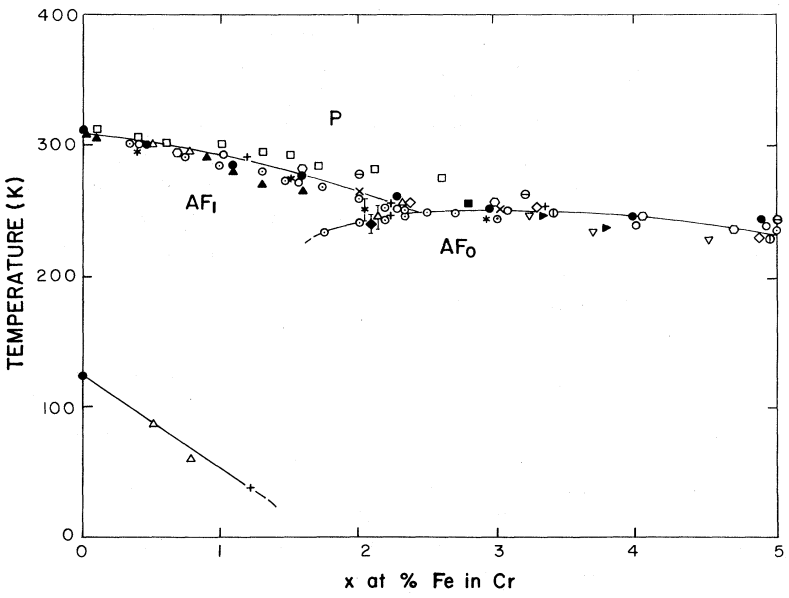

FIG. 14. Magnetic phase diagram of the $Cr_{1-x}Fe_x$ alloy system (for higher concentrations of Fe see Fig. 60): ○ (Suzuki, 1966: χ); ● (Ishikawa *et al.*, 1967: ND); △ (Arrott *et al.*, 1967: ND); ▲ (Arajs *et al.*, 1970: ρ); ⊕ (Arajs and Anderson, 1971: S); ⊖ (Fukamichi and Saito, 1972: β); ■ (Edwards and Fritz, 1973, 1974: US and Fawcett and Vettier, 1982: ND); ✱ (Mori *et al.*, 1976: XRD); ○ (Suzuki, 1976: C); ▶ (Hausch and Török, 1976: β, US); ▽ (Hedgcock *et al.*, 1977: ρ); × (Hedman *et al.*, 1978: χ); ◇ (Kemeny *et al.*, 1979: C); □ (Katano and Mori, 1979: ρ); ◆ (Mizuki *et al.*, 1982: ND); + (Benediktsson *et al.*, 1982: C and χ); ⊙ (Butylenko, 1989: β). The range of coexistence of the AF_0 and AF_I phases is shown for the ND and XRD data by bar lines (from Fawcett and Galkin, 1993).

Fe impurity states. The resistance minimum in binary CrFe alloys, illustrated in Fig. 29, is thought to be due to the same mechanism.

The magnetic properties of CrFe alloys have been studied extensively, both by means of bulk measurements of the magnetic susceptibility, as described in Sec. III (see Table V), and of the inelastic neutron scattering, to determine the spin dynamics in the spin-glass region (Sec. VI.D); and by the use of local probes, including the Mössbauer effect (Sec. IX.A) and diffuse neutron scattering (Sec. IX.B). The magnetic phase diagram shown in Fig. 60 demonstrates the complexity of the problem, with SDW, spin-glass, and ferromagnetic phases being present and, in some cases, coexisting. We must reluctantly conclude, however, that we are still unable to present a comprehensive picture that explains most of the experimental data. In the CrCo alloy system, the zero-field spin echo of ^{59}Co was employed by Kohara and Asayama (1975) to study clustering of the Co atoms (Sec. IX.D).

6. Cr alloys with group-8 nonmagnetic transition metals Ru, Os, Pd, Rh, Ir, and Pt

All these Cr alloy systems, with the exception of CrPd, have phase diagrams similar to those of CrMn and CrRe, as seen in Fig. 10. We have chosen $Cr_{1-x}Ru_x$ as the prototype, as illustrated in Fig. 15, because of the interest in the possibility of coexistence of the SDW with the superconducting state for $x \geq 18$ at. % Ru and because of the unusual magnetoelastic effects seen in dilute CrRu alloys (see Sec. V.C.6).

The commensurate SDW phase appears at a very small concentration of the impurity, $x_L \simeq 0.1$ to 0.3 at. %, and thereafter, for $x > x_L$, the Néel temperature T_N rises much more rapidly with increasing concentration than for $x < x_L$, i.e., $dT_{NC}/dx \gg dT_{NI}/dx$, as seen in Table IV. $T_N(x)$ reaches a plateau at a value between 550 and 650 K for x beyond about 3 to 5 at. % (see Fig. 10), and for those systems in which measurements have been extended sufficiently far, namely, CrRe (Fig. 13), CrRu (Fig. 15), and CrRh, the SDW does not disappear until x exceeds about 15 to 20 at. %. The small value of x_L was explained by Fishman and Liu (1992, 1993a), who realized that it is energetically favorable for the SDW to become commensurate well before the geometric nesting vector reaches the value $2\pi/a$. This also explains qualitatively why T_N continues to rise considerably for $x > x_L$ as the nesting continues to improve with increasing x (see Sec. II.A).

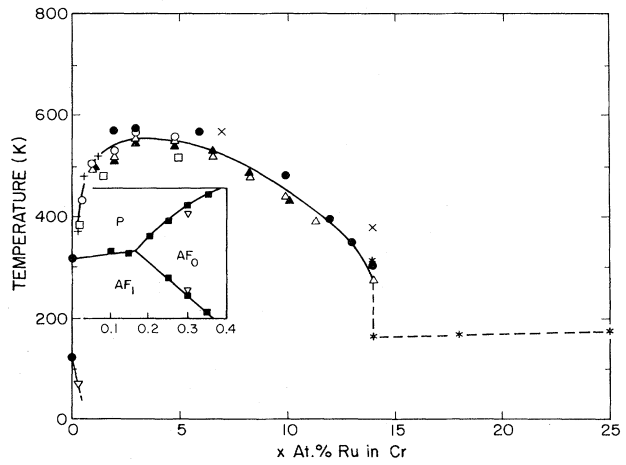

FIG. 15. Magnetic phase diagram of the $Cr_{1-x}Ru_x$ alloy system: ● (Booth, 1964: χ); + (Jayaraman *et al.*, 1970: ρ); × (Bender and Müller, 1970: χ); ○ (Arajs *et al.*, 1970c: ρ); △ (De Young *et al.*, 1973: ρ); △ (Arajs, Moyer, *et al.*, 1975: χ); ■ (Butylenko and Nevdacha, 1980a, 1980b: ρ); □ (Papoular *et al.*, 1981: ND); * (Nishihara *et al.*, 1986: ρ, C, χ); ▽ (Alberts and Boshoff, 1992: US).

References to the literature for Cr alloy systems with group 8 metals whose phase diagrams are not shown here are as follows:

CrOs: Booth (1964)—χ; Butylenko and Gridnev (1964)—ρ,β; Butylenko and Gridnev (1965)—ρ; Arajs *et al.* (1970)—ρ; Butylenko and Nevdacha (1980a, 1980b)—ρ; Hedman *et al.* (1981)—ρ, χ; Bender and Müller (1970)—χ.

CrPd: Abdul-Noor and Booth (1973)—ρ, χ, β; Fukamichi and Saito (1975a)—ρ, β; Moyer *et al.* (1980)—ρ; Butylenko and Nevdacha (1980a, 1980b)—ρ; Yakhmi *et al.* (1985a)—ρ.

CrRh: Booth (1964)—χ; Dadarlat *et al.* (1983)—χ; Butylenko and Nevdacha (1980a)—ρ.

CrIr: Butylenko and Gridnev (1965)—ρ; De Young *et al.* (1971)—ρ; Fukamichi and Saito (1975c)—χ, β; Butylenko and Nevdacha (1980a, 1980b)—ρ; Yakhmi *et al.* (1985b)—ρ.

CrPt: Abdul-Noor and Booth (1973)—ρ, χ, ND; Arajs, Rao, and Anderson (1975)—ρ; Fukamichi and Saito (1975a)—ρ; Booth *et al.* (1978)—ND; Butylenko and Nevdacha (1980a, 1980b)—ρ.

None of these Cr alloys exhibits unusual behavior of the magnetic susceptibility, with the exception perhaps of CrRh, which shows some sign of a Curie-Weiss law above the Néel temperature T_N (see Table V). The temperature dependence of the resistivity shows a maximum below T_N similar in magnitude to that seen in the Cr alloys with group-5 and -6 metals (see Table VI), which in Cr+0.5 at. % Ir was found to be very sensitive to doping with V (see Fig. 34).

Yakhmi, Gopalakrishnan, Iyer, and Gupta (1985) discuss, on the basis of their measurements of the temperature dependence of the resistivity and magnetic susceptibility, a number of features relating to SDW antiferromagnetism in CrPd (and CrMn) alloys, including the depairing effect of impurity scattering, the possibility of local-moment formation on impurities and their role as supplier of electrons to the conduction band, the nonrigid-band characteristics of CrPd alloys, and the exchange enhancement of electron-hole pairing.

The temperature dependence of the resistivity $\rho(T)$ at low temperatures has not been measured in most of these Cr alloys, so that in Table VI no resistance minimum is reported. CrPt shows remarkably strong scattering by the Pt ions, which gives a residual resistivity that is exceeded only in the CrNi alloy system. In the paramagnetic phase, both the resistivity and the thermal expansion exhibit a precursor of the Néel transition, as shown for $\rho(T)$ in CrOs in Fig. 36(a), over a temperature interval that exceeds 100 K around the triple-point composition. This type of behavior, which is also seen in CrRe alloys (Butylenko, 1985), may be an indication of critical fluctuations, as discussed in Sec. IV.B.

The magnetoelastic properties of these Cr alloys, again with the exception of CrPd, are generally similar, as may be seen by an inspection of Table IX and Fig. 47. The

TABLE VI. Characteristics of the dependence on temperature T of the resistivity R for chromium alloy systems $Cr_{1-x}A_x$. The expressions for the resistivity extrema are defined in Eqs. (15) and (40) for the maximum and the minimum, respectively. The ratio f of the impurity resistivity at high temperatures in the paramagnetic phase and at low temperatures is defined in Eq. (49).

Solute	Zero-T limit	Low-T resistivity minimum	$T<T_N$ resistivity maximum	$f=\frac{\delta R_P}{\delta R_0}$ ‡	Reference
A	$\frac{dR_0}{dx}$ (10^{-6} Ω m)	$\left[\frac{\Delta R}{R_0}\right]_{max}$ * [x at. %]	$\left[\frac{\Delta R}{R}\right]_{max}$ † [x at. %]		
Ti	2	no	0.2 [0.6]	0.5	a
V	0.4	0.07 [3.4]	0.2 [2.0]	−5	b
Nb	3	no	0.2 [1.1]	≲0	c
Ta	4	no	0.2 [0.6]	~0	c
Mo	0.4	0.05 [21]	0.3 [13]	≲1	b,d
W	0.8	no	0.25 [5]	~0	b
Mn	2	no	0.4 [20]	2.5	e,f,g
Re	0.6	no	0.6 [5]	~2 (N_2)	b,h
Fe	7	0.025 [0.6,1.86 GPa]	0.8 [5]	≲1	f,k,l
Co	8	0.04 [4,0.62 GPa]	0.2 [3]	~1	f,k,m
Ni	19	0.07 [1.7]	0.15 [0.8]	≲1	n
Ru	4		0.35 [5]	0.5	p,q
Os	3		0.25 [2]	≳1	p
Ir			0.4 [1.4]	≳1 (N_2)	r,s
Pd	5		0.15 [1]	~5 (N_2)	t,u
Pt	16	no	0.2 [1.6]	≲1	v
Au	13		0.15 [0.6]	≲1 (N_2)	w
Al	10	~0.01 [1.9]	0.04 [6]	≃1	x
Ga			0.07 [2.9]		y
Si	16	~0.01 [1.3]	0.2 [2.7]	≲1	z,A
Ge	13	~0.01 [1.1]	0.2 [2]	≳1	B,C
Sn			0.2 [1.2]		D
Sb			0.05 [1.9]		E

*Defined in (40).
†Defined in (44).
‡Defined in (49).
[a]Chiu *et al.* (1971).
[b]Trego and Mackintosh (1968).
[c]Arajs (1969).
[d]Ström-Olsen and Wilford (1980).
[e]Maki and Adahi (1979).
[f]Ohno *et al.* (1967).
[g]Suzuki (1966).
[h]Arajs, Moyer, and Abukay (1980).
[k]Katano and Mori (1980).
[l]Hedgcock *et al.* (1977).
[m]Katano *et al.* (1980).
[n]Arajs (1970c).
[p]Arajs *et al.* (1970).
[q]De Young *et al.* (1973).
[r]De Young *et al.* (1971).
[s]Yakhmi *et al.* (1983).
[t]Moyer *et al.* (1980).
[u]Yakhmi *et al.* (1985a).
[v]Arajs, Rao, and Anderson (1975).
[w]Eroglu *et al.* (1978).
[x]Arajs, Reeves, and Anderson (1971).
[y]Fukamichi (1979).
[z]Arajs and Katzenmeyer (1967b).
[A]Galkin and Tugushev (1991).
[B]Arajs and Katzenmeyer (1967a).
[C]Arajs, Aidun, and Moyer (1980).
[D]Fukamichi *et al.* (1973).
[E]Fukamichi (1978).

maximum in the temperature dependence of the thermal expansivity at the AF_1-AF_0 phase-transition temperature T_{IC}, seen in Figs. 45 and 48 for CrMn and CrRu alloys, respectively, corresponds to a positive value of the pressure dependence of T_{IC}, which is illustrated for CrMn in Figs. 43 and 44. The same effect is seen in CrPt, while the broadening of the minimum in the temperature dependence of the bulk modulus, seen in Fig. 47 for CrRe, CrRu, and CrRh alloys, serves only to show that there are two transitions without giving the signs to be expected for their pressure dependence [see Eq. (78b)].

7. Cr alloys with the group-1 nontransition metal Au

The only available data for the noble metals are those for CrAu reported by Eroglu *et al.* (1978—ρ) and by Alberts (1993—US). Their results are in strong disagreement, since Eroglu *et al.* found a linear temperature dependence of T_N at a rate $dT_N/dx = -32$ K/at. %, as shown in Fig. 10 and tabulated in Table I, whereas Alberts found T_N to be essentially independent of x up to $x = 1.5$ at. % Au. Alberts explained his negative result as being due to Au having a solubility limit of less than 0.1 at. % Au in Cr.

8. Cr alloys with the group-2 nontransition metal Be

$Cr_{1-x}Be_x$ differs from the other Cr alloy systems with nontransition metals in that, while the Néel temperature decreases with increasing impurity concentration x in all these systems (except for CrSb), as seen in Table I, the amplitude μ_0 and wave vector Q of the SDW decrease for CrBe, but both increase with increasing x for the other systems, as seen in Table II. This behavior clearly follows from the fact that CrBe is also unique among these alloy systems in not exhibiting a commensurate SDW phase, since Q (and with it μ_0) must increase as x increases towards the triple point. The phase diagram of CrBe was determined by Sano *et al.* (1981—ND, ρ).

9. Cr alloys with group-3 nontransition metals Al and Ga

The nature of the phase diagram in the $Cr_{1-x}Al_x$ alloy system has only recently been determined definitively (Baran *et al.*, 1992), though it has been studied a good deal. In Fig. 16 we see that there is reasonably good agreement between values of the Néel temperature obtained by different experimental techniques only for $x \lesssim 0.5$ and $x \gtrsim 3$ at. % Al. In the intermediate concentration range, where the triple point must be situated, there is considerable scatter in the experimental data, which may be due to dependence of the Néel transition upon sample quality near the triple-point composition.

We show in Fig. 16 two alternative interpretations of the experimental data. The solid lines correspond to the resistivity data of Alberts and Burger (1978), the neutron-diffraction data of Mizuki *et al.* (1982) and Baran *et al.* (1992), and the susceptibility data of Kuz'menko *et al.* (1986), with $x_L \simeq 1.9$ at. % Al, $T_L \simeq 130$ K. The dashed lines fit the resistivity and thermoelectric power data of Yakhmi *et al.* (1988; see also Yakhmi, Gopalakrishnan, and Iyer, 1987 and Yakhmi, Gopalakrishnan, Iyer, and Stanford, 1987) and the thermal-expansion and bulk modulus data of Alberts and Lourens (1984a), and correspond to a triple point, $x_L \simeq 1.0$ at. % Al, $T_L \simeq 150$ K.

Mizuki *et al.* (1982) found that their alloys having $x = 1.4$ and 1.9 at. % Al gave transitions to AF_1 and AF_0 phases, respectively, which would place the triple point between these limits; but Baran *et al.* (1992) found only the AF_1 phase in a Cr+1.9 at. % Al sample. The Cr+1.4 at. % Al sample has an anomalously low temperature dependence of the SDW wave vector (Fig. 8 of Mizuki *et al.*, 1982), which suggests that it is close to the triple point. Indirect evidence, however, from the temperature dependence of the resistivity for CrAl samples of different concentrations (Alberts, 1985) and from the

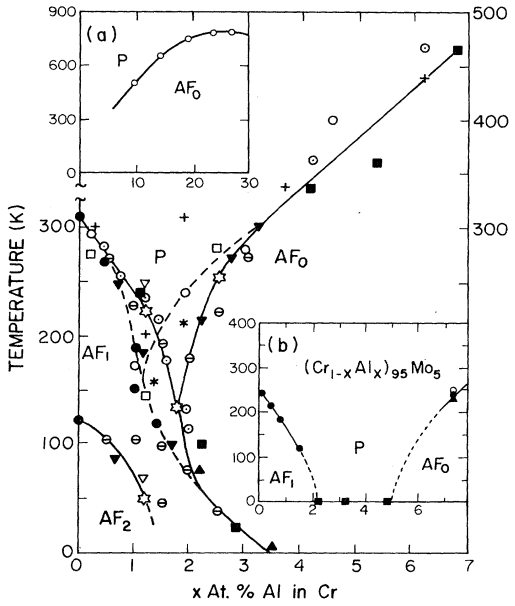

FIG. 16. Magnetic phase diagram of the $Cr_{1-x}Al_x$ alloy system: + (Arajs, Reeves, and Anderson, 1971: ρ); □ (Chakrabarti and Beck, 1971: ρ); ⊙ (Alberts and Burger, 1978: ρ); ▽ (Mikke and Jankowska, 1978b: ND); ■ (Sousa *et al.*, 1980: ρ, S, χ); * (Mizuki *et al.*, 1982: ND); ▼ (Alberts and Lourens, 1984a: US); ⊖ (Kuz'menko *et al.*, 1986: χ); ▲ (Alberts, 1985: ρ); ○ (Yakhmi, Gopalakrishnan, and Iyer, 1987; Yakhmi, Gopalakrishnan, Iyer, and Stanford, 1987: ρ); ● (Yakhmi *et al.*, 1988: S); ☆ (Baran *et al.*, 1992: ND, US). Inset (a) shows the phase diagram at higher concentrations of Al: ○ (Köster *et al.*, 1963: χ); —— (solid line, no data points, for samples containing x=4, 8, 10, 13, 15, 20, 24, and 32 at. % Al; Kallel and Bergevin, 1967: ND). Inset (b) shows the phase diagram for the ternary alloys system $(Cr_{1-x}Al_x)_{95}Mo_5$: ●, ρ; ■, no anomaly in $\rho(T)$ down to temperature T=4 K (after Smit and Alberts, 1987).

pressure dependence of the Néel temperature (Alberts and Burger, 1978; see the inset in Fig. 50) favors a triple point at $x_L \simeq 2$ at. % Al. The line of AF_1-AF_0 transition shown by the dashed line in Fig. 16 is based on data showing an anomaly in the temperature dependence of the susceptibility, but the much steeper solid line is suggested by the recent neutron-diffraction work of Baran *et al.* (1992).

The inset (b) in Fig. 16 shows the remarkable effect of diluting CrAl with 5 at. % Mo. In ternary samples $(Cr_{1-x}Al_x)_{95}Mo_5$, Smit and Alberts (1986) found that antiferromagnetism disappears in the range of concentrations $2 \lesssim x \lesssim 5$ at. % Al, while the Néel temperature is considerably depressed relative to the corresponding CrAl alloys for both the AF_1 and AF_0 phases. Further evidence for the absence of the SDW in this concentration range is provided by the concentration dependence of the residual resistivity $\rho_{\rm imp}(x)$, which only outside the range shows enhancement, in accordance with Eq. (19), due to the electron-hole condensation (Smit and Alberts, 1986). We shall see also in Sec. IV.B that the characteristic humps in the temperature dependence of both the resistance and the thermoelectric power, in the region below the Néel temperature, are absent in $Cr_{1-x}Al_x$ alloys for $x \simeq 2$ at. % Al, but not for lower and higher concentrations.

The behavior of the $Cr_{1-x}Al_x$ alloy system for higher concentrations of Al is quite remarkable. The early magnetic-susceptibility measurements of Köster *et al.* (1963) showing the Néel temperature T_N rising to about 800 K beyond $x > 20$ at. % Al, as illustrated in inset (a) of Fig. 16, were confirmed by neutron-diffraction experiments of Kallel and De Bergeven (1967), who found the same high value of T_N for $x = 33$ at. % Al (i.e., Cr_2Al). Chakrabarti and Beck (1971) found, however, that both the Hall coefficient and the resistivity were large for samples in the range of concentrations $15 \lesssim x \lesssim 25$ at. % Al, with the temperature dependence of the resistivity being negative and of a form characteristic of a narrow-gap semiconductor.

Low-temperature specific-heat measurements on ternary alloys $[Cr_{1-x}(V,Fe)_x]_{0.7}Al_{0.3}$ having concentrations ranging from $x = 0.7$ for V-doped $Cr_{0.7}Al_{0.3}$ to $x = 0.3$ for the Fe-doped alloys, when compared with similar studies on V-doped and Fe-doped samples of $Cr_{0.9}Al_{0.1}$ (Gupta *et al.*, 1962) and $Cr_{0.8}Al_{0.2}$ (Srinivasan and Claus, 1967), appear to conform this picture of an energy gap opening up around the latter composition. This is consistent with the low minimum in the Sommerfeld coefficient for binary $Cr_{1-x}Al_x$ alloys at $x = 20$ at. % Al (Pessall *et al.*, 1964).

Nakata and Kawarazaki (1983) measured the Sommerfeld coefficient γ of the linear term in the specific heat for ternary alloys $(Cr_{1-x}Mo_x)_{1-y}Al_y$ having $y = 5$ and 15 at. % Al, with Mo substituted for Al up to $x = 100$ at. % Mo. The extrapolation of $\gamma(x)$ back to $x = 0$, from the paramagnetic alloys at larger values of x, provides an estimate for the paramagnetic value γ_P in $Cr_{1-y}Al_y$. The measured value $\gamma_{\rm SDW}$ in the binary alloy (Pessall *et al.*, 1964) corresponds to the actual SDW phase. They found that $\gamma_{\rm SDW}(y)$ peaks around $y = 5$ at. % Al and thereafter, for $y \gtrsim 5$ at. % Al, decreases monotonically up to $y \gtrsim 20$ at. % Al, while $\gamma_P(y)$ continues to increase linearly with y up to $y \gtrsim 15$ at. % Al, where $\gamma_P \simeq 4\gamma_{\rm SDW}$.

This very small value of $\gamma_{\rm SDW}$ is consistent with the large value of T_N for $y \simeq 20$ at. % Al, but both are difficult to understand in terms of the canonical nesting model described in Sec. II.A. Akai and Kanamori (1985) propose a model in which Al acts as a vacancy in the Cr matrix and prevents electron transfer in the alloy. This results in narrowing of the d band, which enhances the density of states at the Fermi level and thus increases the Néel temperature.

The amplitude of the SDW in $Cr_{1-x}Al_x$ alloys, for $x > 15$ at. % Al, is larger than in any other Cr alloy system, having a value of about $1\mu_B$, as illustrated in Fig. 5(d). It had been suggested that this situation might arise from a stable configuration of the Cr atom, in which three electrons of t_{2g} symmetry have their spin oppositely polarized to two electrons of e_g symmetry. Costa and Brown (1977), to determine the form factors, performed careful x-ray and neutron powder diffraction experiments on six samples having $11 < x < 28$ at. % Al.

The x-ray scattering data showed that the electrons contributed by Al occupy states in these alloys in which their radial charge density is more $3s$- than $3d$-like, and having t_{2g} rather than e_g symmetry. On the other hand, the neutron-scattering data showed the opposite, with the symmetry of the spin density, although not far from spherical, becoming more e_g-like with increasing x.

It is not possible to reconcile these two results within a rigid-band model, so that the experiments appear to be inconclusive. Costa and Brown state that the increase in amplitude of the SDW is due to expansion of the Cr lattice when Al is introduced, which increases the exchange interaction. But, in fact, the lattice expansion determined by Kallel and De Bergevin (1967) in the range $10 < x < 25$ at. % Al gives a value $d\omega/dx = 0.3$, which is similar to that produced by other impurities that do not show the dramatic increase of the SDW amplitude seen in CrAl.

The composition-temperature phase diagram of CrGa [Kaneko *et al.* (1982)—ρ; Booth *et al.* (1983)—ρ; Alberts and Lourens (1984b)—ρ; Alberts and Lourens (1985)—β,US] appears to be straightforward, except that the triple point occurs at the composition, $x_L = 0.6$ at. % Ga, while the singularity in the magnetoelastic properties, evident in Fig. 52, occurs at about twice this concentration of Ga. Another anomalous feature of the magnetoelastic properties of CrGa alloys is that the maximum in the temperature dependence of the thermal expansivity, seen at the AF_1-AF_0 phase transition at temperature T_{IC}, is inconsistent according to Eq. (78) with the negative sign of the pressure dependence of T_{IC}, seen in Fig. 51. We shall discuss this inconsistency in Sec. V.C.7.

10. Cr alloys with group-4 nontransition metals Si, Ge, and Sn

The phase diagram of the CrSi alloy system, shown in Fig. 17, has the remarkable feature, unique in binary Cr alloys apart from the possibility of similar behavior in CrFe (Fawcett and Galkin, 1992, 1993), of a reentrant commensurate SDW phase. The evidence for this is indirect, but quite convincing: the temperature dependence $d\mathbf{Q}/dT$ of the SDW wave vector $\mathbf{Q}$ in the incommensurate SDW AF_1 phase changes sign at a temperature close to the AF_0 phase, as shown in the inset to Fig. 17. Alberts and Lourens (1988a) did a careful study of the phase diagram close to the triple point and found no evidence for such behavior; but this is not surprising, since the method they used for detecting the phase transitions through the anomalies in the magnetoelastic properties cannot resolve two transitions that are so close in temperature.

CrSi and CrFe are remarkable not only in having the commensurate SDW phase lying at lower temperatures than the incommensurate SDW phase close to the triple point $x < x_L$, but also in having a strongly first-order Néel transition at temperature T_{NC} to the commensurate SDW phase for $x > x_L$ (Sec. VI and Table XV). The magnetic susceptibility has a strong first-order transition at T_{NC} (Hedman *et al.*, 1973), in contrast to the continuous transition seen at T_{NI} in pure Cr (Fawcett, 1988a).

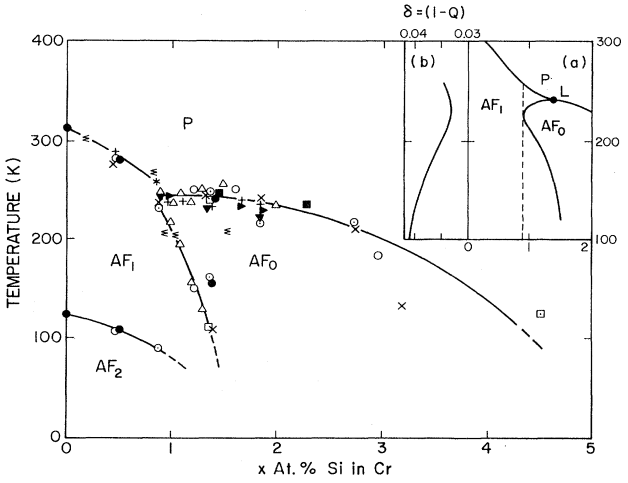

FIG. 17. Magnetic phase diagram of the $Cr_{1-x}Si_x$ alloy system: × (Arajs and Katzenmeyer, 1967: ρ; Arajs, Anderson and Ebert, 1971: S); □ (Hedman *et al.*, 1973: χ); ■ (Fukamichi and Saito, 1975b: ρ, β); ▼ (Jayaraman *et al.*, 1976: ρ); ⊙ (Cable, 1977: ND); △ (Suzuki, 1977: β); ▷ (Åstrom *et al.*, 1977: C); Σ (Dadarlat *et al.*, 1980: χ); ⊡ (Costa *et al.*, 1980: ND); ● (Endoh *et al.*, 1982: ND); + (Benediktsson *et al.*, 1982: χ, C); * (Mizuki *et al.*, 1986: ND); ○ (Anderson *et al.*, 1993: B, β). The insets show (a) the phase diagram around the triple point, with a re-entrant commensurate SDW phase, and (b) the variation of the SDW wave vector $\mathbf{Q}$ along the dashed line corresponding to changing temperature for a sample, Cr+0.85 at. % Si (from Fawcett and Galkin, 1993).

There is similar evidence for a reentrant AF_0 phase in the pressure-temperature phase diagram of a CrSi alloy, as shown in Fig. 53. The two phases $AF_1(L)$ and $AF_1(H)$ are so labeled because of the different sign of $d\mathbf{Q}/dT$ in these regions of the AF_1 phase, as shown in the inset to Fig. 53. The behavior under pressure is complicated by the occurrence of regions where the AF_1 and AF_0 phases coexist.

The phase diagram for CrGe [Suzuki (1978)—β; Arajs, Aidun, and Moyer (1980)—ρ; Iida, Kawarazaki, and Kunitomi (1981)—β, ND; Dadarlat *et al.* (1982)—χ; Booth *et al.* (1983)—ND; van Rijn and Alberts (1986a, 1986b)—ρ], by contrast, is quite normal, and Fig. 55 shows how CrGe is the prototype to illustrate the parallelism generally seen between the composition-temperature and the pressure-temperature phase diagrams. The quite different nature of the CrSi and CrGe alloy systems is also apparent in the strongly first-order character of the Néel transition to the commensurate SDW phase in CrSi (see Table XV), in contrast to the continuous phase transition in CrGe (compare Fig. 3 of van Rijn *et al.*, 1987 with Fig. 1 of Alberts and Lourens, 1988a). We shall discuss the phase diagram of CrSn alloys [Fukamichi and Saito (1972); Fukamichi *et al.* (1973)—ρ, β; Suzuki (1979)—β; Okpalugo *et al.* (1985)—ND] in Sec. II.C.11.

The transport properties of CrSi alloys are anomalous in that the temperature dependence of the Lorenz ratio has a large broad maximum around 60 K, as seen in Fig. 37. The residual resistivity in dilute Cr alloys with the nontransition metals is larger than with most of the transition metals, as seen in Table VI. This result, together with the fact that a low-temperature resistance minimum is seen in CrAl alloys as well as in CrSi and CrGe (see Table VI), may indicate that local impurity states occur in all cases.

This expectation is confirmed for the CrSi alloy system by the observation of peaks, characteristic of impurity-resonance scattering (see Fig. 30), in the temperature dependence of the residual resistivity of ternary alloys of CrSi with (V,Mn), as the Fermi level is tuned by changing the concentrations of V and Mn (Galkin, 1987; Galkin and Fawcett, 1992a), which is in accordance with theory, as discussed in Sec. IV.A.3. Further data on the temperature dependence of the resistivity and thermal expansivity of CrSi (V,Mn) alloys (Galkin *et al.*, 1991; Galkin and Fawcett, 1993) are interpreted in terms of the model of local impurity states by Galkin and Fawcett (1994, unpublished).

Despite this considerable success in understanding the phenomenology of the phase diagrams of Cr alloys with nontransition metals, and even the apparent microscopic understanding of these systems implied by the success of the impurity-state model in describing their properties, we do not in fact know the fundamental nature of their electronic structure. Jayaraman *et al.* (1976) suggested that Si might go interstitially into the Cr lattice, thus enabling it to act as an electron donor and leading to the

occurrence of a commensurate SDW phase, in accordance with the canonical model. Takehashi *et al.* (1980) demonstrated, however, that this is not the case, in experiments on proton channeling and propagation of induced x rays in single crystals of CrSi (and CrAl), which showed the impurity atoms to be substitutional. Münch *et al.* (1983) showed also, by means of an EXAFS study (see Sec. IX.E) in CrGe, that the isoelectronic impurity atom Ge goes into the Cr lattice substitutionally. Jayaranman (1984) reviewed these experiments on the nature of the Si and Ge states in Cr alloys.

Arajs, Aidun, and Moyer (1980) have offered an intriguing explanation for the behavior of substitutional Ge (and Si) in the Cr lattice, that it behaves as if it were an electron donor. Their idea furthermore implies the existence of a virtual impurity level, close to and above the Fermi level, which may correspond to the model of local impurity states that has been so successful in describing the properties of CrSi alloys, as described above.

The scattering potential of Ge in the Cr lattice is repulsive, corresponding to two electronic charges, which according to the Friedel sum rule is screened by two holes from the Cr conduction band. If, however, the scattering potential were strong enough to introduce a virtual level above the Fermi energy, or even to split off a bound state from the top of the band, there would be an excess screening hole density, which would cause the Fermi level to rise, as if electrons were being donated by the Ge atom. Since the triple point in the CrGe alloy system occurs at the composition, $x_L = 0.3$ at. % Ge, while the value of x_L is much larger in CrSi, $x_L = 1.4$ at. % Si (see Table IV), Arajs *et al.* predict that the virtual level in CrGe will be shifted further from the Fermi level than in CrSi. This prediction could be verified by measuring the peaks in the residual resistivity of ternary CrGe(V,Mn) alloys as a function of V or Mn doping (see Fawcett and Galkin, 1991a, 1991b).

The phase diagram of CrSn is discussed in the next section.

11. Cr alloys with the group-5 nontransition metal Sb

The most remarkable feature of the phase diagrams of CrSn and CrSb [Fukamichi (1978)—ρ, β; Okpalugo *et al.* (1985)—ND] is their similarity, despite the difference in valence of Sn and Sb. This result clearly shows that the simple rigid-band model, which works reasonably well for Cr alloys with transition metals in neighboring groups, is not appropriate for Cr alloys with nontransition metals.

The essential constancy of the spin-flip temperature T_{SF} is unique to these two systems. This is not apparent in Table I, where we list the *initial* temperature dependence of T_{SF}; but the schematic magnetic phase diagrams, illustrated in Figs. 9 and 10, show that in no other case does T_{SF} remain about the same with solution of up to 3 to 5 at. % impurity in Cr.

12. Cr alloys with rare-earth metals

Giurgiu *et al.* (1981) found that the magnetic susceptibility χ of $Cr_{1-x}Yb_x$ and $Cr_{1-x}Er_x$ alloys becomes constant and independent of temperature T in the SDW phase down to about $T \simeq 120$ K for only a trace of the impurity $x \simeq 0.007$ at. % Yb or Er. The temperature-independent value in the SDW phase increases rapidly with the concentration x of Yb and Er at a rate $d\chi/dx = 2.5$ and 4.0×10^{-6} emu/(g at. %), respectively, which compares with the roughly constant value $\chi = 3.6 \times 10^{-6}$ emu/g in the paramagnetic phase of pure Cr between the Néel transition and a temperature $T \simeq 700$ K. In the paramagnetic phase, on the other hand, these alloys develop a temperature dependence of a Curie-Weiss nature as the impurity concentration increases (see Table V).

The Néel temperature T_N of these alloys also decreases rapidly with impurity concentration x down to a value $T_N \simeq 240$ K for $x \simeq 0.014$ at. % Yb or Er, but thereafter decreases only slowly. Butylenko *et al.* (1974) found that the anomaly in the temperature dependence of the resistivity $\rho(T)$ gives a Néel temperature T_N that increases slowly with the additions of Tb, Dy, Ho, and Lu up to a concentration $x \simeq 1$ at. %, but remains roughly constant with the addition of Y or La. Butylenko and Gridnev (1964) measured also the thermal expansion in CrLu and CrHf alloys.

The magnitude of the resistivity appears to *decrease* at a rate $d\rho/dx \simeq -1$ $\mu\Omega$ cm/at. % Y or La over the temperature range $200 < T < 373$ K as x increases up to about 1 at. % Y or La (Butylenko *et al.*, 1974, Figs. 2 and 3), which compares with the value $\rho \simeq 13$ $\mu\Omega$ cm, just above the Néel temperature in pure Cr. For higher concentrations, at a given temperature, $\rho(x)$ increases with x, as one expects for impurity scattering. Other light rare-earth impurities in the La period behave in similar fashion; but for alloys with the heavy rare earths, typified by Dy, the increase of $\rho(x)$ with x is monotonic (Butylenko, 1982, Fig. 4).

D. Experiment: ternary systems

The thermal expansivity below the Néel temperature T_N is strongly affected by the negative magnetic contribution, as we shall see in Sec. V, and this may result in a region of negative thermal expansivity below T_N. In ternary alloys there is evidently considerable scope for manipulating the behavior so as to obtain alloys having a low thermal expansivity over a wide temperature range around room temperature. This is called the invar characteristic, and sometimes such alloys are referred to as "invar alloys," though more correctly the term "invar" should be reserved for the $Fe_{64}Ni_{36}$ alloy, whose characteristic behavior was discovered by Guillaume (1897).

For technical applications, invar alloys based on Cr have the advantage over those based on FeNi that, being

antiferromagnetic, they are not vulnerable to ambient magnetic fields. Thus conventional ferromagnetic invar alloys expand or contract in a magnetic field due to the Joule effect, which in some applications vitiates their desirable property of low thermal expansivity.

There has accordingly been a good deal of work on ternary alloys based on Cr in an effort to optimize the thermal and mechanical properties for technical applications requiring an alloy of low thermal expansivity around room temperature. Fukamichi and Saito (1977) have reviewed this work, much of which they have performed with co-workers. We shall not, however, discuss these results, since they do not, nor were they intended to, throw much light on the fundamental physics of SDW Cr alloys.

In several cases ternary alloy systems have been studied to clarify the behavior of a binary alloy. Thus Mo is an atom which, being isoelectronic with Cr, does not change the electron concentration, but which slowly reduces the magnetic interactions as the concentration x of Mo in $Cr_{1-x}Mo_x$ increases, until antiferromagnetism vanishes when $x \simeq 23$ at. % Mo. Ström-Olsen *et al.* (1982) have therefore used Mo as a dopant to study the binary alloy system CrFe, while Smit and Alberts (1986, 1989, 1990) have used it to study CrAl and CrSi. We referred to this work in Sec. II.C in the subsections dealing with the phase diagrams of the binary alloy systems, CrFe, CrAl, and CrSi.

On the other hand, the atoms V and Mn, respectively, decrease and increase the electron concentration, and therefore move the Fermi level. Galkin and co-workers (1986 to 1992) have thus systematically studied the effect of moving the Fermi level through the energy levels of local impurity states associated with Fe and Si atoms in the binary alloys, CrFe and CrSi, by doping with V or Mn. This work is discussed in Sec. IV.B, since the most interesting effects are in the transport properties, but it is also referred to in Sec. II in the subsections for CrFe and CrSi. Other ternary systems are also discussed or referred to in the appropriate subsection of Sec. II.C dealing with the principal binary alloy.

III. MAGNETIC SUSCEPTIBILITY: LOCAL MOMENTS

The static magnetic susceptibility of an AFM system provides rather less information about its nature than in the case of a paramagnetic or ferromagnetic system. The response function to a staggered magnetic field having the same period as the AFM structure, on the other hand, plays the same role in an antiferromagnet as the static magnetic susceptibility in a ferromagnet. This can be measured in effect by neutron scattering, and by the method a good deal of information has been obtained about Cr alloy systems, as we shall see in Sec. VII.

The model of Fedders and Martin (1966), comprising nesting electron and hole spheres of the same radius k_F with a Fermi velocity v_F, gives the essential features of the anisotropy and temperature dependence of the susceptibility of an itinerant-electron SDW system. Above the Néel temperature T_N, the susceptibility is independent of temperature and has the Pauli value χ_0 given in Eq. (12). Below T_N, the components $\chi_\perp$ of the susceptibility tensor perpendicular to the polarization of the SDW (*not* the wave vector **Q**) decrease linearly with temperature,

$$\chi_\perp = \chi_0[1-2(1-T/T_N)] , \tag{11}$$

while along the polarization direction the susceptibility is unchanged,

$$\chi_\parallel = \chi_0 = \frac{\mu_B^2}{\pi^2}\frac{k_F^2}{\hbar v_F} . \tag{12}$$

Arajs, Moyer, *et al.* (1975) found in careful measurements of a series of polycrystalline CrRu alloys that, close to T_N, the temperature dependence of χ is quadratic, rather than linear as implied by Eq. (11). They examined more carefully the algebra of the Fedders and Martin calculation and found that the susceptibility indeed has a quadratic temperature dependence and is essentially isotropic,

$$\chi_\perp \simeq \chi_\parallel \simeq \chi_0\left[1+\frac{\pi^2}{3}\left[\frac{k_B T}{\hbar k_F v_F}\right]^2\right] , \tag{13}$$

whereas Moyer *et al.* found a strongly anisotropic susceptibility.

In a later paper, the same group (Kelly *et al.*, 1979) calculated the temperature dependence of the susceptibility for the canonical model. They found that, taking into account phonon and impurity scattering and allowing the band gap for perfect nesting to be a variable parameter, the theory contained enough parameters to give an excellent fit to the experimental data for CrRu (Arajs, Moyer, *et al.*, 1975) and CrRe (Arajs *et al.*, 1976) between the Néel temperature T_N and about $T_N/2$.

The susceptibility χ becomes more important in those Cr alloy systems in which the impurities form local moments in some temperature range. According to the criterion that the alloy obey a Curie-Weiss law for the temperature dependence of the susceptibility

$$\chi = \frac{C}{T-\Theta}, \quad C = \frac{n_A \mu_A^2}{3k_B} , \tag{14}$$

four impurity atoms, V, Mn, Fe, and Co, carry local moments above the Néel temperature T_N. The Curie constant C in Eq. (14) gives the net moment μ_A per atom listed in Table V, n_A being the number density of atoms A in the alloy $Cr_{1-x}A_x$.

In the case of the impurity atoms, Re, Rh, and Si, there may be some evidence for local moments above T_N in that, for concentrations high enough to be well into the commensurate SDW phase, there are some alloy compositions for which the susceptibility decreases with increasing temperature above T_N. We shall discuss in Sec. IV.A the picture of spin-polarized local states or lo-

cal SDW associated with impurities, that are believed to occur above T_N as well as in the ordered phase. As we shall see, however, the contribution of these states to the susceptibility in the paramagnetic phase is much less well understood than is the effect of local impurity states on the transport properties at low temperatures.

In only one case of all the Cr alloy SDW systems studied, that of CrFe, does the local moment persist into the SDW phase in samples having a low concentration of impurities (Newman and Stevens, 1959). The reciprocal of the susceptibility is roughly linear in temperature below the Néel temperature for concentrations in $Cr_{1-x}Fe_x$ up to at least the composition $x = 9$ at. % Fe, as shown in Fig. 18. The corresponding local moments μ_{Fe} and Curie-Weiss temperatures are listed in Table V. There is some quantitative variation in the results of different workers, but the general trend is for μ_{Fe} to increase with increasing concentration x of Fe, while the Curie-Weiss temperature changes from negative values (antiferromagnetic coupling) to positive values (ferromagnetic coupling) at higher concentrations.

Above the Néel temperature the values of μ_{Fe} are somewhat smaller, according to Hedgcock *et al.* (1977, reference l in Table V), but not for other workers (references k and m). Thus their estimate of the exchange coupling constant for the interaction between the electrons on the nesting parts of the Fermi surface and the Fe moment is suspect, since it is based on the small increase in μ_{Fe} on passing through the Néel transition observed by Hedgcock *et al.*, but not evident in other work.

Friedel and Hedman (1978) have proposed that a single Fe atom is coupled to the SDW, while clusters of Fe atoms are effectively independent of the SDW because they interact so strongly with each other as to overpower their coupling to the SDW. This would explain the decrease in μ_{Fe} that they observe as the SDW phase is entered (references l,m in Table V), but a contrary result is seen in reference k. It is not, however, at all clear how this explains, as claimed, the fact that Fe decreases the Néel temperature while increasing the amplitude of the SDW (see Tables I and II). Attempts to measure superparamagnetic clusters in CrFe alloys by use of diffuse neutron scattering are discussed in Sec. IX.B.

The contrast between the behavior of Fe and the other two ferromagnetic metals Co and Ni, when introduced as an impurity in Cr, is shown clearly in Fig. 19. Ni has no magnetic moment, either in the paramagnetic phase or in the SDW phase, and the temperature dependence of the susceptibility $\chi(T)$ is similar to that of pure Cr, apart from the change in Néel temperature. Both Co and Fe impurities give $\chi(T)$ varying inversely as temperature in the paramagnetic phase. For Fe this inverse temperature dependence continues below the Néel temperature, while $\chi(T)$ decreases for CrCo with decreasing temperature like pure Cr. Similar behavior occurs in ternary alloys of CrCo and CrFe doped with V (Kondorskii *et al.*, 1981).

Shibatani (1971) and Moyer *et al.* (1979) have considered models for local moments interacting with a SDW host. Shibatani showed that it is possible to explain why the Néel temperature T_N decreases with concentration of magnetic impurity for both Fe and Co (see Fig. 10), while the amplitude μ_0 of the SDW remains essentially constant [see Fig. 5(b)]. The depairing effect due to spin and potential scattering acts in opposition to a pairing effect arising from the antiferromagnetic align-

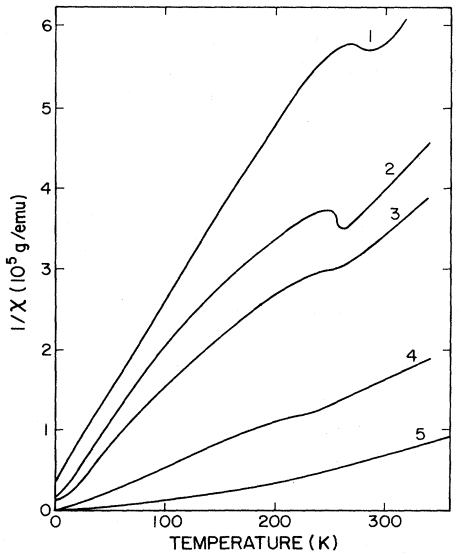

FIG. 18. Temperature dependence of the inverse magnetic susceptibility of $Cr_{1-\chi}Fe_\chi$ alloys for concentrations x in at. %: 1—1.0 (magnitude of $1/\chi$ reduced by a factor 4 to plot on the same scale as the other alloys); 2—3.5; 3—4.7; 4—6.0; 5—9.0 (after Ishikawa *et al.*, 1965).

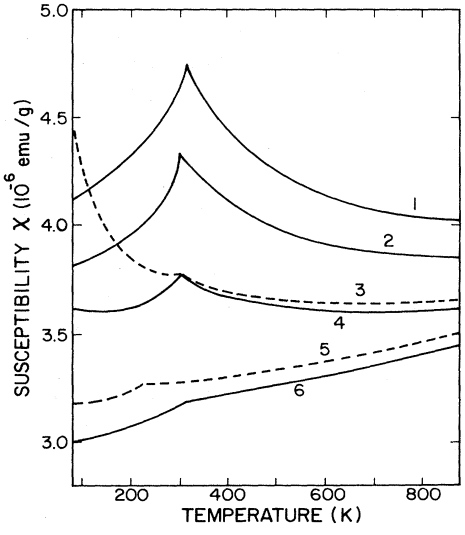

FIG. 19. Temperature dependence of the magnetic susceptibility over a wide temperature range of $Cr_{1-x}Co_x$ alloys in comparison with Cr+1.0 at. % Fe (curve 3) and Cr+1.0 at. % Ni (curve 5), which are shown by dashed lines, for concentrations x in at. %: 1—2.8; 2—1.9; 4—1.0; 6—00 (pure Cr) (Booth, 1966; see also Fig. 209 in Landolt-Börnstein, 1986).

ment of the impurity spins. Since those two effects give opposite temperature dependence, their combined operation may give rise to different behavior of T_N and μ_0. Under certain conditions the theory gives a decreasing T_N with constant μ_0 as the impurity concentration increases.

Moyer *et al.* (1979) extend the work of Shibatani (1971) and Crisan and Anghel (1976) by using an effective spin Hamiltonian. They show how the coupling of the moment on the impurity to the SDW host may be small, which gives rise to the Curie-Weiss law seen in the temperature dependence of the susceptibility in CrFe alloys. They are not able to explain, however, why CrCo, in which the temperature dependence of the susceptibility suggests that the moment is strongly coupled to the SDW, should be so different from CrFe.

The $Cr_{1-x}Mn_x$ alloy system is of particular interest, since Mn itself is an antiferromagnetic metal. As shown in Fig. 12, the Néel temperature T_N increases rapidly with x in the commensurate SDW phase and becomes roughly constant at a high value, $T_N \simeq 700$ K, for $x > 0.2$. Maki and Adachi (1979) found that for Mn concentrations, $0.2 \lesssim x \lesssim 0.6$, the susceptibility below T_N has a component obeying the Curie-Weiss law of Eq. (14), which for $x \gtrsim 0.4$ continues to decrease with increasing temperature above T_N according to roughly the same law. The effective moment is approximately constant, $\mu_{Mn} \simeq 1.5\mu_B$ per atom, while μ_{Mn} rapidly decreases with decreasing x below $x = 0.2$, and disappears for $x \lesssim 0.1$, where the susceptibility is only very weakly temperature dependent.

The analysis of Aidun *et al.* (1985) of their data for the temperature dependence between 300 and 500 K of the susceptibility of $Cr_{1-x}Mn_x$ alloys for $0.02 \leq x \leq 0.16$ gives quite different results, however. They find a component obeying a Curie-Weiss law over the whole of this range, with a very high value for the effective moment, $\mu_{Mn} \simeq 4\mu_B$. It would be desirable to resolve this question, perhaps by analyzing the data of Iusan *et al.* (1973), who measured a complete series of alloys from $x = 0.02$ to $x = 0.30$ at 0.02 intervals, over a very wide temperature range, from 100 to 950 K.

The most surprising occurrence of a moment in the paramagnetic phase is, however, that seen in dilute alloys of the CrV system. This was first observed by Kondorskii *et al.* (1979) and was confirmed recently by Hill *et al.* (1994), who found that the moment disappears abruptly at the Néel transition, giving rise to a sharp drop in the susceptibility as the temperature falls through T_N. The existence of the moment is no doubt related to the suppression of spin fluctuations and the strong effect of a small amount of V dissolved in Cr on several physical properties, as discussed in Sec. II.C.2. There seems, however, to be little effect on the value of the Néel temperature $T_N(x)$ itself, which is a linear function of x in $Cr_{1-x}V_x$ right across the phase diagram, as shown in Fig. 11, with no evidence of anomalous behavior for small values of x.

IV. TRANSPORT PROPERTIES: LOCAL IMPURITY STATES

The importance of transport properties to an understanding of Cr alloy SDW systems was firmly established by Trego and Mackintosh (1968) in an extensive series of measurements on alloys of Cr with V, Mn, Mo, W, and Re. They found an anomaly in the resistivity $R(T)$ that sets in below the Néel temperature T_N,

$$\frac{\Delta R}{R}(T) = \frac{R - R_P}{R} , \tag{15}$$

where $R_P(T)$ is a linear extrapolation into the SDW phase of the resistivity in the paramagnetic phase. This anomaly takes the form of a "hump" similar to that seen in pure Cr, whose magnitude typically increases initially in rough proportionality to the concentration of impurity, as we shall see in Sec. IV.B (Fig. 22).

This resistivity maximum, close to and below the Néel temperature T_N, is seen in all Cr alloy systems; its magnitude and the approximate concentration for which the maximum occurs are listed in Table VI. The initial increase in the resistivity as temperature decreases below T_N is undoubtedly due to the progressive opening up of the energy gap, which leaves less of the Fermi surface available for conduction. Trego and Mackintosh (1968, Fig. 10; or Fawcett, 1988a, Fig. 47) pointed to the strong anisotropy of the maximum in a single-**Q** sample of pure Cr to support this interpretation.

The rapid decrease of $\Delta R/R$ at lower temperatures, as seen for the alloy system CrRe in Fig. 23, which gives rise to the term "hump" to describe the anomaly, i.e., a true maximum in $\Delta R/R$, must, however, be due to the dependence on temperature of the other factor, the relaxation time, which determines the resistivity. This decrease in $\Delta R/R$ is related to the decrease at lower temperatures in density of final states at the Fermi surface to which electrons can be scattered, so that indirectly it, too, is due to the condensation of electrons and holes at the Fermi surface.

Trego and Mackintosh (1968) also measured, for the same five Cr alloy systems, the thermoelectric power S, which is a potent tool for exploring complex systems. In the case of the alloy system CrMn, they seem to have found clear evidence in the temperature dependence of S for a magnon drag contribution. Results for the other alloy systems and by later workers have, however, provided disappointingly little information.

A resistivity minimum at low temperatures was first observed by Arajs *et al.* (1967) in the alloy system $Cr_{1-x}Co_x$ for $x > 2.7$ at. % Co. The effect was attributed to the Kondo mechanism of exchange scattering of electrons by local moments and was studied in detail in both CrCo and CrFe alloys by Mori and co-workers (see Fig. 29). A resistivity minimum is, however, seen in many Cr alloy systems for which there is no reason whatever to expect a local moment on the impurity, and indeed for which there is no evidence for such a moment

in the temperature dependence of the susceptibility. Thus Table VI lists the following alloy systems as showing a resistivity minimum at low temperatures: $Cr_{1-x}A_x$ with A =V, Mo, Fe, Co, Ni, Al, Si, and Ge; whereas an inspection of Table V shows that only CrFe and CrMn exhibit a Curie-Weiss law in the SDW phase. The temperature dependence of the susceptibility suggests that there may be a moment in the paramagnetic phase in $Cr_{1-x}A_x$ with A =Co and Rh (and possibly Re and Si) as well as V, but this is irrelevant to behavior of the resistivity at low temperatures.

In dilute alloy systems with metals other than Cr as the host, the resistance minimum due to impurity atoms is always associated with a susceptibility that increases with decreasing temperature in a manner indicative of the occurrence of local moments (Sarachik *et al.*, 1964). We shall see that the absence of a local moment is only one of several pieces of evidence for believing that the resistivity minimum seen in many dilute antiferromagnetic chromium alloys is in fact not due to the Kondo effect. Even in the case of the $Cr_{1-x}Fe_x$ alloy system, where there is a local moment, the low-temperature resistivity minimum and other anomalous features of the temperature dependence of the resistivity are believed to be due to resonance scattering by local impurity states in the AFM energy gap (Volkov and Tugushev, 1984; Galkin, 1989), as we shall see in Secs. IV.A.3 and IV.B.

In pure Cr films the electrical noise increases by about two orders of magnitude as temperature decreases below the Néel temperature T_N (Michel *et al.*, 1993). This effect is attributed mainly to orientation fluctuations of polarization S domains, with some contribution also from Q domains close to T_N. The association of the noise with S domains is confirmed by the observation in CrMn films that its magnitude is much less in the commensurate SDW phase than in the incommensurate SDW phase (Michel *et al.*, 1993).

A. Theory

1. Electron-hole condensation

We consider first the increase in resistivity caused by condensation of electrons and holes in the nesting octahedra of the canonical model, if no account is taken of the change in relaxation time of the carriers. McWhan and Rice (1967) divide the conductivity into two components, σ_r and σ_n, where σ_r comes from the noncondensing reservoir and σ_n from the nesting parts of the Fermi surface that condense to form electron-hole pairs.

Thus σ_r is unaffected by the condensation, with $\sigma_r=\sigma_{rp}$ at all temperatures T, whereas the conductivity σ_n in the AFM phase is decreased relative to the conductivity σ_{np} at the same temperature extrapolated from the paramagnetic phase in the ratio

$$\frac{\sigma_n}{\sigma_{np}}=\int_{-\infty}^{+\infty}\frac{\Delta^2}{(E^2+\Delta^2)^{3/2}}\frac{dE}{\exp[(E^2+\Delta^2)^{1/2}/k_BT]+1}\ , \tag{16}$$

where $2\Delta(T)$ is the temperature-dependent energy gap. The resistivity anomaly defined in Eq. (15) then follows

$$\frac{\Delta R}{R}=g\frac{\sigma_{np}}{\sigma_p}\ , \tag{17a}$$

where

$$g=\frac{\sigma_{np}-\sigma_n}{\sigma_{np}}=1-\frac{\sigma_n}{\sigma_{np}} \tag{17b}$$

is the fraction of the nesting octahedra that condenses, and

$$\frac{\sigma_{np}}{\sigma_p}=\frac{\sigma_{np}}{\sigma_r+\sigma_{np}} \tag{17c}$$

is the fraction of the total Fermi surface in the octahedra.

The effect of temperature on the carrier scattering rate is obtained from the formal equation for the conductivity tensor

$$\sigma_{ij}=\frac{e^2}{4\pi^3\hbar}\int\tau v_i d\Sigma_j\ , \tag{18a}$$

where $d\Sigma_j$ is an element of Fermi surface transverse to the electric field, the integral in this case being over the part of the Fermi surface where the energy gap has not developed, and v_i is a component of the Fermi velocity; the reciprocal of the relaxation time τ is obtained by adding the relaxation rates due to different processes

$$\frac{1}{\tau}=\frac{1}{\tau_{\rm imp}}+\frac{1}{\tau_{\rm ph}}+\frac{1}{\tau_{ee}}+\frac{1}{\tau_{\rm mag}}\ . \tag{18b}$$

The relaxation rate due to impurities, $\nu_{\rm imp}=1/\tau_{\rm imp}$, might, as in Sec. II.A, be resolved into components corresponding to potential and exchange intraband scattering between the nesting octahedra or between different parts of the reservoir, and interband scattering between the octahedra and the reservoir. Because of the decreasing final density of states as condensation progresses with decreasing temperature, the relaxation rate of those processes involving scattering to the nesting octahedra will decrease with temperature, and the contribution to the resistivity will accordingly decrease.

The relaxation rate $\nu_{\rm ph}=1/\tau_{\rm ph}$ due to scattering by phonons at low temperatures might be expected to vary as T^5 with temperature T, corresponding to the Debye model. But if we include here also magnon scattering due to coherent magnetic excitations, perhaps a T^3 law is more appropriate, corresponding to magnon scattering with $\nu_{\rm mn}=1/\tau_{\rm mn}\sim T^3$, which is in fact the observed power law of the temperature dependence of the resistivity of pure Cr (Akiba and Mitsui, 1972). At higher temperatures, however, as the Néel temperature T_N is approached, the normal linear temperature dependence of

ν_{ph}, corresponding to the Bose statistics for the number of phonons and magnons, might be overwhelmed by a more rapid change as the condensed part of the Fermi surface decreases to zero at T_N and the final density of states increases to its normal value.

The relaxation rate $\nu_{ee}=1/\tau_{ee}$ is normally negligible, except perhaps at low temperatures in pure meals, where the T^2 variation of ν_{ee} with temperature T may be distinguished from the T^5 variation of ν_{ph}. However, in metals having a nesting Fermi surface, there is considerably larger scattering linear in T, according to Virosztek and Ruvalds (1990), who claim that this explains the linear variation of the resistivity over a wide temperature range observed in the normal phase of many high-temperature superconductors. This theory explains also the anomalous character of the frequency dependence of the optical conductivity (Ruvalds and Virosztek, 1991), which resembles that seen in pure Cr (Barker and Ditzenberger, 1970; Ruvalds *et al.*, 1992).

Finally, the relaxation rate $\nu_{mag}=1/\tau_{mag}$ due to spin fluctuations might be important in the region around T_N and also at high temperatures well above T_N in the paramagnetic phase. Moriya (1981) has discussed the contribution of spin fluctuations to the thermodynamic properties, but not the transport properties. We shall see in Sec. IV.B that spin fluctuations clearly contribute to the resistivity in the paramagnetic phase for CrTi (Fig. 35) and CrOs (Fig. 36).

The residual resistance R_{imp} due to scattering by impurities will also be affected by the condensation of parts of the Fermi surface. Takeuchi *et al.* (1980) adopt the simplest approximation that the contribution σ_r of the reservoir to the conductivity is negligible, so that in Eq. (17c), $\sigma_{np}/\sigma_p=1$. This gives an increase in the ratio

$$\frac{R_{imp}}{R^P_{imp}}=\frac{1}{1-g} \tag{19}$$

relative to the residual resistance R^P_{imp} with no condensation, g being the fraction of the nesting part of the Fermi surface that condenses, as defined in Eq. (17b) in terms of contributions to the conductivity.

2. Thermoelectric power

The thermoelectric power due to carrier diffusion is given by the energy derivative of the conductivity,

$$S_{dif}=\frac{\pi^2 k_B^2 T}{3e}\left[\frac{\partial \ln\sigma}{\partial E}\right]_{E_F} \tag{20a}$$

$$\simeq\frac{\pi^2 k_B^2 T}{3e}\left[\frac{\partial \ln\Sigma}{\partial E}+\frac{\partial \ln\langle l\rangle}{\partial E}\right]_{E_F}, \tag{20b}$$

where in Eq. (20b) we make the approximation that the conductivity is the product of the area Σ of the Fermi surface and $\langle l\rangle=\langle \tau v\rangle$, which is the average mean free path over Σ. In an AFM Cr alloy, Σ is the area of the Fermi surface that has not condensed, which might in some cases be very sensitive to energy E. In the temperature region of most interest below the Néel temperature T_N, where the hump in the resistivity is seen, the contribution of the second term may be large when electron-phonon scattering largely determines the mean free path $\langle l\rangle$.

Trego and Mackintosh (1968) discussed a model in which the energy gap 2Δ increases from a value much smaller than the characteristic energy E_{ph} of the phonons to a value $\Delta>E_{ph}$, and showed that $(d\tau_{ph}/dE)_{E_F}$ exhibits a maximum when $\Delta\simeq E_{ph}$. This should give a positive maximum in the temperature dependence of S. Identification of the maximum is suggested with that seen in the temperature region below T_N in nearly all dilute Cr alloys that have been studied, as in Cr itself. The first term in Eq. (20b) has also to be taken into account, however.

Anomalous behavior of the thermoelectric power might be expected at low temperatures due to magnon drag (Trego and Mackintosh, 1968; Blatt *et al.*, 1976). Since the magnon dispersion relations in a SDW system are predicted to be linear (see Sec. IV.A.2 of Fawcett, 1988a), as for phonons, the magnon drag term S_{mag} at low temperatures will have a T^3 law temperature dependence. Thus the total thermopower will be of the form

$$S=S_{dif}+S_{mag}=aT+bT^3\ . \tag{21}$$

At high temperatures S_{mag} might be expected to become negligible as phonon scattering becomes dominant, which would result in a low-temperature hump in the temperature dependence of S.

3. Local impurity states (low temperature)

In our consideration of the theory of local impurity states, we shall be concerned mostly with the electrical resistivity $R(T,H,\mu)$ of commensurate SDW systems, and with its dependence on temperature T, magnetic field **B**, and the position of the Fermi level μ. When we apply the theory to interpret experimental results in Sec. IV.B, we shall see that the Fermi level μ in an alloy $Cr_{1-x}A_x$ may be conveniently tuned by doping with V or Mn. In the resultant ternary alloy, it is found to be a good approximation in the cases of interest to neglect the scattering of electrons by the V or Mn impurities. It appears, too, that the application of pressure changes the Fermi level for reasons that are still not understood, as we shall see in Sec. V.

We follow the treatment of Tugushev (1992), which introduces the new and important concept of local impurity states within the energy gap (the forbidden band) of a commensurate SDW in an itinerant-electron antiferromagnet (Volkov and Tugushev, 1984). Resonant scattering of conduction electrons at these states may lead to greatly enhanced zero-temperature impurity scattering. Depending upon the position of the Fermi level relative to the impurity-state level, one may also see

an initial decrease in resistivity with increasing temperature, or in some cases in anomalously rapid increase. The low-temperature magnetoresistance may also be negative.

All these effects have been analyzed for the case of a commensurate SDW, but as we shall see in Sec. IV.B, in some cases there is experimental evidence also for local impurity states in alloys in which the SDW is incommensurate. Buzdin *et al.* (1986) have analyzed this case and have found that the impurity energy levels are spread over the entire energy gap. The tentative explanation for the observed behavior is that the density of energy levels across the energy gap may have structure, but no analysis exists to support this suggestion.

Other aspects of the behavior of Cr alloy SDW systems to which this theory is relevant include the dependence of the Néel temperature T_N on impurity concentration, and the temperature dependence of the resistivity close to and below T_N. The magnetic susceptibility of the SDW system may also be affected, since a magnetic moment is associated with a single impurity state. It turns out, however, that the moment is frozen in the SDW matrix, and an assembly of random impurities is similar to a spin glass at low temperature, with no net contribution to the susceptibility.

On the other hand, local impurity states may also form above the Néel temperature (Kostina *et al.*, 1985; Buzdin *et al.*, 1986). In this case there is no long-range order, and the resultant moments may lead to the susceptibility's varying inversely with temperature according to a Curie-Weiss law. It is convenient to discuss the theory of local impurity-state susceptibility here rather than in Sec. III, where the experimental evidence for the formation of local moments is discussed.

The impurity scattering Hamiltonian of Nakanishi and Kasuya (1977) given in Eq. (5) is the starting point of the theory of local impurity states in the most general case of a magnetic impurity with both Coulomb and exchange scattering. We shall, however, write down the equations only for the case of Coulomb scattering, since their structure is identical to that for a magnetic impurity, though the definition of the parameters g_α defined for the Coulomb case in Eqs. (22) will of course be different if there is also exchange scattering.

The parameters g_α are defined in terms of the matrix elements V_{ij} between the nesting electron and hole and the reservoir parts of the Fermi surface, for which the densities of states are $\rho_e=\rho_h$ and ρ_r, respectively,

$$g_0=2\pi V_0\rho_e, \quad V_0\equiv V_{ee}=V_{hh}=V_{eh}=V_{he} , \tag{22a}$$

$$g_1=\pi V_1\rho_r, \quad V_1\equiv V_{rr} , \tag{22b}$$

$$g_2=2\pi^2 V_2^2\rho_e\rho_r, \quad V_2\equiv V_{cr}=V_{hr} . \tag{22c}$$

The energy levels of the local impurity states are symmetric relative to the middle of the energy gap 2Δ, to which they are referred to as energy zero, and, in the case when $g_2=0$, are given by

$$E_{\uparrow\downarrow}=\pm\Delta\left[\frac{1-g_0^2}{1+g_0^2}\right] . \tag{23}$$

Equation (23) refers to the case in which the matrix element for scattering between the nesting electron and hole surfaces changes sign when the location $\mathbf{r}_0$ of the impurity moves from spin-up to spin-down antinode of the SDW with

$$V_{eh}=V_{he}^*=V_0\exp(i\mathbf{Q}\cdot\mathbf{r}_0) , \tag{24}$$

$\mathbf{Q}$ being the wave vector, which is parallel to $\mathbf{r}_0$ since the SDW is one dimensional.

The subscript arrows $\uparrow\downarrow$ for the energy levels in Eq. (23) refer to the complete spin polarization of these states. The spin-up arrow for the state of lower energy $E_\uparrow$ corresponds to the spin on the impurity atom being in phase with the SDW, while the spin-down arrow $E_\downarrow$ corresponds to the antiphase state. For another choice of the matrix elements, with no scattering between the electron and hole surfaces,

$$V_{eh}=V_{he}=0 , \tag{25}$$

the energy levels are also symmetric, with

$$E_\pm=\pm\Delta\left[\frac{4-g_0^2}{4+g_0^2}\right] . \tag{26}$$

The subscripts $\pm$ for E in Eq. (26), in contrast to Eq. (23), correspond to the fact that these levels are not spin polarized, with the number of impurity states for each level being twice that for the spin-polarized impurity states whose energy levels are given by Eq. (23).

The symmetric energy-level scheme described by Eq. (23) is shown in Fig. 20(a). For arbitrary choice of the matrix elements, the levels will be asymmetric relative to the midgap, as illustrated schematically in Fig. 20(b), and the local impurity states will be partially spin polarized.

In the approximation $g_2=0$, the energy levels described by Eqs. (23) and (26) have zero width. Level broadening occurs when the matrix elements V_2 for scattering between the nesting surfaces and the reservoir are nonzero. Since the wave function has *sp* symmetry while that of the reservoir has predominantly *d*-symmetry (see Fawcett, 1988a), it is reasonable to suppose that $V_2<V_e,V_1$; and since $\rho_e\sim\rho_h\sim\rho_r$, thus

$$g_0<g_1,g_2 . \tag{27}$$

In this approximation and for the case of Eq. (24), when scattering between the electron and hole surfaces occurs, Eq. (23) becomes

$$E_{\uparrow\downarrow}=\pm\Delta\left\{\left[\frac{1-g_0^2}{1+g_0^2}\right]+i\frac{4g_0g_2}{(1+g_0^2)^2(1+g_1^2)}\right\} . \tag{28}$$

The half-width of these energy levels

$$\gamma=\frac{4\Delta g_0g_2}{(1+g_0^2)^2(1+g_1^2)} , \tag{29}$$

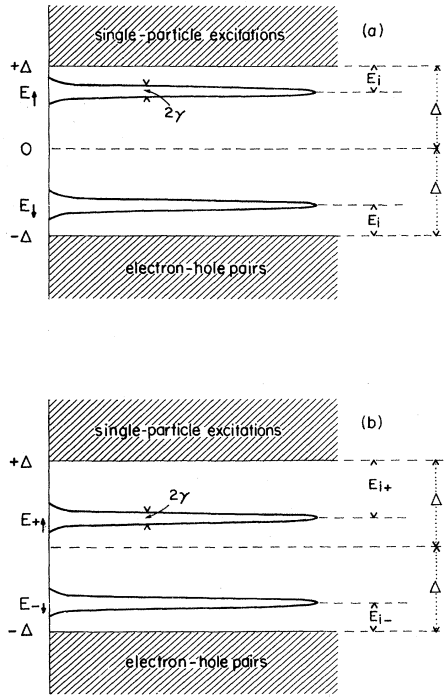

FIG. 20. Energy-level diagram showing the position of the local impurity states relative to the center of the energy gap between the single-particle excitations and the electron-hole pairs: (a) symmetric, corresponding to Eq. (23); (b) asymmetric, for arbitrary choice of the matrix elements V_{ij}.

which may be written relative to the real part of $E_\uparrow$

$$\frac{\gamma}{E_\uparrow}=\frac{4g_0g_2}{(1+g_0^2)(1-g_0^2)(1+g_2^2)} \tag{30}$$

or relative to the ionization energy of the impurity level (see Fig. 20)

$$E_i=\Delta-E_\uparrow\ , \tag{31}$$

gives

$$\frac{\gamma}{E_i}=\frac{2g_2}{g_0(1+g_0^2)(1+g_1^2)}\ . \tag{32}$$

The resonant scattering of reservoir electrons of energy E by the local impurity state is described by the complex scattering rate

$$\nu^*_{\rm res}(E)=\frac{1}{\pi\rho_r}\left[\frac{\gamma}{E-E_0+i\gamma}\right]\ , \tag{33}$$

where the energy level of the impurity state is $E_0=E_\uparrow$ or $E_\downarrow$. This gives a momentum relaxation time at temperature T,

$$\tau_{\rm res}=\frac{\pi\rho_r}{2}\left[1+\left[\frac{E_0-E_F}{\gamma}\right]^2+\frac{\pi^2k_B^2T^2}{3\gamma^2}\right]\ , \tag{34}$$

where E_F is the Fermi energy.

The electrical resistivity at low temperature, $k_BT\ll\gamma\ll k_BT_N$, is of the form

$$R(T)=R_0^0+R^0_{\rm res}+R_{\rm ph}(T)+R_{\rm res}(T)\ , \tag{35}$$

where R_0^0 is the residual resistivity at zero temperature due to nonresonant impurity scattering and $R_{\rm ph}(T)$ is due to scattering by phonons, which is of course a positive contribution. The new and interesting terms in Eq. (35) are those associated with impurity resonance scattering and include an additional contribution to the residual resistivity,

$$R^0_{\rm res}=\frac{bx}{1+\left[\dfrac{E_0-E_F}{\gamma}\right]^2};\quad b=\frac{2m^*}{\pi e^2\rho_r}\ , \tag{36}$$

and a negative temperature-dependent contribution

$$R_{\rm res}(T)=-\frac{axk_B^2T^2}{1+\left[\dfrac{E_0-E_F}{\gamma}\right]^2};\quad a=\frac{\pi^2b}{3\gamma^2}\ , \tag{37}$$

m^* being an average effective mass. As we shall see in Sec. IV.B, where we describe experiments to verify these equations, the resonant scattering contributions given in Eqs. (36) and (37) may be quite large relative to the normal resistivity, $R_0^0-R_0(T)$.

The other low-temperature effect predicted by the theory is the magnetoresistance for temperature, $T\ll T_N$. This may be calculated by substituting $E_F\rightarrow E_F\pm\mu_BB$ in Eq. (36), which gives

$$\frac{R(B)-R(0)}{R^0_{\rm res}}=\frac{\Delta R(B)}{R^0_{\rm res}}=-\frac{\pi\rho_r}{\gamma^2}(\mu_BB)^2\ . \tag{38}$$

This negative magnetoresistance is quite distinct in origin from that associated with the Kondo effect, which occurs as the spin-flip scattering by the local moment is frozen out at high magnetic fields. As temperature T increases, the size of the negative magnetoresistance may increase due to the decrease in the energy gap, in contrast to the model of Al'tshuler and Aronov (1979) for a nonmagnetic weakly disordered Fermi liquid, whose negative magnetoresistance falls monotonically as T increases.

4. Kondo effect

It is appropriate to discuss the predictions for the temperature dependence of the resistivity and the magnetoresistance in the case of a Kondo alloy having local moments with the Kondo temperature T_K in the temperature region of interest (Heeger, 1969). The Kondo resistance begins to increase as temperature decreases below T_K, due to spin-flip scattering, when there is an AFM coupling characterized by a negative exchange parameter J_{sd} between the conduction s electrons and the local-moment d electrons. The increase is logarithmic, with

$$R_K = xR_K^0[1+2J_{sd}N(E_F)\ln(T/T_K)] \; ; \tag{39}$$

but the Kondo resistivity eventually saturates, and the resistivity becomes independent of temperature, when the local moments become compensated at temperatures $T \ll T_K$.

When T_K is small enough that the Kondo resistivity dominates the temperature dependence, a resistivity minimum will necessarily occur as the resistivity begins to increase again at higher temperatures due to electron-phonon scattering. The characteristic power law, $R_{\rm ph} \sim T^5$, of the temperature dependence of this component of the resistivity at temperatures well below the Debye temperature results in a variation of the temperature $T_{\rm min}$ of the minimum varying as the 1/5 power of the impurity concentration, $T_{\rm min} \sim x^{1/5}$. If the power law of the temperature dependence of the resistivity were cubic, as appears to be the case in pure Cr (Ström-Olsen *et al.*, 1982), perhaps because the scattering is mainly by magnons well below the Debye temperature, the variation would be of the form $T_{\rm min} \sim x^{1/3}$.

In the case when the resistivity shows a minimum at low temperature, we define its maximum amplitude

$$\left[\frac{\Delta R}{R_0}\right]_{\rm max} = \frac{R_0 - R_{\rm min}}{R_0} \; , \tag{40}$$

where $R_{\rm min}$ is the value at the minimum. R_0 is the extrapolated resistivity at zero temperature, though in most cases the value at liquid-helium temperature is satisfactory. In the case when the minimum is due to scattering by local states, the residual resistivity is the sum of the two temperature-independent terms in Eq. (35) and

$$R_0 = R_0^0 + R_{\rm res}^0 \; . \tag{41}$$

Application of a magnetic field at temperatures below the resistivity minimum gives rise to a negative magnetoresistance, since the field suppresses the spin-flip scattering of the conduction electrons. Beal-Monod and Weiner (1968) give an equation, which Hedgcock *et al.* (1977) adapt for the case when g is the g factor of the local moment μ_A on the impurity and when $\mu_A B \ll k_B T$,

$$\Delta R_K(B) = R(B=0) - R(B) \simeq \frac{3\pi}{2E_F}\frac{m}{e^2 h} x\Omega J_{sd}^2 M^2 \left[\frac{4}{g^2} + \frac{\mu_B^2}{\mu_A^2}\right] , \tag{42}$$

Ω being the atomic volume of the host, and M the magnetization. The result expressed in Eq. (42) points out the fact that the Kondo effect is generally considered not to occur in a magnetically ordered metal, because the large exchange field suppresses the spin-flip scattering of the conduction electrons. We shall discuss this question in Sec. IV.B in relation to the observed resistivity minimum in the CrFe system, for which a local moment occurs in the SDW phase.

Volkov and Nunaparov (1980), in the first of the series of papers on local impurity states quoted by Tugushev (1992), emphasized that there is no net local moment, in contrast with the Anderson model, in which a spin moment appears on the impurity atom due to the exchange interaction of electrons on the inner shell. There is, however, a redistribution of spin density in the vicinity of the impurity. The electrons of down-spin (say) are repelled from a region around the impurity of radius

$$\xi \sim a\frac{W}{\Delta}\frac{1+g_0^2}{2g_0} \; , \tag{43}$$

where a is the lattice parameter and W is the width of the Cr $3d$ band. With rough estimates, $W \simeq 5$ eV, $2\Delta \simeq 0.16$ eV, and $g_0 \lesssim 1$, we get a large value, $\xi \simeq 100a$. This redistribution of the moment is frozen by the exchange field of the SDW at temperatures well below T_N, and spin-flip processes are strongly suppressed. As a result, a Curie-law susceptibility does not appear. The system is analogous to a frozen spin glass.

These and other features of the theory of local impurity states are on a less firm basis and appear not to be easily accessible as yet to experimental confirmation. Thus Eq. (43) was derived in an unpublished memorandum (see Ref. 10 of Volkov and Tugushev, 1984), while so far as experiment is concerned, a region of spin deficit as large as this would be extremely difficult to confirm by small-angle neutron scattering.

5. Local impurity states (high temperature)

The electron-hole condensation below the Néel transition causes an increase of the resistivity, which falls away again at lower temperatures, as discussed in Sec. IV.A.1, giving rise to a maximum in the resistivity. The maximum value of the resistivity anomaly given in Table VI is rather loosely defined as

$$\left[\frac{\Delta R}{R}\right]_{\rm max} = \left[\frac{R(T) - R_i(T)}{R_i(T)}\right]_{\rm max} . \tag{44}$$

In this equation, $R(T)$ is the resistivity of the AFM Cr alloy, while $R_i(T)$ is the ideal resistivity of a hypothetical nonmagnetic alloy of the same composition, which in this definition includes both phonon and nonmagnetic impurity scattering. In practice $(\Delta R/R)_{\rm max}$ is usually regarded as an experimental quantity, with $R_i(T)$ being estimated by extrapolation between the observed resistivity in the paramagnetic phase and at liquid-helium temperature.

The resistivity close to and below the Néel temperature, $T \lesssim T_N$, was predicted by Volkov and Tugushev (1984) to rise linearly with decreasing temperature T

$$\Delta R = R(T) - R(T_N) \sim x(T_N - T) \tag{45a}$$

because of resonant scattering by the local impurity state. This contrasts with a temperature variation of the form

$$\Delta R = R(T) - R(T_N) \sim [\Delta(T)]^{1/2} \sim (T_N - T)^{1/2} \; , \tag{45b}$$

which follows from Eq. (16), due to decrease of the Fermi-surface area as the electron and hole surfaces condense to form the SDW state. The latter effect causes a strong resistance anomaly below T_N in pure Cr (Fawcett, 1988a, Fig. 47) and presumably is responsible in part for the similar anomaly seen in most AFM Cr alloys. There is also evidence, however, for a contribution like Eq. (45a) from resonant scattering, as we shall see in Sec. IV.B, and, in particular, the size of the resistance anomaly is often observed to increase with the doping concentration x.

Another application of the theory of local impurity states proposed by Volkov and Tugushev (1984) is to explain the dependence of the Néel temperature $T_N(x)$ on the impurity concentration x. Depending upon the sign of $V_0 - V_1$, as defined in Eq. (22), and the position of the Fermi level relative to the midgap, $dT_N(x)/dx$ may be positive or negative. Since the matrix elements V_0 and V_1 are regarded as adjustable parameters, this might enable us to work out the systematics of their variation with the chemical nature of the impurity. One should, of course, also take into account the change in the relative size of the nesting electron and hole surfaces due to the valence difference between the solute and the Cr host.

Buzdin *et al.* (1986) have also considered the formation of a local impurity state in the case of an incommensurate SDW. If the location of the impurity atoms is random, the impurity levels will be spread right across the energy gap. This would presumably make the phenomena associated with resonant scattering at a single impurity level unobservable. In practice, however, the phase of the incommensurate SDW might adjust in response to the perturbation produced by the impurity atom, so that there would be some correlation between their location and the antinode of the SDW. We shall discuss this situation in Sec. IV.B in relation to the experimental results for an incommensurate SDW system which shows some evidence for resonant impurity scattering.

Finally, we shall consider the theory of local impurity states above the Néel temperature T_N, which was first discussed by Kostina *et al.* (1985) in relation to interesting experimental results obtained by Kondorskii *et al.* (1979) and recently confirmed by de Camargo *et al.* (1993) for the temperature dependence of the magnetic susceptibility of CrV alloys above T_N. This situation was analyzed thoroughly by Buzdin *et al.* (1986), and we show in Fig. 21 their phase diagram for the canonical model, which illustrates in the shaded regions above the bulk transition $t_N(h)$ the effect of local SDW states associated with single atom impurities. The line of transitions $t_L(h)$ to these local states is shown only schematically, since the parameters that determine the value of $t_L(h)$ are not known.

The distinction between the shaded regions I and II in Fig. 21 is that, in region I above the commensurate SDW, the amplitude of the local state wave function decreases exponentially away from the impurity atom,

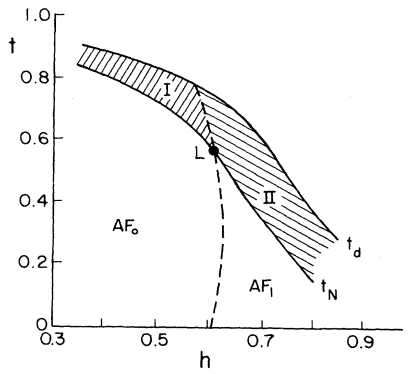

FIG. 21. Phase diagram for the canonical model for reservoir power $\rho=0$ with impurities, showing schematically the line of transitions $t_d(h)$ to local states (from Buzdin *et al.*, 1986).

whereas in region II the wave function varies periodically as it extends into the incommensurate SDW of the Cr matrix. The theory does not predict any specific physical effects at the local SDW transition, but it does predict a spin polarization giving a net magnetic moment associated with the impurity atom. The magnitude of the moment involves several unknown parameters, but its most interesting feature is an inverse temperature dependence [see Eq. (45) of Buzdin *et al.*, 1986]. This result was previously obtained by Kostina *et al.* (1985), and both papers conclude that this leads to a Curie-Weiss law for the temperature dependence of the susceptibility $\chi(T)$ in the temperature interval $T_N < T < T_L$.

We saw in Sec. III that several impurity atoms appear to carry local moments above the Néel transition, which give rise to a Curie-Weiss temperature dependence of the susceptibility. In the case of clearly nonmagnetic impurity atoms, in particular, V, it was claimed by Kostina *et al.* (1985) that this provides evidence for the local SDW state. Men'shov and Tugushev (1989) further claim that the temperature dependence of the nuclear-spin relaxation time above T_N in a CrV alloy (Kontani and Masuda, 1983) supports the theory, but the same behavior is seen also in pure Cr (see Fig. 86 of Fawcett, 1988a). It is also doubtful if CrCo alloys exhibit a local SDW state, since the Curie-Weiss law seen above T_N is probably due to an intrinsic moment on the Co atom, as discussed in Sec. III.

In summary, the theory of local impurity states is strongly supported by the low-temperature experiments, as we shall see in Sec. IV.B. The relevance of these states to the behavior at higher temperatures, both below and above the Néel transition, is not, however, at all clear.

B. Experiment

The resistivity anomaly seen in the CrV alloy system as temperature decreases below the Néel transition is illustrated in Fig. 22. The increasing magnitude of the anomaly in the relative resistivity difference with increasing

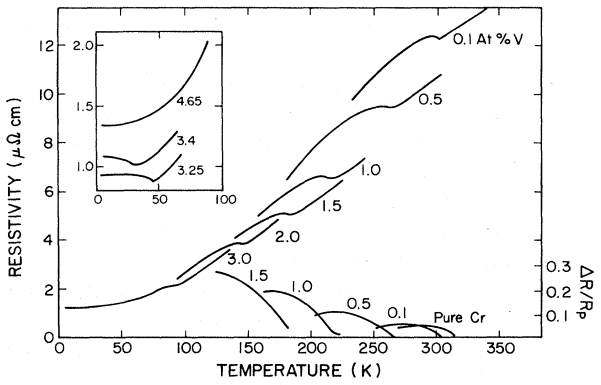

FIG. 22. Temperature dependence of the resistivity of $Cr_{1-x}V_x$ alloys, for compositions ranging from $x=0.1$ to 4.65 at. % V in Cr. The relative resistivity difference $\Delta R/R_P$ shown in the lower-right inset is defined differently from the formulation given in Eq. (15). From Moller *et al.* (1965).

impurity concentration, shown in the lower right of the figure, is typical. In CrRe, however, as illustrated in Fig. 23, the anomaly is, more accurately than in CrV, described as a "hump" at the higher concentrations, since the resistivity decreases rapidly at lower temperatures, giving a true maximum. This behavior is typical of Cr alloys with group-7 and -8 nonmagnetic metals, which all, with the exception of CrPd, show also a rapid increase of the Néel temperature in the commensurate SDW phase with increasing concentration x of the solute. In the case of CrMn, CrRe, CrOs, and CrPt, this extends well beyond the triple point, at $x \gtrsim 1$ at. %. Thus in these alloys, for the higher concentrations, the Néel temperature is well above the Debye temperature Θ_D, so that the rapid decrease in resistivity with decreasing temperature

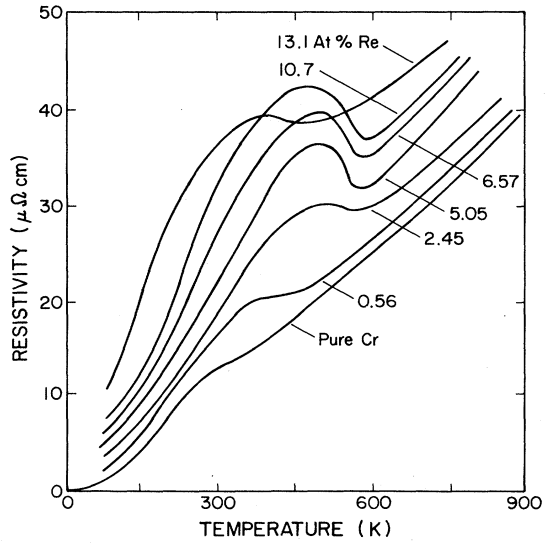

FIG. 23. Temperature dependence of the resistivity of $Cr_{1-x}Re_x$ alloys for compositions ranging from $x=0.56$ to 13.1 at. % Re, with data for pure Cr for comparison (from Arajs, Moyer, and Abukay, 1980).

below the maximum may simply be due to the rapidly decreasing phonon scattering below Θ_D.

The two prominent features of the temperature dependence of the resistivity of Cr alloy systems are best illustrated by two different systems. One of these prototypes is $Cr_{1-x}Mo_x$, whose SDW ordering, as manifested in the temperature dependence of the resistivity, obeys a law of corresponding states (Ström-Olsen and Wilford, 1980), the resistivity anomaly below the Néel transition being explained completely by considering the condensation of electron-hole pairs. This presumably is because Cr and Mo are isoelectronic, so that the nesting of the Fermi surface is not changed significantly in CrMo by changing the electron-to-atom ratio, as occurs, for example, in the CrV alloy system. We shall discuss CrMo alloys first, and consider later the prototypical system $Cr_{1-x}Fe_x$, and ternary alloys having a commensurate SDW such as $(Cr+2.7 \text{ at. \% } Fe)_{1-x}A_x$, with $A=V$ or Mn, which show a resistivity minimum at low temperatures.

The resistivity data for CrMo alloys are shown in Fig. 24. The observed increase in resistivity as temperature falls below the Néel transition can be related to the theoretical equation (16) for the conductivity by use of Eq. (17). Ström-Olsen and Wilford (1980) point out that Eq. (17) assumes that the ratio of the scattering on the nesting part of the Fermi surface to that on the reservoir is constant and independent of temperature in CrMo alloys, just as in pure Cr. This assumption is justified *a*

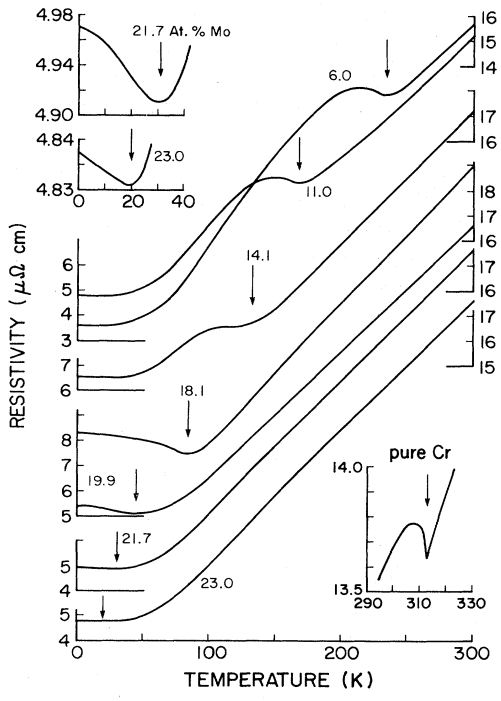

FIG. 24. Temperature dependence of the resistivity of $Cr_{1-x}Mo_x$ alloys for compositions ranging from $x=6.0$ to 23.0 at. %. The low-temperature region is shown enlarged for $x=21.7$ and 23.0 at. % to show the resistance minimum. The resistance around the Néel temperature in pure Cr is also shown for comparison (from Mamiya and Masuda, 1976).

posteriori by the success of the analysis. They use an estimate, $\sigma_{np}/\sigma_p = 0.3$, for the fraction of the total Fermi surface in the nesting octahedra, that seems arbitrary but makes no difference in any case to the qualitative result sought in the analysis.

The extrapolated resistivity R_P from the paramagnetic phase is found empirically to be of the form observed over the whole temperature range in the paramagnetic alloy $Cr_{70}Mo_{30}$,

$$R_P(T) = R_P^1 + A_1 T^3 \quad \text{for } T < T_x \,, \tag{46a}$$

$$R_P(T) = R_P^2 + A_2 T \quad \text{for } T > T_x \,, \tag{46b}$$

with a "crossover" temperature $T_x \simeq 90$ K given by the required continuity in dR_P/dT. The high-temperature form (46b) is evidently consistent with the data in Fig. 24, with roughly similar values of A_2, but different values of R_P^2, for the different alloys. Ström-Olsen and Wilford (1980, Fig. 3) give a plot of the low-temperature data that shows that in this case A_1 is the same for all the alloys, which means that the band structure and temperature-dependent scattering mechanisms are equivalent.

The result of this analysis is proportionality between the observed $(R - R_P)/R_P$ and the temperature dependence of $(1 - \sigma_n/\sigma_{np})$, when the same value $\Delta(0)/k_B T_N = 2.3$ is chosen for the alloys containing 2, 5.3, and 10.8 at. % Mo. For higher concentrations of Mo, the fit is unsatisfactory (Ström-Olsen and Wilford, 1980, Fig. 5). Thus a law of corresponding states describes the temperature dependence of the resistivity for pure Cr and $Cr_{1-x}Mo_x$ for x up to about 10 at. % Mo.

The anomaly in the temperature dependence of the thermoelectric power S of the CrV alloy system, illustrated in Fig. 25, is strikingly similar in form to that in the resistivity R seen in Fig. 22, as reported also by Giannuzzi *et al.* (1970). This is surprising in view of Eq. (20a), which suggests that S should vary as the negative of the logarithmic energy derivative of R. Trego and Mackintosh (1968) discuss the temperature dependence of S in terms of a simple model in which the dominant effect is the decrease in the scattering rate ν_{ph} of electrons by phonons with decreasing temperature due to condensation of the electron and hole surfaces. This practically cancels the increase in R with decreasing temperature due to the decrease in the Fermi-surface area Σ, but in the energy dependence of the two effects, which determines S, the $d \ln \nu_{ph}/dE$ term dominates the $d \ln \Sigma/dE$ term, giving a net positive contribution to S.

The parallelism between the temperature dependence of R and that of S is even more striking in the case of CrFe alloys, as illustrated in Fig. 26 (see also Arajs, 1970b). In this case the first-order Néel transition between the paramagnetic and commensurate SDW phase that sets in beyond the triple point, $x_L \simeq 2.4$ at. % Fe (see Fig. 14), gives a strong first-order singularity in both R and S. A similar effect is seen in the CrSi alloy system, where the first-order step in R, seen for $x > x_L \simeq 0.9$ at. % Si (see Fig. 17), is relatively small, with $\Delta R/R \simeq 10\%$ (Arajs and Katzenmeyer, 1967b); whereas

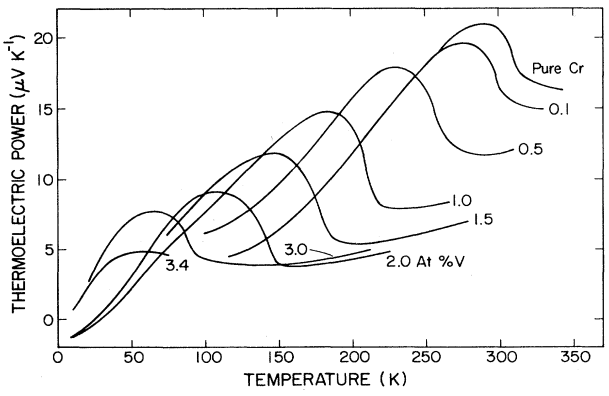

FIG. 25. Temperature dependence of the thermoelectric power of $Cr_{1-x}V_x$ alloys for compositions ranging from $x = 0.1$ to 3.4 at. % V, with data for pure Cr for comparison (from Trego and Mackintosh, 1968).

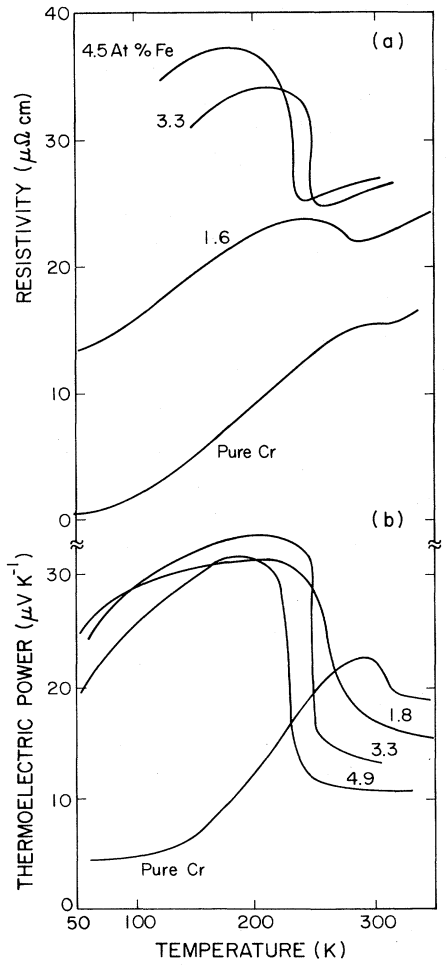

FIG. 26. Temperature dependence of (a) the resistivity and (b) the thermoelectric power of $Cr_{1-x}Fe_x$ alloys for compositions in the range $x = 1.6$–4.9 at. % Fe, with data for pure Cr for comparison (after Ohno *et al.*, 1967; Arajs and Anderson, 1971; and Hedgcock *et al.*, 1977).

the relative step in S is much larger than in R, and, in fact, S changes sign at T_N for $x \gtrsim 2$ at. % Si (Arajs, Anderson, and Ebert, 1971).

The interesting feature of the temperature dependence $S(T)$ of the thermopower of $Cr_{1-x}Mn_x$ alloys in Fig. 27 is the low-temperature hump, which shows a marked enhancement as x increases. Trego and Mackintosh (1968, Fig. 21) show that Eq. (21) satisfactorily describes their data, with the coefficient A of the T^3 term associated with magnon drag increasing rapidly with x as the moment $\langle\mu\rangle$ increases ($d\langle\mu\rangle/dx = 0.14\ \mu_B$/at. % Mn in Table II).

There is no such low-temperature hump in $S(T)$ for CrV alloys, as seen in Fig. 25, since $\langle\mu\rangle$ decreases with x ($d\langle\mu\rangle/dx = -0.12\ \mu_B$/at. % V in Table II). In CrMo, on the other hand, a negative low-temperature hump is seen in the temperature dependence $S(T)$ of the thermoelectric power in Fig. 28 for $x = 5.7$ at. % Mo, which decreases in magnitude for increasing x and disappears completely for $x = 20.8$ at. % Mo. Trego and Mackintosh (1968) attribute this anomaly to phonon drag, and its disappearance at higher concentrations of Mo to the decrease in phonon mean free path caused by scattering from this heavy impurity. Similar, but even more pronounced, negative low-temperature humps in $S(T)$ are seen in CrW alloys (Trego and Mackintosh, 1968, Fig. 6), which is consistent with this explanation, since W is heavier than Mo.

Trego and Mackintosh (1968) point out that V, having approximately the same mass as Cr, has very little effect as an impurity in Cr on the phonon drag, which is approximately the same in Cr+4.65 at. % V as in pure Cr. Unfortunately, no data for $S(T)$ of pure Cr below temperature $\simeq 75$ K (see Fig. 26) appear to have been published.

In $Cr_{1-x}Al_x$ alloys, both $R(T)$ (Arajs, Reeves, and Anderson, 1971) and $S(T)$ (Sousa *et al.*, 1981) show the characteristic hump below the Néel temperature for $x \leq 1.3$ at. % Al, but the hump in the temperature dependence of both resistivity and thermoelectric power disappears at $x \simeq 2$ at. % Al and reappears in both at higher concentrations. This behavior may have something to do

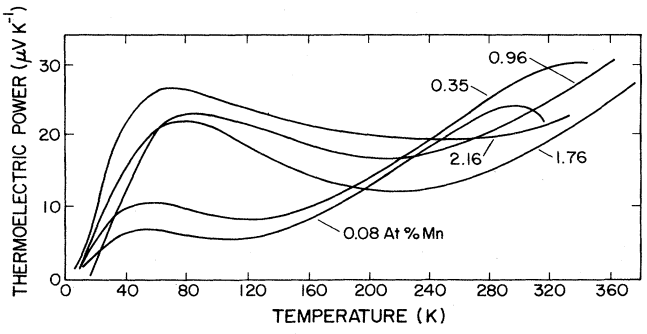

FIG. 27. Temperature dependence of the thermoelectric power of $Cr_{1-x}Mn_x$ alloys for compositions ranging from $x=0.08$ to 2.16 at. % Mn (from Trego and Mackintosh, 1968).

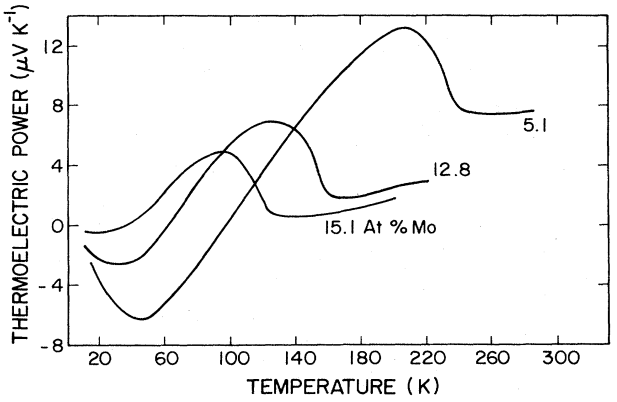

FIG. 28. Temperature dependence of the thermoelectric power of $Cr_{1-x}Mo_x$ alloys for compositions ranging from $x=5.1$ to 15.1 at. % Mo (from Trego and Mackintosh, 1968).

with the extraordinarily large volume dependence of the SDW properties of CrAl alloys around this concentration (see Sec. V.B).

The origin of the low-temperature resistivity (R) minimum seen in several Cr alloy systems has defied satisfactory explanation for many years. The effect is illustrated in Fig. 29, which shows that for some concentrations of Fe the R minimum is followed at lower temperatures by a maximum. The effect of pressure was also studied, and, in fact, for both CrFe and CrCo the size of the R minimum reaches its greatest value at finite pressures, as seen in Table VI.

Katano and Mori (1979) attribute the R-minimum to the Kondo effect, while recognizing that the SDW magnetic ordering should suppress the spin-flip scattering of conduction electrons by localized magnetic moments responsible for the effect. In the CrFe alloys, for low concentrations of Fe, $x \leq 0.6$ at. % Fe, the depth of the R minimum increases with x and the position of $T_{\min}$ varies as $x^{1/3}$, as one would expect for resistivity increasing with temperature T due to magnon scattering. The value of $T_{\min}$, however, decreases between $x = 1.0$ and 1.5 at. % Fe, as seen in Fig. 29, and a maximum appears at low temperatures, followed at higher concentrations by the disappearance of both the R minimum and maximum, with a rapidly decreasing resistivity at the lowest temperatures for $x \gtrsim 2$ at. % Fe. Reference to Eq. (39) shows that this is not at all the expected behavior for a Kondo alloy.

The strongest argument against explaining the R minimum in Cr alloys as being a manifestation of the Kondo effect is, however, the fact that pronounced R minima are seen in CrCo and CrNi alloys (Table VI), in which the impurity Co and Ni atoms do not carry a moment in the SDW phase (Table V). Indeed, the nontransition-metal impurities Al, Si, and Ge, which are clearly nonmagnetic, nevertheless give rise to shallow R minima (Table VI). CrMo and CrV alloys also show R minima even larger than the R minimum seen in CrFe alloys (Table VI), but in both cases the R minimum appears

at high concentrations, close to the critical value when the alloy becomes paramagnetic, so that it is probably due to the normal increase in resistivity below the Néel transition seen in Fig. 22.

Of these Cr alloy systems, only CrFe and CrSi have been studied systematically by doping with V and Mn and by applying pressure (Fawcett and Galkin, 1992, 1993; Galkin and Fawcett, 1994, unpublished). Their behavior is quite similar, so that it seems likely that the same physical mechanism is responsible for the R minimum in these and, by extension, in the other Cr alloy systems; and this mechanism thus operates in CrFe alloys independently of the local moments responsible for the Curie-law susceptibility.

Tugushev (1992), Galkin and Fawcett (Galkin and Fawcett, 1993; Galkin, 1993) explain the temperature dependence of the resistivity in terms of local impurity states. These are formed in the energy gap of a commensurate SDW system, as illustrated in Fig. 20, and described for the symmetric case by Eq. (26). The major predictions of the theory are as follows:

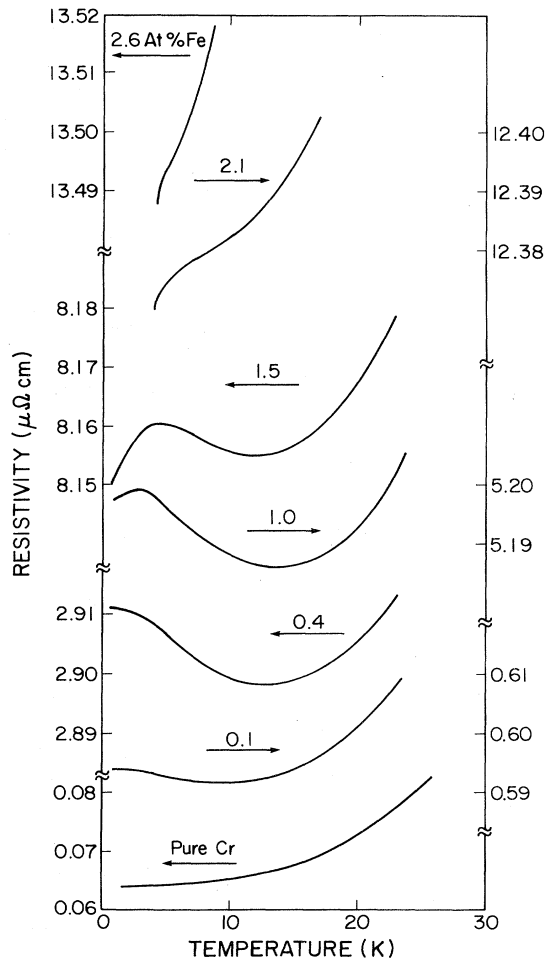

FIG. 29. Temperature dependence below 30 K of the resistivity of $Cr_{1-x}Fe_x$ alloys for x in the range 0.1–2.6 at. % Fe, with data for pure Cr for comparison (from Katano and Mori, 1979).

(1) There is an additional contribution $R^0_{\rm res}$ to the residual resistivity, given by Eq. (36), which is resonant when the Fermi level E_F coincides with the impurity level, $E_0=E_\uparrow$ or $E_\downarrow$.

(2) There is a negative temperature dependence $R_{\rm res}(T)$ of the resistivity, given by Eq. (37), when E_F is close to this resonance; this gives rise to a resistivity minimum in the total resistivity, given in Eq. (35), since at higher temperatures the resistivity $R_{\rm ph}(T)$ due to phonon scattering increases rapidly as T^5 (or T^3 for magnon scattering).

(3) There is a negative magnetoresistance, given by Eq. (38), when E_F is close the E_0.

The first effect in the residual resistivity may be observed by "tuning" the Fermi level E_F through the local impurity level E_0 by doping with V or Mn. This changes E_F in a manner roughly as expected for a rigid-band model, Mn having an extra electron relative to Cr and V being deficient an electron. The resultant variation of the residual resistivity extrapolated to zero temperature,

$$R_0=R^0_0+R^0_{\rm res} \tag{47}$$

from Eq. (35), gives clear evidence for the predicted resonance effect, as seen in Fig. 30. The concentrations giving the peaks in R_0 are $y_{\rm res}=0.4$ at. % V and $x_{\rm res}=0.41$ at. % Mn, the values being equal within the experimental accuracy, which suggests that the symmetric energy-level scheme shown in Fig. 20(a) is appropriate, with E_F lying in the middle of the gap in the commensurate SDW alloy, Cr+2.7 at. % Fe.

The much broader resonance peak seen in Fig. 30 for

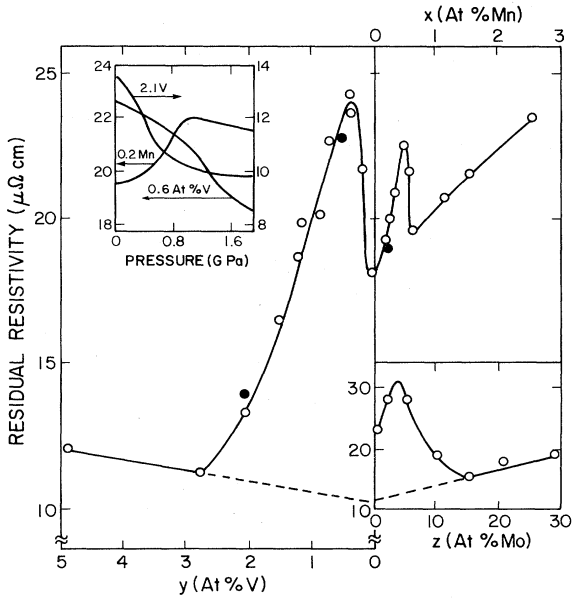

FIG. 30. Residual resistivity at temperature 4.2 K of ternary alloys $(Cr_{1-x}Mn_x)+2.7$ at. % Fe, $(Cr_{1-y}V_y)+2.7$ at. % Fe (from Galkin, 1989), and $(Cr_{1-z}Mo_z)+3$ at. % Fe (V. Yu. Galkin, 1992, unpublished). The inset shows the pressure dependence of the residual resistivity for three of the alloys based on Cr+2.7 at. % Fe, whose data points are shown by solid circles in the main diagram (from Galkin, 1987).

Mo doping of Cr+3 at. % Fe is more difficult to explain, since Mo is isoelectronic with Cr, so that any change in the Fermi level cannot be due to a change in electron concentration. It is interesting to note that for both V and Mo doping the residual resistivity in the paramagnetic alloys rises roughly linearly with y and z, respectively, and extrapolation back to $y=z=0$ gives roughly the same value, $R_0^0 \simeq 10\ \mu\Omega$ cm, which may be assumed to be the value for nonresonant potential scattering.

Since $x_{\rm res} \simeq y_{\rm res}$ for the alloy system based on Cr+2.7 at. % Fe shown in Fig. 30, it is reasonable to assume that the symmetric energy-level scheme shown in Fig. 20(a) is appropriate, with $E_0=E_\uparrow=E_\downarrow$. The value of E_0 may then be estimated from the average value, $(x_{\rm res}+y_{\rm res})/2=0.425$ at. %, if we can estimate the rate of change of the Fermi level with doping. The value obtained from experimental and theoretical estimates of the mean Fermi velocity, combined with the observed change in the SDW wave vector with doping, is $|dE_F/dx|=0.032$ eV/at. % (Fawcett and Galkin, 1991a). The true value may well be different from the commensurate SDW alloy Cr+2.7 at. % Fe, but the resultant estimate, $E_0=0.014$ eV, gives at least a rough idea of the energy-level scheme. The value of the energy gap measured by infrared absorption in a Cr+3 at. % Fe alloy at temperature 80 K (Barker and Ditzenberger, 1970; Kirillova and Nomerovannaya, 1975) is $2\Delta=0.39$ eV, which gives a zero-temperature value, $\Delta=0.20$ eV. Thus $E_0/\Delta=0.07$, and, substituting in Eq. (26), we find that $g_0=0.94$.

In principle, we could determine, from the widths of the local impurity level maxima in $R_{\rm res}^0$, the coefficient g_2, by use of Eq. (29). According to Eq. (22c), this measures the potential scattering between the nesting surfaces e and h, which may thus be compared with coefficient g_0 for *ee* and *hh* potential scattering. Figure 30 shows, however, that the width for V doping is considerably larger than for Mn doping. This may be connected with the fact that the system (Cr+2.7 at. % Fe)$_{1-y}$V$_y$ becomes incommensurate for $y \gtrsim 0.1$ at. % V (Fawcett and Galkin, 1992a, 1992b).

For a lower concentration of Fe in the system (Cr+1.5 at. % Fe)$_{1-y}$V$_y$, the width of the resonance peak is considerably larger, while the resonance peak in (Cr+1.5 at. % Fe)$_{1-x}$Mn$_x$ remains narrow. Galkin and Tugusheva (1988) attribute this to the spreading of the impurity levels right across the energy gap of an incommensurate SDW system, as predicted by Buzdin *et al.* (1986). A similar effect is seen in Cr+1.3 at. % Si doped with V or Mn, while in Cr+3.2 at. % Co both the narrow resonance peaks occur with V doping at $y_{\rm res}=0.2$ and 0.65 at. % V (Fawcett and Galkin, 1992a).

We turn now to the second prediction of the model of local impurity states, namely, the negative temperature dependence of the resistivity R at low temperatures when the Fermi level is close to the resonance impurity level and the resultant resistivity minimum. This effect is seen very clearly in the system (Cr+1.5 at. % Fe)$_{1-y}$V$_y$, illustrated in Fig. 31(a) for curves 3 and 4. In the case of curve 5, for $y=1.1$ at. % V, the Néel temperature has fallen so low, $T_N \simeq 75$ K, that the resistivity minimum above T_N seen in curves 1, 2, 3, and 4, which is associated with the resistivity hump due to electron-hole condensation, merges with the low-temperature resistivity minimum. The behavior under these conditions, which is seen also in Fig. 31(b), is very complicated and requires more detailed analysis than the qualitative discussion

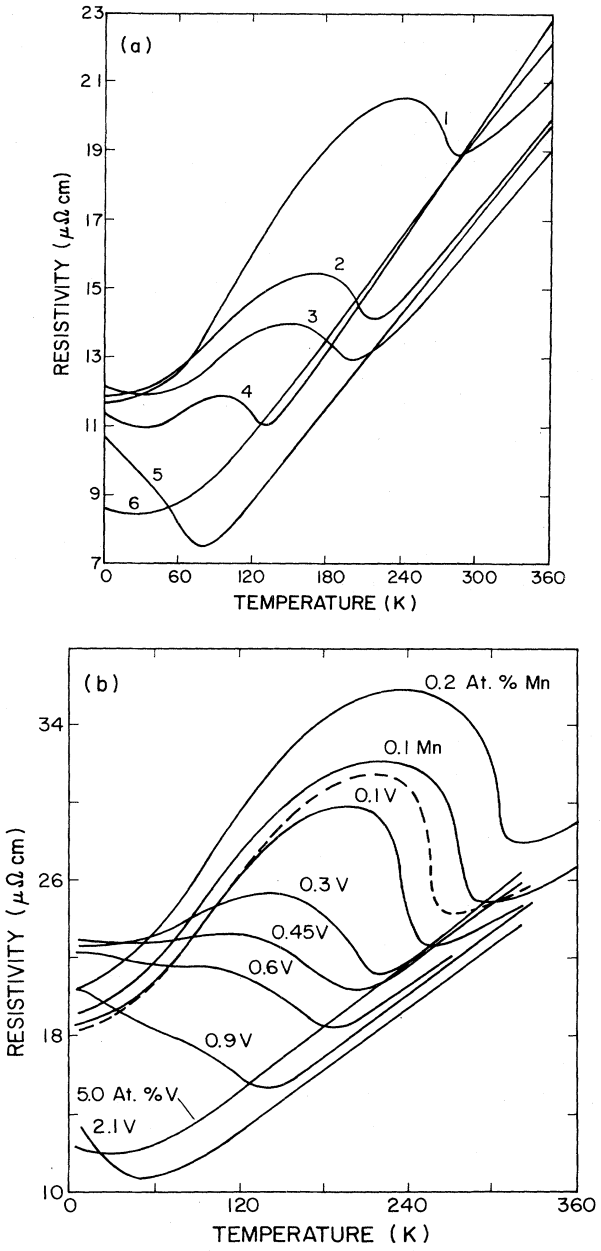

FIG. 31. Temperature dependence of the resistivity of ternary alloys: (a) (Cr+1.5 at. % Fe)$_{1-y}$V$_y$ with concentrations y of V in at. %: 1—0.0; 2—0.3; 3—0.5; 4—0.7; 5—1.1; 6—1.5, and (b) (Cr+2.7 at. % Fe)$_{1-x}$ (V,Mn)$_x$, with the concentrations x of V or Mn shown on the curves, the curve for undoped Cr+2.7 at. % Fe being dashed (after Galkin and Fawcett, 1992).

given by Galkin and Tugusheva (1988). The striking feature of Fig. 31(b) for the system (Cr+2.7 at. % Fe)$_{1-x}$(V,Mn)$_x$, which is commensurate for $x \gtrsim 0.1$ at. % V, is the rapid increase in the residual resistivity as the resonance peak at $x_{res}=0.4$ at. % V is approached from the lower-x commensurate SDW side. This results in a resistivity minimum for $x=0.3$ and 0.45 at. % V; but for $x=0.6$ at. % V, the minimum is lost as the broader minimum due to the increase in resistivity below the Néel temperature takes over (Galkin and Fawcett, 1993).

The temperature dependence of the resistivity is very similar as the Fermi level is tuned by V and Mn doping through the local impurity levels of the commensurate SDW alloy Cr+1.3 at. % Si (Galkin *et al.*, 1991). This gives powerful support to the idea that the complex behavior of the transport phenomena in both CrFe and CrSi alloy systems has the same origin, which is therefore nonmagnetic: it is *not* the Kondo effect.

The effect of V doping on Cr+3 at. % Fe was measured by Åstrom *et al.* (1977), with results similar to Fig. 31(a). A Cr+2 at. % Si alloy exhibits a strong first-order transition (see Sec. II.C.10 and Sec. VI.A, Table XV) at a Néel temperature, $T_N \simeq 230$ K, which is depressed to 130 K by adding only 0.1 at. % V (Benediktsson *et al.*, 1980). Hedman *et al.* (1982) also measured the temperature dependence of the susceptibility in Cr+2 at. % Si doped with up to 3 at. % Fe.

The system (Cr+3 at. % Fe)$_{1-z}$Mo$_z$, which was studied by Ström-Olsen *et al.* (1982), does not show a low-temperature resistivity minimum, possibly because the strong resistivity anomaly around the Néel temperature T_N (see Fig. 26, where the resistivity for Cr+3.3 at. % Fe increases below T_N by 50% above the minimum value just above T_N), together with the very large residual resistivity at the resonance composition, $z_{res}=4$ at. % Mo (see Fig. 30), causes the low-temperature resistivity minimum to disappear into the resistivity minimum around the Néel transition.

The magnetoresistance of a series of commensurate SDW alloys of Cr+2.7 at. % Fe doped with Mn, shown in Fig. 32, exhibits the initial negative term quadratic in field that is predicted by Eq. (38) for the impurity resonance scattering model and also by the Kondo model (Beal-Monod and Weiner, 1968). The sensitivity of the minimum in the magnetoresistance at higher fields to the concentration of Mn suggests that, when the interpretation is available for these and other unpublished magnetoresistance data on ternary Cr alloys (Galkin, 1992), we shall gain considerable insight into these interesting systems (see Figs. 30, 31, and 59 for other experimental results for ternary alloys of CrFe doped with Mn).

Arajs and Dunmyre (1967a, 1967b) and Arajs *et al.* (1976) measured the longitudinal magnetoresistance of CrMn, CrFe, CrCo, and CrNi alloys, and Kondorskii, Kostina, and Trubitsina (1983) of CrCo alloys, at temperature 4.2 K in fields up to 6 T, with inconclusive results. Arajs (1970a) analyzed his transverse magnetoresistance data for Cr$_{1-x}$Fe$_x$ alloys at 4.2 K in terms of a magnetic

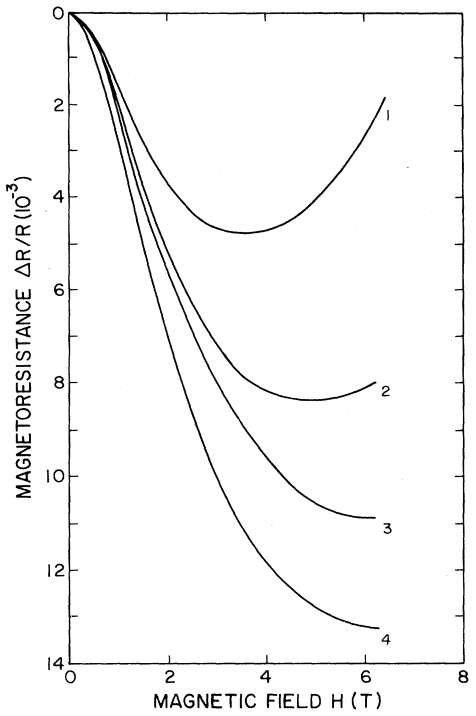

FIG. 32. Magnetoresistance at temperature 4 K of alloys, Cr$_{1-x}$Mn$_x$+2.7 at. % Fe, with concentrations x of Mn in at. %: 1—0.14; 2—0.5; 3—2.5; 4—1.1 (after Galkin, 1992).

component associated with the localized magnetic moments on the Fe atoms, which was negative and increased in magnitude progressively with the concentration x of Fe, and a positive component independent of x. This was thought to give support to the idea that the localized moments in the Fe atoms are the cause of the anomalies in the temperature dependence of the resistivity in CrFe alloys (see Fig. 29), while the relative weakness of the magnetoresistance in CrCo alloys (Arajs *et al.*, 1967) is consistent with the absence of local moments in this system (see Sec. III).

There have been a few studies of the Hall effect in Cr alloys, which are reviewed by Hurd (1972). The results are inconclusive, though it is interesting to note that de Vries (1959) measured the temperature dependence of the Hall effect, as well as the resistivity, in his pioneering study of the effect of 1 at. % of V, Mn, Fe, Cr, and Ni on the transport properties of Cr. The reason is that, in a compensated metal like Cr, the sign and magnitude of the Hall coefficient R_H is determined in a complicated way by the numbers of carriers in different parts of the Fermi surface weighted according to their mobilities. The same is true for dilute alloys of Cr, and R_H provides little information, except in the unique case of the CrAl alloy system, which becomes a narrow-gap semiconductor over a range of concentrations (see Sec. II.C.9).

A remarkable feature of the low-temperature resistivity minimum in Cr alloy systems is the similarity between the effects of applied pressure and that of tuning the Fer-

mi level. This may be seen by comparing Fig. 33 with Fig. 31(b). Katano and Mori (1980) first studied systematically the strong pressure effect in CrFe and CrCo alloys. They also measured a paramagnetic ternary alloy, $Cr_{92}V_8+1$ at. % Fe, which showed a resistivity minimum having the characteristic features of the Kondo effect. It is interesting to note that they find the pressure dependence of the Kondo temperature, $dT_K/dp \simeq 7$ K $(GPa)^{-1}$, to be an order of magnitude smaller than the initial value of dT_{min}/dp for Cr+0.6 at. % Fe and Cr+4 at. % Co. Jayaraman (1984) has reviewed this work, and we shall discuss in Sec. V.D the significance of this parallelism between the effects of pressure and of electron concentration in Cr alloy systems.

The linear increase in resistivity below the Néel temperature T_N predicted by Volkov and Tugushev (1984) in Eq. (45a) will be difficult to distinguish in most cases from the increase associated with condensation of the electron and hole octahedra, which is thought to be responsible for the hump in $\Delta R/R$ below T_N seen in all Cr alloy systems (Table VI). In at least one case, however, the extreme sensitivity of the hump to doping suggests that another mechanism is operative, namely, the tuning of the Fermi level through local impurity states, with consequent change in the scattering. The alloy Cr+0.5 at. % Ir is remarkably sensitive to doping with V, as seen in Fig. 34. The inset shows that the resistivity difference, $\Delta R = R_{max} - R_{min}$, for the hump changes in this alloy with electron-per-atom ratio e_A, measured relative to Cr, at a rate 5 times greater than for $Cr_{1-x}Ir_x$ and 100 times faster than for $Cr_{1-x}V_x$. The difficulty with explaining this in terms of scattering by the local states of the Ir impurity is that $Cr_{95.5}Ir_{0.5}$ has an incommensurate SDW, the triple point being at 0.14 at. % Ir, so that according

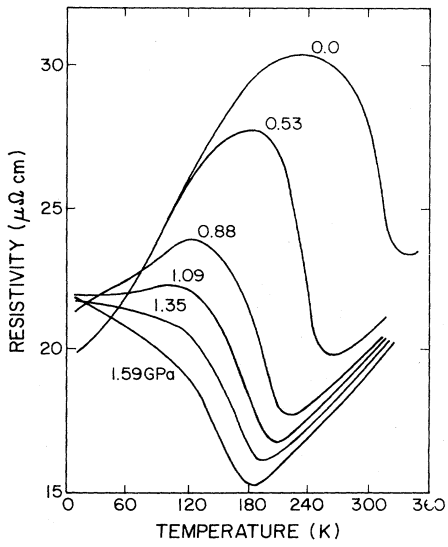

FIG. 33. Pressure dependence of the resistivity of an alloy, Cr+0.25 at. % Mn+2.7 at. % Fe (i.e., in the vocabulary of Fig. 32, x=0.25 at. % Mn), for pressures ranging from 0 (ambient) to 1.59 GPa (from Galkin, 1989).

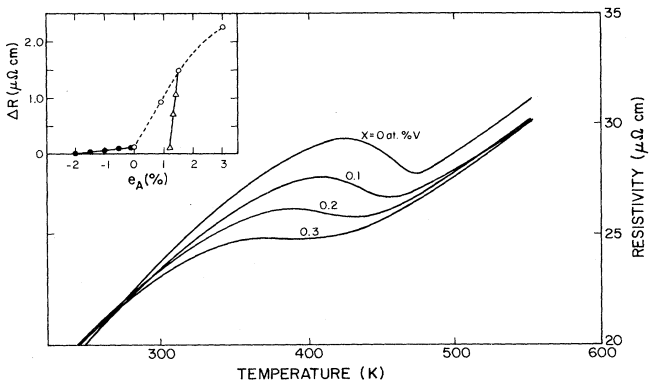

FIG. 34. Temperature dependence of the resistivity around the Néel temperature T_N and the resistivity hump below T_N in alloys $Cr_{1-x}V_x+0.5$ at. % Ir. The inset shows the dependence of the difference between the maximum and minimum resistivity, $R = R_{max} - R_{min}$, as a function of electron-per-atom ratio e_A, for this system in comparison with the CrV and CrIr alloy systems: △—$Cr_{1-x}V_x+0.5$ at. % Ir; O—CrIr; ●—CrV (from Gopalakrishnan *et al.*, 1984).

to Buzdin *et al.* (1986) the impurity levels will be spread right across the energy gap. One would rather expect such extreme sensitivity of the resistivity hump below T_N in a commensurate SDW alloy, but Fig. 31(b) shows that this is not the case in $(Cr+2.7 \text{ at. \% Fe})_{1-x}Mn_x$.

As we shall see in Sec. VII.B, there is clear evidence in the inelastic neutron scattering for SDW fluctuations in Cr alloys above the Néel temperature T_N, and even in an alloy Cr+5 at. % V, that does not order. In Sec. V we shall see that thermal expansion and elastic constant anomalies, which are clearly magnetic in origin because of their close association with the temperature dependence of the order parameter below T_N, also persist to temperatures well above T_N. It is not surprising therefore to find that the resistivity also first begins to show precursor effects of the approaching Néel transition with decreasing temperatures at least 100 K above T_N.

Chiu *et al.* (1971) estimated quantitatively, as illustrated in Fig. 35, the magnetic contribution to the resistivity in the paramagnetic phase in the CrTi alloy system and also in pure Cr. They found that in CrTi it is reasonable to assume that, at temperatures T sufficiently high above T_N, the resistivity curve $R(T)$, after subtracting the residual resistivity, is asymptotic to the ideal resistivity $R_i(T)$ (referred to in Sec. IV.A as the resistivity associated with electron-phonon scattering) as the magnetic contribution $R_m(T)$ vanishes with increasing temperature. They used for $R_i(T)$ an analytic function, comprising a Grüneisen function with the Debye temperature, Θ_D=450 K, of pure Cr, for the electron-phonon scattering and a small positive T^3 term corresponding to *s-d* scattering. They fit this expression to data of Arajs *et al.* (1970) for pure Cr in the temperature range 800–1000 K, well above the appearance of any magnetic contribution. We are mainly interested in the temperature dependence

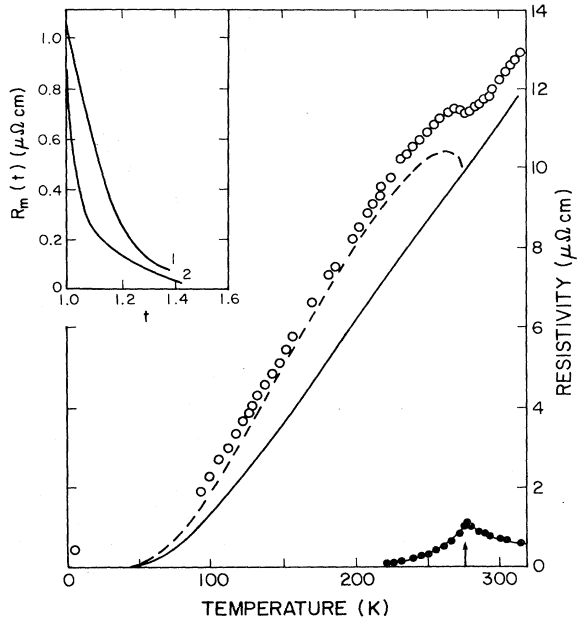

FIG. 35. Analysis of the temperature dependence of the resistivity of an alloy, Cr+0.17 at. % Ti, by subtracting the ideal resistivity R_i (——), enhanced below the Néel temperature, by electron-hole condensation (— — —), from the measured resistivity (○), so as to give the magnetic contribution R_m (●). The arrow indicates the Néel temperature $T_N=276$ K. The inset shows the resultant temperature dependence of R_m above T_N as a function of reduced temperature, $t=T/T_N$, for (1)—pure Cr, (2)—Cr+0.47 at. % Tr (after Chiu *et al.*, 1971).

of the magnetic resistivity $R_m(T)$ above T_N, but we shall include the relatively small and temperature-independent impurity scattering $R_{\rm imp}$ in the equation of Chiu *et al.* [1971, Eq. (16)],

$$R(T)=\frac{R_i(T)+R_m(T)+R_{\rm imp}}{1-\alpha\Delta(T)/\Delta(0)} . \tag{48}$$

The energy-gap function $\Delta(T)$ was assumed to have the temperature dependence of the BCS function, and α is an adjustable parameter typically having a value of about 0.3, which is used to optimize the fit to the resistivity hump below T_N resulting from electron-hole condensation. The inset in Fig. 35 shows that $R_m(T)$ has a similar temperature dependence in the CrTi alloy to that in pure Cr, and, in both, the magnetic scattering decreases rapidly, like critical scattering, with increasing temperature above T_N, going to zero at reduced temperature $t=T/T_N\simeq 1.5$.

In CrRe and CrOs alloys the temperature interval $\Delta T=T_H-T_N$ between the Néel temperature T_N and the disappearance at temperature T_H of $R_m(T)$, which is signaled by the onset of linear temperature dependence at higher temperatures, peaks around the triple point (Butylenko, 1985). The data for $Cr_{1-x}Os_x$ alloys shown in Fig. 36(a) give the plot of $\Delta T(x)$ in Fig. 36(b), which peaks at $x_L=0.2$ at. % Os, the triple-point concentration. A similar result is obtained from thermal-expansion data for both CrOs and CrRe alloys (Butylenko, 1985). Butylenko *et al.* (1980) show also the thermal expansivity and specific heat of dilute CrOs alloys around T_N, and

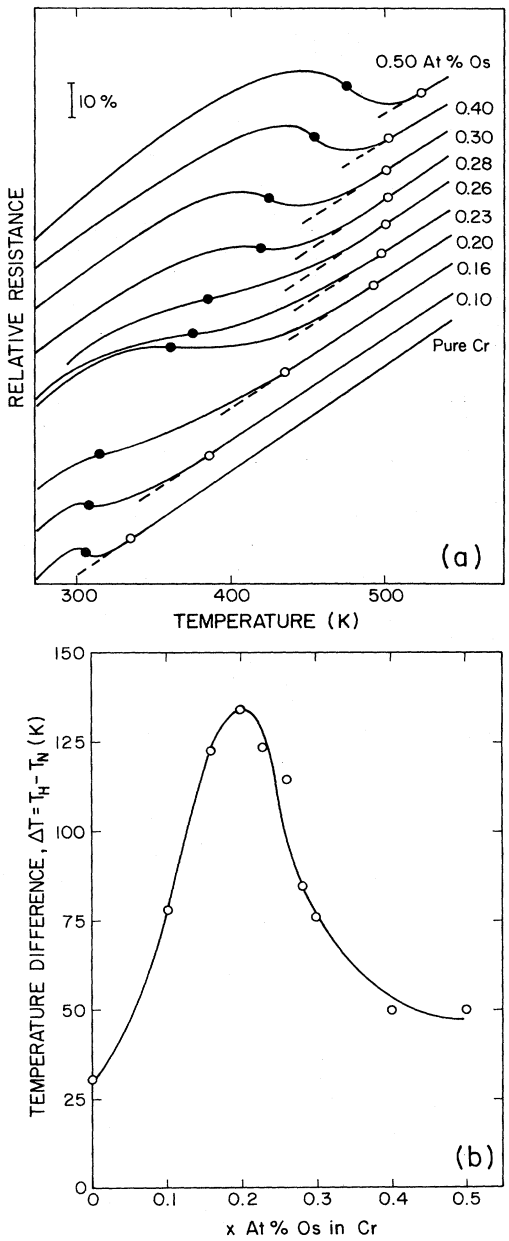

FIG. 36. Temperature dependence of the resistivity of CrOs alloys, around the Néel temperature and up to 550 K: (a) Temperature dependence of the relative resistance, referred to the value at temperature 293 K, of $Cr_{1-x}Os_x$ alloys for compositions ranging from $x=0.10$ to 0.50 at. % Os, with data for pure Cr for comparison. The Néel temperature T_N (●) is defined by the point of inflection of the curve $R(T)$, while the onset of linear temperature dependence in the paramagnetic phase at temperature T_H (○) is indicated by the dashed line extrapolated into the nonlinear region. (b) Temperature difference ΔT between T_H, where the linear temperature dependence of the resistance begins, and the Néel temperature T_N, for $Cr_{1-x}Os_x$ alloys [after Butylenko, 1985, who shows in his Fig. 1 the Néel temperature as occurring at the minimum of the $R(T)$ curve].

exhibit the largest anomaly at the triple-point concentration.

The explanation of this behavior may be that suggested by Butylenko, namely, that close to the triple point critical conditions for the coexistence of several phases occur, with resultant fluctuations that may extend to higher temperatures in the paramagnetic phase. It should be noted, however, that the phase diagram in Fig. 21 is quite different from that obtained if T_H, as defined in Fig. 36, is identified with the temperature predicted for the onset of local impurity states at single atoms. Buzdin *et al.* (1986) find no increase in the temperature interval $\Delta T = T_H - T_N$ around the triple point.

The final topic in the temperature dependence of resistivity of Cr alloys is the remarkable deviation from Matthiessen's rule seen in some systems. Thus in $Cr_{1-x}V_x$ alloys the resistivity in the paramagnetic phase at a given temperature, say, 300 K, drops rapidly when V is first introduced into Cr, as seen in Fig. 22, and only begins to increase with x for $x \gtrsim 1$ to 2 at. % V, whereas the residual resistivity R_0 increases monotonically and is roughly linear in x (Takeuchi *et al.*, 1980).

This initial decrease in resistivity in the paramagnetic phase was found by Vedernikov (1967) to be roughly constant between the Néel temperature and 550 K. It is attributed by Fawcett (1992a) to the suppression of spin fluctuations by the V impurity, which is seen directly in the inelastic neutron scattering (Noakes, Holden, Fawcett, and de Camargo, 1990), as illustrated in Fig. 66 and Table XVI in Sec. VII.B. It is manifested also in a rapid increase in the NMR relaxation rate (Kontani and Masuda, 1983) and in dramatic changes in the magnetoelastic properties (Fawcett, 1992a).

In Table VI, the column labeled

$$f = \frac{\delta R_P}{\delta R_0} \tag{49}$$

gives a very rough estimate of the ratio, for a given low concentration of the solute A, of the change δR_P in the resistivity R_P in the paramagnetic phase at the highest temperature to the change δR_0 in the low-temperature resistivity R_0. In most cases R_0 is the residual resistivity at liquid-helium temperature, but in a few cases, as indicated by the notation N_2, the change in R_0 is estimated by extrapolating from liquid-nitrogen temperature. We see that CrV is indeed very anomalous, with a large negative contribution, greater than $-2\ \mu\Omega$ cm (at. % V)$^{-1}$ to R_P and only 0.4 $\mu\Omega$ cm (at. % V)$^{-1}$ to R_0.

Before discussing the many other anomalous cases listed in Table VI, we should point out that a strict application of Matthiessen's rule, which states simply that impurity scattering is independent of temperature, would predict for a SDW metal a value for the ratio, $f \lesssim 1$. This is because condensation below the Néel transition of electrons and holes at the Fermi surface reduces the effective number of current carriers. In the formulation of Chiu *et al.* (1971), as expressed in Eq. (48), this ratio has the value $f = 1 - \alpha$, since at zero temperature $\Delta(T) = \Delta(0)$, and for $T > T_N$, $\Delta(T) = 0$.

When we inspect Table VI, we find that CrTi, CrMo, CrFe, CrNi, CrRu, CrPt, CrAu, and CrSi have the value $f \lesssim 1$, expected for this simple SDW model. There appears to be no systematic pattern in the anomalous values of the ratio f for the other alloys that might lead to an explanation why impurity scattering in the paramagnetic phase above the Néel transition appears to have no correlation with impurity scattering at low temperature.

The effect of Mo and W impurity on the thermoelectric power S of Cr in the paramagnetic phase is surprisingly large. Arajs, Anderson, and Ebert (1971, Fig. 3) give data up to temperature 360 K, some 50–100 K above the Néel temperature T_N, in alloys containing up to 8.8 at. % Mo and 3.4 at. % W, where the value of S decreases by a factor of about 2 below its value, $S \simeq 16\ \mu V\,K^{-1}$, in pure Cr. At higher temperatures up to 600 K, S remains roughly constant in Cr; but in CrMo alloys, S increases linearly with temperature beyond about 100 K above T_N (Schröder and Tomaschke, 1968), as predicted for the diffusion term in Eq. (20).

In $Cr_{1-x}Ni_x$ alloys also the thermoelectric power at temperature 600 K decreases rapidly with increasing x, being reduced by more than a factor 2 for $x = 4$ at. % Ni, where there is no antiferromagnetism at lower temperatures, and thereafter remaining constant up to $x = 10$ at. % Ni (Schröder and Baum, 1968). This apparent connection between the value of S several hundreds of degrees above the Néel transition and the existence of long-range order is quite remarkable.

Another interesting feature of the CrNi alloy system is the initial rapid dependence of the residual resistivity R_0 on Ni, with $dR_0/dx \simeq 20\ \mu\Omega$ cm/at. % (Arajs, 1970c, Fig. 4; Butylenko and Nevdacha, 1993), which is followed beyond $x \simeq 1$ at. % Ni with a leveling off in R to a constant value, $R_0 \simeq 22\ \mu\Omega$ cm, for $x \gtrsim 3$ at. % Ni.

The high-temperature Lorenz ratio of pure Cr, $L = \kappa/\sigma T$, κ being the thermal conductivity and σ the electrical conductivity at temperature T, is considerably larger than the Sommerfeld value

$$L_0 = \frac{\pi^2}{3}\left[\frac{k_B}{e}\right]^2 = 2.44\times 10^{-8}\ V^2\,K^{-2}\ . \tag{50}$$

In an effort to understand the reason for this behavior, the temperature dependence of κ was measured, with the results shown in Fig. 37, in AFM CrMo and CrSi alloys and in a paramagnetic CrV alloy. In fact, the latter comes closest to reproducing the hump in the temperature dependence of $L(T)$ that develops between 100 and 200 K in Cr.

The SDW alloys all show a hump in $L(T)$ at a temperature of about 50 K, which is attributed to thermal conduction by the lattice (Johannesson *et al.*, 1982). This feature is especially strong in CrSi, where the decrease at higher temperatures is relatively slow and the value of L around the Néel temperature ($T_N \simeq 275$ K; see Fig. 17) is close to that of pure Cr, both having a value a factor $\lesssim 2$

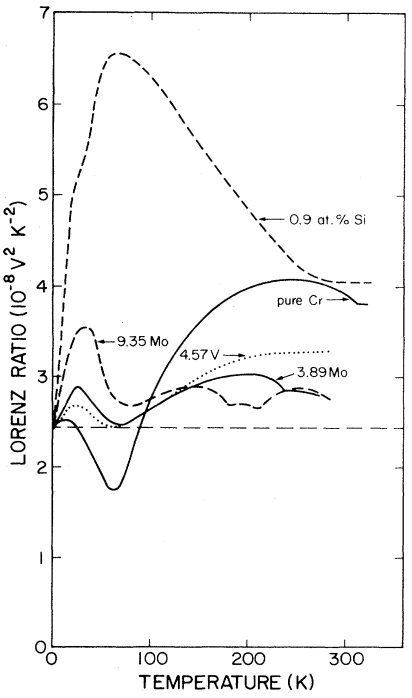

FIG. 37. Temperature dependence of the Lorenz number of pure Cr and Cr alloys with V, Mo, and Si. The curves are labeled with the concentration of the alloys in at. %. The Sommerfeld value, $L_0 = 2.44 \times 10^{-8}$ V^2 K^2, is shown by the horizontal dashed line (after Mitchell and Goff, 1975 and Johanesson *et al.*, 1982).

times larger than L_0. The behavior of a Cr+1.4 at. % Si sample is very similar to that of the Cr+0.9 at. % Si sample shown in Fig. 37, with the first-order transition to the commensurate SDW phase in the former (see Sec. VI.A) having only a small effect.

Subtraction of an electronic component to the thermal conductivity, $\kappa_e = L_0 T/R_0$, R_0 being the residual resistivity, gives the lattice component κ_g, which, in both the CrSi alloys below a temperature $T \lesssim 30$ K, has a T^2 dependence, as expected for phonon-dominated scattering processes. The reason for the very large value of κ_g in the CrSi alloys is not understood, nor why κ_g is absent at low temperatures in pure Cr, where on the contrary $L(T)$ exhibits a *negative* hump.

Mitchell and Goff (1975) give reasons why the large value of L around the Néel transition is associated with the opening of the AFM band gap, but it is not clear why the value is reduced in the Mo alloys and not in CrSi, nor why the high value of L persists above the Néel transition. The minimum in $L(T)$ below 200 K for the alloy Cr+3.9 at. % Mo corresponds to the Néel transition, but the origin of the minimum at $T = 230$ K is not understood. The value of L is high in this temperature region also in the CrV alloy, which exhibits incommensurate SDW fluctuations (Fawcett *et al.*, 1989) even though it does not order for this composition. This suggests that the high value of L in the paramagnetic phase of all the alloys shown in Fig. 37, but especially of the CrSi alloy, and also that of pure Cr, are connected with the nesting Fermi surface.

V. MAGNETOELASTICITY

The thermophysical properties of Cr alloys, like those of pure Cr, show strong effects associated with the volume dependence of their antiferromagnetism. Thus the magnetic Grüneisen parameter Γ_N for Cr alloys, defined in (51) and given below in Table VII, has values typically in the range from that of Cr, $\Gamma_N = -30$ (Fawcett, 1989a) to negative several hundred. Similarly large values of the magnetic Grüneisen parameters Γ_i, defined in (53) in terms of the magnetic contributions to the magnetoelastic properties, are found also in AFM γ-Mn alloys. The values of the magnetic Grüneisen parameter for the ferromagnetic 3*d* metals, Fe, Co, and Ni, on the other hand, are typically of order unity (Fawcett, 1989b).

Moruzzi and Marcus (1992) have found a possible explanation for this strong volume dependence of the thermophysical properties of Cr in a first-principles study of the ground state. They show that Cr in a bcc lattice is *not* magnetic, but a small increase in volume will produce a SDW of substantial amplitude, with little cost in strain energy. Marcus (1994) points out that it is not necessary in their calculations to introduce explicitly nesting of the Fermi surface to deduce the potential for stabilization of the SDW. So long as the action of the SDW in reducing the energy of filled states, when its wave vector spans the Fermi surface, compensates for this small increase in strain energy and the increase in magnetic energy, a new ground state will be produced corresponding to an incommensurate SDW. This has not yet been demonstrated by a first-principles calculation, however, because of the difficulty in treating the large magnetic cell of the SDW found in Cr, which is about 21 lattice spacings long.

The thermal expansion β is the simplest magnetoelastic property to measure and has been studied in many Cr alloy systems. We shall assume in almost all cases that β is isotropic, i.e., that the tetragonal shear strain is negligible relative to the volume strain. The various phase transitions as a function of temperature, including the Néel transition, either to the incommensurate or to the commensurate SDW phase, the spin-flip transition within the incommensurate SDW phase, and the commensurate-incommensurate transition, normally exhibit an anomaly in β and, in some cases, give a first-order change in length. We shall discuss these effects in Sec. VI.

The occurrence of these phase transitions is, however, usually determined from the anomaly in the temperature dependence of the electrical resistivity ρ. The pressure dependence of the Néel temperature, or in some cases that of the other phase-transition temperatures, may thus

be determined by measuring the temperature dependence of ρ under pressure.

For several Cr alloy systems $Cr_{1-x}A_x$, the magnetic phase diagram in the pressure-temperature plane has thus been determined for various concentrations x of the solute metal A. In some cases there is a striking similarity to the phase diagram in the composition-temperature plane at ambient pressure, which is still not understood.

In Fig. 38 we show data on both the pressure dependence and the dependence on electron concentration per atom e_A, relative to Cr, of the Néel temperature for a number of Cr alloys, which illustrate vividly their similarity. We shall see more later, in the discussion of individual Cr alloy systems, of this parallelism between the effects of pressure and concentration of the solute element. The similarity is especially striking in some cases when doping produces a commensurate SDW phase, and pressure restores the incommensurate SDW phase, so that the phase diagrams in the composition-temperature and the pressure-temperature planes are similar, with negative pressure corresponding to increasing e_A. Comparison between the two phase diagrams for those Cr alloy systems in which they have both been measured is made in Table XIII, and the explanation for this parallelism is discussed in Sec. V.D, where we shall see that it is not at all understood.

The pressure dependence of the phase-transition temperature, let us suppose the Néel temperature T_N, may be

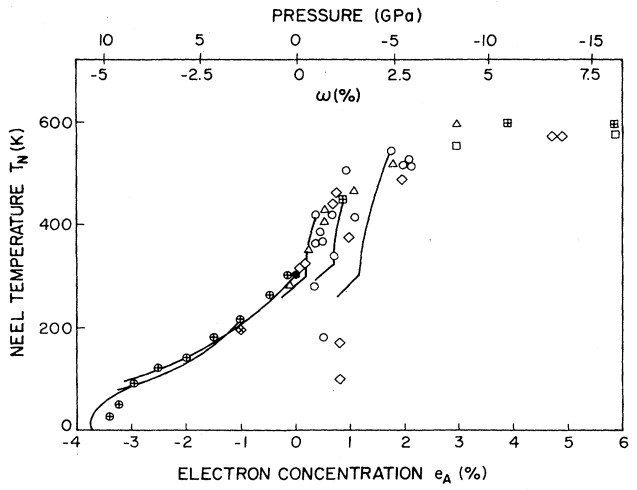

FIG. 38. Dependence of the Néel temperature T_N for different solutes A in Cr alloys $Cr_{1-x}A_x$ on excess concentration per atom e_A, calculated from the concentration x by assuming an electron excess of 2 electrons per impurity atom for group 8 solute metals, 1 for group 7, and -1 for group 5. The dependence of T_N on pressure p is shown for comparison by the solid lines, which are calculated from the experimental data (for CrV as shown in Fig. 39 and for CrMn and CrRu alloys, which exhibit a triple point, as shown in Fig. 43) by use of a scaling factor of 2.8 GPa per 1% e_A. The pressure p and volume change ω scales shown along the top of the diagram correspond to this scaling factor and bulk modulus of 200 GPa: CrV (⊕); CrTa (⊛); Cr (●); CrMn (○); CrMnV (△); CrRe (◇); CrRu (⊞); CrRh (□). From Griessen and Fawcett (1977).

used to calculate a magnetic Grüneisen parameter

$$\Gamma_N = -\frac{d\ln T_N}{d\ln V} = -\frac{d\ln T_N}{d\omega} \simeq \frac{B_N}{T_N}\frac{dT_N}{dp}\ , \tag{51}$$

where $B_N = -(dp/d\omega)_{T_N}$ is the bulk modulus at T_N. A more exact equation (Bloch and Pavlovic, 1969),

$$\Gamma_N = \frac{B_N}{T_N}\frac{dT_N}{dp}\left[1-\beta_N B_N \frac{dT_N}{dp}\right]^{-1}\ , \tag{52}$$

should be used when dT_N/dp is so large that the second term in the bracket in Eq. (52) is not negligibly small. In many cases, however, when dT_N/dp is large there is a pronounced softening of the lattice, and both the thermal expansivity β and the bulk modulus B are anomalously small at the Néel transition; so the Bloch-Pavlovic correction is still small. In Table VII, where we list the values of Γ_N calculated from dT_N/dp, we make the Bloch-Pavlovic correction only when it decreases Γ_N by more than 10%.

Other magnetic Grüneisen parameters may be defined in different temperature regimes by the method developed by Fawcett (1989a; see also Muir *et al.*, 1987a, 1987b). The magnetic contribution $\Delta\beta(t)$ to the thermal expansion is found in most magnetic Cr alloys to be proportional to the magnetic contribution $\Delta B(t)$ to the bulk modulus as a function of reduced temperature, $t = T/T_N$. These magnetic contributions are determined by reference to the volume thermal expansivity (White *et al.*, 1986) and bulk modulus (Alberts, 1990) of Cr+5 at. % V, which is a paramagnetic alloy that does not order magnetically. Following the thermodynamic analysis of Testardi (1975), Fawcett defines corresponding magnetic Grüneisen parameters, as in (76a) and (76b) below,

$$\Gamma_i = -\frac{1}{B_N T_N}\frac{\Delta B(t)}{\Delta\beta(t)}\ , \tag{53}$$

where the subscript i refers to the different temperature regimes, with Γ_{NT} for $t \lesssim 1$ in the ordered phase, and Γ_{SF} for $t \gtrsim 1$, corresponding to spin fluctuations in the paramagnetic phase. A low-temperature magnetic Grüneisen parameter may also be defined from the ratio of the magnetovolume, $\Delta\omega(0)$ at $t=0$, to the magnetic contribution $\Delta B(0)$ to the bulk modulus at zero temperature. This method of analysis for obtaining magnetic Grüneisen parameters from magnetoelastic data has been applied successfully to other AFM (Fawcett, 1989b, 1989c) and ferromagnetic (Fawcett *et al.*, 1992) systems.

Cankurtaran *et al.* (1992) have recently found, in their pioneering work on the pressure dependence of the elastic constants for a Cr+0.3 at. % Ru single crystal, that the acoustic-mode Grüneisen parameters may have a different value, and even a different sign, from the magnetic Grüneisen parameter obtained either from the pressure dependence of the phase-transition temperature or by the indirect methods discussed in Sec. V.B. They believe that this indicates a fundamental problem associated with assumptions used to develop Eq. (51), and by

TABLE VII. Pressure dependence of the Néel temperature T_N and magnetic Grüneisen parameter Γ_N for chromium alloy systems $Cr_{1-x}A_x$. A dagger indicates that the Néel transition is to the commensurate SDW phase; an asterisk indicates that the Bloch-Pavlovic Eq. (52) has been used. In other cases Eq. (51) has been used, since the Bloch-Pavlovic correction is less than 10%, while in some cases the transition is first order so that the thermal expansivity cannot be defined at the transition.

Solute A	Composition x (at. %)	Néel temperature T_N (K)	dT_N/dp [K (GPa)$^{-1}$]	Grüneisen parameter Γ_N	Reference (Figure)
V	1.1–2.6 (5 samples)	230–122	−39–21	−33±2	a
	1.2,2.8	200,105	−27	−30,−50	b (Fig. 39)
	0.45			−32	c
Mo	3–8 (3 samples)			−34±1	d
	8.6, 12	214, 155	−30	−30,−40	b (Fig. 39)
Mn	0.5†	350	−90	−50	e [Fig. 44(b)]
	0.7†	445	−200	−90	f (Fig. 43)
	1.8†	520	−100	−40	
Re	2†–15† (9 samples)	460–630	−50–15	−20–6	g
Fe	2.5†	255	−250	−200	h
	2.8†	250	−200	−180	
	2.1	265	−100	−50	e
Co	1.0–6.1† (6 samples)	67–304	−4.4–15.5	−30–60	k
Ru	0.3†	375	−300	−80	f
	0.6†	475	−130	−27*	
	3.5–14† (5 samples)	490–530	−40–125	−8–25	l
Os	1–10† (7 samples)	420–600	−130–30	−80–15	m (Fig. 49)
Al	1.4†	160	−50	−40	e
	1.9†	210	−300 ($p \leq 0.3$ GPa)	−220	
	0.5	280	−63	−45*	n
	0.8	255	−68	−50*	
	1.2†	235	−70	−50*	
	1.6†	180	−100	−75*	
	1.9†	135	−190	−155*	
	2.0†	155	−240 ($p \leq 0.4$ GPa)	−210*	
Ga	0.5	300	−60	−25*	p
	1.1†–3.0†	370–460	−240–110	−70*–30*	
Si	0.5–1.4† (3 samples)	285–240	−60–300	−45–150	q
	0.9–2.7† (4 samples)	240	−80–300	−40–250	r
	1.85†	230	−500	−450	s
Ge	0.1–1.5† (7 samples)	305–440	−80–130	−50–210	t
	0.4	305	−90	−60	s
	0.6†	380	−300	−600	
	1.0†	435	−200	−100	
Sn	1.0†	314	−60	−20	s
	2.5†	~360	−100	−60	

[a]De Dood *et al.* (1970).
[b]Rice, Barker, *et al.* (1969a).
[c]Furuya *et al.* (1970).
[d]Mori *et al.* (1970).
[e]Mizuki *et al.* (1982).
[f]Jayaraman *et al.* (1970).
[g]Butylenko and Kobzenko (1981).
[h]Edwards and Fritz (1974).
[k]de Koning *et al.* (1980).
[l]Butylenko and Nevdacha (1983).
[m]Butylenko and Nevdacha (1980b).
[n]Alberts and Lourens (1984a).
[p]Kaneko *et al.* (1982).
[q]Endoh *et al.* (1982, Fig. 6).
[r]Jayarman *et al.* (1976).
[s]Hocheimer and Münch (1991).
[t]van Rijn and Alberts (1986a,1986b).

inference also Eq. (53), namely, that the magnetic contribution to the free energy is separable and is a function of a single volume-dependent temperature parameter. The separability of the electronic and lattice contributions to the free energy has been put in question by several authors (Kim, 1989; Moruzzi, 1990; Mañosa *et al.*, 1992).

We discuss first in Sec. V.A a fundamental theory of magnetovolume, which develops the concept of magnetic pressure for itinerant-electron ferromagnets (Janak and Williams, 1976) and assumes that it may be extended both to simple antiferromagnets, i.e., commensurate SDW systems, and to incommensurate SDW systems. The magnetovolume is thus related (Holden *et al.*, 1984; Kaiser and Haines, 1985) to the mean-square moment $\langle\langle \mu^2(t) \rangle\rangle$, where the double brackets denote an ensemble or thermal average, which includes spin fluctuations and rotation of the ordered moment, and indeed refer also to the paramagnetic phase.

Another approach to magnetoelasticity in SDW systems develops, by analogy with the Bardeen-Cooper-Schrieffer theory of superconductivity, an expression for the magnetic Grüneisen parameter Γ_N, defined in Eq. (51), in terms of the volume derivatives of the density of states at the Fermi surface and of an exchange interaction parameter, which is assumed (Fawcett, 1988a) to be the magnetic susceptibility at the SDW wave vector.

In Sec. V.B the Stoner-Wohlfarth model, as developed by Steinemann (1978), gives expressions for the magnetovolume $\Delta\omega(t)$ and the magnetic contribution $\Delta B(t)$ to the bulk modulus in the ordered phase by making the ansatz for the magnetic free energy

$$\Delta F(t) = \Delta\phi(1-t^2)^2 \ . \tag{54}$$

$\Delta\phi$ is the magnetic free energy in the ground state at zero temperature, which is sometimes referred to as the magnetic excitation potential. Magnetic Grüneisen parameters at the Néel temperature and at zero temperature are also defined in this theory. In the Grüneisen-Testardi theory (Fawcett, 1989a) that follows in Sec. V.B, magnetic Grüneisen parameters as defined in Eq. (53) are obtained.

A. Theory: magnetic pressure

Janak and Williams (1976) explained the magnetovolume observed in magnetic metals as being due to spin polarization that splits the electronic energy bands below the magnetic transition temperature, resulting in a gain of exchange energy which is counterbalanced by an increase in the kinetic energy of the electrons. The kinetic-energy-increase may be reduced by increasing the density of states of the electrons by expanding the lattice in all directions, when the sample is cooled through the magnetic transition temperature. An effective repulsive force, known as magnetic pressure, then appears that is proportional to the magnetic energy density and therefore to the square of the magnetic moment. According to Janak and Williams, this argument also applies to cases in which the ordering varies spatially, as for simple antiferromagnets or spin-density waves, so long as a local spin-density functional may be defined.

The negative magnetic contribution to the bulk modulus that is found in most magnetic metals, including Cr and its dilute alloys, also follows from the same considerations in the theory of Janak and Williams. In magnetic $3d$ transition metals and alloys, the large magnetic pressure causes a considerable expansion of the lattice and a reduction of bulk modulus, in reasonable agreement with that observed.

Holden *et al.* (1984) presented a general theory for the magnetic pressure, which subsumes those of several other workers, who developed models in terms of locally rotated and fluctuating exchange fields that align the itinerant $3d$ electrons. They write the magnetic Hamiltonian

$$\mathcal{H} = \left[\frac{V_0}{V}\right]^{\beta_1} \mathcal{H}_b + \left[\frac{V_0}{V}\right]^{\beta_1\beta_2} \mathcal{H}_c \ , \tag{55}$$

where $\mathcal{H}_b$ is a band term corresponding to electron hopping and $\mathcal{H}_c$ a Coulomb term corresponding to electron-electron interaction.

In a ferromagnetic metal,

$$\beta_1 = \frac{d\ \ln N(0)}{d\omega} \tag{56a}$$

and

$$-\beta_1\beta_2 = \frac{d\ \ln I}{d\omega} \ , \tag{56b}$$

where $N(0)$ is the density of states at the Fermi surface and I is the Stoner exchange interaction parameter in

$$\chi = \frac{\chi_0}{1-IN(0)} = \frac{\chi_0}{1-\bar{I}} \tag{57a}$$

for the exchange-enhanced magnetic susceptibility. In a SDW system, Fawcett (1988a) suggests, following Skriver (1981), that $N(0)$ should be replaced by the wave-vector-dependent susceptibility $\chi_0(\mathbf{q})$, giving in the random-phase approximation

$$\chi(\mathbf{q}) = \frac{\chi_0(\mathbf{q})}{1-I_{\chi 0}(\mathbf{q})} \ , \tag{57b}$$

with $\chi(\mathbf{q})$ becoming infinite at the SDW wave vector $\mathbf{Q}$, where $\chi_0(\mathbf{q})$ is a maximum.

The Hamiltonian in Eq. (55) leads to a magnetic pressure

$$p(t) = \frac{\beta_1}{V_0}\left[\Delta U(t) + \frac{I}{4}(1-\beta_2)\langle\langle \mu^2(t) \rangle\rangle\right] \ , \tag{58}$$

where ΔU is the thermal average of the two energies in Eq. (55),

$$\Delta U = \langle\langle \mathcal{H}_b \rangle\rangle + \langle\langle \mathcal{H}_c \rangle\rangle \ , \tag{59}$$

and the ansatz for the Coulomb energy in terms of the thermal average of the magnetic moment μ,

$$\langle\langle \mathcal{H}_c \rangle\rangle = -\frac{I}{4}\langle\langle \mu^2 \rangle\rangle \ , \tag{60}$$

introduces the parameter I and hence β_2 through Eq. (56b). The thermal averages in Eqs. (59) and (60) are considered by Holden *et al.* (1984) to correspond to slow magnetic fluctuations of the order of spin-wave frequencies (~ 0.1 eV), while fast density and spin fluctuations at the speed of electron hopping, having larger energies ($\gtrsim 1$ eV), are not included.

This magnetic pressure is considered to act against the bulk modulus B, giving a magnetovolume

$$\Delta\omega(t) = \frac{\Delta V(t)}{V_0} = \frac{p(t)}{B}$$
$$= \frac{\beta_1}{BV_0}\left[\Delta U(t) + \frac{(1-\beta_2)}{4} I \langle\langle \mu^2(t) \rangle\rangle\right] . \tag{61}$$

Kaiser and Haines (1985) argue that, since the specific heat anomaly around the Néel transition in Cr is very small, giving an internal energy change of only about 10^{-4} eV/atom, $\Delta U(t)$ in Eq. (61) is two or three orders of magnitude smaller than the term involving the moment and may be neglected. The same is true in Cr alloys, and thus we may write

$$\Delta\omega(t) = \frac{C}{B}\langle\langle \mu^2(t) \rangle\rangle \tag{62a}$$

$$= \frac{I}{4BV_0}\beta_1(1-\beta_2)\langle\langle \mu^2(t) \rangle\rangle \tag{62b}$$

$$= \frac{I}{4BV_0}\left\{\frac{d\ln N(0)}{d\omega} + \frac{d\ln I}{d\omega}\right\}\langle\langle \mu^2(t) \rangle\rangle \ . \tag{62c}$$

The well-known equation (62a) is similar to that derived by Wohlfarth (1969) in the Stoner model. Moriya and Usami (1980) employ the same approximation as an ansatz in developing a theory of magnetovolume in a magnetic system with spin fluctuations. In the ordered phase, without spin fluctuations or rotations, the ensemble average for an incommensurate SDW will give the mean-square moment, $\langle \mu^2 \rangle = \mu_0^2/2$, in Eq. (62a), μ_0 being the peak moment, while for a commensurate SDW the term will be simply μ_0^2. The ensemble average over time and space is, however, appropriate in cases where spin fluctuations or rotation of the moment are important, as, for example, in the paramagnetic phase. In Eq. (62a), the bulk modulus B is assumed to be constant, having usually only a small relative change with temperature as compared with the moment.

Fawcett *et al.* (1986a) discuss the experimental value, based on thermal-expansion measurements in pure Cr, of the ratio in Eq. (62a), $C/B = 0.9\%\,\mu_B^{-2}$ (Kaiser and Haines, 1985, estimate, from the same data, a value, $0.8\%\,\mu_B^{-2}$), in relation to the theoretical equations (62b) and (62c). If we use the canonical value $\beta_1 = d\ln N(0)/d\omega = 5/3$ for a d-band metal without hybridization, we obtain by employing an estimate, $I = 56$ mRy, from band-structure calculations, the value $\beta_1\beta_2 = -d\ln I/d\omega = 1.0$.

Such a large value for the volume dependence of the exchange interaction parameter I is not expected from local spin-density functional calculations. Kanamori (1963) showed, however, that an *effective* exchange interaction I may have a negative volume dependence through the increase in screening with volume due to the increase in density of states. Thus, writing

$$I = \frac{I_0}{1 + gI_0N(0)} \ , \tag{63}$$

where g is a constant of order unity, and assuming I_0 and g to be independent of volume, with $g = I_0N(0) = 1$, as a simple example, one finds that

$$\frac{d\ln I}{d\omega} = -\frac{1}{2}\frac{d\ln N(0)}{d\omega} = -\frac{5}{6}$$

(Fawcett *et al.*, 1986a), close to the value -1 required to give the observed magnetoelastic coupling constant C in Eq. (62a).

It is important to note that the theory of Holden *et al.* (1984) and Kanamori's (1963) explanation through Eq. (63) for the observed volume dependence in Cr of the effective exchange interaction are cast in terms of the volume dependence of the density of states $N(0)$ at the Fermi surface. But $N(0)$ is proportional to the *static* susceptibility χ_0 in Eq. (57a), while the staggered susceptibility $\chi_0(\mathbf{q})$ is the appropriate quantity for a SDW system, as in Eq. (57b).

The pressure dependence of the Néel temperature of Cr was considered by McWhan and Rice (1967) from a rather different point of view, in the framework of a two-band itinerant model of antiferromagnetism (Fedders and Martin, 1966). This model is mathematically identical to the Bardeen-Cooper-Schrieffer model for superconductivity, with the formation of a condensate of bound electron-hole pairs, rather than Cooper electron-electron pairs, lying at an energy Δ above the single-particle states. The electron-hole pairs are in the triplet state and therefore carry a spin, so that the condensate is a spin-density wave.

The gap equation corresponding to the energy gap gives a Néel temperature

$$T_N = T_B \exp(-1/N_M I) \ , \tag{64a}$$

so that

$$\frac{d\ln T_N}{dz} = \frac{d\ln T_B}{dz} + \ln\left[\frac{T_B}{T_N}\right]\left[\frac{d\ln N_M}{dz} + \frac{d\ln I}{dz}\right] , \tag{64b}$$

where $k_B T_B$ is of band-energy order and I is the average Coulomb interaction energy responsible for the electron-hole pairing. N_M is the density of states of that fraction of the Fermi surface which at zero temperature disappears because of the formation of the energy gap, and, in Eq. (64b), z is either the fractional volume change ω or

the change in electron concentration e_A.

McWhan and Rice (1967) pointed out that the negative electronic thermal expansivity, linear in temperature, that is seen in Cr at low temperatures (White, 1961) is consistent with the observed negative pressure dependence of T_N (Mitsui and Tomizuka, 1965) if N_M is assumed to increase rapidly with volume. Rice, Jayaraman, and McWhan (1969) developed this model further by use of a joint density-of-states function defined at two energies, the sum and difference of the energies of the interacting electrons and holes. They considered the problem of the disappearance of antiferromagnetism under high pressure and showed that the assumption equivalent to the linear negative pressure dependence of N_M gives an expression in accordance with the observed behavior, as we shall see in Sec. V.C.2.

We shall discuss in Sec. V.D the remarkable similarity between the effects of volume increase and increase in electron concentration, seen in many SDW Cr alloy systems, in the light of these two theories.

B. Theory: thermal expansion and bulk modulus

We restrict our treatment in almost all cases to the volume thermal expansivity β (or, equivalently, its integral with respect to temperature, the magnetovolume $\Delta\omega$) and to the bulk modulus B. Experiment shows that anisotropy of the thermal expansion (Kaiser *et al.*, 1985) and the effect of shear strains (Muir *et al.*, 1987a, 1987b) are very weak in Cr, and results for the shear elastic moduli in Cr alloys show that the volume effects strongly dominate here also.

Steinemann (1978) develops the Stoner-Wohlfarth (SW) theory for a weak itinerant ferromagnet to describe the temperature dependence of β and B and to relate their magnitudes. The theory might be expected to apply to itinerant antiferromagnets (Alberts and Lourens, 1984a). We shall follow the notation of Fawcett and Alberts (1990), who compared and contrasted the predictions of the SW theory with those of the Grüneisen-Testardi (GT) theory.

We adapt Steinemann's analysis to the SDW case by using a volume-dependent Néel temperature function $T_N(\omega)$, whose single-letter subscript distinguishes it from the equivalent function $T_{NT}(\omega)$ of the GT theory. The magnetic free energy is

$$\Delta F(t)=\Delta\phi(1-t^2)^2 , \tag{65a}$$

with

$$\Delta\phi=a[T_N(\omega)]^4 \tag{65b}$$

being a volume-dependent magnetic energy in the ground state, which is sometimes referred to as the "magnetic excitation potential."

Equations (65) give a magnetovolume

$$\Delta\omega(t)=-\frac{4\Delta\phi}{B}\Gamma_{\rm SW}(1-t^2) , \tag{66a}$$

with

$$\Gamma_{\rm SW}=-\frac{d\ln T_N(\omega)}{d\omega} \tag{66b}$$

being the SW Grüneisen parameter. Equation (66a) is of the same form as Eq. (62), since $\mu^2(t)=\mu^2(0)[1-t^2]$ in the Stoner approximation (Wohlfarth, 1968).

The volume thermal expansivity obtained from Eq. (66a),

$$\Delta\beta(t)=\left[\frac{8\Delta\phi}{B}\Gamma_{\rm SW}\right]t , \tag{67}$$

is linear in temperature. This simple result, and the corresponding quadratic temperature dependence of the magnetovolume in Eq. (66a), is equivalent to the assumption that the square of the amplitude of the SDW is quadratic in temperature. Alberts and Lourens (1984a) find that in CrAl, as in other Cr alloy systems, including CrGa, CrSi, and CrGe (Alberts and Lourens, 1988a), the magnetovolume is better described by including also a fourth-order term,

$$\frac{\Delta\omega(t)}{\Delta\omega(0)}=A_0+A_1t^2+A_2t^4 . \tag{68}$$

This is a natural extension of the SW theory for a ferromagnetic metal (Edwards and Wohlfarth, 1968), in which the free energy is expanded in even powers of the moment μ, with $\mu\sim t^2$, and is normally cut off at the quadratic term for a weak itinerant ferromagnet. Baran *et al.* (1992) find that in CrAl the neutron-diffraction intensity, which measures $\mu^2(t)$ in the ordered phase, as well as the magnetic contribution to the bulk modulus, is of the form of Eq. (68).

The magnetic contribution to the bulk modulus obtained from Eqs. (65) is

$$\Delta B(t)=-4\Delta\phi\left[\left[\frac{d\ln T_N}{d\omega}\right]^2(3-t^2)+\frac{1}{T_N}\frac{d^2T_N}{d\omega^2}(1-t^2)\right] . \tag{69}$$

Steinemann's (1978) expressions for the logarithmic derivatives in Eq. (69), and the value for the volume derivative of the density of states in the tight-binding approximation, $d\ln N(0)/d\omega=5/3$ (Heine, 1967), give, according to Alberts and Lourens (1983, who correct a numerical error in Steinemann's analysis),

$$\left[\frac{d\ln T_N}{d\omega}\right]\left[\frac{1}{T_N}\frac{d^2T_N}{d\omega^2}\right]^{-1}=-\frac{3}{10} . \tag{70}$$

We have translated in Eqs. (69) and (70) the notation for a ferromagnet having a Curie temperature T_C to that for a SDW system having a Néel transition T_N, so that we should use for consistency the volume derivative of the susceptibility $\chi_0(\mathbf{Q})$ at the SDW wave vector $\mathbf{Q}$, instead of that of the density of states.

Alberts and Lourens (1983) point out that in Cr alloy

systems the negative of the magnetic Grüneisen parameter, $d\ln T_N/d\omega$ [see Eq. (51)], is normally very large, having typically a value 30, as in pure Cr (see Table VII), so that according to Eq. (70) the second derivative term, $(T_N)^{-1}d^2T_N/dw^2$, is of order 100, making the second term in Eq. (69) small, but not negligible, relative to the first term, which is of order 1000. Indirect experimental evidence (Muir *et al.*, 1987a, 1987b) shows, in fact, that in pure Cr the strain dependence of the Néel temperature is linear in strain to a very good approximation, as is physically reasonable, and the same is true for the Cr alloys that have been analyzed by the methods employed in these papers (see Sec. V.C and Fawcett and Alberts, 1990). Thus it appears that Eq. (69) may be simplified and written

$$\Delta B(t)\simeq -4\Delta\phi\left[\frac{d\ln T_N}{d\omega}\right]^2(3-t^2)\ . \tag{71}$$

We note that the SW theory gives a magnetic contribution at zero temperature to both the magnetovolume and the bulk modulus, from Eqs. (66) and (71), respectively,

$$\Delta\omega(0)=-\frac{4\Delta\phi}{B}\Gamma_{\rm SW} \tag{72a}$$

and

$$\Delta B(0)=-12\Delta\phi\Gamma_{\rm SW}^2\ . \tag{72b}$$

Comparison of these two results provides therefore a measure of the SW Grüneisen parameter

$$\Gamma_{\rm SW}=\frac{1}{3B}\frac{\Delta B(0)}{\Delta\omega(0)}\ . \tag{73}$$

When the second derivative term in Eq. (69) is not negligibly small, the full expression should be used; but, more importantly, in this case there may be an appreciable magnetic contribution to the shear modulus

$$\Delta G(t)=-4\Delta\phi\left[\frac{1}{T_N}\frac{d^2T_N}{d\gamma^2}\right](1-t^2) \tag{74a}$$

with

$$\gamma=\epsilon_{ii}\quad(i=4,5,6)\ . \tag{74b}$$

The shear term in the magnetoelasticity is found to be large in CrRu alloys, for example, where a sizable anomaly appears at the incommensurate-commensurate SDW phase transition, as we shall see in Sec. V.C.6.

We now consider the Grüneisen-Testardi (GT) theory, for which the magnetic free energy in the ordered state below T_N is written (Fawcett, 1989a)

$$\begin{aligned}&\Delta F(t)=f[t_{NT}(\omega)]\ ,\\ &t_{NT}(\omega)=T/T_{NT}(\omega),\quad T<T_N\end{aligned} \tag{75a}$$

and in the paramagnetic phase, above T_N,

$$\begin{aligned}&\Delta F(t)=g[t_{\rm SF}(\omega)]\ ,\\ &t_{\rm SF}(\omega)=T/T_{\rm SF}(\omega),\quad T>T_N\ .\end{aligned} \tag{75b}$$

The Néel temperature function $T_{NT}(\omega)$ (where the T in the subscript denotes Testardi, 1975) is thus distinguished from the spin-fluctuation-temperature function $T_{\rm SF}(\omega)$, in accordance with the experimental fact that in Cr and Cr alloys the two quantities give very different magnetic Grüneisen parameters (Fawcett, 1989a; Fawcett and Alberts, 1990).

It is then argued that, close to the Néel temperature, the second derivative for both $f(t)$ and $g(t)$ will be large compared with the first derivative. In the approximation that the latter can be neglected, two magnetic Grüneisen parameters are thus obtained,

$$\Gamma_{NT}=-\frac{d\ln[T_{NT}(\omega)]}{d\omega}=-\frac{1}{B_NT_N}\lim_{t\le 1}\left[\frac{\Delta B(t)}{\Delta\beta(t)}\right] \tag{76a}$$

and

$$\Gamma_{\rm SF}=-\frac{d\ln[T_{\rm SF}(\omega)]}{d\omega}=-\frac{1}{B_NT_N}\lim_{t\ge 1}\left[\frac{\Delta B(t)}{\Delta\beta(t)}\right]\ , \tag{76b}$$

where B_N is the bulk modulus at T_N.

In practice, in Cr (Fawcett, 1989a) and some Cr alloys (Fawcett and Alberts, 1990, 1992b), AFM compounds (Fawcett, 1989c), and even ferromagnetic alloys (Fawcett *et al.*, 1992), it is found that $\Delta B(t)$ is proportional to $\Delta\beta(t)$ over a wide range of temperature, both below and above T_N, but often the linearity of the plot of $\Delta B(t)$ vs $\Delta\beta(t)$ does not extend to $t=1$. The reason may be the existence of critical fluctuations, which develop close to the ordering transition; but in any case the values of Γ_{NT} and $\Gamma_{\rm SF}$ are determined from the linear regions of the plots, provided they extend over a reasonably wide range of t.

In the case of Cr and Cr alloys, the paramagnetic alloy Cr+5 at. % V, denoted P, is assumed to have no magnetic component in β and B, so that $\Delta\beta$ and ΔB for the SDW system $Cr_{1-x}A_x$ may be defined in terms of the experimental data by

$$\Delta\beta(x,t)=\beta(x,t)-\beta(P,t) \tag{77a}$$

and

$$\Delta B(x,t)=B(x,t)-B(P,t)\ . \tag{77b}$$

Other reference materials, or a construct such as extrapolation of $\beta(t)$ and $B(t)$ from the paramagnetic phase back into the ordered phase (Fawcett *et al.*, 1992), are used for the other systems.

In many cases it is not feasible to analyze the magnetoelastic anomalies at the Néel temperature T_N by use of Eqs. (76), since $\Delta\beta(t)$ and $\Delta B(t)$ may not be proportional over any significant temperature interval. This is usually the case for the phase transition at temperature T_{IC} between the incommensurate AF_1 and the commensurate AF_0 phases. There is, furthermore, no fundamental theoretical basis for using an equation for the difference between the free energy in the two phases of the form of Eq. (75a).

Nevertheless, even in these cases, the relative *sign* of the anomalies $\Delta\beta(T)$ and $\Delta B(T)$ around the phase-transition temperature T_i (T_N or T_{IC}) provides useful information about the sign of the pressure dependence of T_i. This qualitative result may be seen by the use of the Grüneisen-Testardi magnetic free energy as given in Eq. (75); but, being thermodynamic in nature, it does not depend on the specific form of the equation. Following Fawcett (1989a) and Fawcett and Alberts (1992a), we obtain the qualitative equations

$$\Delta\beta(T)=\frac{1}{T_i}\frac{d\Delta\omega}{dT}=\frac{1}{T_i}\frac{d}{dT}\left[\frac{1}{B(T)}\frac{d\Delta F}{d\omega}\right] \sim -\frac{d\ln T_i}{d\omega}\sim+\frac{dT_i}{dp} \tag{78a}$$

and

$$\Delta B(T)=\frac{d^2\Delta F}{d\omega^2}\sim-\left[\frac{d\ln T_i}{d\omega}\right]^2 \tag{78b}$$

for a phase transition at temperature $T_i(\omega)$, where in Eq. (78b) we neglect the second derivative, $(T_i)^{-1}d^2T_i/d\omega^2$, relative to $d\ln T_i/d\omega$.

Equation 78(b) shows that $\Delta B(T)$ is always negative. This in fact is the case in Cr alloy systems, which always soften around the various phase transitions. Thus the sign of the thermal-expansion anomaly $\Delta\beta(T)$ gives directly, according to Eq. 78(a), the sign of the pressure dependence dT_i/dp of the phase-transition temperature. The experimental confirmation of this prediction will be discussed in Sec. V.C.1 in connection with data presented in Table IX, and for specific Cr alloy systems, in particular, CrMn, CrRu, and CrGa, in other parts of Sec. V.C.

This analysis can be made semiquantitative so as to provide a rough estimate of the magnetic Grüneisen parameter Γ_{IC} at the incommensurate-commensurate SDW phase transition by use of an Ehrenfest-like equation,

$$\Gamma_{IC}=-\frac{d\ln T_{IC}}{d\omega}=-\left[\frac{1}{BT}\frac{\Delta B}{\Delta\beta}\right]_{IC}, \tag{79}$$

analogous to Eqs. (76). In Eq. (79) all the quantities are determined at T_{IC}, and the resultant values of Γ_{IC} are compared with $\Gamma_I=B_{IC}\,d\ln T_{IC}/dp$ [see Eq. (51)] in Table X in Sec. V.C.1.

The fact that Γ_{IC} is much smaller than Γ_I for a Cr+0.3 at. % Ru single crystal, as shown in Table X, demonstrates a serious limitation of this method for determining the magnetic Grüneisen parameter. Alberts *et al.* (1992) suggest that Eq. (79) is suitable only for determining the sign, but not the magnitude, of Γ_{IC}, when as in this case the phase transition is strongly first order. The same limitation may be expected to apply to Eq. (79); but, fortunately, in most Cr alloy systems the Néel transition is continuous, or at least weakly first order as in pure Cr.

More serious reservations about the fundamental significance of magnetic Grüneisen parameters determined by these methods are indicated in recent work by Cankurtaran *et al.* (1992) on the pressure dependence of the elastic constants of the same CrRu sample. They find from the pressure dependence of the acoustic-mode frequencies ω_i corresponding to the elastic constants c_i that the acoustic-mode Grüneisen parameters, $\Gamma_i=-d\ln\omega_i/d\ln V$, are much larger than Γ_I. The values of Γ_i are rather different in the incommensurate and commensurate SDW phases. Perhaps only coincidentally, the values of Γ_i in the commensurate SDW phase for the longitudinal and shear modes are roughly equal in magnitude to Γ_{IC} and Γ_{GIC} in Table X, with, however, opposite sign for the longitudinal mode.

The analysis in the low-temperature region is more complicated (Fawcett, 1989a), since a volume-dependent prefactor $\phi(\omega)$ must be introduced to give a nonzero value of $\Delta B(0)$, the magnetic contribution to B at zero temperature. A zero-temperature Grüneisen parameter Γ_0 is, however, easily defined by writing

$$\Delta F=\phi(\omega)h[t],\quad t=T/T_N\gtrsim 0, \tag{80a}$$

which gives

$$\Gamma_0=\frac{1}{B_0}\frac{\Delta B(0)}{\Delta\omega(0)}=-\frac{d\ln\phi'}{d\omega}=-\frac{\phi''}{\phi'}, \tag{80b}$$

where $\Delta\omega(0)$ is the magnetovolume, and B_0 the bulk modulus in the limit of zero temperature.

We note that Γ_0, as defined for the GT theory in terms of the experimental parameters in Eq. (80b), is equal to $3\Gamma_{SW}$, as defined for the SW theory in Eq. (73). The interpretation is different in the two theories. Γ_{GT} is connected to the volume dependence of a prefactor $\phi(\omega)$, as introduced in Eq. (80a), with T_N regarded as constant. On the other hand, Γ_{SW} is the logarithmic derivative with respect to volume of $T_N(\omega)$, as defined in Eqs. (65) and (66). We shall normally use the definition of Γ_0 as defined in Eq. (80b), though H. L. Alberts and coworkers use Γ_{SW}. We note also that in the previous literature (Fawcett, 1989a; Fawcett and Alberts, 1990) Γ_0 was denoted Γ_{GT}.

Another Grüneisen parameter appropriate for the temperature region, $0<t\ll 1$, where both the specific heat C_e per unit volume and the thermal expansivity β_e for pure Cr and some Cr alloys are linear in temperature, in particular for CrV alloys as described in Sec. V.C.2, is

$$\Gamma_e=\frac{\beta_e B(0)}{C_e}. \tag{81}$$

The subscript e denotes electronic, as opposed to the lattice contributions, which are roughly cubic in temperature and dominate at higher temperatures.

The magnetic Grüneisen parameter corresponding to shear strain, ϵ_{ii} ($i=4,5,6$), may be written

$$\Gamma_{GN}=-\frac{d\ln[T_N(\epsilon_{ii})]}{d\epsilon_{ii}}=-\frac{1}{B_N T_N}\lim_{t\to 1}\left[\frac{\Delta G(t)}{\Delta\beta(t)}\right]. \tag{82}$$

This equation refers to pure strain in a single crystal; but in all cases that we consider, the shear modulus G was obtained by measuring the transverse sound velocity in a polycrystalline sample. In fact, CrRu alloys (see Sec. V.C.6) are unique in showing anomalies in the temperature dependence of $G(t)$ as well as $B(t)$, and both occur at the incommensurate-commensurate SDW phase transition at temperature T_{IC}, rather than at the Néel temperature T_N (Alberts and Lourens, 1988b).

C. Experiment: pressure effects and magnetoelastic properties

1. Cr alloy systems in general

The initial pressure dependence of the Néel temperature for all Cr alloy systems in which it has been measured is listed in Table VII. We also give the value of the magnetic Grüneisen parameter Γ_N calculated by use of Eq. (51), with the measured value of the bulk modulus B_N at the Néel temperature T_N, where it is available in the literature, as discussed in the relevant subsection of Sec. V.C. Otherwise, we use the value $B_N = 200$ GPa, which is the approximate value for the paramagnetic alloy Cr+5 at. % V, over the range of temperatures from zero to 500 K (Alberts, 1990); though in cases when Γ_N is large, the value of B_N at the Néel temperature may be considerably smaller.

The values of Γ_N are usually as large as, or in some cases much larger than, the value $\Gamma_N = -27$ for pure Cr. This provides a direct demonstration of the fact that the magnetoelastic coupling is strong throughout the AFM Cr alloy systems.

In Table VIII we list the pressure dependence of the phase-transition temperature for each of the three phase boundaries that intersect at the triple point in the pressure-temperature phase diagram. Again the values are large; and for the incommensurate-commensurate SDW phase transition (IC), the value of dT_{IC}/dp in some cases is more than an order of magnitude larger than the value $dT_N/dp = -50$ K(GPa)$^{-1}$ for pure Cr. We have not listed the corresponding Grüneisen parameters, but they may be easily calculated by use of equations

TABLE VIII. Pressure dependence, near the triple-point temperature T_L and pressure p_L, of the Néel temperature of the transition from the paramagnetic phase to the incommensurate SDW phase (I), T_{NI}, and to the commensurate SDW phase (C), T_{NC}, and of the temperature T_{IC} of the incommensurate-commensurate SDW phase transition for chromium alloy systems $Cr_{1-x}A_x$.

Solute	Composition	Triple point					Reference (figure)
A	x (at. %)	T_L (K)	p_L (GPA)	$\frac{dT_{NI}}{dp}$ (K/GPa)	$\frac{dT_{NC}}{dp}$ (K/GPa)	$\frac{dT_{IC}}{dp}$ (K/GPa)	
Mn	0.7	300	0.5	−50	−350		a
	1.8	290	1.5	−50	−250		(Fig. 43)
	0.5	340	0.6		−230	200	b
							[Fig. 44(b)]
Re	4	400	2.5	−25	−125		c
Fe	2.1					−350	b
	3.0	245	0.05	−150	−50	−150	[Fig. 44(d)]
	2.8	245	0.04	−200	−75	−200	d
Co	2.0	260	0.15	−100	−300	−1500	[Fig. 44(f)]
Ru	0.3	320	0.15	−50	−300		e
	0.6	310	0.75	−50	−500		(Fig. 43)
	0.3	315				300	f
Os	2.5–10	320	~2	−20 to −120	−30 to −120		g
	(7 samples)	to 500					[Fig. 49(a)]
Ga	1.1	260	0.5	−30	−65	−240	h
							(Fig. 51)
	0.7–1.2					−120	i
	(3 samples)						
Si	1.85	130	0.35	−100	−330		j
Ge	0.5	270	0.3	−60	−600	400	k
	0.5	280	0.2	−60	−1200	1600	l
	0.7	270	0.35	−50	−1000	1400	(Fig. 55)

[a]Jayaraman *et al.* (1970).
[b]Mizuki *et al.* (1982).
[c]Butylenko and Kobzenko (1981).
[d]Fawcett and Vettier (1982).
[e]Jayaraman *et al.* (1976).
[f]Alberts *et al.* (1992); Cankuratan *et al.* (1992).
[g]Butylenko and Nevdacha (1980c).
[h]Kaneko *et al.* (1982).
[i]Alberts and Lourens (1984b).
[j]Endoh *et al.* (1982).
[k]Mizuki and Endoh (1982).
[l]van Rijn and Alberts (1986a).

analogous to Eqs. (51) or (52), by substitution of the triple-point temperature T_L instead of T_N, and the value of B at T_L.

With the exception of CrNi and CrPd, all Cr alloy systems $Cr_{1-x}A_x$ with transition metals A of groups 7 and 8 of the periodic table exhibit a triple point at a concentration x_L of A, with the Néel transition for $x > x_L$ being to the commensurate SDW phase. The same is true for alloys with groups-3 and -4 nontransition metals. For these systems, in the concentration range $x_L < x < x_0$, on further decreasing the temperature there is a transition to the incommensurate SDW phase at temperature T_{IC}, with T_{IC} going to zero at $x = x_0$. The only exception to this type of behavior is the CrFe alloy system, for which the transition to the incommensurate SDW phase occurs with *increasing* temperature, for $x \lesssim x_L$ (Ishikawa *et al.*, 1967).

In all systems that have been measured, the thermal expansitivity $\beta(T)$ shows a minimum near the Néel transition from the paramagnetic phase to either the incommensurate or the commensurate SDW phase. The transition at T_{IC} from the incommensurate to the commensurate SDW phase, on the other hand, often shows a *maximum* in $\beta(T)$, as we shall see, for example, in Figs. 45(c) and 45(e) (see also Kondorskii *et al.*, 1978); but in some cases no anomaly at all is seen at this transition. Again CrFe alloys are exceptional, since they show a strongly first-order hysteretic transition to the commensurate SDW phase either from the paramagnetic phase or from the incommensurate SDW phase (Edwards and Fritz, 1973, 1974; Fawcett and Vettier, 1982).

In most cases, when a maximum in $\beta(T)$ is seen at T_{IC}, an anomaly is also seen at this phase transition in the temperature dependence of the bulk modulus $B(T)$, which is always a minimum, like that at T_N, though not as pronounced, as we shall see, for example, in Figs. 48(b) and 48(e). In some cases, when the two phase-transition temperatures T_N and T_{IC} are close, the two minima in $B(T)$ coalesce to form a single broad minimum, as shown, for example, in Figs. 45(d) and 45(f).

The system CrRu is remarkable in that it shows a minimum also in the temperature dependence of the shear modulus $G(T)$ at the incommensurate-commensurate SDW phase transition, as shown in Figs.

TABLE IX. Experimental observation of anomalies in the magnetoelastic properties of Cr alloy systems at the Néel transition at temperature T_N and at the incommensurate-commensurate (IC) SDW phase transition at temperature T_{IC}.

Property	Group	Anomaly at T_N	Anomaly at T_{IC}	Reference
Thermal expansion β	5	CrV	–*	a
	6	CrMo	–	b
	7	CrMn	$\widehat{\text{CrMn}}$†	c,d
		CrRe	×‡	e
	8	CrFe	$\widehat{\text{CrFe}}$§	d,f
		CrCo	×	g
		CrRu	$\widehat{\text{CrRu}}$	g
		CrOs	×	e
		CrPt	$\widehat{\text{CrPt}}$	i
	3	CrAl	×	j
		CrGa	$\widehat{\text{CrGa}}$	k
	4	$\underbrace{\text{CrSi}}$	$\widehat{\text{CrSi}}$	i
		CrGe	$\widehat{\text{CrGe}}$	m
Bulk modulus B or Young's modulus Y‖	5	CrV	–	n
	6	CrMo	–	b
	7	CrMn	CrMn	c
		CrRe(Y)	CrRe(Y)	o
	8	CrFe	CrFe	p
		CrFe(Y)	CrFe(Y)	f
		CrRu	CrRu	h,q
		CrRu(Y)	CrRu(Y)	o
		CrRu(Y)	CrRh(Y)	o
		CrPt	CrPt	i
	3	CrGa	CrGa	k
		CrAl	×	s

TABLE X. (*Continued*).

Property	Group	Anomaly at T_N	Anomaly at T_{IC}	Reference
	4	CrSi	×	l
Shear		CrGe	CrGe	m
modulus G ¶	8	CrFe	CrFe(Y)	p
		×	CrRu	h,q
	4	CrSi	×	l,r

*CrV and CrMo are also listed for completeness, though these Cr alloy systems do not exhibit a commensurate SDW phase. The dash symbol (–) indicates accordingly that the *IC* SDW phase transition does not exist. To our knowledge this tabulation of elastic constant references is thus complete, but thermal-expansion data exist for some other Cr alloy systems, in particular, CrN, CrLu, CrHf, CrTa, and CrW (Butylenko and Gridnev, 1964).

†The hat symbol ($\hat{A}$) indicates that the thermal-expansion anomaly at T_{IC} in the CrA alloy system is a maximum.

‡The cross symbol (×) indicates that no anomaly is observed at this transition.

§The under-bracket symbol $\underset{\frown}{\mathrm{Cr}A}$ indicates that a first-order transition occurs at T_N or T_{IC} in the CrA alloy system.

‖The notation (Y) for both the transition at T_N and that at T_{IC} indicates that a broad, deep minimum was observed in B and/or Y which, as described in the text, is interpreted as being the result of the coalescence of two unresolved minima.

¶Cr alloy systems in which the shear modulus G was measured, but no anomaly was observed either at the Néel transition or at the *IC* SDW phase transition: CrCo, CrAl, CrGa, and CrGe, and also the two systems CrV and CrMo that do not have a triple point.

[a]White *et al.* (1986).
[b]Venter *et al.* (1986).
[c]Alberts and Lourens (1987).
[d]Butylenko (1989).
[e]Butylenko (1985).
[f]Hausch and Török (1977).
[g]Alberts and Lourens (1983).
[h]Alberts and Lourens (1988b).
[i]Alberts and Lourens (1988c).
[j]Alberts and Lourens (1984a).
[k]Alberts and Lourens (1985).
[l]Alberts and Lourens (1988a).
[m]van Rijn *et al.* (1987).
[n]de Camargo and Brotzen (1982).
[o]Munday (1971).
[p]Edwards and Fritz (1973,1974).
[q]Alberts and Boshoff (1992).
[r]Anderson *et al.* (1993).
[s]Baran *et al.* (1992).

48(c) and 48(f). The only other Cr alloy systems that exhibit an anomaly in the shear modulus are CrFe and CrSi, but this anomaly, also a minimum, is associated with the strongly first-order transition at T_N seen in these systems.

While $B(T)$ exhibits minima at both T_N and T_{IC}, reference to Table IX shows that the thermal expansion $\beta(T)$ always exhibits a minimum at T_N, but either a maximum at T_{IC} or no anomaly at all, with CrFe being exceptional, as noted earlier, because of the first-order transition to the commensurate SDW phase. Thus, according to Eq. (78a), the pressure dependence of T_{IC} is positive for the Cr alloys systems CrMn, CrRu, CrPt, CrGa, CrSi, and CrGe, while dT_N/dp is always negative, as for pure Cr. This prediction is confirmed in CrMn (Mizuki *et al.*, 1982), CrRu (Sidek *et al.*, 1993), and CrGe (van Rijn and Alberts, 1986a), while the pressure-temperature phase diagram has not been measured for CrPt. In CrSi the incommensurate-commensurate SDW phase boundary, as determined by neutron-diffraction measurements under pressure (Endoh *et al.*, 1982), is poorly defined, so that dT_{IC}/dp cannot be determined. Only CrGa, for which dT_{IC}/dp is negative (see Fig. 51), seems to contradict this prediction, as we shall discuss in Sec. V.C.7.

Values are given in Table X for the magnetic Grüneisen parameter Γ_{IC} obtained from the Ehrenfest-like equation (79) applied to the magnetoelastic anomalies at the incommensurate-commensurate SDW phase transition. The shear-strain magnetic Grüneisen parameter Γ_{GIC} is estimated for CrRu from data present-

TABLE X. Magnetic Grüneisen parameters of Cr alloy systems $Cr_{1-x}A_x$ at the incommensurate-commensurate (*IC*) SDW phase transition. Γ_{IC} is the volume strain and Γ_{GIC} the shear-strain magnetic Grüneisen parameter, while Γ_I is obtained from the pressure dependence of T_{IC}.

Solute *A*	Concentration *x* (at. %)	Γ_{IC}	Γ_I	Γ_{GIC}	Reference
Mn	0.23	?	200		1/2*
	0.33	?			
Ru	0.3	5	215	1	3/4
	0.5	5		3	
Pt	0.3	<5			5
Ga	1.4	25	−60		6/7,8
Ge	0.7	10	170		9/10

*The notation 1/2 means that Γ_{IC} (and Γ_{GIC} in the case of CrRu) is obtained from data in Ref. 1, and Γ_I from Ref. 2. The question mark (?) here means that Γ_{IC} can in principle be determined for this system, but not in practice from the data given in Ref. 1.

[1]Alberts and Lourens (1987).
[2]Mizuki *et al.* (1982).
[3]Alberts and Lourens (1988b).
[4]Alberts *et al.* (1992); Cankurtaran *et al.* (1992).
[5]Alberts and Lourens (1988c).
[6]Alberts and Lourens (1985).
[7]Kaneko *et al.* (1982).
[8]Alberts and Lourens (1984b).
[9]van Rijn *et al.* (1987).
[10]van Rijn and Alberts (1986a).

ed in Sec. V.C.6, by use of the equation for shear strain analogous to Eq. (79).

We proceed in Sec. V.C to discuss the magnetoelasticity experimental data for individual Cr alloy systems. We note that no data are available for CrTi, CrNb, CrTa, CrW, CrNi, CrPd, CrIr, CrAu, ,CrBe, and alloys of Cr with rare-earth metals, all of which Cr alloy systems were discussed in Sec. II.C.

2. Cr alloys with the group-5 transition metal V

The CrV alloy system has featured large in the history of research on AFM Cr alloys and, in particular, on their magnetoelastic properties. The results of Rice, Barker, *et al.* (1969) for two CrV alloys, shown in Fig. 39, and those of de Dood *et al.* (1970), listed in Table VII, were found to be consistent with Eq. (64) for the nesting Fermi-surface model of an antiferromagnet. The values of dT_N/dp for the two CrV samples shown in Fig. 39 are not given in Table VII, since it is misleading to give the value averaged over a wide pressure range when $T_N(p)$ is exponential in form.

Rice, Jayaraman, and Mewhan (1969) point out that the way in which antiferromagnetism vanishes for the Cr+2.8 at. % V alloy, and for the two CrMo alloys shown in Fig. 39, is consistent with the form they predict, $T_N(p) \sim (p_c - p)^{1/2}$, where p_c is a critical pressure. They show that this form is consistent with the gap equation for a more general two-band model than that considered by Fedders and Martin (1966).

Roberts *et al.* (1983) and White *et al.* (1986) used a paramagnetic alloy, Cr+5 at. % V, as the reference to determine by subtraction the magnetic contribution to the thermal expansion of pure Cr and an alloy Cr+0.5 at. % V. The magnetic contributions to the bulk

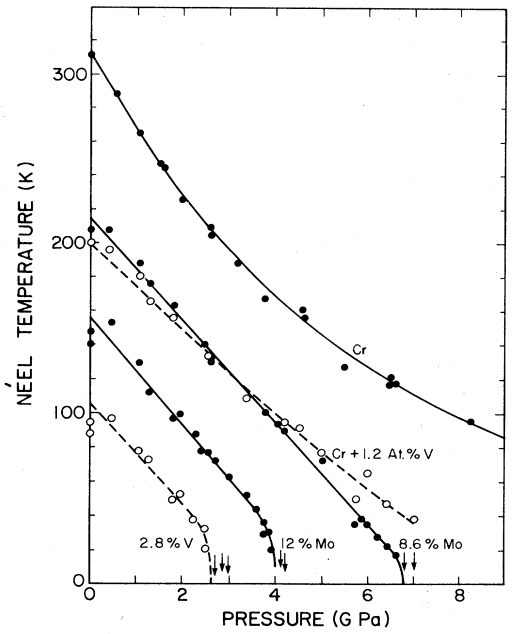

FIG. 39. Pressure dependence of the Néel temperature T_N for pure Cr and Cr alloys with V and Mo. The vertical arrows show pressures at which no anomaly in the temperature dependence of the resistivity, which was used to determine T_N, could be observed down to temperature 4.2 K (from Rice, Barker, *et al.*, 1969).

TABLE XI. Ground-state magnetovolume $\omega_0(x)$ and low-temperature electronic Grüneisen parameters for $Cr_{1-x}V_x$ alloys (from Kaiser *et al.*, 1985; see also Fawcett *et al.* 1986b).

x	(at. %)	0	0.5	1.5	2.5	3.45	5
T_N	(K)	311	263	150	105	28	para.
B_e/T	(10^{-8} K^{-2})	−1.08	−1.14	−1.50	−1.56	−1.80	−0.33
ω_0	(10^{-6})	1430	920		165	10	
ω_0/T_N^2	(10^{-8} K^{-2})	1.47	1.32		1.50	1.27	
C_e/T	(mJ mol^{-1} K^{-1})	1.45	1.5	1.6	1.8	2.1	2.3
Γ_e		−10.5	−11	−13	−12	−12	
Γ_E		−35	−30	−35	−50	−150	

modulus of pure Cr was determined in a similar fashion (Muir *et al.*, 1987a, 1987b) by subtraction from that of Cr+5 at. % V, which was published later (Alberts, 1990). This method of comparing the thermal expansion and bulk modulus of a Cr alloy with those of Cr+5 at. % V, in order to determine their magnetic contributions, has been used extensively by H. L. Alberts and co-workers. In some cases the magnetic contributions thus obtained have been used to determine the magnetic Grüneisen parameters by use either of the Stoner-Wohlfarth analysis or of the Grüneisen-Testardi analysis described in Sec. V.B.

The change in nature of the Néel transition from first order in pure Cr to continuous in an alloy containing as little as 0.2 at. % V (Fawcett, Roberts, *et al.*, 1986; de Camargo *et al.*, 1988) is an interesting magnetoelastic effect, which is believed not to be specific to V as an impurity. It is suggested (Fawcett *et al.*, 1991) that this effect may be related to the decrease in the spin-fluctuation Grüneisen parameter γ_{SF} in the paramagnetic phase defined in Eq. (76b), which is produced by doping with V (Fawcett, 1988b). Both effects are no doubt associated with the existence of a moment on the V atom in the paramagnetic phase (see Sec. II.C.2 and Sec. III), but no theory relevant to this situation is available.

The effect of V doping on the thermal expansion of Cr has also been important in guiding efforts to develop a more fundamental understanding of magnetovolume effects in Cr alloy systems. Kaiser and Haines (1985) analyzed the data of White *et al.* (1986) for Cr+0.5 at. % V, following the formalism of Holden *et al.* (1984) described in Sec. V.A. The relevance of the Cr alloy results to the spin-split state proposed by Hirsch (1990) as an alternative to the SDW state was discussed by Kaiser *et al.* (1992) and Kaiser and Oles (1993), who adduce a considerable body of evidence to demonstrate the inadequacies of this proposal.

Finally, we show in Table XI the data for the low-temperature thermal expansion (White *et al.*, 1986) and specific heat (Heiniger *et al.*, 1965; Takeuchi *et al.*, 1980). The electronic Grüneisen parameter Γ_e calculated by use of Eq. (81) is seen to be roughly constant, but the value is considerably smaller than the magnetic Grüneisen parameters of pure Cr, which are typically of the order of magnitude 50 (Fawcett, 1989a).

A magnetic Grüneisen parameter Γ_E having more physical significance may be obtained by using a definition,

$$\Gamma_E(x)=\frac{\Delta\beta_e(x)B(0)}{\Delta C_e(x)} \tag{83a}$$

with

$$\Delta\beta_e(x)=\beta_e(x)-\beta_e(P),\quad \Delta C_e(x)=C_e(x)-C_e(P)\ , \tag{83b}$$

where $\beta_e(P)$ and $C_e(P)$ are the thermal expansivity and electronic specific heat per unit volume of the paramagnetic alloy Cr+5 at. % V. Thus $\Delta\beta_e$ and ΔC_e may be regarded as magnetic contributions, which define a magnetic Grüneisen parameter in the spirit of the Grüneisen-Testardi Eqs. (76) and (77). The resultant values of Γ_E given in Table XI are, in fact, more similar in magnitude to the values for Γ_N of the Cr alloys in Table VII and the values Γ_i of the Grüneisen-Testardi parameters shown in Figs. 64 and 72 for the Cr alloy systems CrMo and CrAl, respectively.

Kaiser *et al.* (1985) point out that the rough proportionality between $\omega_0(x)$ and $T_N^2(x)$ shown in Table XII, together with the proportionality between T_N and the amplitude μ_0 of the SDW wave observed in many Cr alloy systems, as illustrated in Fig. 7, shows that the magnetovolume is proportional to μ^2, as expected from a fundamental theory of the magnetoelastic coupling (see Sec. V.A).

Other studies of magnetoelastic effects in CrV alloys include de Camargo and Brotzen's (1982) measurements of the elastic constants for Cr+0.67 at. % V and Cr+1.5 at. % V, and the ultrasonic attenuation around the Néel transition (Castro *et al.*, 1986).

3. Cr alloys with the group-6 transition metal Mo

We have chosen the $Cr_{1-x}Mo_x$ alloy system to illustrate in Fig. 40 the temperature dependence of the thermal expansivity and bulk modulus as the concentra-

TABLE XII. Ground-state magnetovolume $\omega_0(x)$ for $Cr_{1-x}Mn_x$ alloys (after Hausch *et al.*, 1976).

x	(at. %)	0	1.0	1.6	2.9	7.0	19.5
T_N	(K)	311	492	550	590	680	750
ω_0	(10^{-6})	1430	5100	5400	5600	6300	8400
ω_0/T_N^2	(10^{-8} K^{-2})	1.5	2.1	1.8	1.6	1.7	1.5

tion x of the solute metal is varied, in the case when the behavior in the alloys is not too different from that in pure Cr over a reasonably wide range of x.

The plot of $\Delta B(t)$ vs $\Delta\beta(t)$, as defined in Eqs. (77), for a typical alloy in this system that is illustrated in Fig. 41, shows linearity over a reasonably wide range of t both above and below the Néel temperature. In both cases deviation from linearity occurs close to the Néel transition, at $t=1$, perhaps due to critical fluctuations.

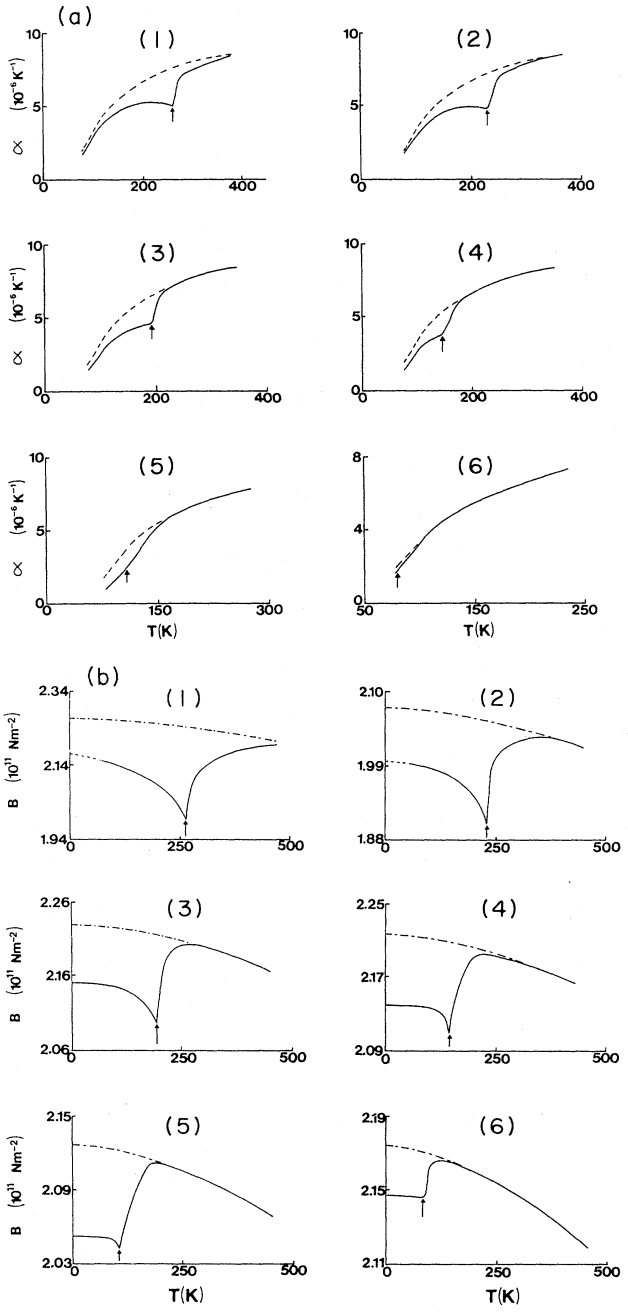

FIG. 40. Temperature dependence of (a) the linear thermal expansivity α (1/3 β) and (b) the bulk modulus B for the $Cr_{1-x}Mo_x$ alloy system. The concentration of Mo in at. % for the alloys is (1) 2.8; (2) 6.3; (3) 7.9; (4) 10.9; (5) 13.9; and (6) 17.4. The dashed line in (a) and dot-dashed line in (b) show the temperature dependence for the paramagnetic alloy Cr+5 at. % V, with the curves in (b) being displaced along the B axis so as to be asymptotic to the curve showing $B(T)$ for the CrMo alloy. The vertical arrow shows the Néel temperature estimated from the singularity in $B(T)$. From Venter *et al.* (1986).

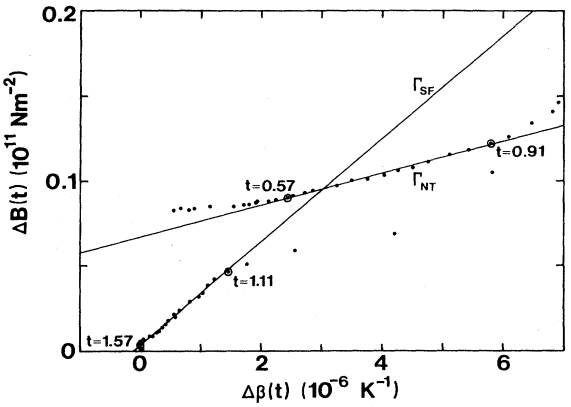

FIG. 41. Comparison of the magnetic contributions to the bulk modulus $\Delta B(t)$ and volume thermal expansivity $\Delta\beta(t)$ in Cr+6.25 at. % Mo. The reduced temperature $t=T/T_N$ is relative to the Néel temperature $T_N=230$ K. The lines are least-squares fits to the data points between and including the circled points, for which values of t are shown (from Fawcett and Alberts, 1990).

The dependence of the various magnetic Grüneisen parameters Γ_i defined in Eqs. (51), (76), and (79) on the alloy concentration x, illustrated in Fig. 42, shows monotonic variation for Γ_{SF} and Γ_{NT}, with $\Gamma_{SF}\simeq 3\Gamma_{NT}$ as for pure Cr (Fawcett, 1989a). Both Γ_{SF} and Γ_{NT} appear to extrapolate to zero at about $x=13$ at. % Mo, but both Γ_0 and Γ_N are increasing fairly rapidly with x at this

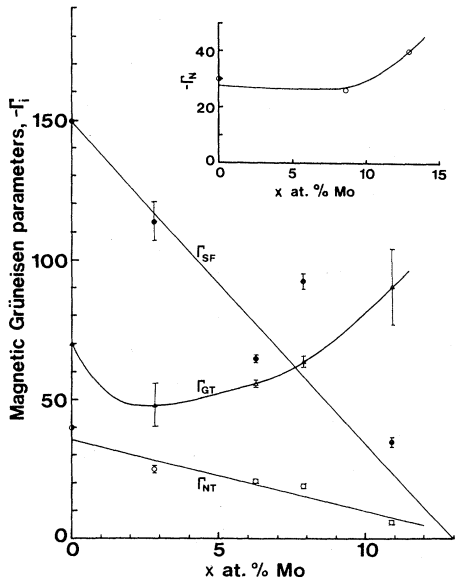

FIG. 42. Magnetic Grüneisen parameter Γ_i in the $Cr_{1-x}Mo_x$ alloy system: ●, Γ_{SF} for temperature, $T>T_N$; ○, Γ_{NT} for $T<T_N$; △, Γ_{GT} (3 Γ_{SW}) for zero temperature. Inset: ○, Γ_N for $T=T_N$ (from Fawcett and Alberts, 1990).

composition. This is interesting and unexpected behavior for a system in which the Néel temperature $T_N(x)$ decreases linearly to zero at $x=23$ at. % Mo, and which is sometimes assumed to be isomorphous with pure Cr.

Venter *et al.* (1986) showed, however, that, if one assumes a law of corresponding states for the $Cr_{1-x}Mo_x$ alloy system and interprets Eq. (62) to mean that the change in magnetovolume at zero temperature from that in pure Cr produced by the substitution of Mo may be written

$$\Delta\omega(x,0)=K\Delta\langle\mu^2(x,0)\rangle\ , \tag{84}$$

then the change in the mean-square moment determined by neutron diffraction (Cywinski and Hicks, 1986) agrees very well with their data, with $K=9.0\times10^{-3}$ $(\mu_B/\text{at. \% Mo})^{-2}$.

4. Cr alloys with group-7 transition metals Mn and Re

The pressure dependence of the Néel temperature T_N is shown in Fig. 43 for two $Cr_{1-x}Mn_x$ alloys having a composition $x>x_L=0.3$ at. % Mn, the triple-point concentration (see Fig. 12 and Table IV). The value of dT_N/dp at the triple point is considerably less for the transition to the incommensurate AF_1 phase than to the commensurate AF_0 phase, though both are negative (see Table VIII). The value of dT_{IC}/dp listed in Table VIII was obtained from the phase diagram shown in Fig. 44(b), which was determined by neutron diffraction (Mizuki *et al.*, 1982).

A parallel exists between the phase diagrams showing the effect of doping with Mn, shown in Fig. 44(a) (the triple point at $x_L=0.3$ at. % Mn is not shown), and the effect of negative pressure, shown in Fig. 44(b). This

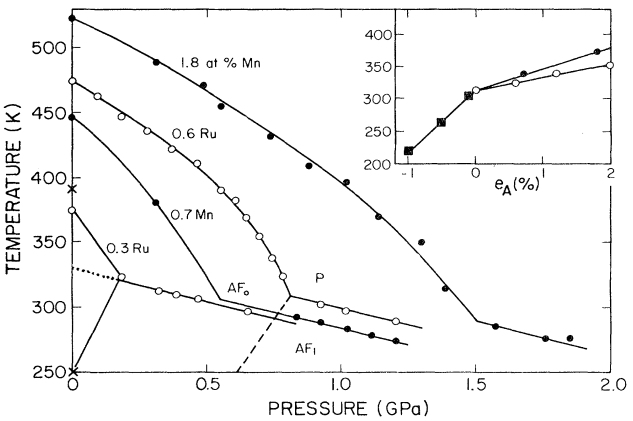

FIG. 43. Phase diagram in the pressure-temperature plane for Cr alloys with Mn and Ru. The dashed line showing the transition from the incommensurate to the commensurate SDW phase for Cr+0.6 at. % Ru is schematic. The dotted line shows the construction used to determine the Néel temperature T_{NI} of the incommensurate SDW phase by extrapolation to zero pressure. The values of T_{NI} are shown in the inset as a function of excess electron concentration e_A for these alloys and also for CrV alloys (■). After Jayaraman *et al.* (1970), with data for Cr+0.3 at. % Ru at ambient pressure (X) from Alberts and Lourens (1988b).

parallel between the composition-temperature and the pressure-temperature phase diagrams is seen in several other systems, and the result is especially striking when, as in $Cr_{1-x}Fe_x$, the incommensurate AF_1 phase lies at higher temperature than the commensurate AF_0 phase, as is seen in both Figs. 44(c) and 44(d). We shall discuss this interesting result further in Sec. V.C.5.

The thermal expansion and bulk modulus of CrMn alloys show interesting temperature dependence for concentrations x close to and above the triple point x_L, as shown in Fig. 45. According to Alberts and Lourens (1987), $x_L=0.20$ at. % Mn, and the composition $x=0.23$ at. % Mn shows peaks in the temperature dependence of the thermal expansivity $\beta(T)$ of opposite sign, with a broad and deep minimum in that of the bulk modulus $B(T)$. There are similar but even stronger effects for $x=0.33$ at. % Mn. These results are entirely consistent with the sign of the pressure dependence of T_N and T_{IC}, as illustrated in Fig. 44(b), in accordance with Eq. (78a).

The thermal expansivity maximum at the incommensurate-commensurate SDW phase transition corresponds to a point of inflection in the plot of strain ϵ vs temperature T, with $d\epsilon/dT$ being a maximum. This is seen clearly for $x>x_L\simeq0.3$ at. % Mn in the data for $Cr_{1-x}Mn_x$ alloys shown in Fig. 46. Butylenko and Nevdacha (1981) also measured the pressure dependence of the Néel temperature and attempted to construct the three-dimensional phase diagram for this system in temperature-pressure-composition space.

The inset to Fig. 43 shows the dependence on electron concentration of the Néel temperature to the hypothetical incommensurate phase at ambient pressure, which is obtained by extrapolating the P-AF_1 line of phase transitions back to zero pressure, as shown for the alloy Cr+0.3 at. % Ru. The data for V, Mn, and Ru solutes are consistent with the expressions derived by Zittartz (1967) for the depression of the Néel transition by the depairing effect produced by the scattering of electrons by the impurity

$$T_{NI}(x)=T_{NI}(0)-\frac{\pi}{4}\gamma x\ . \tag{85}$$

Ru appears to be a stronger scatterer than Mn, but the average suppression for the three metals follows Eq. (85), with $\gamma=40$ K/at. % (Jayaraman *et al.*, 1970).

The ground-state magnetovolume $\omega_0(x)$ in $Cr_{1-x}Mn_x$ alloys follows roughly the same law of corresponding states as that in CrV alloys, when compared with the Néel temperature $T_N(x)$. Comparison of Table XII for CrMn alloys with Table XI for CrV alloys shows that in both ω_0 is roughly proportional to T_N^2, with about the same constant of proportionality. The value of ω_0/T_N^2 is a little larger in the CrMn alloys, especially for the dilute alloys with $x=1.0$ and 1.6 at. % Mn, which may be due to a relatively rapid increase of ω_0 as the system passes through the triple point at $x_L=0.3$ at. % Mn (see Fig. 12). The pressure dependence of $T_N(p)$ in $Cr_{1-x}Mn_x$ alloys, however, which at low concentrations gives a plot

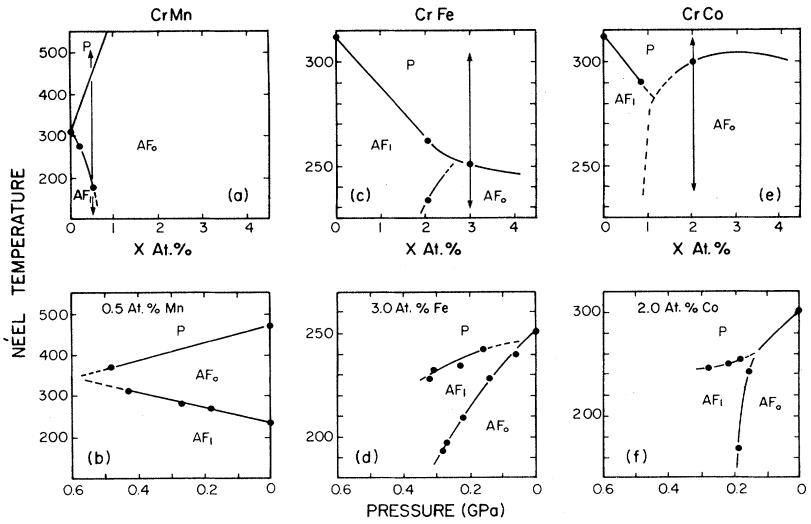

FIG. 44. Phase diagrams in the composition-temperature (x-T) and pressure-temperature (p-T) planes for Cr alloys with Mn, Fe, and Co. The vertical arrow in each (x-T) diagram shows the composition for which the (p-T) diagram is determined (from Mizuki *et al.*, 1982).

having negative curvature, with $d^2T_N/dp^2 < 0$, as seen in Fig. 43, changes over to a plot of positive curvature between $x = 5.3$ and 11.6 at. % Mn (Butylenko and Nevdacha, 1980c).

In much more concentrated $Cr_{1-x}Mn_x$ alloys, with $x \gtrsim 0.5$, a giant negative thermal-expansion anomaly develops at low temperatures (Shiga *et al.*, 1986; White *et al.*, 1989), but this should be regarded as being in the regime of AFM Mn, rather than Cr, alloys (see Sec. II.C.4).

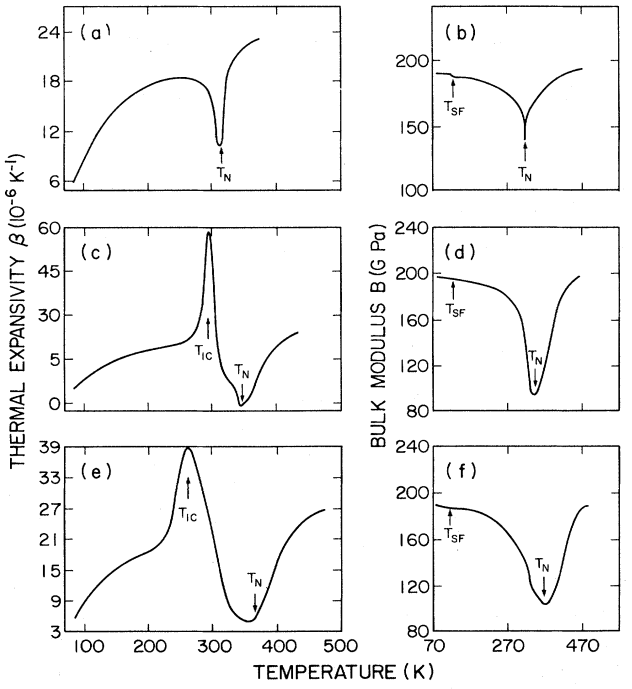

FIG. 45. Temperature dependence of the thermal expansivity and the bulk modulus for three $Cr_{1-x}Mn_x$ alloys having concentrations x of Mn around the triple point $x_L = 0.20$ at. % Mn: (a,b), $x = 0.09$; (c,d), $x = 0.23$; (e,f) $x = 0.33$ at. % Mn (data of Alberts and Lourens, 1987; from Fawcett and Alberts, 1992a).

In $Cr_{1-x}Re_x$ alloys we encounter again, as in CrMn alloys, the broad and deep minimum in the temperature dependence of the bulk modulus (Alberts, 1989) at concentrations, $x \gtrsim 0.3$ at. % Re, close to and above the triple point, which Fig. 13 shows to be at $x_L \lesssim 0.3$ at. % Re. This softening was first seen in early work by Munday (1971), who found the effect in the Young's modulus Y for CrRe, CrRu, and CrRh alloys, as shown in Fig. 47. Both CrRu and CrRh, like CrRe, have a triple point at a low concentration x_L, with the deep λ-type minimum in Y seen for $x \gtrsim x_L$. The explanation is undoubtedly that given for the similar but rather broader minimum for $B(T)$ in CrMn alloys seen in Figs. 45(d) and 45(f), i.e., the close proximity of the Néel transition to the incommensurate-commensurate phase transition at T_{IC}, both having a large magnetic Grüneisen parameter. No

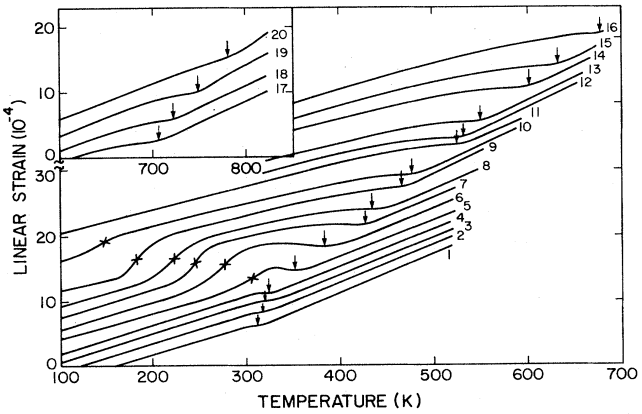

FIG. 46. Temperature dependence of the linear strain for $Cr_{1-x}Mn_x$ alloys having concentrations x in at. % Mn: 1—0.0; 2—0.1; 3—0.2; 4—0.3; 5—0.4; 6—0.5; 7—0.6; 8—0.7; 9—1.0; 10—1.25; 11—1.5; 12—2.0; 13—3.0; 14—4.0; 15—5.0; 16—6.0; 17—10; 18—20; 19—30; 20—34. The Néel temperature T_N is indicated by an arrow, and the incommensurate-commensurate SDW phase transition by a cross (after Butylenko, 1989).

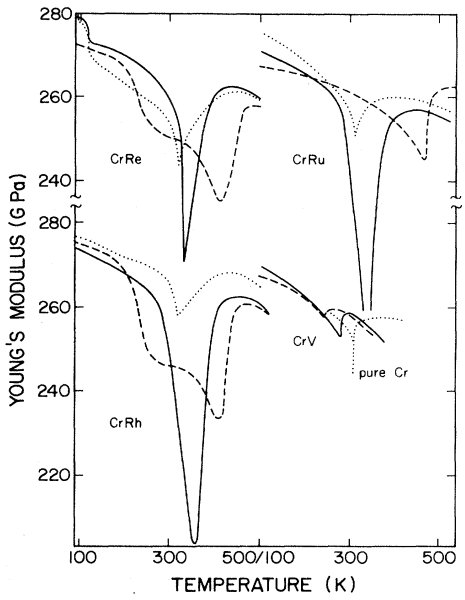

FIG. 47. Temperature dependence of the Young's modulus for CrRe, CrRu, and CrRh alloys having concentration x of the solute A in $Cr_{1-x}A_x$ around the triple points x_L, with data for CrV alloys and pure Cr for comparison. The concentrations x for the three samples of each Cr alloy system, and the triple-point concentration x_L, are

Solute (at. %)	Re	Ru	Rh	V	line
x_L	0.3	0.16	0.11		
x	0.15	0.15	0.12	0	· · · ·
x	0.30	0.27	0.20	0.29	——
x	0.62	0.69	0.30	0.61	– – –

(from Munday, 1971).

such effect occurs in CrV alloys, where no triple point exists, and the anomaly in the Young's modulus shows only a small steplike decrease, as seen in Fig. 47. In the case of CrRe, however, thermal-expansion measurements have not been done for alloys close to the triple point, so that it is not known whether the temperature dependence of the expansivity shows a minimum at T_N followed by a maximum at T_{IC}, as in CrMn [see Figs. 45(c) and 45(e)].

Boshoff *et al.* (1993) measured the various elastic moduli in single crystals of both CrRe and CrRu containing 0.3 and 0.5 at. % of each dopant. Their beautiful data illustrate the power of magnetoelastic studies of good uniform-composition single crystals to help us understand the nature of the various phase transitions in Cr alloys.

Butylenko and Kobzenko (1981) measured the pressure dependence of the Néel temperature in $Cr_{1-x}Re_x$, using the anomaly in the resistivity, and found also an incommensurate-commensurate transition at $T_{IC} \lesssim 400$ K for $x = 2$, 3, and 4 at. % Re, which suggests that the pressure-temperature phase diagram is similar to the concentration-temperature phase diagram, with increasing x corresponding to negative pressure, as for CrMn alloys [see Figs. 44(a) and 44(b)]. The initial pressure dependence decreases with increasing x, so that the magnetic Grüneisen parameter Γ_N defined in Eq. (51) decreases monotonically from about 20 for $x = 2$ to about 6 for $x = 15$ at. % Re.

5. Cr alloys with group-8 magnetic transition metals Fe and Co

The most interesting feature of the CrFe alloy system is the occurrence of the incommensurate SDW phase *above* the commensurate in the concentration-temperature phase diagram, as seen in Figs. 14 and 44(c). Similar behavior occurs in the pressure-temperature phase diagram, shown in Fig. 44(d), when pressure is applied to a $Cr_{1-x}Fe_x$ alloy having a composition $x > x_L = 2.3$ at. % Fe. Thus the two phase diagrams are quite similar, with increase of x corresponding to negative pressure, in both the CrFe and CrMn alloy systems, as seen in Fig. 44, except that the pressure dependence of the Néel temperature T_N at the transition to the AF_1 phase is negative, whereas decreasing x increases T_N for the corresponding branch of the phase diagram in Fig. 44(c).

This "rotation" of the branch of the pressure-temperature phase diagram in CrFe, corresponding to a change of sign of the pressure dependence of the incommensurate-commensurate SDW phase-transition temperature T_{IC}, was first observed by Syono and Ishikawa (1967), who contrasted it with the behavior of a CrMn alloy. We shall discuss further the nature of the various phase transitions in the CrFe alloy system in Sec. VI. The transitions to the commensurate SDW phase are strongly first order (Syono and Ishikawa, 1967), with volume increase with decreasing temperature through the transition of magnitude, $\Delta\omega \simeq 10^{-3}$ (Hausch and Török, 1977), which is much larger than that seen at the weak first-order transition in pure Cr, $\Delta\omega \simeq 3\times 10^{-5}$ (Fawcett, Roberts, *et al.*, 1986). This explains to some extent why the ratio of the ground-state magnetovolume $\omega_0(x)$ to the square of the Néel temperature $T_N(x)$ has a value, $\omega_0/T_N^2 = 5.0\pm 0.5$, for $x = 2.0$ to 6.8 at. % Fe (Hausch and Török, 1977), that is considerably larger than the values 1.4 ± 0.1 for CrV alloys (see Table XI) and 1.8 ± 0.3 for CrMn alloys (see Table XII).

Hausch and Török (1977) also measured the Young's modulus Y and bulk modulus B around the Néel temperature T_N in CrFe alloys and found a λ-type anomaly at T_N in the temperature dependence of both, similar to those seen for CrRe, CrRu, and CrRh by Munday (1971), as shown in Fig. 47. They also found a small λ-type anomaly in the shear modulus G measured by the torsional method, but *not* by the ultrasonic-velocity method, which shows a small steplike decrease as temperature decreases through T_N (see also Alberts and Lourens, 1992).

Hausch and Török attribute the difference in behavior observed by the two methods to a torsion-flexure coupling in the torsion measurements that induces a λ-type anomaly in G through the large λ-type anomaly in Y.

The steplike transition in G near T_N for CrFe alloys contrasts with the behavior seen in most other Cr alloys, in which no anomaly occurs for G. A steplike behavior in G near T_N is also observed for CrSi alloys in the concentration range where first-order discontinuous changes occur in the thermal expansion at the Néel transition to the commensurate SDW phase (Alberts and Lourens, 1988a).

Alberts and Lourens (1992) measured the temperature dependence from 4 to 300 K of the bulk modulus (and in most cases also the thermal expansion) of antiferromagnetic $Cr_{1-x}Fe_x$ alloys with x ranging from 0.5 to 15 at. % Fe (their results for $16 \leq x \leq 30$ at. % Fe will be discussed in Sec. VI.D). They determined the magnetic Grüneisen parameter Γ_0 defined in Eq. (80b) and analyzed their data using a version of Steinemann's (1978) analysis, with the magnetic free energy written in the form $\Delta F(t,\omega)=\varphi(\omega)f[T/T_0(\omega)]$, that is more general than Eq. (65). The resultant value of $-d\ln T_0/d\omega$ interestingly is found in each alloy to be close to the value of Γ_0, both varying irregularly from a maximum value of about -20 to a minimum of -50 for $-1.5 \leq x \leq 10$.

Mizuki *et al.* (1982) found the phase diagram in the pressure-temperature plane for CrCo and CrFe alloys to be similar, as shown in Figs. 44(f) and 44(d), respectively. They speculated that the similarity to the phase diagram in the concentration-temperature plane seen for CrFe [compare Figs. 44(c) and 44(d)] would also occur in CrCo, and they predicted the phase diagram shown in Fig. 44(e). The phase diagram for CrCo is, however, conventional in form, as shown in Fig. 10, with the incommensurate-commensurate SDW transition temperature T_{IC} occurring for concentrations $x > x_L$, *larger* than the triple-point concentration x_L.

Alberts and Lourens (1983) used Eq. (66a) to calculate the magnetic excitation potential $\Delta\phi$ for the CrCo alloy system from the ground-state magnetovolume $\Delta\omega(0)$ and the magnetic Grüneisen parameter, which they obtained from the pressure dependence of the Néel temperature (de Koning *et al.*, 1980) by use of Eq. (52). The resultant values range between $\Delta\phi=-170$ and -340 μeV/atom, as compared with $\Delta\phi=-370$ μeV/atom for pure Cr. These values are considerably smaller in magnitude than those of itinerant-electron ferromagnets, such as ferromagnetic invar, for which $\Delta\phi$ is of the order of 10 to 20 meV/atom. The difference is due to the much smaller values of the ground-state magnetovolume of the Cr alloy system as compared with that of invar.

6. Cr alloys with group-8 nonmagnetic transition metals Ru, Os, Rh, and Pt

The existence of a triple point at a very low concentration x_L of the dopant for all these metals (see Table IV and Fig. 10) was indicated, in the light of Eq. (78b), by the early measurements of Munday (1971), who observed a broad and deep minimum in the temperature dependence of the Young's modulus for concentrations $x \gtrsim x_L$, as seen in Fig. 47.

Alberts and Lourens (1988b) measured the temperature dependence of the elastic constants and of the thermal expansion for polycrystalline samples of $Cr_{1-x}Ru_x$ for two concentrations, $x=0.3$ and 0.5 at. % Ru, somewhat above the triple-point concentration, $x_L=0.16$ at. % Ru. The thermal expansivity $\beta(T)$ illustrated in Fig. 48 shows a minimum at the Néel temperature T_N and a maximum at the incommensurate-commensurate SDW phase-transition temperature T_{IC} similar to those seen for CrMn alloys, as illustrated in Figs. 45(c) and 45(e). For CrRu, however, the two minima in the temperature dependence of the magnetic contribution to the bulk modulus $\Delta B(T)$ shown in Fig. 48 are also clearly resolved, instead of forming a single broad minimum as seen for CrMn in Figs. 45(d) and 45(f). Thus we can conclude that dT_N/dp is negative and dT_{IC}/dp positive, giving a phase diagram in the pressure-temperature plane like that shown for CrMn in Fig. 44(b). This is consistent with the observed pressure-temperature phase diagram of CrRu shown in Fig. 43.

Recent measurements of the pressure dependence of the elastic constants of this alloy reported by Alberts *et al.* (1992) and Cankurtaran *et al.* (1992) show, however, that dT_{IC}/dp is about 300 K(GPa)$^{-1}$. This gives a

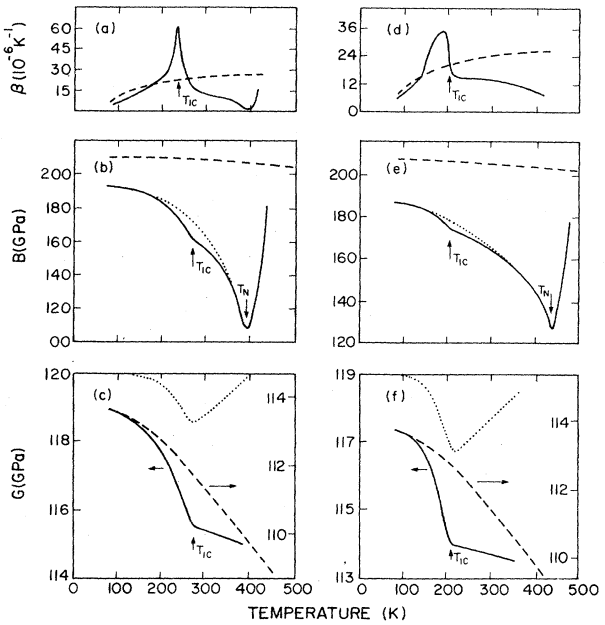

FIG. 48. Temperature dependence of the thermal expansivity β, bulk modulus B, and shear modulus G for two polycrystalline $Cr_{1-x}Ru_x$ alloys having composition $x=0.3$ at. % Ru (a), (b), and (c); and $x=0.5$ at. % Ru (d), (e), and (f). The dashed lines in panels (a) and (d) are the thermal expansivity; and in panels (b) and (e), the bulk modulus of Cr+5 at. % V. The references used to determine the magnetic contributions are, however, the sketched curves asymptotic to the CrRu curves, as shown for B [· · · · in (b) and (e)] and G [— — — in (c) and (f)], but not shown for β. The resultant temperature dependence of ΔG is shown (· · · ·) in (c) and (f). Data of Alberts and Lourens (1988b); from Fawcett and Alberts (1992).

value for the magnetic Grüneisen parameter, $\Gamma_{IC}=215$, when substituted in the equivalent expression to Eq. (51), which is very much larger than that estimated by the use of Eq. (79) from the magnitude of the anomalies $\delta\beta(T)$ and $\delta B(T)$, as given in Table X. Alberts *et al.* (1992) suggest that the reason for this discrepancy is that the Ehrenfest-like Eq. (79) is suitable only for determining the *sign* of Γ_{IC}, but not its magnitude, when the transition is strongly first order. The marked hysteresis of T_{IC}, which is about 20 K at ambient pressure in Cr+0.3 at. % Ru (Cankurtaran *et al.*, 1992), and large change in length (Alberts and Lourens, 1988b) show this to be the case for this sample.

The temperature dependence of the shear modulus $G(T)$ also shows a clear anomaly at T_{IC} for these two CrRu alloys, as seen in panels (c) and (f) of Fig. 48. This behavior is unique in Cr alloy systems and enables us to evaluate a magnetic Grüneisen parameter for shear strain, as defined in Eq. (82). The dotted curves showing $\Delta G(T)$ in panels (c) and (f) of Fig. 48 were estimated by use of the data for Cr+5 at. % V displaced vertically so as to be asymptotic in each case to the continuous curve $G(T)$ at lower temperature. The maximum value of $\Delta G(T)$, which was obtained by subtraction of the two curves, occurs at a temperature some 40 K higher than the value of T_{IC} estimated from the peak in $\beta(T)$ shown in panels (a) and (d). The ratio of these maximum values nevertheless seems to serve best to estimate roughly the shear magnetic Grüneisen parameter Γ_{GIC} by substitution in the analog of Eq. (82) for the AF_1-AF_0 (IC) phase transition.

In the case of the magnetic contribution $\Delta B(T)$ to the bulk modulus, however, the decrease towards the deep minimum at T_N begins at a temperature below T_{IC}, and the dotted curves sketched in panels (b) and (e) of Fig. 48 show our estimate for this decrease. This curve, and *not* that for the nonmagnetic reference material Cr+5 at. % V, is clearly the appropriate reference for $B(P,T)$ to use in Eq. (77b) for estimating $\Delta B(T)$.

The resultant values of Γ_{GIC} given in Table X are of order unity, being somewhat less, but comparable in magnitude, to the value of Γ_{IC}. There is, of course, no reason why one should expect the two magnetic Grüneisen parameters to be comparable in magnitude, or even to have the same sign. Indeed, in other Cr alloy systems, with the exception of CrFe, we find the condition $\Gamma_{GIC} \ll \Gamma_{IC}$ (and $\Gamma_{GN} \ll \Gamma \ll \Gamma_N$), so that anomalies are not seen at all in the shear modulus at either of the two phase transitions.

Measurements by Alberts and Boshoff (1992) on a single-crystal sample of Cr+0.3 at. % Ru give a remarkably sharp change, perhaps a first-order step, in the elastic moduli and especially in the shear moduli, c_{44} and $(c_{11}-c_{12})/2$, at the incommensurate-commensurate SDW phase transition. The estimates of Γ_{IC} and Γ_{GIC} obtained from the single-crystal data by substituting the values of the step changes in Eqs. (76) and (82) are, however, roughly the same as those for the polycrystalline samples given in Table X.

Measurements of the pressure dependence of the elastic constants in this sample were referred to above and discussed in Sec. V.B (Alberts *et al.*, 1992; Cankurtaran *et al.*, 1992). The elastic constants are considerably larger in the incommensurate than in the commensurate SDW phase, and the phase transition is markedly hysteretic both in temperature and in pressure. There is a remarkable longitudinal mode softening with increasing pressure in both phases, which gives acoustic-mode Grüneisen parameters that are negative, having a larger magnitude with strong temperature dependence in the commensurate SDW phase.

A comprehensive study by Boshoff *et al.* (1993) of the temperature dependence of the various elastic moduli in single crystals of Cr+0.3 and 0.5 at. % Ru, in comparison with CrRe crystals of the same composition, should be referred to for further insight into this interesting system.

Butylenko and Nevdacha (1980b) measured the temperature dependence of the resistivity $\rho(T)$ of $Cr_{1-x}Os_x$ alloys in the range $1<x<10$ at. % Os under pressure up to almost 8 GPa and, from the anomaly in $\rho(T)$ at the Néel transition shown in Fig. 49(a), constructed the composition-pressure-temperature phase diagram shown in Fig. 49(b). The surface of AF_1-AF_0 phase transitions is absent, because $\rho(T)$ does not show an anomaly there. The surface of Néel transitions to the AF_0 phase shows a line of saddle points, corresponding to the maximum in temperature along the line of triple points.

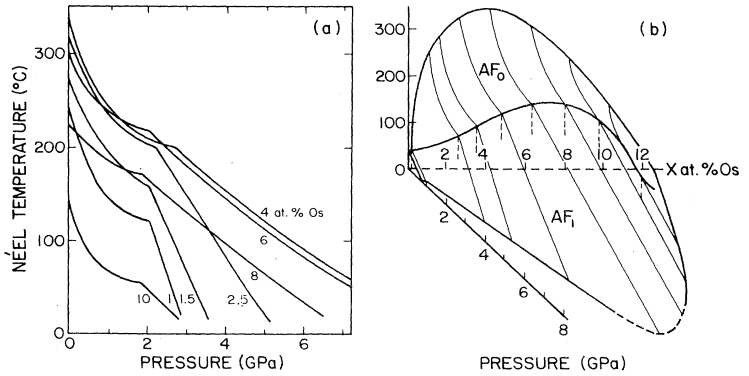

FIG. 49. Pressure dependence of the Néel temperature T_N in a set of $Cr_{1-x}Os_x$ alloys: (a) $T_N(p)$ curves for different concentration x of Os as indicated; (b) composition-pressure-temperature phase diagram constructed from the $T_N(p)$ curves in (a). From Butylenko and Nevdacha (1980c).

7. Cr alloys with group-3 nontransition metals Al and Ga

The CrAl alloy system exhibits extraordinarily strong magnetoelastic effects. Alberts and Burger (1978) found a pressure dependence, $dT_N/dp = -240$ K(GPa)$^{-1}$, for the Néel temperature T_N of an alloy containing $x \lesssim 2.0$ at. % Al. The series of alloys $Cr_{1-x}Al_x$ that they measured gave a magnetic Grüneisen parameter Γ_N, calculated by use of Eq. (52), that increased monotonically with x, as listed in Table VII and illustrated in the inset to Fig. 50, up to a value of magnitude greater than 200 for $x \gtrsim 2.0$ at. % Al.

Fawcett and Alberts (1990) analyzed the magnetoelastic data of Alberts and Lourens (1984a), using the Grüneisen-Testardi method, with the results shown in Fig. 50. They found that the singularity in the magnetoelastic properties occurs at about $x = 2.2$ at. % Al, where both Γ_{SF} and Γ_0, defined in Eqs. (76b) and (80b), reach the astounding value $\Gamma_i \sim -1300$. Γ_{NT} is also large for this alloy, but could not be determined, since the Néel transition cannot be distinguished in the bulk modulus data (see Fig. 3 of Alberts and Lourens, 1984a).

Measurements of the elastic constants of CrAl alloys by Baran *et al.* (1992) and Alberts (1994) show several interesting features. The anomaly in the temperature dependence at the spin-flip transition in a Cr+1.2 at. % Al sample is strong in the shear moduli as well as in the bulk modulus. The anomaly in the bulk modulus at the Néel transition to the incommensurate SDW phase is like that in CrMn [Fig. 45(d)], whereas the transition to the commensurate SDW phase in a Cr+2.6 at. % Al sample shows a steplike change. Finally, the magnetic contribution to the bulk modulus persists up to a temperature $T > 400$ K, more than 3 times the Néel temperature, $T_N = 134$ K, in a Cr+1.9 at. % Al sample, whereas the magnetic contribution to the tetragonal shear modulus, $\frac{1}{2}(c_{11} - c_{12})$, disappears abruptly at T_N.

Figure 51(a) shows the phase diagram in the pressure-temperature plane for a $Cr_{1-x}Ga_x$ alloy having a composition $x > x_L = 0.6$ at. % Ga, which on comparison with the phase diagram in the concentration-temperature plane, sketched in Fig. 9, is seen to have the common feature that negative pressure corresponds to increasing the doping concentration (cf. Fig. 44). The fact that $|dT_{IC}/dp|$ is larger than $|dT_{NI}/dp|$ was confirmed by Alberts and Lourens (1984b), who did not determine dT_{NC}/dp.

A study of the temperature dependence of the bulk modulus $B(T)$ and the thermal expansivity $\beta(T)$ by Alberts and Lourens (1985) was analyzed by Fawcett and Alberts (1992b) using the Grüneisen-Testardi method, with the results shown in Fig. 52. There appears to be a singularity at a concentration $x \simeq 1$ at. % Ga, where all the magnetic Grüneisen parameters become large, which is about a factor 2 greater than the triple-point concen-

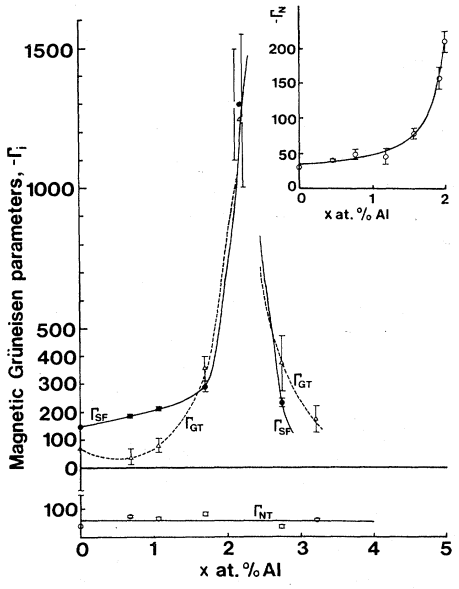

FIG. 50. Magnetic Grüneisen parameter Γ_i in the $Cr_{1-x}Al_x$ alloy system: ●, Γ_{SF} for temperature, $T > T_N$; ○, Γ_{NT} for $T < T_N$ (lower panel); △ and — — —, Γ_{GT} (3 Γ_{SW}) for zero temperature. Inset: ○, Γ_N for $T = T_N$ (from Fawcett and Alberts, 1990).

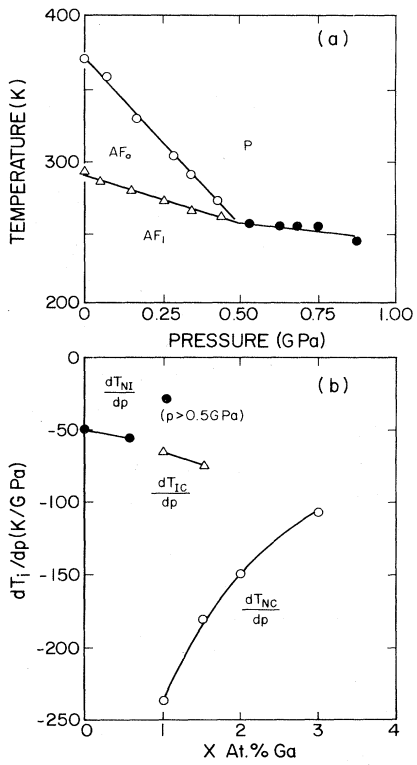

FIG. 51. Pressure dependence of the phase transitions in the $Cr_{1-x}Ga_x$ alloy system: (a) phase diagram in the pressure-temperature plane for an alloy containing $x = 1.1$ at. % Ga; (b) dependence on composition of the pressure dependence of the Néel temperature to the incommensurate SDW phase (dT_{NI}/dp), and of the incommensurate-commensurate SDW phase-transition temperature (dT_{IC}/dp). From Kaneko *et al.* (1982).

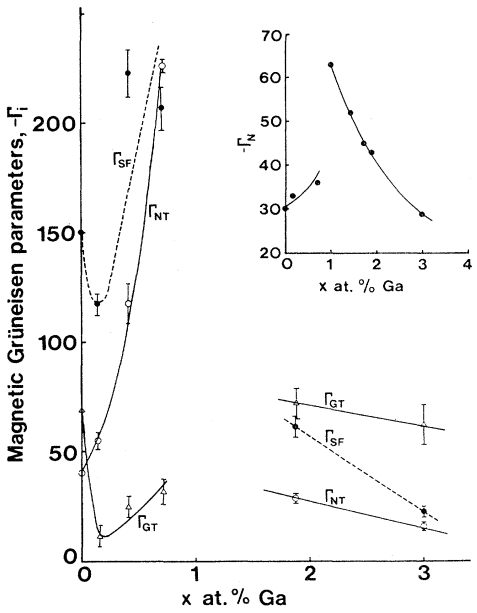

FIG. 52. Magnetic Grüneisen parameter Γ_i in the $Cr_{1-x}Ga_x$ alloy system: ● and — — —, Γ_{SF} for temperature, $T > T_N$; ○, Γ_{NT} for $T < T_N$; △, Γ_{GT} (3 Γ_{SW}) for zero temperature. Inset: ●, Γ_N for $T = T_N$ (Fawcett and Alberts, 1992b).

tration $x_L \simeq 0.5$ at. % Ga.

A puzzling feature of the magnetoelastic data, when compared with the phase diagram of Fig. 51, is the fact that $\beta(T)$ exhibits a minimum at the Néel temperature T_N and a maximum at the incommensurate-commensurate SDW phase-transition temperature T_{IC}, as is seen in Fig. 1 of Alberts and Lourens (1985) for five concentrations of Ga in the range $x = 0.83$ to 1.72 at. % Ga; while their Fig. 3 shows a broad minimum in $B(T)$ for the three lower concentrations and two resolved minima for the two higher concentrations. According to Eq. (78a), this means that dT_N/dp is negative as observed, but dT_{IC}/dp is positive in contradiction to the observations shown in Fig. 51.

This apparent failure of the CrGa alloy system to conform with the expected behavior may indicate problems resulting, for example, from sensitivity of samples to defects such as internal strain that may be introduced in an uncontrolled way during their preparation. This may account for the very strange result that the triple point is reported to be at a concentration $x_L = 0.6$ at. % Ga (see Table IV and Fig. 9); the singularity in the magnetoelastic properties is at $x \simeq 1.0$ at. % Ga (see Fig. 52). One expects this singularity to occur at the triple point, where, as seen in Table VIII, the pressure dependence of the Néel temperature T_N deceases considerably between the transition to the commensurate and to the incommensurate SDW phase, i.e., $|dT_{NI}/dp| \ll |dT_{NC}/dp|$ in every case (including CrGa itself), except for CrFe, for which dT_{NI}/dp is about 3 to 4 times larger than dT_{NC}/dp.

Alberts and Lourens (1985, Figs. 1 and 3) took a different approach to the analysis of their magnetoelastic data. For concentrations of Ga greater than x_L, the two phase transitions at T_N and T_{IC} are identified as being, respectively, at the inflection point on the high-temperature side of the $B(T)$ and $\beta(T)$ minima, and at the inflection point on the low-temperature side of the $B(T)$ minimum and between the $\beta(T)$ minimum and maximum. This identification conforms with the idea that the magnetovolume $\Delta\omega(t)$ may be described by Eq. (68), with $t = T/T_N$, but with different coefficients A_0, A_1, and A_2 for the commensurate and incommensurate SDW phases. Thus the thermal-expansion data may be described approximately by two parabolic curves in a plot of $\Delta\omega(t)$ vs t^2 (see Alberts and Lourens, 1985, Fig. 5). The resultant values of the mean-square moment in the incommensurate SDW phase and of the moment in the commensurate SDW phase, obtained by substituting the ground-state magnetovolume in Eq. (62) with the same value for the coefficient C/B, are in reasonably good agreement with neutron-diffraction data.

8. Cr alloys with group-4 nontransition metals Si, Ge, and Sn

The $Cr_{1-x}Si_x$ alloy system, like CrFe, exhibits a remarkably large first-order Néel transition in length (Suzuki, 1977) when the concentration x exceeds $x_L = 1.0$ at. % Si, the triple-point concentration, so that the ordered phase immediately below the Néel temperature is a commensurate SDW. We shall discuss this effect in detail in Sec. VI.B, when we shall see that the explanation of Nakanishi and Kasuya for the behavior of the CrFe involves the local moment on the Fe atom, and the unique feature of the CrFe alloy system that the incommensurate SDW phase for $x < x_L$ lies *above* the commensurate SDW phase, as seen in Fig. 14. This is not the case, however, for CrSi (see Fig. 17), and some other explanation must be sought.

Lourens and Alberts (1993) have measured a single crystal of Cr + 1.6 at. % Si, with special reference to the critical behavior of the thermal expansion and the magnetoelastic properties and the strong first-order effects seen at the Néel transition.

Smit and Alberts (1989), in an effort to gain more understanding of this interesting system, introduced Mo to reduce the strength of the SDW in Cr (Ström-Olsen and Wilford, 1980), through broadening the *d* band and hence reducing the density of states (Cywinski and Hicks, 1986). They obtained the remarkable result that a fixed amount of 3% Mo introduced into the $Cr_{1-x}Si_x$ alloy in place of Cr [the $(Cr_{0.97}Mo_{0.03})_{1-x}Si_x$ or "Si series" of ternary CrMoSi alloys] suppresses completely the commensurate SDW phase, and with it the first-order transition.

Smit and Alberts (1990) then took an alloy with a fixed amount, $x = 1.4$ at. % Si, and varied the concentration of Mo [the $(Cr_{1-x}Mo_x)_{0.986}Si_{0.014}$ or "Mo series" of ternary CrMoSi alloys]. Again the results were interesting, as we shall see.

The temperature dependence of the thermal expansivi-

ty $\beta(T)$ in the $Cr_{1-x}Si_x$ alloy series shows a deep minimum for transitions to the incommensurate SDW phase, for $x < x_L = 1.0$ at. % Si, which becomes singular, corresponding to the first-order transition to the commensurate SDW phase for $x > x_L$. The incommensurate-commensurate SDW phase transition at temperature T_{IC}, which moves rapidly to lower temperatures as x increases beyond x_L (see Fig. 17), gives a strong maximum in $\beta(T)$. This indicates, according to Eq. (78a), that dT_{IC}/dp should be positive, while dT_N/dp, as usual, is negative.

In fact, this prediction is hard to verify, since the two phases coexist all the way to 4.2 K from a temperature of about 150 K, which is therefore not a clearly defined phase-transition temperature. The pressure-temperature phase diagram shown in Fig. 53 is very complicated. The Néel temperature T_{NC} to the AF_0 phase decreases rapidly with pressure (see Table VIII), but the triple point is poorly defined because the AF_0 and $AF_1(H)$ phases coexist. We adopt here a new notation, with $AF_1(H)$ signifying the high-temperature incommensurate SDW phase, while another mixed phase region comprising AF_0 and $AF_1(L)$ phases occurs at temperatures $T < T_{IC}(L) = 150$ K, in Fig. 53. The phase boundary T_{LH} between the low-temperature mixed phase and the $AF_1(H)$ phase is defined by the fact that, with increasing temperature, the incommensurability parameter δ increases just as in pure Cr, while above T_{LH} δ *decreases.*

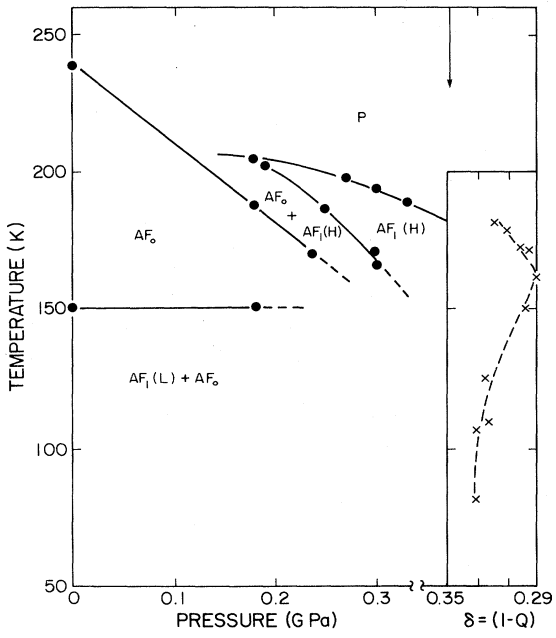

FIG. 53. Magnetic phase diagram of Cr+1.4 at. % Si in the pressure-temperature plane. AF_1 (H) and AF_1 (L) are high- and low-temperature incommensurate SDW phases that have temperature dependence of the incommensurability parameter δ of opposite sign, as plotted in the inset, which corresponds to a pressure of 0.37 GPa, as indicated by the vertical arrow (after Endoh *et al.*, 1982).

This interesting behavior is matched by that seen at ambient pressure in a CrSi alloy close to the triple point, as illustrated in the inset in Fig. 17. It appears that in both the pressure-temperature and composition-temperature phase diagrams the AF_0 phase is reentrant. According to this explanation, the $AF_1(H)$ and $AF_1(L)$ regions in Fig. 53 correspond to the same incommensurate SDW phase, but with different signs of the temperature dependence of δ according to whether, with increasing temperature, one approaches or moves away from the AF_0 phase.

The phase diagrams in the concentration-temperature plane for both the Si series and the Mo series of CrMoSi ternary alloys are shown in Fig. 54, with the phase diagram for $Cr_{1-x}Si_x$ for comparison. The 3 at. % Mo in the Si series completely suppresses the commensurate SDW phase, and, in fact, the SDW disappears altogether when $x \gtrsim 2.1$ at. % Si. The dashed line through the data points is fit to a theory of Dadarlat *et al.* (1980), which they had previously used to explain the concentration dependence of the Néel temperature in $Cr_{1-x}Si_x$. The fit is remarkably good to the data for the Si series and implies that Si changes T_N by two mechanisms, a scattering mechanism that causes electron-hole pair-breaking (Zittartz, 1967) and a distortion of the Fermi surface that can lead to an increase of $T_N(x)$ with increasing x (Crisan and Anghel, 1976) as seen beyond x_L in $Cr_{1-x}Si_x$.

The theory of Dadarlat *et al.* (1980) does not, however, predict a commensurate SDW phase; so it is inappropriate for the Mo series (as well as for $Cr_{1-x}Si_x$), since with 1.4 at. % Si the series starts at $x = 0$ at. % Mo with such a phase. Smit and Alberts (1990) found instead that the canonical model, as formulated by Machida and Fujita (1984), could reproduce all the features of the phase diagram shown in Fig. 54 quite well, with the addition of Mo increasing the nesting parameter h in Eq. (1) and thus eventually restoring the incommensurate SDW phase, as illustrated in Fig. 1(b) or 1(c).

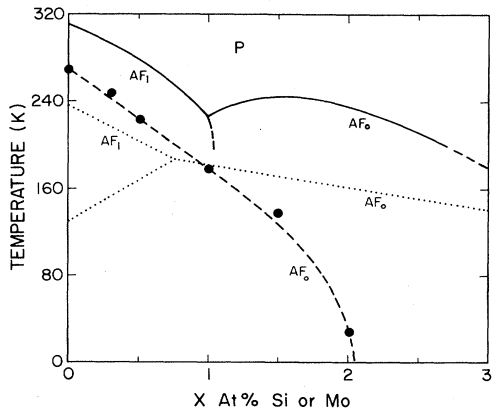

FIG. 54. Magnetic phase diagrams of $(Cr_{0.97}Mo_{0.03})_{1-x}Si_x$, (● and — — —), and of $(Cr_{1-x}Mo_x)$ $Si_{0.014}$ (· · · ·), with the magnetic phase diagram of $Cr_{1-x}Si_x$ for comparison (after Smit and Alberts, 1989, 1990).

It is not at all clear, however, why Mo should be regarded as an electron acceptor, since, being isoelectronic with Cr, it is usually considered simply to reduce the strength of the magnetic interaction, which thus causes the SDW amplitude and Néel temperature to decrease (Cywinski and Hicks, 1986). Si, on the other hand, appears to act like an electron donor, since it causes the commensurate SDW phase to appear. We note, however, that positron channeling experiments in CrSi (Takahashi *et al.*, 1980) have ruled out the tentative prediction (Jayaraman *et al.*, 1976) that Si occupies interstitial sites in the bcc structure of Cr and thus donates electrons.

The magnitude of the moment in commensurate SDW CrSi alloys is anomalously large in relation to the Néel temperature, as may be seen by inspection of Fig. 7. The incommensurate SDW CrSi alloys are not different in this respect from the other alloys shown in Fig. 7.

The $Cr_{1-x}Ge_x$ alloy system is much better behaved than CrSi. For $x > x_L = 0.4$ at. % Ge, the Néel transition at T_N to the commensurate SDW phase is still continuous (van Rijn and Alberts, 1986a), unlike CrSi. The temperature dependence of the thermal expansivity $\beta(T)$ exhibits a minimum at $T_N \simeq 400$ K and a strong maximum at the incommensurate-commensurate SDW phase transition at $T_{IC} \simeq 175$ K for $x = 0.7$ at. % Ge (see van Rijn *et al.*, 1987, Fig. 3), with a strong minimum in the bulk modulus $B(T)$ at T_N and a shallow minimum at T_{IC} (see van Rijn *et al.*, 1987, Fig. 1). Thus, in accordance with Eq. (78a), dT_N/dp is negative and dT_{IC}/dp positive, as confirmed by the measurements of van Rijn and Alberts (1986a) shown in Fig. 55 (see also Fig. 8 in Hochheimer and Münch, 1991).

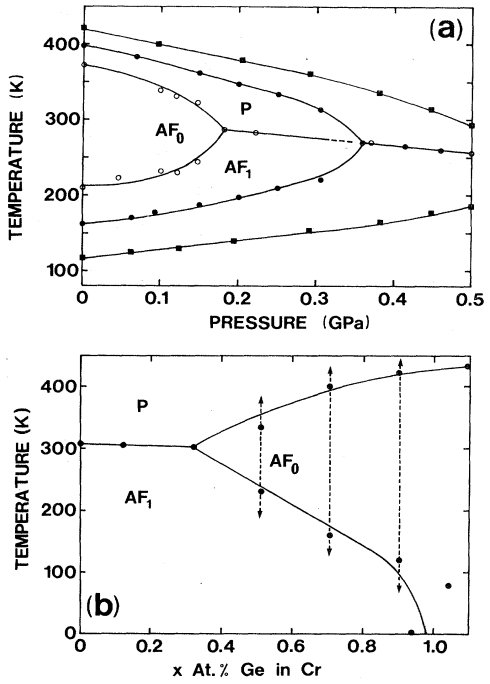

FIG. 55. Magnetic phase diagrams of $Cr_{1-x}Ge_x$ alloy system in (a) the pressure-temperature plane for these concentrations; ○—$x=0.51$ at. % Ge; ●—$x=0.70$ at. % Ge; and ■—$x=0.89$ at. % Ge; and in (b) the composition-temperature plane, where the vertical arrows show the compositions at which the pressure dependence is shown in (a). After van Rijn and Alberts (1986a).

D. Pressure and composition: comparison between the effects of volume change and electron concentration

The empirical correspondence between the application of pressure and decreasing electron concentration in Cr SDW alloy systems was first pointed out by Rice *et al.* (Rice, Barker, *et al.*, 1969; Rice, Jayaraman, and McWhan, 1969). Griessen and Fawcett (1977) reviewed the situation graphically, as illustrated in Fig. 38, as an introduction to their analysis in relation to Fermi-surface effects, as discussed below.

Figure 55 illustrates very clearly the parallelism between the effects of doping and pressure in the CrGe alloy system, which is seen with more or less verisimilitude in almost all the Cr alloy systems that show a transition to the commensurate SDW phase, as well as those that do not, like CrV, as illustrated in Fig. 38. We shall complete our account of the magnetoelastic properties of individual Cr alloy systems by listing in Table XIII the figures showing the concentration-temperature phase diagrams for such systems, and in those cases in which the pressure-temperature phase diagram has been measured,

TABLE XIII. Comparison of the phase diagrams for Cr alloy systems $Cr_{1-x}A_x$ in the composition-temperature (x-T) plane and the pressure-temperature (p-T) planes. "Identical" means that both negative pressure p and increasing solute concentration x lead to a commensurate SDW phase, with corresponding pairs of the three values of $-dT_i/dp$ and dT_i/dx at the triple point having the same sign (compare the values in Tables IV and VIII). "Similar" means that both negative pressure p and increasing solute concentration x lead to a commensurate SDW, but with $-dT_i/dp$ and dT_i/dx at the triple point having different signs or not being determined for one or more corresponding branches of the two phase diagrams. "Complex" means that simple comparison of the two phase diagrams is not feasible, and reference should be made to the papers quoted.

Solute	x-T Fig.	p-T Fig. or Ref.	Comparison
Mn	12,44(a)	43,44(b)	Identical
Re	13	a	Similar
Fe	14,44(c)	44(d),58	Similar
Co	10	44(f)	Similar
Ru	15	43	Identical
Os	10	49	Similar
Al	16	b,c	Complex
Ga	9	51	Similar
Si	17	53	Complex
Ge	9,55(b)	55	Identical

[a]Butylenko and Kobzenko (1981).
[b]Alberts and Burger (1978).
[c]Mizuki *et al.* (1982).

where it is to be found in order to compare the two phase diagrams.

The derivatives dT_i/dx and dT_i/dp, with respect to concentration and pressure, respectively, of the three transition temperatures T_{NI}, T_{NC}, and T_{IC}, near the triple point may also be compared by inspection of Tables IV and VIII. In most cases the derivatives with respect to concentration and negative pressure have the same sign, as expected from Fig. 38. In these cases the ratio of the magnitudes of the derivatives may be estimated for comparison with the scaling factor, 2.8 GPa per 1% e_A, used in constructing Fig. 38, with appropriate choice of the valence difference from Cr, e.g., two electrons per atom for the group-8 metals. With this scaling factor, Fig. 55 would lead us to consider, however, that each Ge impurity atom contributes one-quarter electron.

In only one case, that of CrAl, does an alloy system show a triple point in the concentration-temperature plane and not in the pressure-temperature plane, at least for the concentrations and pressure ranges listed for this system in Table VII. The systems CrRh, CrIr, and CrPt have not been measured under pressure; but by analogy with the behavior of Cr alloy systems with the other group-8 metals showing a triple point in the concentration-temperature plane, namely, CrFe, CrCo, CrRu, and CrOs, we expect the former systems to have a triple point in the pressure-temperature plane also.

Perhaps the most striking similarity between the effects of pressure and electron concentration are seen when we compare the temperature dependence of the resistivity $\rho(T)$ for a series of alloys in the ternary system (Cr+2.7 at. % Fe)$_{1-x}$(V,Mn)$_x$ with the pressure dependence of $\rho(T)$ in two alloys in the series, as illustrated in Figs. 31(b) and 33 (see also Figs. 1, 2, and 3 of Galkin and Fawcett, 1993). The scaling factor between pressure and electron concentration is about the same as in Fig. 38 (Fawcett and Galkin, 1993). A similar value for the scaling factor is obtained when we compare the effects of doping and pressure on the residual resistivity R_0 in the system Cr+2.7 at. % Fe (V,Mn) (Galkin, 1987). Figure 30 shows a peak in R_0 for a sample containing 0.2 at. % Mn at a pressure of about 1 GPa (inset), which is equivalent to shifting e_A by 0.65% to reach the peak for 0.45 at. % doping seen in the main figure. Nityananda *et al.* (1972) obtained similar results for the effect of 0.5 at. % Ru dopant in Cr+3 at. % Fe on the temperature dependence of the resistivity $\rho(T)$ under pressure. Their curves are very similar to those of Fig. 2 in Fawcett and Galkin (1993), and both give a triple point at a pressure of about 9 kbar.

We must at this point, however, restrain our enthusiasm and examine the effect of changing electron concentration and hydrostatic pressure upon the Fermi surface, in order to provide a fundamental basis in terms of the changes in its nesting properties for their supposed equivalence. Griessen and Fawcett (1977) pointed out that, in fact, the response of the Fermi surface to hydrostatic pressure might be expected to be quite different from its dependence on electron concentration. For example, in a hypothetical compensated metal like Cr, consisting of an electron and a hole band, the geometrical nesting vector $\tilde{\mathbf{Q}}$ ($=1-\tilde{\boldsymbol{\delta}}$, with both $\tilde{\mathbf{Q}}$ and $\tilde{\boldsymbol{\delta}}$ measured in units of $a^*=2\pi/a$) remains constant under pressure, because the linear dimensions of both the electron and the hole Fermi surfaces change by the same amount.

This is indeed confirmed by the observed pressure dependence of the Fermi surface in the two paramagnetic metals Mo and W, which are isoelectronic with Cr and have a very similar Fermi surface. Fawcett *et al.* (1980) review the de Haas–van Alphen experiments, which show that for both metals the volume dependence of the nesting vector has a value $d\ln\tilde{Q}/d\omega\simeq-0.1$. To put this value in perspective, we compare it with the volume dependence of the SDW wave vector Q of Cr determined both from neutron diffraction and from experiments on the de Haas–van Alphen effect under pressure, each of which gave a value, $d\ln Q/d\omega=1.1$ (see Table XV in Fawcett, 1988a), that is about 10 times larger and opposite in sign to $d\ln\tilde{Q}/d\omega$. Thus the volume dependence of the geometrical nesting vector $\tilde{\mathbf{Q}}$ between the electron and hole octahedra obtained from the Fermi-surface measurements in Mo and W is an order of magnitude smaller and opposite in sign to that of the SDW wave vector Q.

We are driven to the conclusion that the close similarity between the effects of volume increase and increase in the electron concentration in Cr alloy systems does *not* mean that they are equivalent (Fawcett, 1994). The existing theories discussed in Sec. V.A provide no solution to this problem. Thus, in the theory of McWhan and Rice (1967), an increase in electron concentration e_A improves the match between the nesting electron and hole Fermi surfaces and thereby increases the quantity N_M in Eq. (64a); hence T_N increases according to Eq. (64b), with $z\equiv e_A$. When we consider the effect of volume increase, however, and use the value, $\beta_1\beta_2=-d\ln I/d\omega=1.0$, obtained in Sec. V.A by analyzing the thermal expansion of Cr in terms of the theory of Holden *et al.* (1984), we obtain by substituting in Eq. (64b) the values, $d\ln T_B/d\omega\simeq-d\ln N(0)/d\omega\simeq-5/3$, $T_B/T_N\simeq30$ and a *small negative* value for $d\ln T_N/d\omega$ instead of the *large positive* value, $d\ln T_N/d\omega\simeq30$. We have no explanation for this disconcerting result, though we note that the manner in which the quantity I is defined is quite different in the two theories discussed in Sec. V.A. There is a clear need to reconsider these theories and to develop a comprehensive and fundamental analysis of the magnetoelastic properties of SDW Cr alloy systems.

We discuss finally the extent to which changes in volume produced by substituting impurity atoms in the Cr lattice might account for the strong volume effects observed in Cr alloy systems. The lattice parameter in Cr is about 10% smaller than that of its bcc neighbors in the periodic table, V, Mo, and Mn (the high-temperature phase). Thus alloying with them, and other group 5, 6, and 7 metals, increases the atomic volume, as given in the

TABLE XIV. Contribution of volume change to the change in the Néel temperature T_N of Cr when alloyed with V, Mo, and Mn.

Solute A	a $d\omega/dx$	b $(d\ln T_N/dx)_{vol} = (d\omega/dx)(d\ln T_N/d\omega)$	c $d\ln T_N/dx$
V	0.11	3	−26
Mo	0.36	11	−45
Mn	0.17	5	16

[a]Fractional volume change per mol (Pearson, 1958, 1967).
[b]Value $(d\ln T_N/dx)_{vol}$ expected from the volume change alone, with $d\ln T_N/d\omega = 30$ (Fawcett. 1988a).
[c]Observed value of $d\ln T_N/dx$.

first column of Table XIV (Pearson, 1958). Comparison with the observed volume dependence of the Néel temperature T_N, given in the second column, yields in the third column the expected dependence of T_N upon impurity concentration due to volume changes alone.

Only in the case of CrMn are the sign and order of magnitude of this effect the same as that of the observed value of $d\ln T_N/dx$, given in the last column of Table XIV. Thus the negative values of dT_N/dx for alloys with group-5 and -6 metals (see Table I) are due to *electronic* effects acting in *opposition* to the considerably smaller effects of volume change on alloying.

VI. PHASE TRANSITIONS

A. Néel transition

The Néel transition in pure Cr itself is not understood at all well. The first-order nature of the transition has been discussed by several theorists (see Fawcett, 1988a), without resolving the question of its origin. The change in the nature of the Néel transition in dilute alloys (Fawcett and Noakes, 1993) offers some promise of solving this problem, while yet opening up new questions. Thus V dissolved in Cr was long regarded simply as the prototype system for demonstrating the depression of the Néel temperature with decreasing electron concentration. But now we know, as documented in Sec. II.C.2, that its effects are much more pervasive.

Without doubt, some other impurity atoms produce similar effects to V, since there is no reason to suppose that the remarkable changes it produces are specific to one chemical element. No other dilute alloys have, however, been scrutinized with anything like the same care, and evidence for similar behavior with other impurities is only fragmentary. Thus Nb, Ti (Chiu *et al.*, 1971), and perhaps Ta (Arajs, 1969), produce a decrease of resistivity in the paramagnetic phase when dissolved in Cr. The dilute alloy Cr+0.4 at. % Mo may have a continuous Néel transition (Fawcett, Roberts, *et al.*, 1986), though the existence of a latent heat in Cr+0.6 at. % Mo, as quoted in Table XV, suggests otherwise. $Cr_{1-x}Mo_x$ alloys have a magnetic Grüneisen parameter in the paramagnetic phase that decreases with increasing x, as in $Cr_{1-x}V_x$ alloys (Fawcett and Alberts, 1990), but much less rapidly.

Young and Sokoloff (1974) produced the most likely explanation for the weak first-order Néel transition seen in pure Cr. They found that, for some values of the parameters, the canonical model gives a first-order transition connected with the existence of relatively strong SDW harmonics. The fact that both the second- and the third-harmonic content of the SDW decrease with V doping, and conversely increase with Mn doping as illustrated in Fig. 63, and that the other group-7 metal Re gives a clearly first-order transition in Cr+0.18 at. % Re (Lebech and Mikke, 1972; Fawcett and Noakes, 1993), supports this idea. Fishman and Liu (1992, 1993c) have extended Young and Sokoloff's theory to include impurity scattering, however, and find that both group-7 (Mn and Re) and group-5 (V) impurities should give a continuous Néel transition.

The critical behavior of the resistivity in pure Cr was studied by Akiba and Mitsui (1972) and Rapp *et al.* (1978), but there have been no corresponding measurements in Cr SDW systems. The work on CrMn alloys by Sousa *et al.* (1975) and Ausloos (1977) was done on alloys containing so much Mn that one should rather regard them as Cr-doped Mn alloys than SDW alloys of Cr. Smit and Alberts (1994) measured thermal expansion and ultrasonic velocity and attenuation in single crystals of Cr + 0.05 at. % Mn and Cr=0.1 at. % Mn. Their data suggest that in both the Néel transition is continuous. Yakhmi *et al.* (1984), however, observed a discontinuity at T_N in the temperature dependence of the resistivity in Cr doped with 0.1, 0.2, and 0.3 at. % Mn, while Kondorskii *et al.* (1978) obtained a clear first-order transition in the thermal expansion in a Cr + 0.3 at. % Mn sample.

The critical neutron scattering in Cr+0.2 at. % V was found by Noakes, Holden, and Fawcett (1990) to have essentially the same values for the critical exponents as in pure Cr, a rather surprising result in view of the drastic reduction in the intensity of the scattering produced by the V doping (see Sec. VII.B). The critical exponent for the correlation length has the mean-field value $\nu = 1/2$ (cf. $\nu = 0.7$, in Cr+5 at. % Mn, according to Als-Nielsen *et al.*, 1971), which when combined with the relative intensity of inelastic scattering, above and below the Néel

transition, gives the value $\beta \simeq 0.3$ for the critical exponent for the order parameter.

The elastic scattering in both Cr and Cr+0.2 at. % V, as well as neutron diffraction in CrAl alloys (Baran *et al.*, 1992), shows an intensity of the Bragg peak linear in temperature below and close to T_N, which appears to give the mean-field value $\beta = 1/2$. The value of β obtained from inelastic scattering is more accurate, however, since the Bragg peak comprises both coherent and quasielastic scattering.

The determination of the first-order nature of the Néel transition of a Cr alloy is of course impossible if the sample is not of uniform composition and, as is often the case, the Néel temperature T_N depends strongly on the concentration of the impurity. Even in the case of pure Cr, the latent heat of the weak first-order Néel transition

TABLE XV. Latent heat L at first-order phase transitions in chromium alloy systems $Cr_{1-x}A_x$. Parenthetical values in the fourth column are determined from the first-order length change and the pressure dependence of the phase-transition temperature by means of the Clausius-Clapeyron equation. The first-order transitions to the commensurate phase in CrFe and CrSi (indicated with a dagger) alloy systems exhibit hysteresis, as illustrated in the case of CrFe under pressure in Fig. 58. In some cases the phase transition is fairly wide, but it is difficult to ascertain whether this is due to coexistence of the two phases or simply to inhomogeneity of the sample composition. The average value of the phase-transition temperature is given here, and the reference should be consulted for information about hysteresis and breadth of the transition.

A	x (at. %)	T_i (K)	L (J/mol)	Reference
Pure Cr		$T_{NI}=312$	1.0(<1.4)	a
Mo	0.6	$T_{NI}=303$	0.8	b
W	0.3	$T_{NI}=303$	0.9	b
Mn	0.45	$T_{NC}=447$	continuous	c
		$T_{IC}=180-310$	0.028(0.03)	
	0.7	$T_{NC}=467$	continuous	c
		$T_{IC}=150-220$	0.026(0.038)	
Re	0.18	$T_{NI}=320$	($\simeq 1$)	d
Fe†	0.4 to 2.0	$T_{NI}=300$ to 260	0.15 to 0.7	e
	1.2	$T_{NI}=292$	1.3	f
	2.22	$T_{NI}=254$	1.2	f
		$T_{IC}=248$	0.4	
	3.35	$T_{NC}=252$	12.6	f
	3.5	$T_{NC}=237$	12.5	g
	5	$T_{NC}=228$	13	g
	6.5	$T_{NC}=211$	5	g
	8	$T_{NC}=199$	3	g
Co	0.4	$T_{NI}=298$	0.44	b
	2.2	$T_{NC}=300$	continuous	b
	2.7	$T_{NC}=325$	continuous	b
Ru	0.3	$T_{NC}=402$	continuous	h
		$T_{IC}=256$	9.5	h
Al	0.3	$T_{NI}=300$	0.36	b
	1.9	$T_{NC}=310$	continuous	b
Si†	0.46	$T_{NI}=287$	0.7	f
	0.98	$T_{NI}=237$	0.4	f
	1.12	$T_{NC}=238$	5.6	f
		$T_{IC}=132$	0.3	
	1.39	$T_{NC}=234$	2.5	f
	1.4	$T_{NC}=240$	(8)	k
	1.67	$T_{NC}=237$	4.2	f
	1.85	$T_{NC}=234$	5.4	f

[a]Fawcett (1988a).
[b]Benediktsson *et al.* (1975).
[c]Geerken *et al.* (1982).
[d]Mukherjee *et al.* (1994).
[e]Suzuki (1976).
[f]Benediktsson *et al.* (1982).
[g]Maystrenko and Polovov (1977).
[h]Sidek *et al.* (1993).
[k]Endoh *et al.* (1982).

is difficult to determine, because of the strong strain dependence of T_N, which results in smearing of the transition in a sample having internal strain due to lattice defects.

This experimental problem depends largely on the particular chemistry of the Cr alloy system. Thus CrV alloys of a high degree of uniformity appear to be available with appropriate annealing, so that the continuous transition seen in a sample of Cr+0.5 at. % V is just as sharp as the weak first-order transition with critical fluctuation effects seen in pure Cr, both occurring in a temperature interval of about 3 K (Fawcett, Roberts, *et al.*, 1986). The transition remains sharp on doping presumably because the correlation length of the SDW is larger than the characteristic length associated with the statistical variation of composition for a random substitutional alloy, which might otherwise have been expected to produce a smearing over about 7 K, since the Néel temperature is depressed by nearly 50 K. In other alloy systems, where the impurity tends to cluster, or with samples prepared with inadequate annealing to produce uniformity of composition, an apparently continuous transition may in fact be a first-order transition smeared over a range of temperature.

The latent heat at a first-order phase transition may be measured either directly, for example, by the use of a differential calorimeter (Benediktsson *et al.*, 1975), or indirectly from the first-order length change combined, in the Clausius-Clapeyron equation, with the pressure dependence of the transition temperature. The results of such measurements of the latent heat are given in Table XV for the Néel transition in various Cr alloy systems, both to the incommensurate (T_{NI}) and commensurate (T_{NC}) SDW phase, and at the incommensurate-commensurate SDW phase-transition temperature T_{IC}. The data for the latter phase transition will be discussed in Sec. VI.B.

We note first in Table XV that, while V introduced into Cr causes the Néel transition to become continuous, the first-order character seen in pure Cr seems to persist when the isoelectronic impurity atoms Mo and W are introduced. The Néel transition to the incommensurate SDW is also weakly first order, with a latent heat of about 1 J/mol, for all the Cr alloy systems that have been measured in which a triple point exists, namely, CrRe, CrFe, CrCo, CrAl, and CrSi.

On the other hand, the Néel transition to the commensurate SDW phase is continuous, so far as is known, for all Cr alloy systems except CrFe and CrSi, for which there is a strong first-order transition with a latent heat about an order of magnitude larger than for pure Cr, as shown in Table XV. The absence of a latent heat at this transition has been ascertained directly for the systems CrMn, CrCo, and CrAl (see Table XV); and the absence of discontinuities in the temperature dependence of the resistivity, and/or thermal expansion and elastic constants, suggests that this is true also for the other systems that exhibit a triple point, namely, Cr alloys with group-8 transition metals, and also CrGa and CrGe.

The behavior of CrAl is difficult to understand, since Baran *et al.* (1992) find a discontinuity in the bulk modulus at the Néel transition in a Cr+1.2 at. % Al sample, with strong ultrasonic attenuation like that seen at the first-order Néel transition in pure Cr (Fawcett, 1988a), but no discontinuity in the neutron-diffraction intensity.

Sternlieb *et al.* (1994) found that cooling in a magnetic field of 6 T through the Néel transition into the commensurate SDW phase of a Cr+0.7 at. % Mn sample produced a preferred polarization direction **S** transverse to the field, which relaxed when the field was removed. This means that field-cooling to produce a single **S** domain appears to be ineffective, as expected. It was surprising, however, to find that field-cooling through the first-order transition from the incommensurate to the commensurate SDW phase, which in this high quality sample was quite sharp, and hysteretic by only about 20 K, failed to produce a single Q domain, as had been hoped.

B. Incommensurate-commensurate spin-density-wave phase transition

The schematic phase diagrams for the four Cr alloy systems shown in Fig. 56 illustrate the variety of behavior observed at the phase transitions. In CrMn the incommensurate-commensurate SDW phase transition is first order and strongly hysteretic, but has a latent heat about 30 times smaller than that of pure Cr (Geerken *et al.*, 1982). The phase diagram for CrRe is thought to be similar to that for CrMn, with a first-order and continuous Néel transition, respectively, to the incommensu-

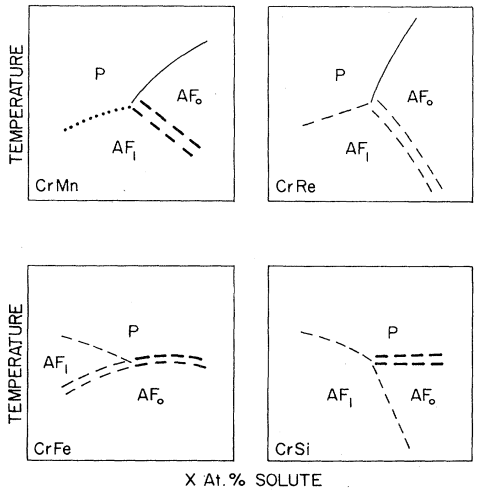

FIG. 56. Schematic phase diagrams for various Cr alloy systems. The nature of the phase transition is indicated: continuous (——); first order (— — —); not known (· · · ·); weak first order, with hysteresis (= = = =); strong first order, with hysteresis (= = = =).

rate and commensurate SDW phases (Lebech and Mikke, 1972), and a hysteretic and therefore first-order AF_0-AF_1 phase transition (Trego and Mackintosh, 1968).

The phase diagram of CrFe is distinctly different from that of any other Cr alloy system in that the AF_0 phase lies below the AF_1 phase, while CrFe and CrSi differ from all other Cr alloys in that the Néel transition to the AF_0 phase is strongly first order, with a large latent heat (see Table XV) and some hysteresis. Kemeny *et al.* (1979) believe that this phase transition in CrFe is more correctly described as a nucleation-controlled process, similar to the crystallization of a supercooled liquid, in which the AFM sample enters a superheated metastable magnetic phase before becoming paramagnetic. This so-called avalanche transition gives rise to a strong dependence of the apparent specific heat on heating rate, which is distinct from thermal diffusion effects.

Most features of the x-T phase diagram of the CrFe alloy system have been explained by the elegant theory of Nakanishi and Kasuya (1977). They add a magnetostrictive term to the free energy for the canonical model of nesting electron and hole octahedra, with a reservoir of power ρ defined in Eq. (4), by writing

$$\mathcal{J}=F(h+\eta\omega)+\tfrac{1}{2}B\omega^2 . \tag{86}$$

The second term is the elastic energy, ω being the volume strain and B the bulk modulus, while the magnetostrictive term introduces a linear volume dependence through the parameter $\eta\omega$ added to the nesting parameter h defined in Eq. (1). They assume exchange scattering in the Hamiltonian of Eq. (5), as appropriate for Fe atoms that carry a moment, and employ a scattering parameter, $g_1=0.24\pi T$, to describe electron-phonon scattering (Sato and Maki, 1974).

Figure 3 shows a variety of phase diagrams obtained by Nakanishi and Kasuya for different choices of the parameters, but in Fig. 57(a) the parameters are chosen to optimize the fit to the actual phase diagram of CrMn, for which the appropriate value for reservoir power ρ is between 2 and 3.

Parameters for calculation of the CrFe phase diagram were the same, with the addition of an impurity scattering of 257 K/at. % Fe and with the inclusion of parameters relating to the magnetostrictive term, like the measured value of the pressure dependence of the Néel temperature in pure Cr. With the triple point located at the point $x_L=2.5$ at. % Fe, $T_L=255$ K, the phase diagram shown in Fig. 57(b) was obtained. Transitions to the commensurate SDW phase are all first order, and the AF_0-AF_1 line is similar to the line for $\rho=\infty$ in the CrMn phase diagram shown in Fig. 57(a). The agreement with the actual phase diagram of CrFe, shown in Fig. 19, is excellent.

The magnetostrictive term in Eq. (86) increases the power ρ of the reservoir to an effective value r given by the relation

$$\frac{1}{r+1}=\frac{1}{\rho+1}-\frac{4\rho_0\eta^2}{B} , \tag{87}$$

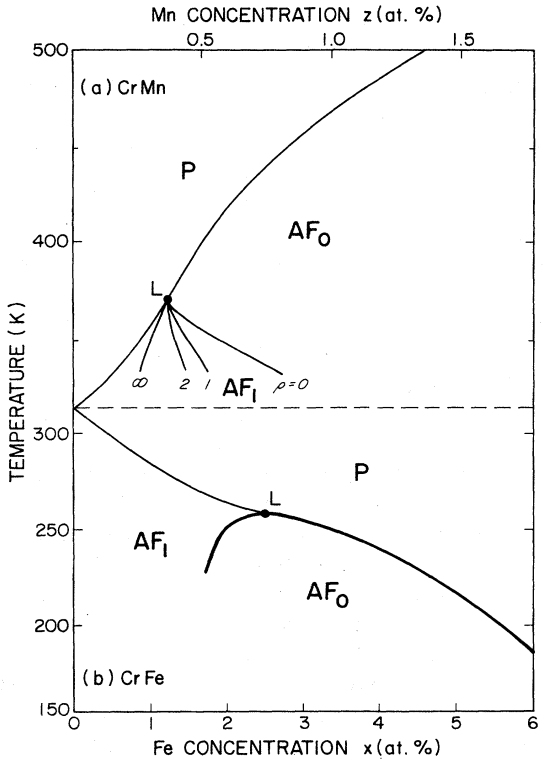

FIG. 57. Magnetic phase diagrams of (a) $Cr_{1-z}Mn_z$ with different AF_0-AF_1 lines of transition corresponding to different values of the power ρ of the reservoir [see Eq. (4)], and (b) $Cr_{1-x}Fe_x$ with the heavy line indicating the first-order nature of the transitions to the AF_0 phase from both the P phase and the AF_1 phase (after Nakanishi and Kasuya, 1977; Fawcett and Galkin, 1992b).

where $\rho_0=\rho_e=\rho_h$ is the electron/hole octahedron density of states, assumed equal for simplicity. The physical explanation for this effect is that the first-order transition results in a flow of electrons from the Fe impurities to the electron and hole octahedral Fermi surfaces, thus effectively enhancing the power of the reservoir. The calculated first-order strain at the Néel transition to the AF_0 phase is of order 5×10^{-4}, in good agreement with experiment, which corresponds to an electron flow of about 0.1 electron per Fe atom.

The second role of the Fe impurities is to reduce the energy-gap order parameter, by virtue of the electron-hole depairing produced by the strong exchange scattering, which overwhelms the effect of the improved nesting associated with the electron flow and results in the overall decrease of T_N with increasing x in the phase diagram of Fig. 57(b). In $Cr_{1-z}Mn_z$, without impurity scattering, T_N increases with z as in Fig. 57(a) because of the improved nesting of the electron and hole Fermi surfaces, resulting from electrons contributed by the Mn atoms, increases the energy gap and therefore T_N. Thus we have in the theory of Nakanishi and Kasuya a most satisfactory explanation for the unusual phase diagram of CrFe, though the fundamental origin of the magneto-

strictive term is still not understood.

The parallelism between the composition-temperature and pressure-temperature phase diagrams discussed in Sec. V.C and illustrated in Figs. 44(c) and 44(d) offers the possibility of studying the variation of the incommensurability parameter $\delta = 1 - Q$, Q being the SDW wave vector, as one approaches the triple point continuously by varying the pressure. The results, illustrated in Fig. 58, show that δ decreases slowly with decreasing pressure along the P-AF_1, line of phase transitions, and then falls abruptly to zero at the triple point. This result shows clearly that the triple point in CrFe, and presumably in other Cr alloys, is *not* a Lifshitz point, as had been speculated. The fact that the nature of the critical scattering in the paramagnetic phase a little above the Néel transition remains the same, as the triple point is approached, leads to this conclusion (Fawcett and Vettier, 1982).

Figure 59 shows the result of varying the Mn concentration in ternary CrFeMn alloys, for which the binary CrFe alloy has an incommensurate SDW phase. The addition of Mn causes the system to approach the triple point in a manner similar to decreasing pressure in Fig. 58(a); but for both ternary alloys, a *re-entrant* commensurate SDW phase is observed, as illustrated in Fig. 59. These phase diagrams were determined from the anomalies in the temperature dependence of the thermal expansion (Fawcett and Galkin, 1992, 1993; Galkin and Fawcett, 1993), and the various phase transitions show

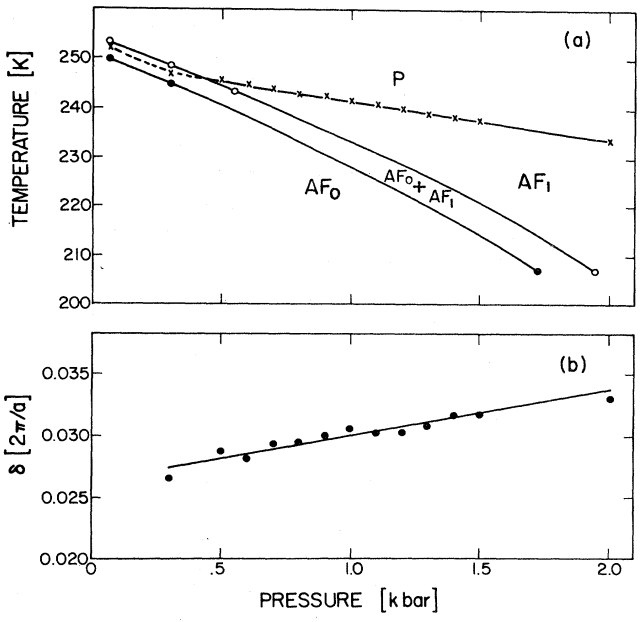

FIG. 58. Pressure dependence of Cr+2.8 at. % Fe: (a) phase diagram in the pressure-temperature plane showing the limits of superheating (○) and supercooling (●) at the first-order transition from paramagnetic P to commensurate AF_0 and incommensurate AF_1 SDW phases, with the points × defining the line of continuous P-AF_1 transitions, (b) incommensurability parameter δ along the P-AF_1 line (from Fawcett and Vettier, 1982).

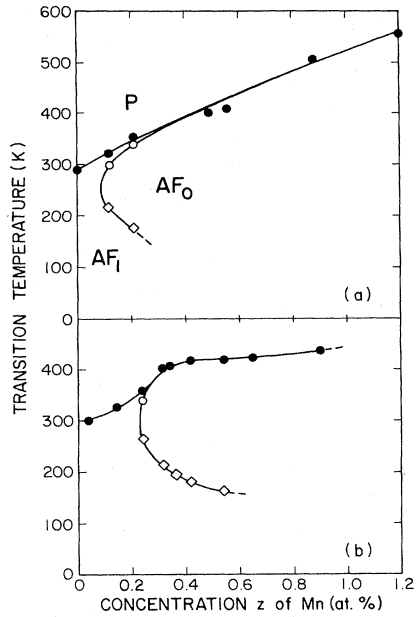

FIG. 59. Magnetic phase diagrams of (a) (Cr+1.5 at. % $Fe)_{1-z}Mn_z$ and (b) (Cr+0.5 at. % $Fe)_{1-z}Mn_z$: ●— — — T_N; ○— — — T_{IC}; ◇— — — T_{IC} (from Fawcett and Galkin, 1992).

interesting contrasts in their nature. It would be most interesting to explore the pressure-temperature phase diagram of some of these ternary alloys.

CrSi also exhibits a strong first-order length change of the Néel transition to the commensurate SDW phase, with a somewhat smaller step in the opposite direction at the incommensurate-commensurate SDW phase transition (Suzuki, 1977). Unlike the CrFe system, however (Butylenko, 1989), these two first-order transitions occur in samples having compositions close to the triplet point but with $x \gtrsim x_L$, since the phase diagram of CrSi is normal, in that the AF_1 phase lies below the AF_0, except very close to the triple point (see Fig. 17).

Galkin *et al.* (1991) extended the theory of Nakanishi and Kasuya to explain an interesting feature of the phase diagram of $Cr_{1-x}Si_x$, that the Néel temperature initially decreases, but goes through a minimum value close to the triple-point concentration x_L and therefore increases with x. This is a consequence of the resonant scattering at the local impurity state in the energy gap (Volkov and Tugushev, 1984) associated with the Si atom (Galkin, 1987), which we discussed in Sec. IV.A. The scattering parameter g_{Si} also includes the usual potential scattering term and is of the form

$$g_{Si} = \begin{cases} g_0, & E_F \leq E_0 , \\ g_1(E_F - E_0), & E_F > E_0 , \end{cases} \tag{88}$$

corresponding to the dependence of the resonant scattering on the position of the Fermi level E_F relative to the Si impurity level E_0. The addition of Si to Cr is assumed also to shift E_F in the same direction as does Mn, but at a somewhat lower rate, corresponding to an increase in the

electron concentration in the canonical model.

In fact, the magnetostrictive term is quite unable to explain the minimum in $T_N(x)$ around the triple point, as Suzuki (1977) found when he applied the Nakanishi-Kasuya theory to account for the first-order changes in length that he observed. The fact that a similar variation of $T_N(x)$ is found in several other Cr alloy systems with nontransition metals, including Al, Ga, and Ge, as illustrated in Figs. 9 and 16, suggests that scattering by these impurities also might have a resonant character.

Fishman and Liu (1993c) find, using the Young and Sokoloff (1974) three-band model, that impurity scattering, which in this case may result in the incommensurate SDW phase lying at lower temperatures than the commensurate SDW phase, may also give a first-order transition between these phases, unlike the canonical model (see Sec. II.A). They claim, in particular, that the *IC* transition in CrMn alloys is first order for this reason, whereas Nakanishi and Kasuya (1977) obtained a continuous transition, as illustrated in Fig. 57(a).

The difficulty with this explanation is that, in fact, CrMn is exceptional in having a first-order *IC* transition, since apart from CrFe, whose anomalous behavior is due to a magnetostrictive effect, all the other systems considered in Table XV (CrCo, CrAl, and perhaps CrSi) have a continuous *IC* transition. We can be sure that other systems not listed in Table XV would have been reported if, like CrMn (e.g., Geerken *et al.*, 1982), they had shown spectacular effects due to a first-order *IC* transition; and their absence suggests that the *IC* transition is nearly always continuous.

C. Spin-flip transition

The first-order phase transition at temperature T_{SF} in pure Cr, where the polarization direction in the transverse SDW phase AF_1 "flips" into the direction of the wave vector **Q** in the longitudinal SDW phase AF_2, is most clearly seen in neutron-diffraction measurements, because of the dependence of scattering intensity on the angle between the polarization direction and the momentum transfer to the scattered neutrons. The phase diagrams for CrRe, CrFe, CrBe, CrAl, CrSi, and CrGe show a branch corresponding to the spin-flip transition determined in this way.

The spin-flip transition also gives rise to anomalies in the temperature dependence of the thermal expansion (β), elastic constants (US); and magnetic susceptibility (χ), with only a very weak anomaly, if anything at all, in the resistivity and other physical properties. Thus, apart from neutron diffraction experiments, the spin-flip transition has been observed in only a few Cr alloy systems, including CrTi (Chiu *et al.*, 1971: χ); CrW (Hedman *et al.*, 1974: χ); CrAl (Alberts and Lourens, 1984a: US; Baran *et al.*, 1992: ND and US); CrRu (Alberts and Boshoff, 1992: US); and CrPt (Alberts and Lourens, 1988c: US).

Arrot and Werner (1969) explained why the spin-flip transition temperature always decreases on alloying, as seen in Table I. The depression of the spin-flip temperature, as observed in the magnetoresistance of a Cr(001) thin film (Mattson *et al.*, 1991), is associated with stress due to differential thermal expansion. This experiment points the way, however, to work on Cr alloy films that will be interesting.

D. Spin-glass phase between the spin-density-wave and ferromagnetic phases

When the impurity atom carries a moment, as in the case of Fe dissolved in Cr, which is discussed in Sec. III, the interesting possibility arises of the existence of a spin-glass state, intermediate between the AFM phase at low concentrations of Fe and the ferromagnetic phase that must develop at sufficiently high concentrations. The nature of the Fe moment, and of the interaction between the SDW and the moment, has been investigated by diffuse neutron elastic scattering, as we shall see in Sec. IX.B. We shall discuss here measurements, as a function of Fe concentration and of temperature, of the bulk magnetization, with and without field cooling, to reveal spin-glass characteristics; of elastic neutron scattering to determine the SDW moment and, with the resistivity, the Néel temperature; and of quasielastic neutron scattering to determine the correlation length and relaxation time of the magnetically correlated clusters of Fe moments, which appear to coexist with the SDW at low temperatures over a wide range of concentrations.

Ishikawa *et al.* (1965) first observed spin-glass-like behavior in the form of magnetic remanence at low temperatures for compositions in the range $x=9$ to 15 at. % Fe. Ström-Olsen *et al.* (1979) observed a peak in the zero-field susceptibility, which they used to determine a spin-glass freezing temperature $T_G=9$ K in a sample Cr+14 at. % Fe. The Néel temperature $T_N=65$ K, determined from the inflection point in the temperature dependence of the resistivity, was in good agreement with the value obtained from elastic neutron-scattering measurements of the temperature dependence of the SDW amplitude. In a ternary alloy, Cr+2 at. % Mo+14 at. % Fe, in which the Cr was diluted with Mo so as to reduce the AFM interaction, the zero-temperature amplitude of the SDW and the Néel temperature were both reduced by a factor of about 2 ($T_N=30$ K) while the spin-glass freezing temperature increased by about the same factor ($T_G=17$ K). In both samples, the marked difference between the temperature dependence of the susceptibility for the field-cooled state and for zero-field cooling provided clear evidence for the existence of a spin-glass state.

Alberts and Lourens (1992) found an anomaly in the sound velocity at the spin-glass transition for $16 \leq x \leq 20$ at. % Fe, but not in the antiferromagnetic alloys with $x=12$ and 15 at. % Fe. They found no anomaly in either the thermal expansion ω or the sound velocity at the Cu-

rie temperature for $20 \leq x \leq 30$ at. % Fe.

Babic *et al.* (1980) pursued another aspect of the behavior of AFM CrFe alloys by measuring the susceptibility in very high pulsed magnetic fields up to 33 T. They thus extended the measurements of Ishikawa *et al.* (1965) and observed superparamagnetism at low temperatures for compositions in the range $x=2.4$ to 14 at. % Fe, showing the existence of ferromagnetic clusters of Fe atoms.

The definitive work on the CrFe alloys system in the region of interest was performed by Burke and Rainford (1978, 1983) and Burke *et al.* (1983). They used a series of $Cr_{1-x}Fe_x$ samples, ranging in composition from about $x=5$ to more than 20 at. % Fe, which were arc melted several times, vacuum annealed, and water quenched to achieve homogeneity of composition. The spin-glass freezing temperature shown as a function of x in the inset to Fig. 60 was determined from the peak in the low-field susceptibility, which shows a broad maximum as a function of temperature.

The AFM phase boundary was determined from neutron-diffraction, magnetic-susceptibility, and electrical resistivity data, and extrapolates to a critical concentration for antiferromagnetism at zero temperature, $x_A=16\pm0.5$ at. % Fe. The SDW and spin-glass states coexist between x_A and $x \leq 10$ at. % Fe; and for compositions in this range, the Néel temperature T_N and the SDW moment μ_0 at zero temperature remain proportional to each other with the same scaling factor as that outside the spin-glass region, $\mu_0/T_N=(3.1\pm0.1)\times10^{-3}$ μ_B K^{-1}. Although this fact is rather larger than usual for commensurate SDW systems, for which in Fig. 7 we see $d\mu_0/dT_N \simeq 1.1\times10^{-3}$ μ_B K^{-1}, with both CrSi and CrFe having an anomalously high value, Burke and Rainford (1978) point out that the constancy of the factor

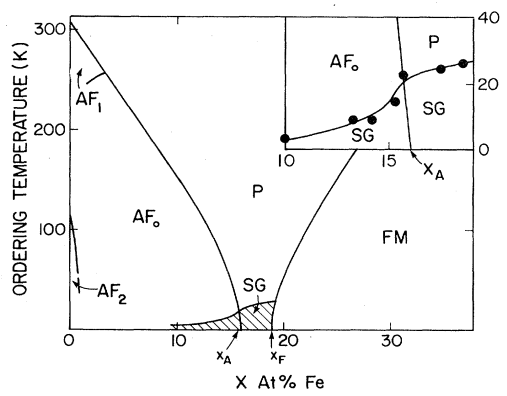

FIG. 60. Magnetic phase diagram of the $Cr_{1-x}Fe_x$ alloy system showing the antiferromagnetic phase boundary extending from lower concentrations $x \leq 5$ at. % Fe, as shown in Fig. 14, to the critical concentration $x_A=16$ at. % Fe (Burke and Rainford, 1978), the spin-glass (SG) freezing-temperature data points ● (Burke and Rainford, 1983a), and the ferromagnetic (FM) phase boundary starting at the critical concentration $x_F=19$ at. % Fe (after Burke and Rainford, 1983b; see also Figs. 110, 112, and 114 in Landolt-Börnstein, 1986).

in the CrFe system demonstrates the remarkable fact that the essential nature of the SDW remains unchanged even close to the critical concentration for antiferromagnetism, despite the development of the coexistent spin-glass state.

The ferromagnetic phase boundary in Fig. 60 was determined from magnetization measurements, with a critical concentration for ferromagnetism at zero temperature, $x_F=19$ at. % Fe. We shall not discuss the neutron small-angle scattering work of Burke *et al.* (1983) used to explore the magnetic properties in the ferromagnetic region, since this is beyond the scope of the present review. The spin dynamics of the Cr+10 at. % Fe alloy in the spin-glass region, measured by Burke and Rainford (1983) using time-of-flight neutron spectroscopy, is, however, of great interest in showing the magnetic properties of the coexistent SDW and spin-glass state.

The correlation length of 5 to 10 Å is essentially constant up to temperature 250 K (Burke and Rainford, 1983, Fig. 7). The relaxation time at the Néel temperature, $T_N=175$ K, is about 10^{-11} s, corresponding to a Lorentzian energy half-width of 1 meV for the scattering, and varies smoothly through T_N (Burke and Rainford, 1983, Fig. 5). This means that clusters of Fe moments are only marginally affected by the development of the SDW, with the relaxation rate tending to the normal Korringa law of proportionality with temperature. The correlation length increases by about 20% between 250 and 10 K, while the Fe moments tend to relax more rapidly with the onset of the SDW.

No theoretical analysis has been performed to describe the coexistent SDW and spin-glass state. Kakehashi (1987) reproduced fairly well the other features of the phase diagram shown in Fig. 60, using a theory with local-environment effects at finite temperature, by suitable choice of the parameters, which include nearest-neighbor ferromagnetic and AFM exchange, respectively, between Fe-Fe and Cr-Cr atoms. It is speculated that inclusion of next-nearest-neighbor exchange might produce the spin-glass state.

E. Transition from spin-density-wave to superconducting phase

Petalas and Baltensperger (1968) showed that, in principle, an electron gas in the SDW state can simultaneously exhibit superconductivity. The SDW and superconducting states have in fact been found to coexist in quasi-one-dimensional organic structures, under pressure or in a magnetic field (see, for example, Fawcett, 1989d; Ishiguro and Yamaji, 1990). Their theoretical description by Machida (1982) and Fenton (1985) supposes the quasi-one-dimensional Fermi surface to comprise regions that nest and give rise to the SDW, and other regions for which the electron-electron interaction is sufficiently attractive as to cause condensation into Cooper pairs, resulting in superconductivity. Gulásci and Gulásci (1986) analyzed the possibility for the coexistence of SDW and

superconductivity for the canonical two-band model, while Daemon and Overhauser (1989) consider superconductivity within the framework of the Bardeen-Cooper-Schrieffer theory for a SDW metal.

Heavy-fermion systems, for example, UPt_3 and URu_2Si_2, exhibit coexistent SDW and superconducting states in three dimensions, but their fundamental understanding is still lacking. The high-temperature perovskite oxide superconductors are quasi-two-dimensional systems that may also exhibit AFM order. Interest in the SDW aspect of high-temperature superconductors has been keen because of the spin-bag model proposed by Kampf and Schrieffer (1990) as a possible mechanism for their superconductivity, mediated by SDW fluctuations, under the assumption that some physical mechanism locks the SDW state in incommensurability with the lattice. Impurity atoms can reduce the SDW energy gap, which leads to an increase of the SDW fluctuations and thereby to an increase in the attractive interaction between the quasiholes. The SDW model holds promise, in view of the strong belief by some that the fundamental mechanism responsible for high-temperature superconductivity is magnetic in origin.

Interest in the nature of the phase boundary in a Cr alloy system between the SDW phase and the superconducting phase, and the possibility of coexistence of the two states, goes back to the work of Muheim and Müller (1964) on $Cr_{1-x}Re_x$. Their data for the Sommerfeld coefficient of the electronic specific as a function of x are shown in Fig. 61, together with their observation of superconductivity in samples containing $x \geq 20$ at. % Re. More recent work by Damaschke and Felsch (1986) shown in Fig. 61 indicates superconductivity of x as low as 14 at. % Re, with a superconducting transition temperature of about 1 K. The Néel transition has been observed by Alberts (1989), through the anomaly in the temperature dependence of the elastic constant, for x as high as 17 at. % Re, with a Néel temperature of 370 K, as shown in Fig. 61. Damaschke and Felsch (1986) caution, however, against the premature conclusion that this provides firm evidence for the coexistence of antiferromagnetism and superconductivity in this system, since there are severe metallurgical problems, as discussed extensively by Muheim and Müller, in preparing a sample of uniform composition, because of the high vapor pressure of Cr at the liquidus temperature.

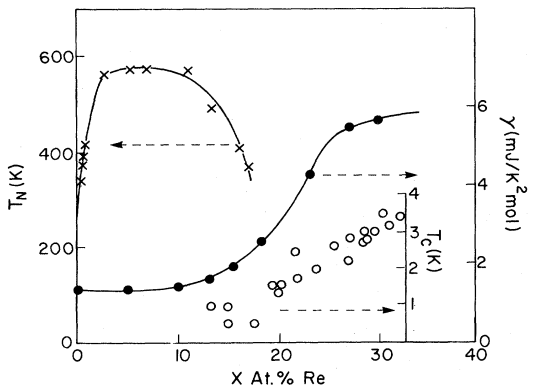

FIG. 61. Antiferromagnetism, superconductivity, and electronic specific heat of the $Cr_{1-x}Re_x$ alloy system: ×— — —Néel temperature T_N (Alberts, 1989, gives references for the data points); ●— — —Sommerfeld coefficient γ of the low-temperature electronic specific heat (Muheim and Müller, 1964); ○— — —superconducting transition temperature (Damaschke and Felsch, 1986, give references for the data points).

Alberts (1989) also found no evidence in the temperature dependence of the elastic constants to support the identification with the Néel transition, by Nishihara *et al.* (1985), of a broad maximum in the susceptibility, centered at temperature ~150 K, for $x=20$, 26, and 30 at. % Re. Alberts (1988c) also endeavored to validate a similar claim by Nishihara *et al.* (1986) to have observed a coexistent SDW and superconducting state in $Cr_{1-x}Ru_x$ alloys for $x \geq 18$ at. % Ru, but found no anomaly in the temperature dependence of the elastic constants for the alloy compositions that showed peaks in the susceptibility.

Alberts *et al.* (1991) also measured ternary alloys $(Cr_{1-x}Mo_x)_{75}Ru_{75}$, with $x=0$, 3, 6, and 10 at. % Mo, in order to vary the strength of the AFM interaction and to see the effect on the superconducting transition temperature. The experiment was, however, inconclusive, since all the samples were superconducting, with approximately the same transition temperature, $T_C \simeq 2$ to 2.5 K, while none of them showed any evidence in the temperature dependence of the elastic constants for a Néel transition.

Nishihara *et al.* (1985) also measured the NMR of the Re nuclei in their superconducting $Cr_{1-x}Re_x$ alloys and claimed to find evidence for hyperfine fields, which would indicate the existence of a SDW. Further experiments with local probes, as described in Sec. IX.D, should be performed to explore this important question of the coexistence of SDW and superconducting states in these Cr alloys.

VII. STRUCTURE AND EXCITATIONS

The powerful technique of neutron scattering, to which Squires (1978) provides an introduction, has been used extensively to determine the structure of Cr alloys by elastic scattering (neutron diffraction) and, to a lesser extent, to study magnetic excitations by inelastic scattering. Incoherent neutron scattering has been used as a local probe to study the magnetic structure around a single impurity or cluster of impurities, as described in Sec. IX.B.

A. Elastic neutron scattering

We have already in Sec. II.B summarized a good deal of the neutron-diffraction data for Cr alloys in Table II

and Figs. 5 and 6, which show the dependence of the SDW wave vector Q and rms moment $\langle\mu\rangle$ on alloy composition. Further aspects of the structure of the SDW in Cr alloys that have been explored in diffraction experiments (most neutron, but also a few x ray) include the temperature dependence of Q and $\langle\mu\rangle$, and the dependence of the harmonic content of the SDW on doping. In the latter connection, the relation between the incommensurability parameter, $\delta=1-Q$, and the amplitude of the third-harmonic and the second-harmonic strain wave relative to that of the fundamental SDW is of particular interest, since theoretical analysis gives predictions about them (Young and Sokoloff, 1974; Kotani, 1975).

The curves in Fig. 62 showing the temperature dependence of Q for several Cr alloys (see also recent work on CrAl alloys by Baran *et al.*, 1992) exhibit in several cases the interesting property that the SDW appears to lock into the lattice at a "pinning temperature," typically, $T_p \gtrsim 100$ K, with Q remaining constant at lower temperatures. Venema *et al.* (1980) emphasize the fact that the SDW is locked to the lattice by pointing out that, if thermal expansion were to be taken into account, the value of Q for a SDW of fixed wavelength would increase very rapidly above about 100 K, as shown by the dotted curve in Fig. 62, since Q is expressed in units of $a^*=2\pi/a$.

The existence of a pinning temperature in the Cr alloys may be a sample-dependent property, as it appears to be

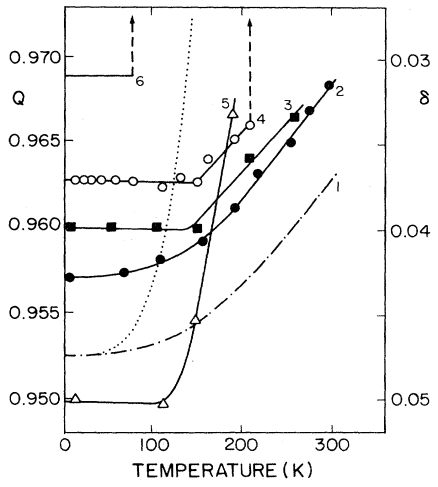

FIG. 62. Temperature dependence of the SDW wave vector $Q=1-\delta$ (both in units of $a^*=2\pi/a$): 1 (—·—·—·) Cr (Gibbs *et al.*, 1988); 2 (●) Cr+0.4 at. % Fe (Ishikawa *et al.*, 1967); 3 (■) Cr+0.8 at. % Fe (Arrott *et al.*, 1967); 4 (○) Cr+0.5 at. % Mn (Fawcett *et al.*, 1978); 5 (△) Cr+1.0 at. % Ni (Endoh *et al.*, 1968); 6 (— — —) Cr+0.8 at. % Re (Lebech and Mikke, 1972). The curves for the CrMn and CrRe alloys terminate at the transition to the commensurate SDW phase where the incommensurability parameter δ becomes identically zero. The dotted curve (· · · ·) illustrates the temperature dependence of Q if the SDW wave vector were assumed to be fixed at the low-temperature value, so that Q would increase with temperature like the lattice parameter.

in pure Cr. Thus Fawcett *et al.* (1978, see Fig. 2) find in Cr clear evidence for pinning at a temperature $T_p \simeq 60$ K, while Gibbs *et al.* (1988) report a continuous variation of Q down to helium temperatures.

The temperature dependence of the wave vector at higher temperatures, and as the Néel transition is approached, is considerably larger for the CrNi system than for pure Cr and the other Cr alloys illustrated in Fig. 62. The same is true for CrCo (Endoh *et al.*, 1968).

We turn now to consider the temperature dependence of the rms moment $\langle\mu\rangle$, which in Cr alloys undergoing an incommensurate-commensurate (AF_1-AF_0) SDW phase transition is difficult to measure, since the neutron-scattering intensities of all the satellites in the AF_1 phase have to be measured for comparison with the single Bragg peak in the AF_0 phase. The occurrence of a spin-flip transition also causes an apparent discontinuity in $\langle\mu\rangle$ at the transition (see Fig. 2 of Werner *et al.*, 1967) due to extinction effects (Fawcett *et al.*, 1986a).

Further problems are associated with the occurrence of a "central peak" at the commensurate position in many cases when the SDW is incommensurate. This may be due to internal strain, which induces regions of AF_0 phase in an AF_1-phase sample, just as in pure Cr (Fawcett, 1988a); or to poor resolution, which results in the neutron spectrometer picking up the off-axis satellites in a polydomain sample in a sweep along one of the cube axes (Noakes, Holden, Fawcett, and de Camargo, 1990); or to quasielastic scattering associated with the commensurate diffuse scattering identified in pure Cr by Grier *et al.* (1985). Finally, the occurrence of a first-order Néel transition leads to a drop in the rms moment of unknown magnitude, which may be spread around the Néel temperature due to inhomogeneity of composition. Perhaps for these several reasons, there appear to be no neutron-scattering data for Cr alloys that can be compared meaningfully with the predicted variation with temperature of the rms moment as the BCS function (Overhauser, 1962).

The phenomenological description of the strain wave and odd harmonics of the SDW seen in pure Cr was reviewed by Fawcett (1988a), with some reference also to results for Cr alloys. Thus the ratio of the amplitude S_3 of the third harmonic to the amplitude S_1 of the fundamental decreases rapidly as the incommensurability parameter, $\delta=1-Q$, increases in a series of Cr samples doped with V and Mn (see Fig. 30 of Fawcett, 1988a). These data are reproduced in Fig. 63(a), together with data for the amplitude Δ/a of the strain wave, also plotted as a function of δ, in Fig. 63(b). We note incidentally that the displacement amplitude Δ must be clearly distinguished from the strain amplitude Δa in such a plot, since $\Delta a = \Delta\sin(4\pi\delta)$. In Fig. 63(b) we also plot vs δ the ratio of $\Delta a/a$ to S_1, which must vanish as δ goes to zero because of this relation.

The theoretical curves for the samples of the third harmonic and of the strain wave, relative to the amplitude of the fundamental, as a function of δ, shown in Figs. 63(a)

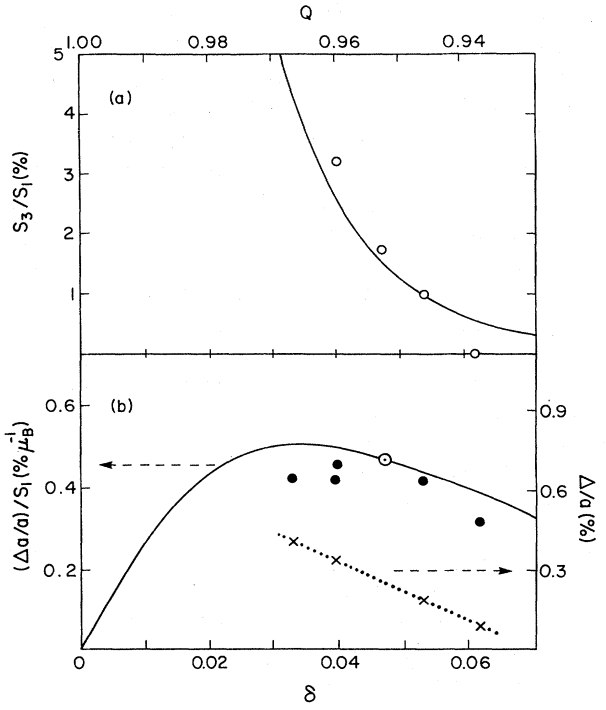

FIG. 63. Relation between the amplitudes of the SDW harmonics and the incommensurability parameter $\delta = 1 - \mathbf{Q}$ (both measured in units of $a^* = 2\pi/a$): (a) ○ — — —the relative amplitudes of the third-harmonic and fundamental analyzed from the experimental data of Iida, Tsunoda, *et al.*, (1981) with the rigid-spin model compared with (——) the theoretical curve calculated by Kotani (1975) using $\Delta_\infty = 0.034$; (b) × — — —displacement amplitude $\Delta a/a$ relative to S_1 from data of Iida, Kohno, *et al.* (1981); (——) the theoretical curve calculated by Machida and Fujita (1984) using $\Delta_\infty = 0.044$ and adjusting the vertical scale at the data point ⊙ for pure Cr (from Fawcett, 1993).

and 63(b), respectively, were calculated by Machida and Fujita (1984) using an exact solution of the canonical model of imperfect-nesting Fermi surfaces, which describes the snoidal-wave modulation of the SDW. The fit to the experimental data is good, though we note that the absolute amplitude of the strain wave is not calculated in this theory. In addition, somewhat different values of the energy parameter Δ_{00} are used in Figs. 63(a) and 63(b) to obtain the best fit in each case. We note that Δ_{00} (denoted δ_0 by Machida and Fujita, 1984) is the energy gap at zero temperature for the perfect-nesting model, corresponding to $\mathbf{H} = 0$ in the schematic energy-band structure (see Fig. 50 of Fawcett, 1988a), which is given in units, $\hbar a^* v_F/2$, and is to be distinguished from the zero-temperature energy gap Δ_0.

B. Inelastic neutron scattering

We shall give only a brief review of the theory, emphasizing those features relevant to the available experimental data. We shall describe the latter more thoroughly, since there are several remarkable features that call for further experimental study and further theoretical analysis.

Efforts to verify the early theoretical results of Fedders and Martin (1966), who showed that the spin-wave velocity for a model of nesting electron and hole spheres should be close in value to the Fermi velocity, were reviewed by Fawcett (1988a). This work (Sinha *et al.*, 1969, 1977; Als-Nielsen *et al.*, 1969, 1971) was performed on samples of Cr doped with several atomic percent Mn to give a commensurate SDW phase, which was considered simpler to study than an incommensurate SDW sample having six magnetic Bragg satellites around the commensurate position for a polydomain single crystal. We shall see, however, that doping changes qualitatively several features of the inelastic neutron scattering, and both incommensurate and commensurate SDW samples should be studied by theory and experiment.

In fact, the spin-wave excitations are barely resolved even in the most favorable case of a commensurate SDW sample at high-energy transfer. It turns out, however, that a much more striking feature of the experimental data is the large variation between different alloys in the temperature dependence of the intensity of the inelastic neutron scattering, which was discussed only perfunctorily in the theoretical analysis. Furthermore, the remarkable commensurate diffuse (CD) scattering, which was first reported in Cr alloys by Mikke and Jankowska (1978b, 1979) and was later the subject of extensive experimental study in pure Cr, as reviewed by Fawcett (1988a), is not predicted by any theory.

Liu (1970) extended the work of Fedders and Martin (1966) to finite temperatures and included phonon scattering, following Zittartz (1967). The spin-wave line shapes that he calculated around the Néel temperature, $0.97 \leq t \leq 1.03$, where $t = T/T_N$ is the reduced temperature, are barely resolved, like those observed experimentally; but the well-resolved spin waves predicted at intermediate and low temperature are not seen.

Although Sato and Maki (1974) did a more comprehensive analysis and calculated the spin waves in the AF_1 and AF_0 phases as well as the critical behavior through T_N into the paramagnetic phase, for the canonical model of unequal Fermi surfaces, they neglected phonon scattering and thus missed those features of Liu's theory resulting from suppression of T_N and reduction of the energy gap to zero at temperatures lower than T_N (Liu, 1986).

The same criticism applies to the analysis of Zhu and Walker (1986), who confirmed the result of Sato and Maki that the spin-wave velocity, like the order parameter, goes to zero at T_N like $(T_N - T)^{1/2}$. Liu (1986) had pointed out that, since the gap is zero close to T_N with phonon scattering, all spin waves are overdamped, so that one cannot define a velocity.

Fishman and Liu (1992 ,1993a ,1993b) have addressed recently the problem of explaining the inelastic scattering in the paramagnetic phase of Cr and its alloys (Noakes,

Holden, and Fawcett, 1990; Noakes, Holden, Fawcett, and de Camargo, 1990) and also in a paramagnetic alloy, Cr+5 at. % V, associated with nesting of the Fermi surface (Fawcett, Werner, *et al.*, 1988, 1989). Their three-band model was described in Sec. II.A, and we shall give here only a brief account of the results of their calculations. At a reduced temperature, $t=T/T_N=1.025$, the incommensurate peaks in the dynamic susceptibility are little changed in width by impurity scattering when the ordered phase is an incommensurate SDW (Figs. 9 and 10). When the ordered phase is commensurate, the inelastic-scattering peaks with no scattering are still incommensurate (Figs. 11 and 12, dashed curves, Fishman and Liu, 1993a), since for the parameters chosen the nesting vector is still far from commensurate. In this case, on the other hand, introducing scattering causes the incommensurate inelastic peaks to collapse into a commensurate central peak (Figs. 11 and 12, solid curves, Fishman and Liu, 1993a). When the mismatch between the electron and hole surfaces is so large that the alloy never orders even at zero temperature, inelastic scattering is seen with greatly reduced intensity (Figs. 13 and 14, Fishman and Liu, 1993a) and decreasing slowly with increasing temperature (Figs. 3 and 4, Fishman and Liu, 1993b).

The observed variation of the temperature dependence of the inelastic scattering $I(t)$ between different Cr alloys shown in Fig. 64 is amazing. The increase of $I(t)$ in a CrMn alloy as temperature decreases below T_N, shown in Fig. 64 (Sinha *et al.*, 1977), is very strange and was not observed in a recent study of a good Cr+0.7 at. % Mn sample (Sternlieb *et al.*, 1993). Another commensurate SDW sample, CrFeSi (curves 1, 2, and 3 in Fig. 64 for the three AF_0 alloys are shown by heavy lines), has a roughly constant intensity below T_N. The two AF_1 alloys, Cr+0.18 at. % Re and CrAl (curves 4 and 5), show $I(t)$ decreasing rapidly as temperature decreases below T_N, like pure Cr (Tsunoda *et al.*, 1972; Grier *et al.*, 1985). The AF_0 sample Cr+0.8 at. % Re (curve 3) is intermediate in behavior, but $I(t)$ decreases by a factor of about 2 at the AF_0-AF_1 transition and thus moves towards the lower values apparently characteristic of the AF_1 phase. In the paramagnetic phase, the intensity decreases with increasing temperature in all cases, but only the variation for CrMn is sketched in Fig. 64.

Another remarkable feature of inelastic neutron scattering in SDW systems is illustrated in Fig. 65. These results of Mikke and Jankowska (1978b) were the first clear evidence for commensurate diffuse scattering, which has been studied intensively in pure Cr, as reviewed by Fawcett (1988a), and reported more recently by Stirling *et al.* (1989), Pynn *et al.* (1992), and Sternlieb *et al.* (1994). Figure 65(a) shows well-resolved Bragg peaks at wave vector $\mathbf{Q}=(0.0,1\pm\delta)$, $\delta\lesssim 0.05$, with the central peak being due to the off-axis Bragg peaks picked up because of the relatively low resolution of the spectrometer. The fact that $I(1+\delta)>I(1-\delta)$ is probably

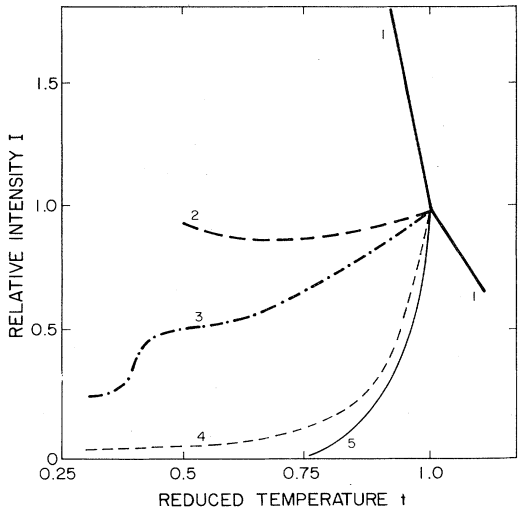

FIG. 64. Temperature dependence (corrected for the Bose-Einstein population factor) of the integrated inelastic neutron scattering at constant energy transfer ΔE for scans of the scattering vector along the cube axis in several Cr alloys: 1 (——) Cr+2 at. % Mn (AF_0) for $\Delta E=8$ and 16 meV; 2 (— — —) Cr+0.8 at. % Fe+0.3 at. % Si (AF_0) for $\Delta E=10$ meV; 3 (—·—·—) Cr+0.8 at. % Re (AF_0 with phase transition to AF_1) for $\Delta E=2$ and 4 meV; 4 (— — —) Cr+0.18% Re for $\Delta E=4$ and 8 meV; 5 (——) Cr+0.5 at. % Al (AF_1) for $\Delta E=2$ meV (after Mikke and Jankowska, 1978b,1979).

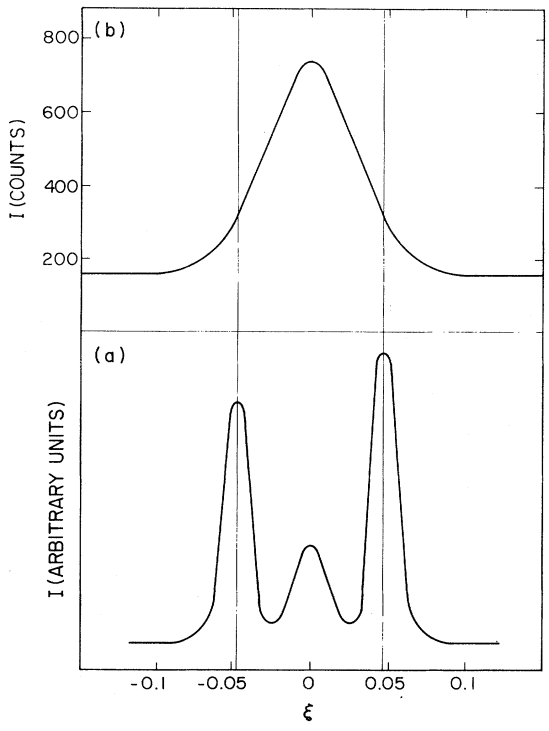

FIG. 65. Commensurate diffuse neutron scattering at reduced temperature $t=0.94$ in Cr+1.2 at. % Al. The scattering wave vector ξ is measured in units of a^* relative to (0,0,1), with $\mathbf{Q}=(0,0,1\pm\delta)$: (a) elastic-scattering intensity I showing that $\delta<0.05$; (b) inelastic scattering at energy transfer $\Delta E=6$ meV (from Mikke and Jankowska, 1978b).

due to misalignment, since the form factor of the moment invariably leads to the inequality having the opposite sign.

The inelastic scattering in Fig. 65(b) shows, however, no sign of these Bragg peaks, the single peak centered at (0,0,1) having, in fact, a width rather smaller than 2δ. Similar behavior is seen for the other incommensurate SDW alloy Cr+0.18 at. % Re (Mikke and Jankowska, 1980), for which the temperature dependence of the integrated intensity I is similar to that of the CrAl alloy (see curves 4 and 5 in Fig. 64). A similar effect was seen by Grier *et al.* (1985) in pure Cr, and they termed the scattering responsible for the inelastic peak at (0,0,1) "commensurate diffuse" (CD) scattering.

Commensurate diffuse scattering may also occur in the AF_0 alloys; but since the Bragg peak in this case is also at (0,0,1), the dramatic disappearance of the incommensurate SDW Bragg peaks for inelastic scattering is no longer a clear signal of such behavior. It seems likely, however, that the very different temperature dependence of the intensity for CrMn, and perhaps for CrFeSi and Cr+0.8 at. % Re (see curves 1, 2, and 3 in Fig. 64), indicates some other scattering mechanism for the commensurate SDW alloys.

The critical scattering in the paramagnetic phase in pure Cr and in a dilute alloy Cr+0.2 at. % V was measured by Noakes *et al.* (Noakes, Holden, and Fawcett, 1990; Noakes, Holden, Fawcett, and de Camargo, 1990), and the results for the critical exponents are presented in Sec. VI.A. The most interesting features of these data are, however, illustrated in Fig. 66 and presented in Table XVI. The equation for the dynamic susceptibility that was found to describe accurately the neutron-scattering intensity as a function of both energy transfer up to $\hbar\omega \simeq 16$ meV and scattering wave vector ξ through the inelastic peaks, as shown in Fig. 66 and Fig. 2 of Fawcett *et al.* (1991), in the case of both pure Cr and the doped sample, had been given by Sato and Maki (1974),

$$\chi(\mathbf{q},\omega)=\frac{(\chi^0/r^2)A^2}{A^2[\kappa^2+R(\mathbf{q})]^2+\omega^2}\ , \tag{89}$$

where χ^0 is the coefficient of the Curie-law susceptibility in the noninteracting limit, r is the length scale of the magnetic interaction, A is the "magnetic stiffness," and κ

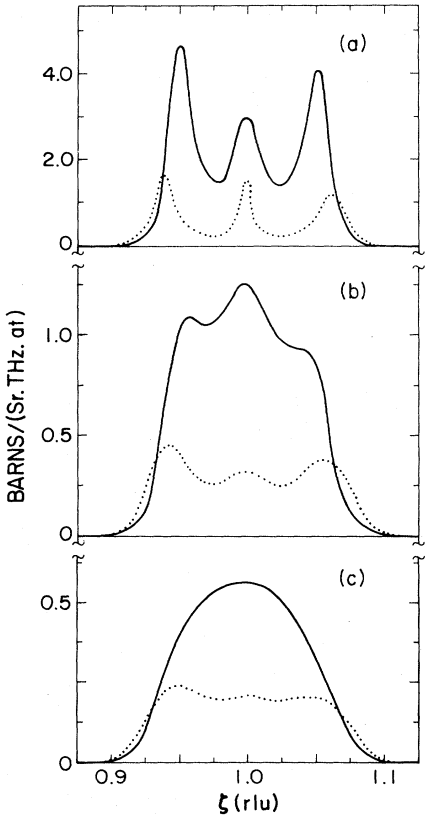

FIG. 66. Neutron-scattering wave vector ξ scans along the cube axis [001] in the paramagnetic phase for Cr (— — —) and Cr+0.2 at. % V (. . . .) at the same reduced temperature, $t=1.027(2)$. The constant energy transfers are (a) $\hbar\omega=0$, (b) $\hbar\omega=2$ meV, and (c) $\hbar\omega=4$ meV. The data points to which these curves are fit are shown in Figs. 1 and 2 of Noakes, Holden, Fawcett, and de Camargo (1990). From Fawcett *et al.* (1991).

is the inverse correlation length. The self-energy function $F(\mathbf{q})$ may be written

$$R(\mathbf{q})=\frac{1}{4\delta^2}[(|\mathbf{q}|^2-\delta^2)^2+4(q_x^2q_y^2+q_x^2q_z^2+q_y^2q_z^2)]\ , \tag{90}$$

which is the simplest polynomial of fourth order in $\mathbf{q}=\mathbf{Q}-(0,0,1)$ that conveniently represents the sixfold

TABLE XVI. Parameters of the Sato-Maki model for Cr and Cr+0.2 at. % V at the same reduced temperature, $t=1.027$ (2) (Fawcett *et al.*, 1991). The fourth column gives susceptibility for incommensurate peaks at low energy, the fifth the incommensurability parameter $\delta=1-Q$, the sixth the energy difference between commensurate and incommensurate fluctuations, and the seventh the inverse correlation length scaled by temperature factor.

	$\frac{10^3\chi^0}{r^2}$ $\left[\frac{\mu_B^2}{\text{A}^2\text{ at.}}\right]$	10^{-3} A^2 (THz Å^2)	$\frac{10^0\chi^0}{r^2A^2\kappa^4}(t-1)^2$ $\left[\frac{\mu_B^2}{\text{THz at.}}\right]$	$10^2\delta$ (1/A)	$\frac{A^2\delta^2}{4}$ (THz)	$\frac{10\kappa}{(t-1)^{1/2}}$ (1/A)
Cr+0.2 at. % V	0.59	0.96	3.4	9.4	2.14	6.5
Cr	1.21	0.80	13.4	7.8	1.22	5.8
Ratio			0.26	1.2	1.75	1.1

symmetry exhibited by the satellites at SDW wave vector **Q** around the commensurate position (0,0,1).

It must be emphasized first that Eqs. (89) and (90) give scattering centered at the positions of the six Bragg peaks that would be seen for elastic scattering in a polydomain incommensurate SDW sample below T_N. Thus there is no CD scattering in the paramagnetic phase at the commensurate position (0,0,1). The peak seen at (0,0,1) in all three ξ scans shown in Fig. 66 is entirely caused by an experimental artifact, due to picking up scattering from the four off-axis satellites as the spectrometer resolution function moves through this position. The collapse of the incommensurate peaks seen for quasielastic scattering in Fig. 66(a) into a single broad peak centered at (0,0,1) in the case of pure Cr for energy transfer $\hbar\omega=4$ meV, as seen in Fig. 66(c), is predicted by Eqs. (89) and (90) to occur for $\hbar\omega$ larger than the energy difference $A^2\delta^2/4$ between incommensurate and commensurate SDW fluctuations. Reference to column (3) of Table XVI shows that this is the case for pure Cr, but not for Cr+0.2 at. % V, which explains why for the latter the incommensurate peaks can still just be seen in Fig. 66(c).

The most interesting aspect, however, of the dynamic susceptibility of the dilute Cr alloy system is the close similarity it bears to that seen in the high-temperature superconducting cuprates, whose physical significance is discussed in Sec. I. Thus the insulating antiferromagnetic La_2CuO_4 shows spin waves a little below the Néel temperature $T_N=325$ K, having a velocity $\hbar c=0.75$ eV Å (Hayden *et al.*, 1991), close to the value of about 1 eV Å for the commensurate SDW alloy Cr+5 at. % Mn (Fawcett, 1988a).

When La_2CuO_4 is doped with Sr it becomes a high-temperature superconductor and develops incommensurate SDW fluctuations, which are described by the two-dimensional equivalent of Eqs. (89) and (90), with a value for the magnetic stiffness, $A^2=0.93$ T Hz Å, close to those quoted in Table XVI for the incommensurate SDW case (Mason *et al.*, 1992; Aeppli *et al.*, 1993). The nature of the damped spin waves for these remarkable materials, the insulating antiferromagnet that becomes with doping a superconductor, is shown in Fig. 67, which could serve just as well to illustrate the behavior in the paramagnetic phase in the Cr alloy system. Mason *et al.* (1992) point out that the value of A^2 in the high-temperature superconducting cuprate is close to $\hbar^2/2m$, which shows that quasiparticles with mass close to the free-electron mass m are responsible for the incommensurate fluctuations, as of course we know to be the case in the Cr alloy system.

The other remarkable feature of the experimental data illustrated in Fig. 64 is the decrease in dynamic susceptibility by a factor 4 [see column (1) of Table XVI] produced by doping with only 0.2 at. % V, which we relate to the effects of V doping on other physical properties in Sec. II.C.2. The inelastic scattering for a Cr+0.5 at. % V sample has been measured to see if the intensity decreases still further, but the data have not yet been analyzed (Noakes, Fawcett, and Holden, 1993). In Cr+0.18 at. % Re, on the other hand, the intensity increases relative to that in pure Cr by about a factor 2 (Noakes *et al.*, 1994).

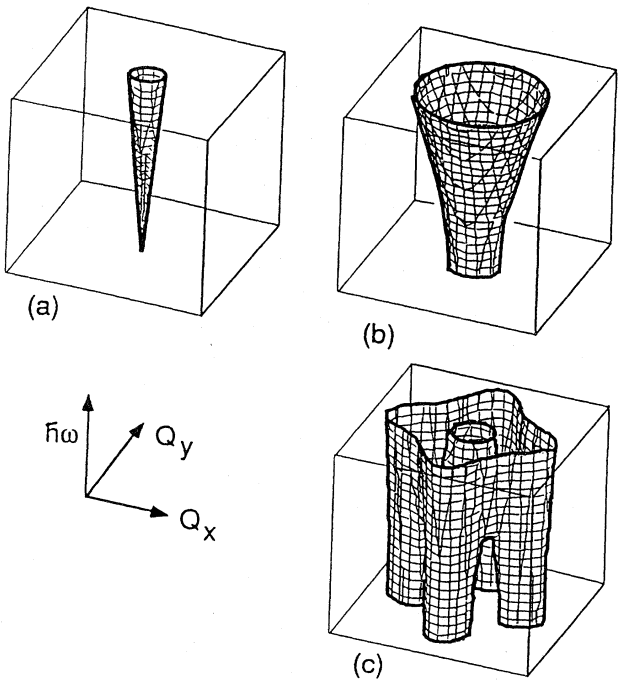

FIG. 67. Schematic of the damped spin waves' dispersion relation in the $La_{2-x}(Ba,Sr)_xCuO_4$ system, each contour at constant energy $\hbar\omega$ corresponding to the $\frac{1}{4}$-maximum intensity: (a) spin-wave poles in La_2CuO_4; (b) overdamped commensurate fluctuations in $La_{1.95}Ba_{0.05}CuO_4$; (c) incommensurate fluctuations in superconducting $La_{1.86}Sr_{0.14}CuO_4$ (from Aeppli *et al.*, 1994).

The incommensurate SDW instability at the nesting vector **Q** manifests itself quite clearly in a Cr alloy that is paramagnetic down to zero temperature, but is close to a composition that orders antiferromagnetically. Thus Cr+5 at. % V does not order (see the phase diagram in Fig. 11), but the dynamic susceptibility $\chi(\mathbf{Q},\omega)$ shows two peaks in inelastic scattering at positions corresponding to an incommensurability parameter, $\delta=0.084$, which is consistent with the variation of $\mathbf{Q}=1-\boldsymbol{\delta}$, with V concentration obtained from the SDW Bragg peaks in the lower concentrations (Fawcett, Werner, *et al.*, 1988).

These excitations, termed "incommensurate SDW paramagnons" (Fawcett, Werner, *et al.*, 1988, 1989), are unique in paramagnetic transition-metal alloys. Unlike the commensurate diffuse excitations in the paramagnetic phase of pure Cr, which peak in intensity at about 10 meV (Grier *et al.*, 1985), the SDW paramagnons continue to increase up to the highest energies of order 80 meV to which they have been measured (Werner *et al.*, 1993).

Thus the characteristic energy of the spin fluctuations in Cr+5 at. % V at a temperature of 300 K is at least an order of magnitude larger than in pure Cr, even 200 K above its Néel temperature. This result is consistent with

the severe reduction in the intensity of scattering by about two orders of magnitude in Cr+5 at. % V at 300 K relative to that in pure Cr at the Néel temperature. A similar trend is seen in dilute alloys, for which the scattering intensity is reduced relative to Cr by a factor 4 in Cr +0.2 at. % V (Noakes, Holden, Fawcett, and de Camargo, 1990) as shown in Fig. 66. The temperature dependence of the dynamic susceptibility in Cr+5 at. % V is weak, decreasing by only about 50% between 10 and 300 K (Werner *et al.*, 1993). Inelastic scattering with a spallation neutron source has been performed at 10 K on the Cr + 5 at. % V sample (Hayden, Aeppli, *et al.*, 1993), with the interesting result that dynamic susceptibility $\chi(Q,\omega)$ in a (100) plane changes from a 4-peak structure at energy transfer 25 meV to a single commensurate peak at 90 meV. The energy dependence of the integrated scattering has not yet been analyzed.

Resonant lattice modes were first observed in Cr alloys in a Cr+3 at. % W sample (Bjerrum-Moller and Mackintosh, 1965). The inelastic neutron-scattering data for the dispersion relation of the phonon modes in this crystal, compared with those in pure Cr, are shown in Fig. 68.

The theory for the scattering of neutrons by local phonon modes is reviewed by Mackintosh and Bjerrum-Moller (1968), who show that the frequency shift $\Delta\omega$ at low frequencies produced for an impurity concentration x is

$$\frac{\Delta\omega}{\omega}=-\frac{1}{2}x\left[\frac{M'-M}{M}\right] \tag{91}$$

in the case when, as here, the mass M' of the impurity atom is greater than M of the host (when $M'<M$, a new localized mode appears at a frequency above the frequency distribution of the host lattice). At high frequencies $\Delta\omega$ increases rather more rapidly and then, as seen in Fig. 68, drops rapidly to zero above a resonant frequency ω_0, whose value is not given explicitly in the theory.

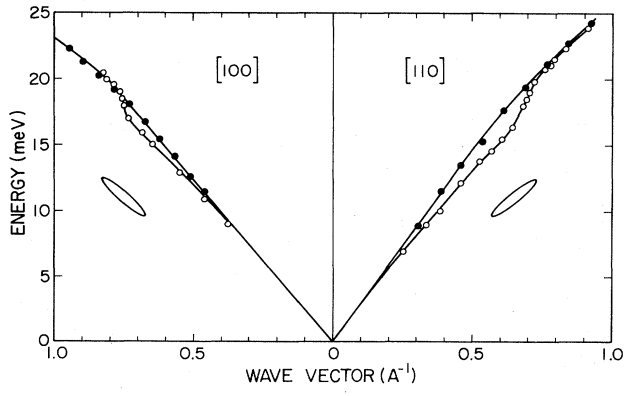

FIG. 68. Dispersion curves for transverse lattice waves propagating in the [100] and [110] directions in ●— — — Cr, and ○— — — Cr+3 at. % W. The half-value contours for the Gaussian resolution function for the neutron-scattering spectrometer are shown (from Mackintosh and Bjerrum-Moller, 1968).

The width γ of the phonon mode also increases to a maximum value at ω_0 given by

$$\frac{\gamma}{\omega_0}=\frac{2\sqrt{3}}{\pi}x\left[\frac{M'}{M}-1\right]^{3/2}. \tag{92}$$

The experimental data shown in Fig. 68 agree reasonably well with Eq. (91) at low frequencies and agree qualitatively with the resonance form predicted by the theory. There are, however, some discrepancies, which indicate that the force constants in the vicinity of the defects are different from those in the pure metal. The increase in the width γ of the phonon modes at the resonant frequency is at least a factor 2 larger than that predicted (Mackintosh and Bjerrum-Moller, 1968).

Cunningham *et al.* (1970) measured several more dilute crystals of Cr doped with W. Their data for the frequency shift were fit quite well by a model having changes in the force constants as variable parameters, as well as the mass increment (Cohen and Gilat, 1972; Kesharwani and Agrawal, 1972).

Mackintosh (1985) measured the phonon-dispersion relation of Cr+10 at. % V along the (100) axis and found that the minimum at the zone boundary is considerably less pronounced than the same feature in pure Cr. The latter has been attributed to a Kohn anomaly associated with either a nesting vector spanning the hole octahedron of the Fermi surface, or between the electron and hole octahedra (see Fawcett, 1988a, Figs. 34 and 60, Table VII). It would be desirable to study also Cr+5 at. % V, whose lattice vibrations in relation to thermophysical properties are of special interest, because of the use of an alloy of this composition as a paramagnetic reference material in experiments on pure Cr and SDW Cr alloys (White *et al.*, 1986; Alberts, 1990), and because of the observation of incommensurate SDW paramagnons in this alloy (Fawcett, Werner, *et al.*, 1988).

VIII. ENERGY-BAND STRUCTURE

A. Optical properties: energy gap

The dependence on frequency ω of the optical reflectivity $R(\omega)$ of a SDW antiferromagnet may be used to determine its energy gap, as reviewed by Fawcett (1988a) in the case of pure Cr. One may simply plot vs ω the absorptivity, $A(\omega)=1-R(\omega)$; or a Kramers-Kronig analysis may be performed to obtain the complex conductivity, $\sigma_1(\omega)+i\sigma_2(\omega)$. A peak in $\sigma_1(\omega)$, or $A(\omega)$, determines the frequency corresponding to the energy gap. The peak may be distinguished more clearly from the normal variation of $R(\omega)$, due to other nonmagnetic band-structure effects, by determining the frequency dependence of the ratio R_L/R_P of the reflectivity R_L at low temperature to R_P at a temperature above the Néel transition.

The data for pure Cr and for alloys of Cr with V, Mo, Mn, Re, Fe, and Ru are shown in Fig. 69. In the case of

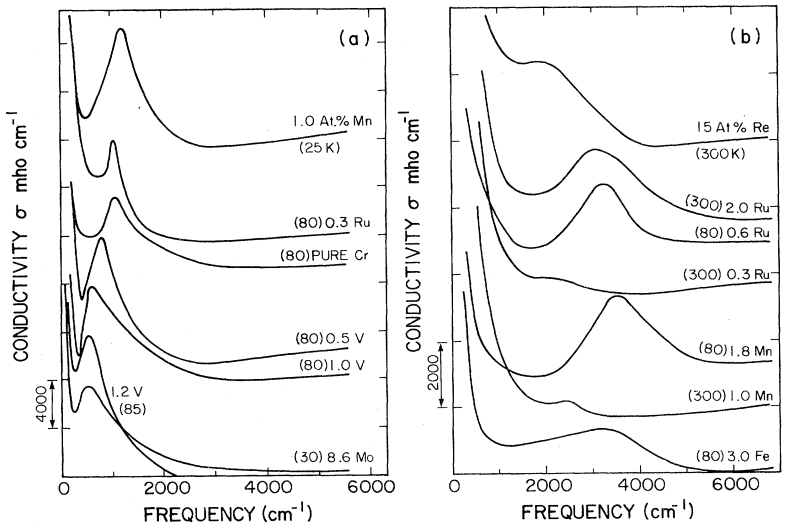

FIG. 69. Frequency dependence of the optical conductivity of Cr alloys: (a) incommensurate SDW alloys; (b) commensurate SDW alloys (from Barker and Ditzenberger, 1970).

the incommensurate SDW alloys in Fig. 69(a), the peak in σ_1 occurs at a frequency corresponding to a wave number around or below 1000 cm^{-1}. When the corresponding energy gap 2Δ is plotted vs the Néel temperature T_N of the alloy as in Fig. 70, it is seen that they are roughly proportional. This is to be expected for an itinerant-electron antiferromagnet resulting from the condensation of electron-hole pairs, since the theory is formally analogous to the Bardeen-Cooper-Schrieffer theory of superconductivity (Overhauser, 1962; Fedders and Martin, 1966). The constant of proportionality between Δ and T_N is found to be, as illustrated in Fig. 70, a value somewhat larger than the value 3.5 for this ratio predicted for a weakly coupled superconductor (Bardeen *et al.*, 1957).

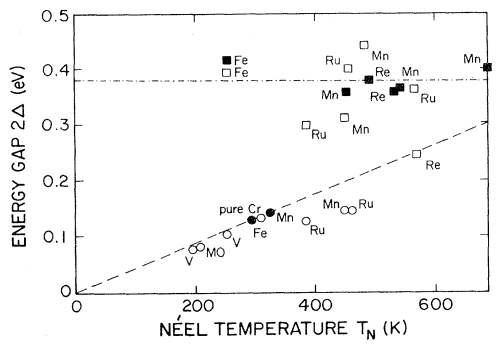

FIG. 70. Energy gap 2Δ in Cr alloys determined at low temperatures from the peak in the infrared reflectivity for incommensurate SDW alloys (○ and ●) and commensurate SDW alloys (□ and ■) plotted against the Néel temperature T_N. The chain line is a guide to the eye suggesting a constant value, $2\Delta = 0.38$ eV, for the gap in the commensurate SDW systems. The dashed line of slope, $2\Delta/k_B T_N = 5.0$, shows the proportionality of the gap to the Néel temperature in the commensurate SDW systems. ● (Bos and Lynch, 1970); ■ (Lynch *et al.*, 1975); ○ and □ (Barker and Ditzenberger, 1970). The two data points for the Cr+1.0 at. % Mn sample having $T_N = 450$ K and $T_{IC} = 60$ K correspond to peaks in the curves plotted in Fig. 54(a) at 25 K (commensurate SDW) and in Fig. 54(b) at 300 K (incommensurate SDW), and similarly for Cr+0.3 at. % Ru, having $T_N = 385$ K and $T_{IC} = 70$ K (after Barker and Ditzenberger, 1970).

The data plotted in Fig. 70 show in three cases a point for both the incommensurate and the commensurate SDW phases, since the corresponding curves shown in Fig. 69 were measured at different temperatures, at which the sample was in one or the other phase. In the case of the CrAl alloy system, however, two strong minima were seen in the reflectivity ratio R_L/R_P, with R_L measured at the same low temperature, $T_L = 30$ K, for compositions at which the sample has an incommensurate SDW at all temperatures. The spectrum for Cr+0.52% Al (Lind and Stanford, 1984) is very similar to that for pure Cr (Machida *et al.*, 1984: see Fig. 76 in Fawcett, 1988a) and yields the same values, $\Delta_1 = 0.12$ eV and $\Delta_2 = 0.45$ eV, for the two energy gaps as in Cr at zero temperature (see Fig. 77 in Fawcett, 1988a). For higher concentrations of Al, however, the spectra are difficult to interpret.

Machida (1984) developed the theory of Kotani (1974b) based on the canonical model and considering the effect of higher harmonics of the incommensurate SDW. He found that the resultant dispersion relation of the quasiparticles contains two energy gaps. These were seen clearly in the infrared reflectivity of pure Cr by Machida *et al.* (1984; see Figs. 76 and 77 of Fawcett, 1988a), but there is no sign of two gaps in the low-temperature data for incommensurate SDW alloys shown in Fig. 69 (a), nor, for that matter, in pure Cr. Machida *et al.* believe that the single large energy gap characteristic of the commensurate SDW alloys in Figs. 69 and 70 corroborates the Machida-Kotani theory.

B. Electronic properties: Fermi surface

The principal tools for the experimental study of the Fermi surface in Cr and Cr alloys have been the de Haas–van Alphen (dHvA) effect and the low-

temperature electronic specific heat. Interpretation of the dHvA effect in Cr alloys hinges on the effect on the Fermi surface of changing the electron concentration with doping, due to change in magnitude of the nesting vector **Q** between the electron and hole surface.

The change in the Sommerfeld coefficient γ of the linear term in the low-temperature specific heat is likewise related to the change in the fraction of the Fermi surface that is "gapped," due to the formation of the SDW, and therefore that does not contribute to the electronic specific heat. This fraction increases with the electron concentration (and conversely), since the increase of the nesting vector **Q** in the canonical model of the Fermi surface, in which the electron octahedron in pure Cr is smaller than the hole octahedron, and the approach to perfect nesting and the commensurate SDW phase extends the gapped region, thereby increasing also the Néel temperature.

Graebner's (1971) experiment on a commensurate SDW phase alloy, Cr +1.76 at. % Mn, was an extension of his definitive work on the dHvA effect in pure Cr (Graebner and Marcus, 1968: see Sec. V.B in Fawcett, 1988a). The residual resistivity ratio at low temperatures in his sample was only 10, due to impurity scattering, so that the amplitude of the dHvA signal was greatly reduced from that in pure Cr. Three branches of the dHvA spectrum were, however, clearly seen, with two arising from mixing of the hole pockets in the paramagnetic Fermi surface due to the AFM interactions responsible for the SDW of wave vector $\mathbf{Q}=2\pi/a$ (see Sec. V.B in Fawcett, 1988a). This interpretation gives results in fair agreement with the calculations of Asano and Yamashita (1967).

Gutman and Stanford (1971) measured the dHvA effect for Cr alloys in the classic systems, CrV and CrMn, and found linear variation of three dHvA frequencies with electron concentration x at rates roughly consistent with the calculations of Asano and Yamashita (1967). Griessen *et al.* (1976) further analyzed their data to show that they correspond to a dependence of the nesting vector on the electron concentration, $d\ \ln\mathbf{Q}/dx = 2.2\pm0.2$. This value compares reasonably well with the value 1.7 ± 0.3, obtained by Komura (1967b) from neutron-diffraction measurements (see Table II, and note that $d\mathbf{Q}/dx \simeq d\ \ln\mathbf{Q}/dx$, since $\mathbf{Q}\lesssim 1$). A somewhat smaller value, $|d\ \ln\mathbf{Q}/dx| \simeq 0.8$, was obtained by Schwartzman *et al.* (1989) in a calculation of the wave-vector dependent susceptibility $\chi(q)$ for CrV and CrMn alloys, for which the sign of $d\mathbf{Q}/dx$ is of course opposite. The magnitude of **Q** was obtained from the peak in $\chi(q)$ close to the Brillouin zone boundary. One should note that in this calculation the peak associated with nesting of the electron and hole surfaces is not the absolute maximum of $\chi(q)$, as it is in a more recent calculation by McMullan (1993).

The proposal by Overhauser (1962) that the SDW in Cr is due to electron-hole condensation at the Fermi surface, and the subsequent development of the canonical two-band model, stimulated measurements of the low-temperature specific heat in Cr alloys to see whether corresponding Fermi-surface effects were evident in the thermophysical properties. The most extensive series of measurements were performed by Heiniger (1966), whose data for CrV, CrRu, and CrOs alloys, illustrated in Fig. 71, show the expected effect. The dashed line interpolating between the paramagnetic alloys, Cr+5 at. % V and Cr+15 at. % Os, is based on a comparison with the concentration dependence of γ with that for the paramagnetic 4*d* and 5*d* alloy systems, Nb-Mo-Re and Ta-W-Re (see Fig. 6 of Heiniger, 1966).

There appears to be a reduction of almost 50% in the value of γ in Cr below what would be seen in the paramagnetic state, if it could be stabilized at low temperature. With V doping, γ rapidly increases towards the paramagnetic value, as the Néel temperature T_N decreases (see Fig. 11). With Ru and Os doping, the deviation from the dashed curve for the hypothetical paramagnetic state initially increases, corresponding to an increase in the gapped area of the Fermi surface, but not nearly so rapidly as T_N increases (see Fig. 10). For higher concentrations of Ru and Os, γ rises rapidly with x as the alloy concentration approaches the paramagnetic phase boundary. The variation of the Debye temperature in these alloys is interesting and, to our knowledge, has not been explained.

We list in Table XVII the initial dependence of the Sommerfeld coefficient on solute concentration for several Cr alloys. We do not include data for CrRu or CrOs, since the variation for these alloys is quite nonlinear, as seen in Fig. 71. The values of $d\gamma/dx$ for CrV, CrMo, and CrW are roughly proportional to the corresponding values of dT_N/dx, which are given in Table I. This is the behavior we expect qualitatively from the canonical model.

On the other hand, for the alloys with the ferromagnetic metals, CrFe, CrCo, and CrNi, the values of $d\gamma/dx$ are much larger and the relative values bear no relation

TABLE XVII. Dependence of the Sommerfeld coefficient γ of the term linear in temperature in the electronic specific heat on solute concentration x in chromium alloy systems $Cr_{1-x}A_x$.

Solute	$\frac{d\gamma}{dx}$	Reference
A	(mJ mol^{-1} K^{-2})	a
V	20	a
Mo	3.5	a
	4.5	b
W	5.5	a
Fe	$\gtrsim 100$	c
Co	35	d
Ni	$\lesssim 100$	e

[a]Heiniger (1966).
[b]Mamiya and Masuda (1976).
[c]Cheng *et al.* (1960).
[d]Kuentzler and Moody (1980).
[e]Baum and Schröder (1971).

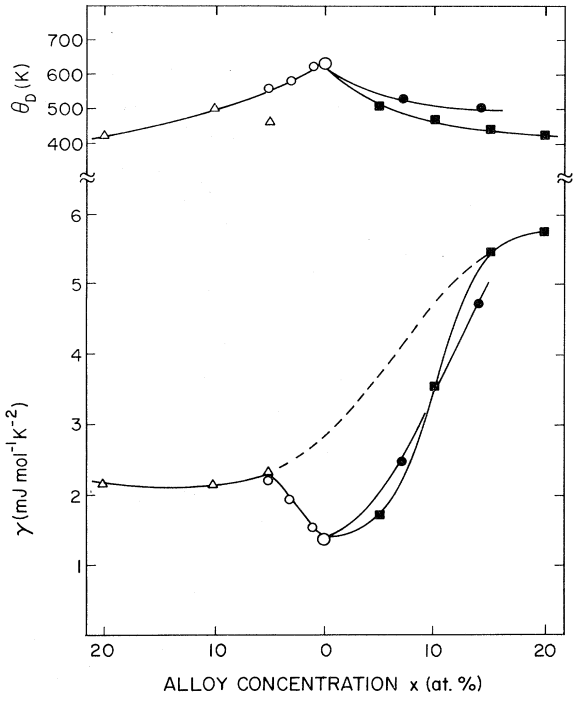

FIG. 71. Dependence of the Sommerfeld coefficient γ and the Debye temperature Θ_D on alloy concentration x for Cr alloys: ○ and △ (Cheng *et al.*, 1960) — — — CrV; ●— — — CrRu; ■— — — CrOs (from Heiniger, 1966; see also Fig. 17 in Landolt-Börnstein, 1986).

to those of dT_N/dx (see Table I). As for so many other properties of these alloys, it appears that other magnetic processes are at work.

IX. MICROSCOPIC PROPERTIES: LOCAL PROBES

Local magnetic probes provide microscopic information: the magnetic state and environment of a probe location in the material, averaged over all such locations in the sample without regard for any long-range correlations. Most of the techniques discussed below are at their most revealing when the probe site is crystallographically and magnetically unique, resulting in a simple, distinctive experimental signal. As the number of sites producing different signals increases, individual features crowd together and may cease to be resolvable. As this happens, the experimenter must rely more and more on models with large numbers of adjustable parameters to fit the data, but more than one model may then be consistent with the data.

In alloy samples in which one species' concentration is in the range of tenths of a percent or more, local clustering on the scale of one or two nearest-neighbor shells may occur and can produce significant probe environment variations and, again, multiple signals in each spectrum, in what would otherwise be considered homogeneous samples. In the incommensurate SDW phase, there should not normally be a magnetically unique probe site; so broad unresolved spectra and model-dependent results are to be expected. Occasionally, however, magnetically unique probe sites are discovered in this phase, in which case their very existence must be explained. A recent conference report on nuclear methods in magnetism (Litterst and Kalvius, 1989) provides an overview of several of the local probe techniques.

A. Mössbauer effect

The Mössbauer effect is a nuclear decay probe of the solid state. It provides, among other things, direct information about the magnetic field at the probe nucleus, which can be used to deduce the magnetic state and environment of the probe ion's electron cloud around the nucleus.

Most studies of the Mössbauer effect in Cr alloys have been in the CrFe system, because the ^{57}Fe resonance is the most popular one to measure and because all other common Mössbauer species are heavier and much harder to dissolve uniformly in the Cr host. Even for ^{57}Fe in Cr alloys, the quality of the sample at the time of measurement must be considered carefully.

Measurements are usually performed in transmission through a polycrystalline sample, since the extra information to be gained from measuring multiple orientations of a single crystal is usually regarded as not being worth the effort. To make a polycrystalline sample thin enough to pass most of the low-energy Mössbauer photons, many researchers resort to filing an ingot to produce a powder, a process that must induce some strain. Strain, however, is known to modify significantly the magnetic properties of pure Cr (Fawcett, 1988a). Only when transition temperatures agree with those of unfiled samples of the same composition should the filed samples be considered unstrained.

The discussion here is generally limited to those papers discussing Fe in Cr at concentrations below the onset of ferromagnetic ordering. Most of the measurements have been at concentrations where commensurate rather than incommensurate SDW ordering occurs. However, the small number of measurements that have been done at concentrations low enough for incommensurate SDW ordering show behavior similar to that at higher concentrations; so the incommensurate SDW phase has not clearly been seen with the Mössbauer effect. The early conference report by Goldanskii and Herber (1968) still provides the best introduction to this technique.

This is the local probe with the longest history in Cr alloys, beginning with Wertheim's (1961) observing only a slight broadening of the spectrum of very dilute ^{57}Fe in Cr at 4.2 K in comparison with the paramagnetic phase. This broadening was later interpreted (Kimball *et al.*, 1963) as being due to a small (relative to ^{57}Fe in other magnetically ordered hosts measured to that date) hyperfine field at the ^{57}Fe nucleus of $\mathbf{B} \simeq 3.5$ T. Normally such a small hyperfine field indicates a corresponding

small local moment on the Fe ion (Herbert *et al.*, 1972). The temperature dependence of the magnetic susceptibility, however, indicates large local moments on Fe ions in the Cr matrix, while showing that all other dilute dopants (even Mn and Co) look very similar to their host Cr ions in the SDW phase (Sec. III and Table V).

Herbert *et al.* (1972) studied four $Cr_{1-x}Fe_x$ alloys having concentration $x=0.2$ to 10 at. % Fe, both in zero field and in an applied field. Data quality was good enough to begin to deduce hyperfine field probability distributions for the first time; and fairly detailed results for the temperature dependence were also obtained, which clearly showed that the hyperfine field disappears at the Néel temperature. We note that, in order to deduce a hyperfine field distribution, it is usually necessary to assume that the isomer shift and quadrupole interaction each have a single value for all sites in the sample, independent of the variation of the hyperfine field (Window, 1971a). The samples of concentration, $x=0.2$, 0.5, and 5 at. % Fe, all showed similar Mössbauer behavior. The authors concluded that in those samples the Fe ion must be in a spin-compensated, Kondo-like state, though not perfectly compensated, leaving a small net moment fairly strongly coupled to the SDW. This result is, however, difficult to reconcile with the susceptibility data given in Table III, which correspond to a temperature dependence of a Curie-Weiss nature, with a large local moment for samples of CrFe in this concentration range.

Blum and Grozdins (1964) had determined that the hyperfine splitting in polycrystalline Cr+0.5 at. % Fe increases in applied field, and had concluded that the "sign" of the hyperfine field is positive, contrary to the behavior of the hyperfine interaction at ^{57}Fe in most hosts; but their modeling of the response of the host SDW to the field was too simplistic. Herbert *et al.* (1972) performed a more sophisticated analysis for their applied field data, deducing a negative hyperfine field (see Rao, 1985, for a table of hyperfine fields at probe impurity nuclei in magnetically ordered elements, in general). The Cr+10 at. % Fe sample behaved differently from the more dilute ones, displaying much broader spectra, with hyperfine field distributions extending up to about 14 T, consistent with the later work of Shiga and Nakamura (1976: see their data for ^{90}Cr in Fig. 72). This is now in the concentration range where spin-glass ordering occurs, as seen in Fig. 60, at a distinct temperature well below the Néel transition; the explanation proposed by Herbert *et al.* is that the Fe is now dense enough in the host for ferromagnetic Fe-Fe interactions, particularly in clusters of locally even higher Fe density, to begin to generate local Fe moments comparable with that in iron metal.

As an alternative to the interpretation in terms of a small static moment, for Fe concentrations below the onset of spin-glass behavior, Frankel and Blum (1973), using a model of Housley and Dash (1964), proposed that spin-density waves are still moving through the lattice and are not static and pinned at temperature 4.2 K; so further cooling should result in higher observed hyperfine fields when a completely static situation is achieved. Shinjo *et al.* (1974), however, observed no change between temperatures 4.2 K and 80 mK in a sample of Cr+0.3 at. % Fe.

Shiga and Nakamura (1976) deduced ^{57}Fe hyperfine field distributions at temperature 5 K for a set of CrFe alloys with Fe concentrations from 10 to 40 at. %, those with ≥ 20 at. % being ferromagnetic. A broad probability peak displaced away from zero characterized the strongly ferromagnetic samples. The most probable value decreased smoothly as Fe concentration was reduced, but not to zero, as ferromagnetic ordering was lost and first spin-glass and then AFM phases developed (see Fig. 60). Below 20 at. % Fe, with no ferromagnetism, a second, low-field peak developed in the probability distribution, the two peaks being of comparable size for the 10 at. % Fe sample. In the nonferromagnetic range of interest here, the authors attributed the high-field peak to ferromagnetically coupled Fe clusters with large moment per Fe atom, and the low-field peak to isolated Fe ions, "probably" with small moment. Later (Shiga and Nakamura, 1980), they studied samples with lower Fe concentration, finding that the high-field probability peak becomes merely a shoulder at 6 at. % Fe and disappears by 3 at. %, as shown in Fig. 72.

Kuwano and Ono (1977, 1979) measured the temperature dependence of the ^{57}Fe hyperfine field in samples of composition of 3 to 19 at. % Fe, seeing magnetic transitions that would now be labeled SDW, spin-glass freezing, and apparently other transitions in between.

Nikolaev and Bezotosnyi (1979) measured the pressure dependence of the Mössbauer effect of the ^{57}Fe hyperfine field up to 1 GPa at temperature 78 K in samples containing 0.5 to 3.5 at. % Fe, observing changes small in comparison to experimental uncertainties, but with a general trend to decrease with pressure. This is beyond the range, however, of the clearly established pressure-temperature phase diagram, which is shown in Fig. 44(d) for Cr+3 at. % Fe, so that it is not clear in what magnetic state, and how close to any magnetic transition temperature, the samples were. The change in the hyperfine field H_i with pressure is large, about 2%/kbar, which corresponds to a magnetic Grüneisen parameter, $\Gamma_{MB}=-d\ln/d\omega\simeq -40$.

Szuszkiewicz *et al.* (1981) interpreted the ^{57}Fe isomer shift, a measure of *s*-electron density at the Fe nucleus, together with positron annihilation data, over the entire range of Fe concentration and concluded that there is net electron transfer from Fe to Cr in the ferromagnetic alloys, but the transfer is reversed below 20 at. % Fe. The precise relation of the *s*-electron density to the magnetic behavior is, however, not clear.

The next most popular Mössbauer resonance after ^{57}Fe is ^{119}Sn. In the late '60s and early '70s, Street, Window, and collaborators (Street and Window, 1966; Street *et al.* 1968; Window, 1970) measured the latter in dilute CrSn and CrMnSn samples. The value of their results is limit-

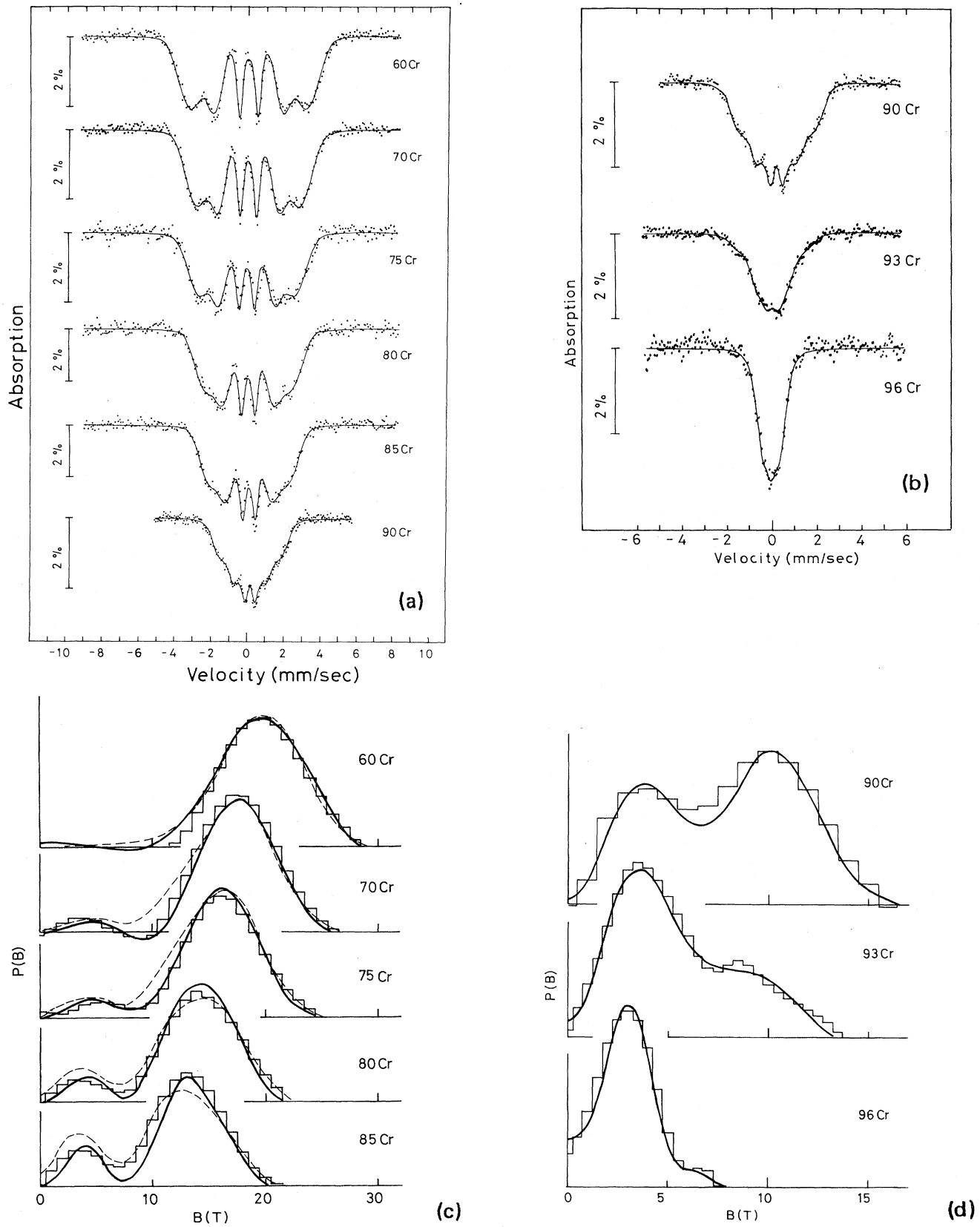

FIG. 72. Mössbauer spectra of Cr-Fe alloys: (a),(b) ^{57}Fe spectra of a set of Cr-Fe samples of concentrations from 4 at. % Fe ("96Cr") to 40 at. % Fe ("60Cr"), all at temperature 5 K; and (c),(d) hyperfine field probability distributions deduced from them (from Shiga and Nakamura, 1980).

ed by the poor quality of Sn distribution in the Cr host in samples that could be produced with the technology of the day. In a study of ^{57}Fe in CrMn, Window (1971a) admits to "large uncertainty in manganese concentration and possible nonuniformity in the . . . samples."

Dubiel (1984) found a clear change in the ^{119}Sn Mössbauer signal at the spin-flip transition in Cr+0.4 at. % Sn. The individual spectra were sufficiently complicated to require multiple Sn sites in fitting, which the author attributed to Sn clustering. There is no discussion in the paper of the distribution of fields to be expected in the incommensurate SDW phase. There was hysteresis of the spin-flip transition behavior in warming and cooling. Dubiel and collaborators went on to study both the ^{57}Fe and ^{119}Sn Mössbauer effects in Cr+13.5 at. % Fe+0.7 at. % Sn (Dubiel *et al.*, 1985b) and at ferromagnetic Fe concentrations (Dubiel *et al.*, 1984, 1985a). In the nonferromagnetic CrFeSn sample, the ^{57}Fe hyperfine field distribution at temperature 4.2 K shows a two-peak structure similar to the results of Shiga and Nakamura discussed earlier. As temperature is raised, this structure collapses to a distribution in which zero is the most likely field by 40 K, but the authors claim that there is enough structure to indicate consistency with the phase diagram, shown in Fig. 14, with the Néel temperature being near 90 K. There is also indication of spin-glass freezing between temperatures 10 and 20 K. For the ^{119}Sn spectra, lack of reflection symmetry about the center implies a significant relation between isomer shift and hyperfine field, and simple deduction of a hyperfine field distribution was accordingly not possible. Fits were made to a multiple-site model instead. Surprisingly, the hyperfine fields in the Sn spectra decreased only slightly around 85 K, near the nominal Néel temperature, and remained finite to the highest temperatures measured, above 300 K. The interpretation of this result in terms of some kind of Fe magnetism persisting in the sample to above room temperature would be more forceful if it were clear that no such effort occurs in the absence of Fe; but these authors have not published spectra of CrSn alloys without Fe for temperatures higher than 10 K above the spin-flip transition.

B. Diffuse neutron scattering

In addition to the coherent neutron scattering that measures long-range-ordered phenomena, as discussed in Sec. VII, incoherent (often referred to as "diffuse") neutron scattering also occurs. This measures single-site properties, with contributions from site-disorder effects, including isotopic differences in neutron-scattering cross section, and from disordered local magnetic moments. Reliable separation of the magnetic from the nuclear incoherent scattering has, in practice, required polarization analysis.

Fawcett (1988a) reviewed attempts to detect truly incoherent magnetic neutron scattering in pure Cr, leading to the surprising conclusion that essentially there is none. All of the magnetic response of Cr, above or below the Néel temperature, is SDW-like; and as the SDW amplitude wanes with increasing temperature, the moment lost from the SDW does not become disordered, it disappears. The application of this technique in alloys of Cr has focused on the CrFe system, particularly in an attempt to find the large Fe moments uncoupled from the SDW that seem to be needed to explain magnetic-susceptibility results in these phases (see Sec. III).

The first incoherent neutron-scattering measurements on a single crystal of Cr+2.8 at. % Fe were by Holden and Fawcett (1978). They did not measure neutron polarization, and so were forced to construct a model of the nuclear incoherent scattering by using the then-accepted values of the nuclear cross sections. This model by itself, with no magnetic incoherent scattering, was consistent with their data; so they concluded that there is no local magnetic difference between a Cr site and an Fe site. But in the same year, Cywinski and Hicks (1978) published new, lower values for those cross sections, reopening the issue. They went on to perform a polarization-analyzed incoherent neutron-scattering study of polycrystalline Cr+6.5 at. % Fe (Cywinski and Hicks, 1980), in which the nuclear incoherent scattering provided evidence for Fe-Fe clustering, but the local Fe moment was not distinguishable from the Cr host. They suggested that the unusual magnetic properties of CrFe alloys should be attributed to large clusters of Fe atoms developing moments correlated over the size of the clusters to become "superparamagnetic," which would not be detectable by their experiment.

Kajzar *et al.* (1981) later presented a study of incoherent neutron scattering in 1.3 T applied field from samples with 1.5, 2.4, 12, and 14.2 at. % Fe in Cr, and coupled the analysis to measurements of high-field static magnetization in the same samples (Babic *et al.*, 1980). They saw clear evidence for Fe clustering in the two higher Fe-concentration samples and, in the form factor of the magnetic incoherent scattering, for superparamagnetic moments correlated on similar scales. Since these two concentrations are in the range where spin-glass freezing seems to take place below the Néel transition, it is reasonable to consider these clusters as being participants in the spin glass, while the host material supports the SDW. The two lower-concentration samples showed only marginal Fe clustering, with no magnetic incoherent scattering. Costa *et al.* (1981) reported briefly on low-field magnetic incoherent neutron scattering in Cr+12 at. % Fe and Cr+10 at. % Co.

A more detailed study of the Cr+2.8 at. % Fe crystal of Holden and Fawcett (1978) was performed by Moze *et al.* (1988), using the ability of the ILL D7 instrument to collect data simultaneously at multiple positions along an arc in reciprocal space, with polarization analysis at all positions. Measurements of several orientations of the sample with respect to the neutron polarization allowed better control of systematic uncertainties than in the ear-

lier experiment. No significant Fe clustering was found in the sample, and a moment of $2.1\mu_B$, coupled to the SDW in the vicinity, was found on the isolated Fe ions. No substantial disturbance of the Cr moments around the Fe was seen. Companion measurements on a polycrystalline Cr+4 at. % Fe sample were judged to be consistent with the model of the Cr+2.8 at. % Fe single crystal, with Fe moment $1.8\mu_B$. The moments observed are large enough to be in disagreement with the results of Cywinski and Hicks (1980), and Moze *et al.* were not able to explain all of the difference. Since no Fe clustering was observed, this data set itself says nothing about the magnetism of clusters, and the authors note that a superparamagnetic species of some sort is required to explain the body of susceptibility data. The idea that pairs of Fe close enough together in the host couple to each other and decouple from the SDW (Friedel and Hedman, 1978) is not ruled out by their data.

C. Perturbed angular correlation

The full name, "time-differential γ-γ perturbed angular correlation," being long, this technique will be referred to as simply PAC. It is described well in an article by Mahnke in Litterst and Kalvius (1989). It is another nuclear decay probe providing similar information to the Mössbauer effect, in principle, with the advantage that only an extremely small amount of the probe species need be present to be useful, and the disadvantage that radioactive material must be handled in the making of every sample. Early measurements (Benski, 1972; Benski *et al.*, 1975) suffered from poor sample quality. Then a process of trial and error was needed to find a really good probe nucleus. ^{181}Ta was found to be magnetically not sensitive enough: only one Larmor precession period was seen in the useful time window (Teisseron *et al.*, 1978). ^{100}Rh was too sensitive: the Larmor precession was difficult to resolve with the time resolution of the apparatus (Peretto *et al.*, 1979). ^{111}Cd was found to be the most useful (Venegas *et al.*, 1980). In all three cases, measurements were made of samples with tens of at. ppm (at. ppm $\equiv 10^{-4}$ at. %) impurity, so that the bulk magnetic state of the samples was essentially that of pure Cr. All three resonances showed a distribution of local hyperfine fields consistent with a sine-wave amplitude SDW in the incommensurate phase, that is not phase locked to the impurity position (Teisseron *et al.*, 1979),

$$P(B)=\frac{2}{\pi}\frac{1}{(B_0^2-B^2)^{1/2}} \quad \text{for } B<B_0 \ , \tag{93}$$

which they call the Overhauser distribution (Overhauser, 1960). It was then surprising to find that PAC of ^{99}Ru in Cr+0.2 at. % Ru indicates no hyperfine field at Ru nuclei from room temperature down to 4.2 K (Rao *et al.*, 1980). Standing in isolation as it does, this result is difficult to explain.

The observation of the Overhauser distribution for the hyperfine field shows that these probes at very low concentrations do not in fact perturb the SDW; i.e., they neither clamp it nor distort its shape. The temperature dependence of the hyperfine field at the Ta atom, however (but not at the Cd atom), deviates from that of the amplitude of the SDW as determined by neutron diffraction (see Fig. 85 of Fawcett, 1988a).

Subsequently, PAC of ^{111}Cd as a very dilute probe in Cr+0.8 at. % Mn (Peretto *et al.*, 1981) clearly showed the difference between the incommensurate SDW phase at low temperature and the commensurate SDW phase at intermediate temperatures, as illustrated in Fig. 73. In the commensurate SDW phase, however, rather than the expected single hyperfine field value, a Gaussian distribution of fields around a central value was observed. This was interpreted as being due to each Mn ion causing a long-range spin disturbance. Near and above the Néel temperature, the hyperfine field distribution developed a two-peak form, indicating that a fraction of the Cd sites continue to see something approximating magnetic order in the supposedly paramagnetic phase. This behavior was found in three different samples and was attributed to the existence of superparamagnetic clusters similar to those seen in CrFe alloys.

Van Cauteren *et al.* (1984) used ion implantation as an alternative way of getting ^{111}Cd into Cr alloys for PAC experiments. There was evidence of radiation-damage effects in the PAC spectra, which could be partially an-

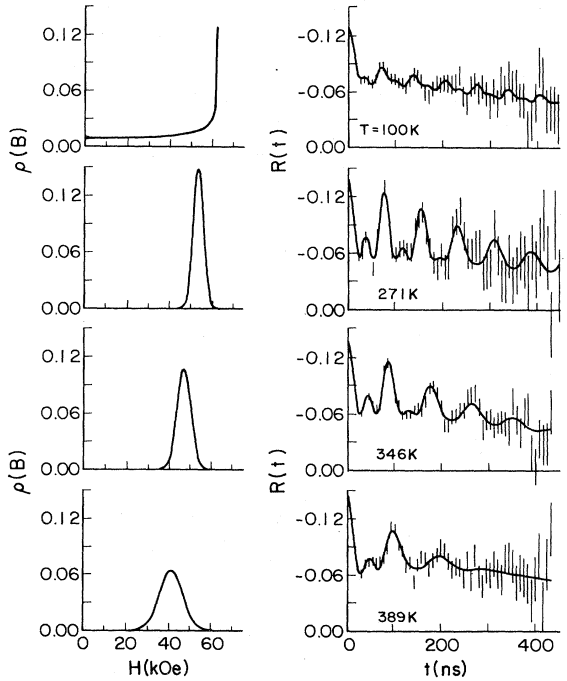

FIG. 73. ^{111}Cd PAC spectra (right-hand side) in Cr+0.8 at. % Mn at various temperatures, with fit lines generated by the hyperfine field distributions shown on the left-hand side. At the lowest temperature, $T=100$ K, the sample is in the incommensurate SDW phase; at the other three temperatures, it is in the commensurate SDW phase (from Peretto *et al.*, 1981).

nealed away, and it is not clear that all the implanted probe ions sat at the desired substitutional (cubic) site in the lattice; so their conclusions must be treated cautiously.

Brenier *et al.* (1982) used nuclear orientation (NO) of ^{101}Rh, a technique related to PAC, where the anisotropy of emission direction of a single-photon nuclear deexcitation is measured with respect to a net nuclear-spin orientation induced by application of a magnetic field. A net orientation can only be induced at temperatures low enough that the thermal fluctuation energy scale is smaller than the nuclear splittings caused by the applied field. Brenier *et al.* measured very dilute ^{101}Rh in Cr in the temperature range of tens of mK and in magnetic fields of several tesla. The sample was polycrystalline, and this limits the amount of information that can be extracted without reliance on modeling of the magnetic response of crystallites at various angles to the external field. They concluded that assuming the Overhauser distribution of local fields at the probe site to be represented by an incommensurate SDW, unperturbed by the presence of the probe ion, fits their data better than a model with a magnetic moment on the Rh ion.

D. Nuclear magnetic resonance

In a simplistic description of NMR, splittings are induced between the multiple levels of a magnetic nucleus, usually by an applied magnetic field, and internal magnetic interactions in the material act as perturbations. The complex splittings that result are then measured by matching the frequency (photon energy) of a simultaneously applied rf electromagnetic field, which causes detectable rf absorption. Sophisticated measurements often involve the application of short field pulses, to produce particular polarized initial nuclear states, followed by later pulses to measure the rate of depolarization of those states. The technique is popular enough to have several textbooks devoted to it, the most readable being Slichter's (1978).

^{53}Cr can be used for NMR; but at its natural abundance of 9.5%, it is difficult to detect, by comparison with natural abundances of such isotopes as ^{51}V and ^{55}Mn in CrV and CrMn alloys. As in the Mössbauer measurements discussed earlier, most of the NMR measurements have been done on samples filed or crushed to powder, and again the strain thus induced may affect the magnetic properties. Most researchers appear to have been unconcerned: in a couple of cases, heat treatments were performed *before* filing, and not after. In one early paper (Ostenburg *et al.* 1962), the Knight shift in the paramagnetic phase was measured both before and after annealing, and no difference was seen.

Earliest measurements were of the Knight shift, the difference between the observed NMR frequency and the frequency to be expected from the applied field alone. These were made above the Néel temperature, or at alloy compositions in which no magnetic ordering occurs. Barnes and Graham (1962) were able to observe the ^{53}Cr Knight shift in CrV alloys containing less than 3 at. % V, at room temperature (and 40 °C in pure Cr), observing a roughly constant value of 0.69%. They also observed the ^{51}V Knight shift Δ at room temperature across the nearly complete composition range from pure V to Cr+0.25 at. % V, finding a broad maximum near the same value, $\Delta=0.69\%$, in the vicinity of 63 at. % Cr, falling to near 0.56% at both ends of the concentration range, in pure V and in nearly pure Cr. The latter was reproduced by Ostenburg *et al.* (1962) and compared to the ^{51}V Knight shift in VTi and VTc alloys. The Cr concentration dependence of the ^{51}V Knight shift is not simply proportional to the total density of states at the Fermi level deduced from specific-heat measurements (Cheng *et al.*, 1960), which falls smoothly as Cr content increases. The Knight shift, however, is proportional to the V-site *s*-electron density at the Fermi level, because only this part is nonzero at the probe nucleus; so Ostenburg *et al.* proposed that the *s*-wave character of the conduction band varies with concentration, peaking near 63 at. % Cr.

Butterworth (1964) performed the first (pulsed, spin-echo NMR) measurement of spin-lattice relaxation in Cr alloys, again using ^{51}V in CrV alloys from pure V to Cr+5 at. % V, none of which order magnetically. An exponential probe nucleus spin-relaxation time called T_1 is measured. Data are usually presented as $1/(T_1T)$ to some power, where T is the temperature at which T_1 was measured, because this quantity is most directly related to the magnetic environment in which the probe ion sits. Butterworth argues that in a conduction-electron paramagnet, which does not have magnetic ordering, $1/(T_1T)$ should be temperature independent, as he observed in his samples. This Korringa-type relaxation should give a value of $1/T_1T$ which, to a first approximation, is proportional to the square of the density of states at the Fermi level, as he also observed.

Barnes and Graham (1965) showed that the sharp paramagnetic ^{51}V and ^{53}Cr NMR lines disappear abruptly at the Néel transition and thus can be used to determine the transition temperature. In this study, the filings used were annealed before the NMR measurements.

Takenaka and Asayama (1971, 1973) measured the ^{55}Mn spin echo at temperatures 1.4 and 4.2 K in CrMn samples with Mn concentrations from about 3 to 60 at. %, all of which should be commensurate antiferromagnets. These measurements were zero field in the sense that no magnetic field was applied in the interval between the aligning and sensing pulses. The internal field at the nucleus dropped from over 6 T for the 3 at. % Mn sample to near 4 T for samples with more than 40 at. % Mn. The internal field is usually proportional to the magnetic moment on the Mn ion; so it appears that this moment decreases as the Mn concentration increases, in contrast to the average saturation moment, as measured by neutron scattering and shown in Fig. 5(a), which rises rapidly with the first few percent Mn added to pure Cr and then levels off. The authors refer to ^{182}W

Mössbauer work by Kunitomi and Kanashiro, which apparently has never been published, to argue that the Cr ion moment increases with Mn concentration, the sum of the two ion moments at each concentration being consistent with the measured average moment. The temperature-independent quantity $1/T_1T$, characteristic of Korringa relaxation, was the same at temperatures 1.4 and 4.2 K in all samples and rose dramatically with Mn concentration from near 0.7 $(\text{sec K})^{-1}$ for 3 at. % Mn to greater than 20 $(\text{sec K})^{-1}$ for samples near 50 at. % Mn. Since the low-temperature Sommerfeld coefficient of the specific heat exhibits similar behavior (Cheng *et al.*, 1960), however, this again appears to be mostly an effect of the changing density of states at the Fermi level.

Kohara and Asayama (1975) measured the zero-field spin echo of ^{59}Co in CrCo alloys containing from 1.1 to 16.5 at. % Co at temperature 1.4 K. While all the samples were almost certainly magnetically ordered at that temperature, the nature of the ordered state is uncertain beyond about 4 at. % Co (see Fig. 10). In the 1.1 at. % Co sample, one spin-echo peak was observed, centered near 66 MHz. As the Co concentration increased, a second peak at lower frequency emerged, and then a third at yet lower frequency. The positions of the peaks did not vary much with composition, but their relative intensities varied in a manner close to the probabilities for the number of nearest-neighbor Co ions to be expected in a random alloy. Thus it appears that the 66-MHz peak is generated by isolated Co ions, the lower frequency by Co ions with one nearest-neighbor Co, and the lowest frequency by Co ions with two nearest-neighbor Co ions. Kohara and Asayama discuss a mechanism of partial cancellation of the hyperfine field due to the ^{59}Co's own electron cloud by the contribution of nearest-neighbor moments to explain why the hyperfine field for Co-Co nearest neighbors is smaller than for isolated Co ions.

In the same paper (Kohara and Asayama, 1975), the authors show that they were able to detect ^{51}V *applied field* spin echo at temperature 1.4 K in the incommensurate SDW phase of Cr+2 at. % V and Cr+3 at. % V. A paramagnetic 4 at. % V sample showed a sharp response at 10 MHz near 0.9 T, while in the incommensurate SDW samples the signal is broadened by the distribution of local fields in a manner consistent with Kontani *et al.* (1975). The latter deduced a specific line shape to be expected in swept applied field (constant rf frequency) spin-echo measurements of an incommensurate SDW phase, with a narrow central peak and broad wings, as shown in Fig. 74. They then observed spectra of similar shape for ^{53}Cr, ^{95}Mo, and ^{97}Mo in CrMo alloys with Mo concentrations from 13 to 23 at. %, at temperature 1.4 K, but they did not fit the theoretical shape to the data.

The internal field at ^{59}Co obtained from these measurements is $B_{\text{int}}=6.6$ T. Matsumara and Asayama (1977) report nuclear magnetic relaxation data for ternary samples, $Cr_{1-x}V_xCo_z$ and $Cr_{1-y}Mo_yCo_z$, for $z=1$ and 3 at. % Co and $x \leq 0.05$ (V), $y \leq 0.25$ (Mo). B_{int} decreases

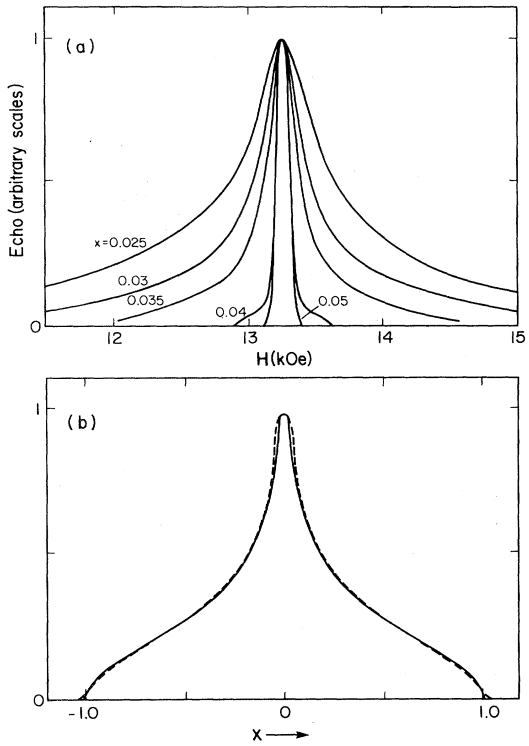

FIG. 74. NMR spectra for Cr-V alloys: (a) Spin echo of ^{51}V in magnetic field H at frequency 15 MHz and temperature in the AF_1 phase of $Cr_{1-x}V_x$ alloys (from Kontani *et al.*, 1983); (b) the corresponding theoretical line shape (solid line), and as it would be detected with typical NMR spectrometer resolution (dashed line). From Kontani *et al.* (1975).

linearly with x or y, as Cr is diluted with either V or Mo, respectively, having about the same value for the two Co concentrations.

Kohara (1981) measured the zero-field spin echo of ^{27}Al in CrAl alloys with compositions from 8 to 24 at. % Al, at temperatures 1.5 and 4.2 K, all samples described as being in the commensurate SDW phase. The hyperfine field at the ^{27}Al ion increased smoothly with Al concentration through this range, as did the Néel temperature (Fig. 16), and saturation sublattice moment (Fig. 7). $1/(T_1T)$ was the same at the two measuring temperatures, but dropped from 0.4 $(\text{sec K})^{-1}$ for Cr+8 at. % Al to 0.14 $(\text{sec K})^{-1}$ for Cr+24 at. % Al; the authors had expected it to increase with Al concentration.

Meanwhile, Kontani and Masuda (1979) used their applied-field spin-echo technique line-shape theory to measure the spin-lattice relaxation of ^{51}V in the incommensurate SDW phase and across the Néel transition into the paramagnetic phase in CrV alloys containing from 3.8 to 6 at. % V. They observed that $1(T_1T)$ is *not* independent of temperature, as expected in the paramagnetic phase near the Néel transition. They then (Kontani and Masuda, 1981) developed a theory of this being the result of critical spin fluctuations: $(T_1T)_{\text{SF}}$ should be proportional to $(T-T_N)^{1/2}$ at temperatures just above the Néel temperature T_N. Kontani *et al.* (1983) demon-

strated reasonable fits of the theory to data for CrV alloys having V concentrations down to 1 at. % V, and Kontani and Masuda (1983) did the same for ^{53}Cr in pure Cr and Cr+2 at. % V.

Kohara *et al.* (1984) measured zero-field and applied-field spin echo of ^{185}Re and ^{187}Re in CrRe alloys containing from 6 to 26 at. % Re, in the temperature range 1.3 to 4.2 K. In the lower part of this range, the samples are in the commensurate SDW phase, with the Néel transition well above room temperature (see Fig. 13), while in the higher part of this range, superconductivity occurs below 4 K and there may or may not be a magnetic transition around 150 K, as discussed in Sec. VI.E. In the "merely commensurate SDW phase" low-concentration samples, broad zero-field spin-echo response is seen, indicative of magnetic ordering in a general sense, centered in the vicinity of 30 to 40 MHz. As the Re concentration increases into the superconducting range, the zero-field pattern at 4.2 K, above the superconducting transition temperature, shifts upward to center in the range 50 to 55 MHz. This is evidence of internal magnetic fields in the samples and hence at least of frozen magnetic moments, if not long-range magnetic order, unless all the patterns are due to distributions of quadrupole interactions, which is conceivable but unlikely. The temperature at which this freezing sets in is not clear, because spin-echo measurements cannot easily be done much above 4.2 K. Applied-field dependence of the spin-echo intensity at 1.3 K in the higher concentration samples is consistent with a superconducting vortex state at low fields, which is destroyed by fields consistent with a superconducting vortex state at low fields, which is destroyed by fields consistent with values of the upper critical field of these type-II superconductors (Damaschke and Felsch, 1986). The value of $1/(T_1T)$ in the resistive, normal state is independent of temperature, but increases rapidly for Re concentrations past 12 at. % or so, in the same manner as the Sommerfeld coefficient of the specific heat (Muheim and Müller, 1964). This indicates that the density of states at the Fermi level starts to increase rapidly at about the same concentration as superconductivity sets in. Below the superconducting transition temperature, in the high-concentration samples, the temperature dependence of T_1 is roughly consistent with an exponential in $1/T$, as is to be expected with the opening of the superconducting gap.

Shiga *et al.* (1986) measured the zero-field spin echo of ^{55}Mn in CrMn alloys containing more than 58 at. % Mn, but this range of concentrations is beyond the scope of this article. NMR studies of CrFe alloys have concentrated on the ferromagnetic Fe-rich part of the phase diagram, again beyond the purview of this article, with samples of no more than 26 at. % Cr (Dubiel and Lutgemeier, 1981; Lutgemeier and Dubiel, 1982).

E. Other local probes

Electron paramagnetic resonance (EPR, sometimes called electron spin resonance, ESR) is similar to NMR in principle, but it uses the magnetic moments of electrons instead of nuclei. Standley and Vaughan (1969) provided an early introduction to the technique, which is still perhaps the best.

Salamon and Feigl (1968) detected EPR in CrFe alloys with Fe concentrations from 1.6 to 3.5 at. %. The signal intensity increased as the square of Fe concentration, and was thus attributed to special behavior of Fe-Fe near-neighbor pairs, because no detectable signal is expected from isolated Fe moments interacting only with the conduction electrons of a metallic host. The model proposed by the authors is incipient superparamagnetic behavior of iron clusters, as discussed above in the sections on the Mössbauer effect and diffuse neutron scattering. Salamon and Feigl do not in fact use the term "superparamagnetic," but later workers in EPR do when comparing data on other Fe systems to this work (see Burr *et al.*, 1970). The sharp resonance observed above the Néel temperature T_N rapidly broadens below the transition, but was followed for several tens of kelvins below T_N in these samples.

In muon spin relaxation (μSR), a beam of low-energy positively charged muons (μ^+) can be produced with essentially 100% spin polarization by particle accelerators. The magnetic-moment orientation of each muon that stops in a sample evolves as it interacts magnetically with moments in the sample, until the muon decays, with a lifetime of 2.2 μs; the direction of each muon's spin at the time of decay is indicated by the direction of the outgoing decay positron. Thus μSR can provide information about local magnetic fields at various sites, typically interstitial, in a material. See Chappert and Grynszpan (1984) for a readable introduction to this technique. Several groups (Kossler *et al.*, 1977; Grebinnik *et al.*, 1979; Weidinger *et al.*, 1981) measured μSR in pure Cr, with some sample dependence in the details, but agreement in general behavior. The muon is very sensitive to moments of electronic scale: for temperatures between about 12 and 45 K, the initial muon polarization relaxes away so fast that it is difficult to detect, and in these early experiments no signal was seen below about 45 K. At higher temperatures, the muon hops from site to site fast enough to cause significant "motional decoupling," which is analogous to motional narrowing in NMR, and the muon spin-relaxation rate can be detected by typical μSR apparatus. Weidinger *et al.* (1981) observed a discrete jump in the relaxation rate at the spin-flip temperature; above the Néel transition, the muon spin does not relax at all. Once the muon is in motion, the observer is primarily learning about diffusion and trapping phenomena of "a light isotope of hydrogen," however, and little can be learned about the magnetism of the host.

Major *et al.* (1986) discovered that, at temperatures below 12 K, zero-field μSR spectra exhibit coherent oscillation at about 85 MHz. The signal is of reduced amplitude, but it means that a fraction of the implanted muons see local magnetic fields in a narrow distribution around 0.62 T. This field is consistent with calculations of the

dipole field for a muon sitting in the tetrahedral interstitial site near the peak of the incommensurate SDW. This seems to require, then, that the muon contact hyperfine field be essentially zero, and that the muon and the peak SDW amplitude somehow attract each other, probably through interaction of the local-structure distortion the muon must cause around its site and the charge-density-wave disturbance that accompanies the SDW (see Fawcett, 1988a). Templ *et al.* (1990) conducted a more extensive study. They found that the oscillating signal persists, but at very small amplitude, down to dilution-refrigerator temperatures. This temperature dependence of amplitude may be a "trap" effect: when the muon first stops in the material at low temperature, it may get stuck in a site that is not the one of lowest energy, and the latter may be the one that generates the interesting signal. It may need to make one energy-reducing hop to get to that site, but may not be able to cross an energy barrier to get there if the temperature is too low. On the other hand, there may be other pinning sites competing with the muon for the peak of the SDW wave form, and the others might be more effective than the muon at low temperature. Meanwhile, an increasing relaxation rate of the oscillating signal as temperature rises toward 12 K indicates that thermally assisted muon hopping has started at these temperatures. Templ *et al.* claimed to see some signal at all temperatures, with the maximum relaxation rate occurring around 19 K; so this is probably the temperature at which interaction between the muon and the SDW sets in. Zero-field μSR coherent oscillation has recently been observed in the commensurate SDW phase of Cr+3 at. % Mn in a similar temperature range (Noakes *et al.*, 1992), but at a substantially lower frequency, near 41 MHz, which is difficult to understand.

In extended x-ray-absorption fine-structure (EXAFS) experiments, the energy of a monochromatic x-ray beam, usually generated by an electron storage ring "light source," is tuned across one or more absorption edges of the ions in the sample. The detailed behavior of the absorption as a function of energy provides information on the location of the charges of other ions in the immediate vicinity of the absorbing ion. This is an electric charge probe, not a magnetic probe. In the sole publication on EXAFS of Cr alloys (Münch *et al.*, 1983), it was shown that the vast majority, perhaps all, of the Ge ions in Cr-Ge alloys with concentrations from 0.4 to 1.0 at. % Ge sit at substitutional sites (see Sec. II.C.10).

X. CONCLUDING SUMMARY

We began our review with a discussion of magnetic phase diagrams of Cr alloy systems in the composition-temperature plane. The fundamental idea, that increasing the electron concentration improves the nesting of the Fermi surfaces responsible for the electron-hole condensation that gives rise to the SDW, and thereby leads to the onset of a commensurate SDW phase as the impurity concentration increases, with a rapidly increasing Néel temperature T_N, explains the behavior of most Cr alloy systems with group-7 and -8 metals; while, conversely, T_N falls and the wave vector decreases with increasing concentration of group-4 and -5 metals.

This idea has been developed to take into account impurity scattering, which in general simply decreases T_N, but in a particular system may give rise to an exotic feature like that seen in CrFe (Figs. 14 and 57), that the commensurate SDW phase lies at lower temperatures in the phase diagram than the incommensurate SDW phase, and also that the phase transition to the commensurate SDW phase is strongly first order (Fig. 58). The behavior of CrFe alloys has been explained by introducing a magnetostrictive term into the free energy, whose physical explanation is a flow of electrons from the Fe impurities to the nesting electron and hole surfaces. Nakanishi and Kasuya (1977) do not explain the origin of this process, but suggest that it is related to the existence of a local moment on the Fe atom. No such moment exists on the Si atom in CrSi alloys, however, but a similar strongly first-order Néel transition to the commensurate SDW phase occurs (but not also from the incommensurate SDW phase as in CrFe: see Fig. 56), which along with the normal phase diagram is explained by a similar theory (Galkin *et al.*, 1991).

There are several other Cr alloys systems which exhibit unique behavior that has not been explained. For example, the rapid decrease of T_N with Ni impurity (Fig. 10) and the strong temperature dependence of the wave vector in CrNi alloys (Fig. 62) remain a mystery. The $Cr_{1-x}Al_x$ alloy system exhibits several remarkable features, including semiconducting behavior in the transport properties for $15 \lesssim x \lesssim 25$ at. % Al (Chakrabarti and Beck, 1971), the largest magnetic Grüneisen parameters for any Cr alloy system (Fig. 50), and the highest observed values for the Néel temperature T_N and the SDW amplitude [Figs. 5(d), 7, and 16(a)]. Akai and Kanamori (1985) propose a model to explain the high values of T_N in terms of the Al atom acting as a vacancy in the Cr matrix. They do not present a microscopic theory for this behavior, however, and the onset of a commensurate SDW phase in the alloys with other group-3 and -4 nontransition metals, which would seem to correspond to these substitutional atoms acting as donors to increase the electron concentration, also remains a mystery. CrPd, alone among Cr alloys with group-8 metals, does not exhibit a commensurate SDW phase; CrRu alloys are unique in showing strong shear magnetoelastic effects (Fig. 48); etc. These many cases of unique behavior in particular Cr alloys systems call for microscopic theories to explain them.

The transport properties exhibit several features, each common to several Cr alloy systems, that are only poorly understood. These include the resistivity hump in the region of temperatures below the Néel transition (Figs. 23 and 34; Table VI), which is seen also in the temperature dependence of the thermoelectric power (compare Figs. 22 and 25; Fig. 26), and the peak in the temperature

dependence of the Lorenz ratio seen in a few systems, but especially in CrSi (Fig. 37).

The interesting features seen in the transport properties of CrFe and CrSi alloys doped with V or Mn (Figs. 29, 30, 31, and 32), on the other hand, are reasonably well understood in terms of local impurity states (Volkov and Tugushev, 1984). The unique existence of local moments in the SDW phase in CrFe alloys has given rise to many experimental studies by use of a variety of techniques, without finding any satisfactory explanation.

Enough has been said already in Sec. V.D about the similarity between the effects of pressure, and of changing the electron concentration, in Cr alloy systems. No microscopic theory exists to explain the strong magnetovolume effects seen in pure Cr (Fawcett, 1988a), and the study of Cr alloys has not thus far significantly clarified this fundamental problem. The effects of pressure on Cr alloys are, however, in their own right, of great interest, and may assist in developing a microscopic theory to explain their properties at ambient pressure.

The persistence in Cr alloys, as in pure Cr, of the effects of spin fluctuations in the paramagnetic phase, to temperatures well above the Néel transition, is of considerable interest. One hopes that some connections, perhaps fundamental rather than merely formal, can be made with the spin fluctuations that play an important role in heavy-fermion compounds and in AFM systems relating to high-temperature superconductors (Fig. 67). Manifestations of spin fluctuations in the physical properties of Cr alloy systems are seen in the resistivity (Figs. 35 and 36), the magnetoelastic effects (Figs. 40 and 47), and the nuclear magnetic relaxation (Fig. 86 in Fawcett, 1988a).

There is a great deal of current interest in the properties of magnetic layer structures based on transition metals with interfaces that are sharp on an atomic scale. Perhaps the most exciting systems are sandwiches and superlattices with magnetic layers separated by nonmagnetic (i.e., nonferromagnetic and so lacking any spontaneous magnetization) spacer layers, such as Fe/Cr, Co/Cr, Co/Ru, Fe/Cu, Co/Cu, and Fe/Mo. These all show oscillatory magnetic coupling between the Fe or Co layers, which oscillate between ferromagnetic and antiferromagnetic with increasing thickness of the spacer layer.

The properties of Fe/Cr superlattices, in particular, have been studied intensively since Grünberg *et al.* (1986) first discovered AFM coupling between the Fe layers and since giant negative magnetoresistance was observed by Baibich *et al.* (1988). A discussion of these fascinating effects would take us too far afield, but one should keep in mind the possibility that the properties of a Cr alloy system may turn out to be relevant to those of a layer structure made up from the same chemical species. We refer the reader accordingly to the following recent experimental and theoretical articles of a review nature on superlattices and sandwiches exhibiting effects similar to those seen in Fe/Cr: Barthélémy *et al.* (1990); Levy *et al.* (1991); Mathon (1991); Mattson *et al.* (1991). Many invited papers on magnetic multilayers were presented at the International Conference on the Physics of Transition Metals held in Darmstadt, Germany, in July 1992. Those making explicit reference to spin-density waves in systems involving chromium layers include the papers by Bader (1993), Herman *et al.* (1993), Leng *et al.* (1993), and Loewenhaupt *et al.* (1993).

ENDORSEMENT

Two of the authors (E.F. and J.V.Y.) wish to state their intention that no agency should derive military benefit from the publication of this paper. Authors who cite this work in support of their own are requested to qualify similarly the availability of their results.

ACKNOWLEDGMENTS

We are grateful to Professor S. A. Werner for advice and encouragement. This work was supported by the Natural Sciences and Engineering Council of Canada (E.F., V.Yu.G., and J.V.Y.), the South African Foundation for Research and Development (H.L.A.), the U.S. DOE under Grant No. DE-FG05-88ER45353 (D.N.), and the Bhabha Atomic Research Centre (J.V.Y.).

REFERENCES

Abdul-Noor, S. S., and J. G. Booth, 1973, Phys. Lett. **43A**, 381.
Abdul-Noor, S. S., and J. G. Booth, 1975, J. Phys. F **5**, L11.
Abrikosov, A. A., and L. P. Gorkov, 1960, Zh. Eksp. Teor. Fiz. **39**, 1781 [Sov. Phys. JETP **12**, 243 (1960)].
Aeppli, G., H. A. Mook, T. E. Mason, S. M. Hayden, A. D. Taylor, T. G. Perring, K. N. Clausen, P. Littlewood, S.-W. Cheong, and Z. Fisk, 1994, "Neutron scattering and magnetic dynamics in insulators, metals and superconductors," Proceedings of the E. Fermi School, Varenna (1992), in press.
Aidun, R., S. Arajs, and C. A. Moyer, 1985, Phys. Status Solidi B **128**, 133.
Akai, H., and J. Kanamori, 1985, J. Phys. Soc. Jpn. **54**, 3537.
Akiba, C., and T. Mitsui, 1972, J. Phys. Soc. Jpn. **32**, 644.
Alberts, H. L., 1985, J. Phys. F **15**, L171.
Alberts, H. L., 1989, Physica B **161**, 87.
Alberts, H. L., 1990, J. Phys. Condens. Matter **2**, 9707.
Alberts, H. L., 1993, J. Alloys Compounds **191**, L17.
Alberts, H. L., 1994, J. Appl. Phys. in press.
Alberts, H. L., and A. H. Boshoff, 1992, J. Magn. Magn. Mater. **104–107**, 2031.
Alberts, H. L., and S. J. Burger, 1978, Solid State Commun. **28**, 771.
Alberts, H. L., P. J. Ford, H. Rahdi, and G. A. Saunders, 1992, J. Phys. Condens. Matter **4**, 2793.
Alberts, H. L., and J. A. J. Jourens, 1983, J. Phys. F **13**, 873.
Alberts, H. L., and J. A. J. Lourens, 1984a, Phys. Rev. B **29**, 5279.
Alberts, H. L., and J. A. J. Lourens, 1984b, Solid State Commun. **50**, 1063.
Alberts, H. L., and J. A. J. Lourens, 1985, J. Phys. F **15**, 2511.

Alberts, H. L., and J. A. J. Lourens, 1987, J. Phys. F **17**, 727.
Alberts, H. L., and J. A. J. Lourens, 1988a, J. Phys. F **18**, 123.
Alberts, H. L., and J. A. J. Lourens, 1988b, J. Phys. F **18**, L213.
Alberts, H. L., and J. A. J. Lourens, 1988c, J. Phys. (Paris) **49**, C8-215.
Alberts, H. L., and J. A. J. Lourens, 1992, J. Phys. Condens. Matter **4**, 3835.
Alberts, H. L., D. S. McLachlan, T. Germishuyse, and M. Naidoo, 1991, J. Phys. Condens. Matter **3**, 1793.
Allen, J. W., and C. Y. Young, 1975, in *Magnetism and Magnetic Materials,* AIP Conference Proceedings No. 24, edited by C. D. Graham, Jr., G. H. Lander, and J. J. Rhyne (AIP, New York), p. 410.
Allen, J. W., and C. Y. Young, 1977, Phys. Rev. B **16**, 1103.
Als-Nielsen, J., J. D. Axe, and G. Shirane, 1971, J. Appl. Phys. **42**, 1666.
Als-Nielsen, J., and O. W. Dietrich, 1969, Phys. Rev. Lett. **22**, 290.
Al'tshuler, B. L., and A. G. Aronov, 1979, Sov. Phys. JETP **50**, 968 [Zh. Eksp. Teor. Fiz. **77**, 2028 (1979)].
Anderson, R. A., H. L. Alberts, and P. Smit, 1993, J. Phys. Condens. Matter **5**, 1733.
Angelescu, N., G. Nenciu, and N. S. Tolnchev, 1984, J. Phys. F **14**, 2155.
Antonoff, M. M., 1977, Physica **91B**, 193.
Antonoff, M. M., 1978, Int. Phys. Conf. Ser. No. 39 (edited by M. J. G. Lee, J. M. Perz, and E. Fawcett), 613.
Antonoff, M. M., 1986, J. Magn. Magn. Mater. **54–57**, 1305.
Antonoff, M. M., 1988, J. Phys. (Paris) **49**, C8-85.
Arajs, S., 1968, J. Appl. Phys. **39**, 673.
Arajs, S., 1969, Can. J. Phys. **47**, 1005.
Arajs, S., 1970a, Phys. Status Solidi **37**, 329.
Arajs, S., 1970b, J. Less-Common. Met. **22**, 519.
Arajs, S., 1970c, Phys. Status Solidi **1(a)**, 499.
Arajs, S., R. Aidun, and C. A. Moyer, 1980, Phys. Rev. B **22**, 5366.
Arajs, S., and E. E. Anderson, 1971, Physica **54**, 617.
Arajs, S., E. E. Anderson, and E. E. Ebert, 1971, Nuovo Cimento **4B**, 40.
Arajs, S., E. E. Anderson, J. R. Kelly, and K. V. Rao, 1974, AIP Conf. Proc. **24**, 412.
Arajs, S., T. F. DeYoung, and E. E. Anderson, 1970, J. Appl. Phys. **41**, 1426.
Arajs, S., and G. R. Dunmyre, 1966, J. Appl. Phys. **37**, 1017.
Arajs, S., and G. R. Dunmyre, 1967a, J. Appl. Phys. **38**, 1157.
Arajs, S., and G. R. Dunmyre, 1967b, J. Appl. Phys. **38**, 1892.
Arajs, S., G. R. Dunmyre, and S. J. Dechter, 1967, Phys. Rev. **154**, 448.
Arajs, S., and W. E. Katzenmeyer, 1967a, J. Phys. Chem. Solids **28**, 1459.
Arajs, S., and W. E. Katzenmeyer, 1967b, J. Phys. Soc. Jpn. **23**, 932.
Arajs, S., G. Kote, C. A. Moyer, J. R. Kelly, K. V. Rao, and E. E. Anderson, 1976, Phys. Status Solidi B **74**, K23.
Arajs, S., C. A. Moyer, and D. Abukay, 1980, Phys. Status Solidi B **101**, 63.
Arajs, S., C. A. Moyer, J. R. Kelly, and K. V. Rao, 1975, Phys. Rev. B **12**, 2747.
Arajs, S., K. V. Rao, and E. E. Anderson, 1975, Solid State Commun. **16**, 331.
Arajs, S., K. V. Rao, H. U. Åstrom, and T. F. DeYoung, 1973, Phys. Scr. **8**, 109.
Arajs, S., N. L. Reeves, and E. E. Anderson, 1971, J. Appl. Phys. **42**, 1691.
Arrott, A. S., 1966, "Antiferromagnetism in Metals," in *Magnetism,* edited by G. T. Rado and H. Suhl (Academic, New York), Vol. II B, p. 295.
Arrott, A. S., 1972, "Long Range Magnetic Order in Disordered Alloys: Antiferromagnetism," in *Magnetism in Alloys,* edited by P. A. Beck and J. J. Weber (AIME, Cleveland), p. 187.
Arrott, A. S., and S. A. Werner, 1969, "Neutron Diffraction studies of Cr and Cr Alloys," in *Magnetic and Inelastic Scattering of Neutrons by Metals,* edited by T. J. Rowland and P. A. Beck (Gordon and Breach, New York).
Arrott, A. S., S. A. Werner, and H. Kendrick, 1967, Phys. Rev. **153**, 624.
Asano, S., and J. Yamashita, 1967, J. Phys. Soc. Jpn. **23**, 714.
Åstrom, H. U., H. Gudmundsson, L. Hedman, and K. V. Rao, 1977, Physica **86–88** B&C, 332.
Ausloos, M., 1977, J. Magn. Magn. Mater. **5**, 156.
Babic, B., F. Kajzar, and G. Parette, 1980, J. Phys. Chem. Solids **41**, 1303.
Bader, S. D, 1993, Int. J. Mod. Phys. B **7**, 414; *Physics of Transition Metals,* Proceedings of the International Conference, Darmstadt, Germany, July 1992, edited by P. M. Oppeneer and J. Kübler (World Scientific, Singapore), Vol. I, p. 414.
Baibich, M. N., J. M. Broto, A. Fert, F. Nguyen Van Dau, F. Petroff, P. Etienne, G. Creuzet, A. Friederich, and J. Chazelas, 1988, Phys. Rev. Lett. **61**, 2472.
Barak, Z., E. Fawcett, D. Feder, G. Lorincz, and M. B. Walker, 1981, J. Phys. F **11**, 915.
Baran, A., H. L. Alberts, A. M. Strydom, and P. de V. du Plessis, 1992, Phys. Rev. B **45**, 10 473.
Bardeen, J., L. N. Cooper, and J. R. Schrieffer, 1957, Phys. Rev. **108**, 1175.
Barker, A. S., Jr., and J. A. Ditzenberger, 1970, Phys. Rev. B **1**, 4378.
Barnes, R. G., and T. P. Graham, 1962, Phys. Rev. Lett. **8**, 248.
Barnes, R. G., and T. P. Graham, 1965, J. Appl. Phys. **36**, 938.
Barthélémy, A., A. Fert, M. N. Baibich, S. Hadjoudj, F. Petroff, P. Etienne, R. Cabanel, S. Lequien, F. Nguyen Van Dau, and G. Creuzet, 1990, J. Appl. Phys. **67**, 5908.
Bastow, T. J., 1966, Proc. Phys. Soc. London **88**, 935.
Baum, N. P., and K. Schroder, 1971, Phys. Rev. B **3**, 3847.
Beal-Monod, M. T., and R. A. Weiner, 1968, Phys. Rev. **170**, 552.
Behera, S. N., and K. S. Viswanathan, 1969, Can. J. Phys. **47**, 477.
Bender, D., and J. Müller, 1970, Phys. Kondens. Mater. **10**, 342.
Benediktsson, G., H. U. Åstrom, and K. V. Rao, 1975, J. Phys. F **5**, 1966.
Benediktsson, G., H. Gudmundsson, L. E. Hedman, A. Jayaraman, A. Kjerulf, K. V. Rao, and H. A. Åstrom, 1980, J. Magn. Magn. Mater. **15–18**, 283.
Benediktsson, G., L. Hedman, H. U. Åstrom, and K. V. Rao, 1982, J. Phys. F **12**, 1439.
Benski, H. C., 1972, Phys. Lett. A **42**, 295.
Benski, H. C., J. Berthier, G. Teisseron, and S. Choulet, 1975, Phys. Lett. A **51**, 467.
Bjerrum-Moller, H., and A. R. Mackintosh, 1965, Phys. Rev. Lett. **15**, 623.
Blatt, F. J., P. A. Schroeder, C. L. Foiles, and D. Greig, 1976, *Thermoelectric Power of Metals* (Plenum, New York).
Bloch, D., and A. S. Pavlovic, 1969, *Advances in High Pressure Research* (Academic, New York), p. 41.
Blum, N., and L. Grozdins, 1964, Phys. Rev. A **136**, 133.
Booth, J. G., 1964, Phys. Status Solidi **7**, K157.

Booth, J. G., 1966, J. Phys. Chem. Solids **27**, 1639.
Booth, J. G., M. M. R. Costa, J. Rodriguez-Carjaval, and J. A. Paixao, 1991, J. Magn. Magn. Mater. **104–107**, 735.
Booth, J. G., M. M. R. Costa, and K. R. A. Ziebeck, 1983, J. Magn. Magn. Mater. **31–34**, 285.
Booth, J. G., K. R. A. Ziebeck, and R. Chagnon, 1978, J. Phys. F **8**, 1303.
Bos, L. W., and D. W. Lynch, 1970, Phys. Rev. B **2**, 4567.
Boshoff, A. H., H. L. Alberts, P. de V. du Plessis, and A. M. Venter, 1993, J. Phys. Condens. Matter **5**, 5353.
Brenier, R., I. Berkes, G. Marest, and P. Peretto, 1982, Hyp. Int. **12**, 71.
Burke, S. K., R. Cywinski, J. R. Davis, and B. D. Rainford, 1983, J. Phys. F **13**, 451.
Burke, S. K., and B. D. Rainford, 1978, J. Phys. F **8**, L239.
Burke, S. K., and B. D. Rainford, 1983, J. Phys. F **13**, 441.
Burr, C. R., W. Zingg, and M. Peter, 1970, Helv. Phys. Acta **43**, 771.
Butterworth, J., 1964, Proc. Phys. Soc. London **83**, 71.
Butylenko, A. K., 1985, Zh. Tekh. Fiz. **55**, 1624 [Sov. Phys. Tech. Phys. **30**, 942 (1985)].
Butylenko, A. K., 1989, Fiz. Met. Metalloved. **68**, 873 [Phys. Met. Metallogr. (USSR) **68**, 37 (1989)].
Butylenko, A. K., and V. N. Gridnev, 1964, Ukr. Fiz. Zh. (Russ. Ed.) **9**, 325.
Butylenko, A. K., and V. N. Gridnev, 1965, Fiz. Met. Metalloved. **19**, 205 [Phys. Met. Metallogr. (USSR) **19**, 47 (1965)].
Butylenko, A. K., and N. S. Kobzenko, 1981, Ukr. Fiz. Zh. (Russ. Ed.) **26**, 199.
Butylenko, A. K., and V. V. Nevdacha, 1980a, Dokl. Akad. Nauk Ukr. SSR, Ser. A, No. **5**, 67.
Butylenko, A. K., and V. V. Nevdacha, 1980b, Dopov. Akad. Nauk Ukr. SSR, Ser. A, No. **5**, 66.
Butylenko, A. K., and V. V. Nevdacha, 1980c, Ukr. Fiz. Zh. (Russ. Ed.) **25**, 137.
Butylenko, A. K., and V. V. Nevdacha, 1981, Ukr. Fiz. Zh. (Russ. Ed.) **25**, 1390.
Butylenko, A. K., and V. V. Nevdacha, 1982, Zh. Tekh. Fiz. **52**, 149 [Sov. Phys. Tech. Phys. **27**, 102 (1982)].
Butylenko, A. K., and V. V. Nevdacha, 1983, Ukr. Fiz. Zh. (Russ. Ed.) **28**, 294.
Butylenko, A. K., and V. V. Nevdacha, 1993, Ukr. Fiz. Zh. (Russ. Ed.) **75**, 80.
Butylenko, A. K., V. V. Nevdacha, and V. A. Chernenko, 1980, Ukr. Fiz. Zh. (Russ. Ed.) **25**, 1424.
Butylenko, A. K., A. N. Rakitzkii, and N. L. Shofman, 1974, Metallofizika **50**, 77 (in Russian); we are indebted to Dr. G. Grechnev for a translation of this paper.
Buzdin, A. I., V. N. Men'shov, and V. V. Tugushev, 1986, Zh. Eksp. Teor. Fiz. **91**, 2204 [Sov. Phys. JETP **19**, 2264 (1986)].
Buzdin, A. I., and V. V. Tugushev, 1983a, Fiz. Tverd. Tela (Leningrad) **25**, 882 [Sov. Phys. Solid State **25**, 506 (1983)].
Buzdin, A. I., and V. V. Tugushev, 1983b, Zh. Eksp. Teor. Fiz. **85**, 735 [Sov. Phys. JETP **58**, 428 (1983)].
Cable, J. W., 1977, J. Magn. Magn. Mater. **5**, 112.
Cankurtaran, M., G. A. Saunders, Q. Wang, P. J. Ford, and H. L. Alberts, 1992, Phys. Rev. B **46**, 1157.
Castro, E. P., P. C. de Camargo, and F. R. Brotzen, 1986, Solid State Commun. **57**, 37.
Chakrabarti, D. J., and P. A. Beck, 1971, J. Phys. Chem. Solids **32**, 1609.
Chappert, J., and R. I. Grynszpan, 1984, Eds., *Muons and Pions in Materials Research* (North-Holland, Amsterdam).
Cheng, C. H., C. T. Wei, and P. A. Beck, 1960, Phys. Rev. **120**, 426.
Chiu, C. H., M. H. Jericho, and R. H. March, 1971, Can. J. Phys. **49**, 3010.
Cohen, S. S., and G. Gilat, 1972, Solid State Commun. **11**, 1269.
Costa, M. M. R., J. G. Booth, K. R. A. Ziebeck, and P. J. Brown, 1981, J. Appl. Phys. **52**, 1681.
Costa, M. M. R., and P. J. Brown, 1977, J. Phys. F **7**, 493.
Costa, M. M. R., K. R. A. Ziebeck, and P. J. Brown, 1980, J. Phys. F **10**, 2793.
Crisan, M., and A. Anghel, 1976, J. Magn. Magn. Mater. **1**, 267.
Cunningham, R. M., L. D. Muhlestein, W. M. Shaw, and C. W. Tompson, 1970, Phys. Rev. B **2**, 4864.
Cywinski, R., and T. J. Hicks, 1978, J. Phys. C **11**, L899.
Cywinski, R., and T. J. Hicks, 1980, J. Phys. F **10**, 693.
Cywinski, R., and T. J. Hicks, 1986, J. Magn. Magn. Mater. **54–57**, 999.
Dadarlat, D., A. Giurgiu, and I. Pop, 1980, Solid State Commun. **34**, 109.
Dadarlat, D., T. Petrisor, A. Giurgiu, and I. Pop, 1983, Phys. Status Solidi B **117**, 155.
Dadarlat, D., T. Petrisor, and I. Pop, 1982, Phys. Status Solidi B **113**, K111.
Daemon, L. L., and A. W. Overhauser, 1989, Phys. Rev. B **39**, 6431.
Damaschke, B., and W. Felsch, 1986, Z. Phys. B **63**, 179.
de Camargo, P. C., and F. R. Brotzen, 1982, J. Magn. Magn. Mater. **27**, 65.
de Camargo, P. C., E. P. Castro, and E. Fawcett, 1988, J. Phys. F **18**, L209.
de Camargo, P. C., E. Fawcett, and J. M. Perz, 1990, J. Appl. Phys. **67**, 5265.
De Dood, W., J. De Dood, and F. P. De Chatel, 1970, Physica **47**, 337.
de Koning, L., H. L. Alberts, and S. J. Burger, 1980, Phys. Status Solidi A **62**, 371.
De Vries, G., 1959, J. Phys. (Paris) **20**, 438.
De Young, T. F., S. Arajs, and E. E. Anderson, 1971, AIP Conf. Proc. **5**, 517.
De Young, T. F., S. Arajs, and E. E. Anderson, 1973, J. Less-Common Met. **32**, 165.
Dubiel, S. M., 1984, Phys. Rev. B **29**, 2816.
Dubiel, S. M., 1988, Port. Phys. **19**, 223.
Dubiel, S. M., and H. Lutgemeier, 1981, Phys. Lett. A **84**, 396.
Dubiel, S. M., C. Sauer, and W. Zinn, 1984, Phys. Rev. B **30**, 6285.
Dubiel, S. M., C. Sauer, and W. Zinn, 1985a, Phys. Rev. B **31**, 1643.
Dubiel, S. M., Ch. Sauer, and W. Zinn, 1985b, Phys. Rev. B **32**, 2745.
Edwards, D. M., and E. P. Wohlfarth, 1968, Proc. R. Soc. London Ser. A **303**, 127.
Edwards, L. R., and I. J. Fritz, 1973, AIP Conf. Proc. **18**, 401.
Edwards, L. R., and I. J. Fritz, 1974, AIP Conf. Proc. **24**, 414.
Endoh, Y., Y. Ishikawa, and H. Ohno, 1968, J. Phys. Soc. Jpn. **24**, 263.
Endoh, Y., J. Mizuki, and Y. Ishikawa, 1982, J. Phys. Soc. Jpn. **51**, 2826.
Eroglu, A., S. Arajs, C. A. Moyer, and K. V. Rao, 1978, Phys. Status Solidi B **87**, 287.
Falicov, L. M., 1992, Phys. Today **46**(10), 46.
Fawcett, E., R. Griessen, and C. Vettier, 1978, Inst. Phys. Conf. Ser. No. 39 (edited by M. J. G. Lee, J. M. Perz, and E. Fawcett), 592.
Fawcett, E., 1979, unpublished.

Fawcett, E., 1988a, Rev. Mod. Phys. **60**, 209.
Fawcett, E., 1988b, J. Phys. (Paris) **49**, C8-225.
Fawcett, E., 1989a, J. Phys. Condens. Matter **1**, 203.
Fawcett, E., 1989b, Physica B **159**, 12.
Fawcett, E., 1989c, Physica B **161**, 83.
Fawcett, E., 1989d, Fiz. Nizk. Temp. **15**, 797 [Sov. J. Low Temp. Phys. **15**, 518 (1989)].
Fawcett, E., 1992a, J. Phys. Condens. Matter **4**, 923.
Fawcett, E., 1992b, Physica **180–181**, 179.
Fawcett, E., 1993, unpublished.
Fawcett, E., 1994, "Why are the effects of pressure and composition change often similar in antiferromagnetic chromium alloys," *Metallic Alloys: Experimental and Theoretical Perspectives,* edited by J. S. Faulkner and R. G. Jordan (Kluwer, Dordrecht), in press.
Fawcett, E., M. Acet, M. Shiga, and E. F. Wassermann, 1992, Phys. Rev. B **45**, 2180.
Fawcett, E., and H. L. Alberts, 1990, J. Phys. Condens. Matter **2**, 6251.
Fawcett, E., and H. L. Alberts, 1992a, J. Phys. Condens. Matter **4**, 613.
Fawcett, E., and H. L. Alberts, 1992b, "Magnetic Grüneisen Parameters in Cr Alloys with Ga and Ge," unpublished.
Fawcett, E., and V. Yu Galkin, 1991, J. Phys. Condens. Matter **3**, 7167.
Fawcett, E., and V. Yu Galkin, 1992a, J. Magn. Magn. Mater. **104–107**, 759.
Fawcett, E., and V. Yu Galkin, 1992b, J. Magn. Magn. Mater. **109**, L139.
Fawcett, E., and V. Yu. Galkin, 1993, J. Magn. Magn. Mater. **119**, 329.
Fawcett, E., R. Griessen, W. Joss, M. J. G. Lee, and J. M. Perz, 1980, "The effect of strain on the Fermi surface," Chap. 6 of *Electrons at the Fermi Surface,* edited by M. Springford (Cambridge University, Cambridge, England), p. 278.
Fawcett, E., T. M. Holden, and D. R. Noakes, 1991, Physica B **174**, 18.
Fawcett, E., A. B. Kaiser, and G. K. White, 1986a, Phys. Rev. B **34**, 6248.
Fawcett, E., A. B. Kaiser, and G. K. White, 1986b, J. Magn. Magn. Mater. **54–57**, 1021.
Fawcett, E., W. C. Muir, T. M. Holden, and P. C. de Camargo, 1988, Zh. Eksp. Teor. Fiz. **94**, 379 [Sov. Phys. JETP **67**, 646 (1988)].
Fawcett, E., and D. R. Noakes, 1993, Int. J. Mod. Phys. B **7**, 624; *Physics of Transition Metals,* Proceedings of the International Conference, Darmstadt, Germany, July 1992, edited by P. M. Oppeneer and J. Kübler (World Scientific, Singapore), Vol. II, p. 624.
Fawcett, E., R. B. Roberts, R. Day, and G. K. White, 1986, Europhys. Lett. **1**, 473.
Fawcett, E., and C. Vettier, 1982, J. Phys. (Paris) **43**, 1365.
Fawcett, E., S. A. Werner, A. Goldman, and G. Shirane, 1988, Phys. Rev. Lett. **61**, 558.
Fawcett, E., S. A. Werner, A. Goldman, and G. Shirane, 1989, Physica B **156–157**, 715.
Fedders, P. A., and P. C. Martin, 1966, Phys. Rev. **143**, 245.
Fenton, E. W., 1985, Solid State Commun. **54**, 633.
Fishman, R. S., and S. H. Liu, 1992, Phys. Rev. B **45**, 12 306.
Fishman, R. S., and S. H. Liu, 1993a, Phys. Rev. B **47**, 11 870.
Fishman, R. S., and S. H. Liu, 1993b, J. Phys. Condens. Matter **5**, 3959.
Fishman, R. S., and S. H. Liu, 1993c, Phys. Rev. B **48**, 3820.
Fishman, R. S., and S. H. Liu, 1993, Int. J. Mod. Phys. B **7**, 620; *Physics of Transition Metals,* Proceedings of the International Conference, Darmstadt, Germany, July 1992, edited by P. M. Oppeneer and J. Kübler (World Scientific, Singapore), Vol. II, p. 620.
Frankel, R. B., and N. A. Blum, 1973, J. Phys. Chem. Solids **34**, 1565.
Friedel, J., and L. E. Hedman, 1978, J. Phys. (Paris) **39**, 1225.
Fukamichi, K., 1978, Phys. Status Solidi A **49**, K37.
Fukamichi, K., 1979, J. Phys. F **9**, L85.
Fukamichi, K., and H. Saito, 1972, J. Phys. Soc. Jpn. **33**, 1485.
Fukamichi, K., and H. Saito, 1974, AIP Conf. Proc. **17**, 45.
Fukamichi, K., and H. Saito, 1975a, Phys. Status Solidi A **30**, K197.
Fukamichi, K., and H. Saito, 1975b, J. Phys. Soc. Jpn. **38**, 287.
Fukamichi, K., and H. Saito, 1975c, J. Less-Common Met. **40**, 357.
Fukamichi, K., and H. Saito, 1977, Sci. Rep. Ritu. **26A**, 299.
Fukamichi, K., Y. Suzuki, and H. Saito, 1973, J. Jpn. Inst. Metals **37**, 927 [J. Jpn. Inst. Metals **16**, 133 (1975)].
Furuya, Y., N. Mori, and T. Mitsui, 1970, J. Phys. Soc. Jpn. **28**, 257.
Galkin, V. Yu., 1987, Fiz. Met. Metalloved. **624**, 1199 [Phys. Met. Metallogr. (USSR) **64**, 150 (1987)].
Galkin, V., 1989, J. Magn. Magn. Mater **79**, 327.
Galkin, V. Yu., 1992 (unpublished).
Galkin, V. Yu., 1993, Int. J. Mod. Phys. B **7**, 638; *Physics of Transition Metals,* Proceedings of the International Conference, Darmstadt, Germany, July 1992, edited by P. M. Oppeneer and J. Kübler (World Scientific, Singapore), Vol. II, p. 638.
Galkin, V. Yu., and. E. Fawcett, 1993, J. Magn. Magn. Mater. **119**, 321.
Galkin, V. Yu, and E. Fawcett, 1994, "Magnetic phase diagrams and impurity resonance scattering of CrFe and CrSi, and their ternary alloys with V and Mn III theory: temperature dependence of resistivity," unpublished.
Galkin, V. Yu., V. V. Tugushev, and T. E. Tugusheva, 1986, Fiz. Tverd. Tela (Leningrad) **28**, 2290 [Sov. Phys. Solid State **28**, 1282 (1986)].
Galkin, V. Yu., V. V. Tugushev, and T. E. Tugusheva, 1991, Fiz. Tverd. Tela (Lengingrad) **33**, 9 [Sov. Phys. Solid State **33**, 4 (1991)].
Galkin, V. Yu., and T. E. Tugusheva, 1988, Fiz. Tverd. Tela (Leningrad) **30**, 845 [Sov. Phys. Solid State **30**, 487 (1988)].
Geerken, B. M., R. Griessen, G. Benediktsson, H. U. Åstrom, and C. van Dijk, 1982, J. Phys. F **12**, 1603.
Giannuzzi, A., H. Tomaschke, and K. Schroder, 1970, Philos. Mag. **21**, 479.
Gibbs, D., K. M. Mohanty, and J. Bohr, 1988, Phys. Rev. B **37**, 562.
Giurgiu, A., I. Pop, M. Popescu, and Z. Gulacsi, 1981, Phys. Rev. B **24**, 1350.
Goldanskii, V. I., and R. Herber, 1968, Eds., *Chemical Applications of Mössbauer Spectroscopy* (Academic, New York).
Gopalakrishnan, I. K., J. V. Yakhmi, and R. M. Iyer, 1984, J. Magn. Magn. Mater. **46**, 207.
Graebner, J. E., 1971, in *Proceedings of the 12th International Conference on Low Temperature Physics, Kyoto,* edited by E. Kanda (Academic, New York), p. 601.
Graebner, J. E., and J. A. Marcus, 1968, Phys. Rev. **175**, 659.
Grebinnik, V. G., I. I. Gurevich, A. I. Klimov, V. N. Majorov, A. P. Manych, E. V. Melnikov, B. A. Nikolsky, A. V. Pirogov, A. N. Ponomarev, V. I. Selivanov, V. A. Suetin, and V. A. Zhukov, 1979, Hyp. Int. **6**, 103.

Grier, B. H., G. Shirane, and S. A. Werner, 1985, Phys. Rev. B **31**, 2882.
Griessen, R., and E. Fawcett, 1977, Physica **91B**, 205.
Griessen, R., D. J. Stanley, and E. Fawcett, 1976, Solid State Commun. **19**, 1185.
Grünberg, P., R. Schreiber, Y. Pang, M. B. Brodsky, and H. Sowers, 1986, Phys. Rev. Lett. **57**, 2442.
Guillaume, C. E., 1897, Compt. Rend. **125**, 235.
Gulásci, M., and Zs. Gulásci, 1986, Phys. Rev. B **33**, 6147.
Gunther, L., and M. M. Antonoff, 1983, J. Magn. Magn. Mater. **31–34**, 1077.
Gupta, K. P., C. H. Cheng, and P. A. Beck, 1962, J. Phys. Radium **23**, 721.
Gutman, E. J., and J. L. Stanford, 1971, Phys. Rev. B **4**, 4026.
Hamaguchi, Y., E. O. Wollan, and W. C. Koehler, 1965, Phys. Rev. **138**, A737.
Hausch, G., M. Shiga, and Y. Nakamura, 1976, J. Phys. Soc. Jpn. **40**, 903.
Hausch, G., and E. Török, 1977, Phys. Status Solidi A **40**, 55.
Hayden, S. M., G. Aeppli, E. Fawcett, T. Fielding, and J. Lowther, 1993, "Magnetic fluctuations in the nested Fermi liquid Cr + 5 at. % V," unpublished.
Hayden, S. M., G. Aeppli, R. Osborn, A. D. Taylor, T. G. Perring, S.-W. Cheong, and Z. Fisk, 1991, Phys. Rev. Lett. **67**, 3622.
Hayden, S. M., T. E. Mason, G. Aeppli, H. A. Mook, S.-W. Cheong, and Z. Fisk, 1993, unpublished.
Hedgcock, F. T., J. O. Strom-Olsen, and D. F. Wilford, 1977, J. Phys. F **7**, 855.
Hedman, L., H. U. Åstrom, K. V. Rao, and S. Arajs, 1975, J. Magn. Magn. Mater **1**, 141.
Hedman, L., A. Kjerulf, K. V. Rao, K. Svensson, and H. U. Åstrom, 1982, Phys. Scr. **25**, 893.
Hedman, L., C. A. Moyer, J. R. Kelly, S. Arajs, G. Kote, and K. Garbe, 1981, J. Appl. Phys. **52**, 1643.
Hedman, L. E., K. V. Rao, and H. U. Åstrom, 1978, J. Phys. (Paris) **39**, C6-788.
Hedman, L., K. Svensson, K. V. Rao, and S. Arajs, 1973, Phys. Lett. **45A**, 175.
Hedman, K., K. Svensson, K. V. Rao, S. Arajs, and H. U. Åstrom, 1974, J. Low Temp. Phys. **14**, 545.
Heeger, A. J., 1969, *Local Moments and Nonmoments in Metals,* Solid State Physics Vol. 23 (edited by F. Seitz *et al.*; Academic, New York), p. 283.
Heine, V., 1967, Phys. Rev. **153**, 673.
Heiniger, F., 1966, Phys. Kondens. Mater. **5**, 285.
Heiniger, F., E. Bucher, and J. Muller, 1965, Phys. Lett. **19**, 163.
Herbert, I. R., P. E. Clark, and G. V. H. Wilson, 1972, J. Phys. Chem. Solids **33**, 979.
Herman, F., M. Van Schilfgaarde, and J. Sticht, 1993, Int. J. Mod. Phys. B **7**, 425; *Physics of Transition Metals,* Proceedings of the International Conference, Darmstadt, Germany, July 1992, edited by P. M. Oppeneer and J. Kübler (Wrld Scientific, Singapore), Vol. I, p. 425.
Hill, P., N. Ali, A. J. A. de Oliveira, W. A. Ortiz, P. C. de Camargo, and E. Fawcett, 1994, J. Phys. Condens. Matter, in press.
Hirai, K., 1993, J. Phys. Soc. Jpn. **62**, 690.
Hirsch, J. E., 1990, Phys. Rev. B **41**, 6828.
Hochheimer, H. D., and R. Münch, 1991, Philos. Mag. B **63**, 979.
Holden, A. J., V. Heine, and J. H. Samson, 1984, J. Phys. F **14**, 1005.
Holden, T. M., and E. Fawcett, 1978, J. Phys. F **8**, 2609.
Housley, R. M., and J. G. Dash, 1964, Phys. Lett. **10**, 270.
Hsu, Jen-Hwa, and Y. W. Fu, 1994, J. Appl. Phys., in press.
Hurd, C. M., 1972, *The Hall Effect in Metals and Alloys* (Plenum, New York).
Iida, S., S. Kawarazaki, and N. Kunitomi, 1981, J. Phys. Soc. Jpn. **50**, 3612.
Iida, S., M. Kohno, Y. Tsunoda, and N. Kunitomi, 1981, J. Phys. Soc. Jpn. **50**, 2581.
Iida, S., Y. Tsunoda, Y. Nakai, and N. Kunitomi, 1981, J. Phys. Soc. Jpn. **50**, 2587.
Ishiguro, T., and K. Yamaji, 1990, *Organic Superconductors* (Springer, New York).
Ishikawa, Y., S. Hoshino, and Y. Endoh, 1967, J. Phys. Soc. Jpn. **22**, 1221.
Ishikawa, Y., R. Tournier, and J. Filippi, 1965, J. Phys. Chem. Solids **26**, 1727.
Iusan, V., I. Pop, and V. I. Chechernikov, 1973, Phys. Status Solidi B **58**, 785.
Janak, J. F., and A. R. Williams, 1976, Phys. Rev. B **14**, 4199.
Jayaraman, A., 1984, Mat. Res. Soc. Symp. Proc. **22**, 89.
Jayaraman, A., R. G. Maines, K. V. Rao, and S. Arajs, 1976, Phys. Rev. Lett. **37**, 926.
Jayaraman, A., T. M. Rice, and E. Bucher, 1970, J. Appl. Phys. **41**, 869.
Johanesson, Ch., H. U. Åstrom, and K. V. Rao, 1982, Phys. Scr. **25**, 751.
Kaiser, A. B., and E. M. Haines, 1985, J. Phys. F **15**, 1765.
Kaiser, A. B., and A. M. Olés, 1993, Int. J. Mod. Phys. B **7**, 634; *Physics of Transition Metals,* Proceedings of the International Conference, Darmstadt, Germany, July 1992, edited by P. M. Oppeneer and J. Kübler (World Scientific, Singapore), Vol. II, p. 634.
Kaiser, A. B., A. M. Olés, and J. Major, 1992, Phys. Rev. B **45**, 7477.
Kaiser, A. B., G. K. White, and E. Fawcett, 1985, Phys. Rev. B **32**, 7438.
Kajzar, F., G. Parette, and B. Babic, 1981 J. Phys. Chem. Solids **42**, 501.
Kakehashi, Y., 1987, Phys. Rev. B **35**, 4973.
Kallel, A., and F. De Bergevin, 1967, Solid State Commun. **5**, 955.
Kampf, A., and J. R. Schrieffer, 1990, Phys. Rev. B **41**, 6399.
Kanamori, J., 1963, Prog. Theor. Phys. **30**, 275.
Kaneko, T., K. Shirakawa, and K. Fukamichi, 1982, J. Appl. Phys. **53**, 2459.
Katano, S., and N. Mori, 1979, J. Phys. Soc. Jpn. **46**, 691.
Katano, S., and N. Mori, 1980, J. Phys. Soc. Jpn. **49**, 1812.
Katano, S., N. Mori, and K. Nakayama, 1980, J. Phys. Soc. Jpn. **48**, 192.
Kelly, J. R., C. A. Moyer, and S. Arajs, 1979, Phys. Rev. B **20**, 1099.
Kemeny, T., B. Fogarassy, S. Arajs, and C. A. Moyer, 1979, Phys. Rev. B **19**, 2975.
Kesharwani, K. M., and B. K. Agrawal, 1972, Phys. Rev. B **6**, 2178.
Kim, D. J., 1989, Phys. Rev. B **39**, 6844.
Kimball, C., W. D. Gerber, and A. Arrott, 1963, J. Appl. Phys. **34**, 1046.
Kirillova, M. M., and L. V. Nomerovannaya, 1975, Fiz. Met. Metalloved. **40**, 983 [Phys. Met. Metallogr. (USSR) **40**, 69 (1975)].
Koehler, W. C., R. M. Moon, A. L. Trego, and A. R. Mackintosh, 1966, Phys. Rev. **151**, 405.

Kohara, T., 1981, J. Phys. Soc. Jpn. **50**, 451.
Kohara, T., and K. Asayama, 1975, J. Phys. Soc. Jpn. **39**, 1263.
Kohara, T., K. Asayama, Y. Nishihara, and Y. Yamaguchi, 1984, Solid State Commun. **49**, 31.
Komura, S., Y. Hamaguchi, and N. Kunitomi, 1967a, J. Phys. Soc. Jpn. **23**, 171.
Komura, S., Y. Hamaguchi, and N. Kunitomi, 1967b, Phys. Lett. **24A**, 299.
Komura, S., and N. Kunitomi, 1965, J. Phys. Soc. Jnp. **20**, 103.
Kondorskii, E. I., T. I. Kostina, and V. Yu. Galkin, 1978, Inst. Phys. Conf. Ser. **39** (ed. M. J. G. Lee, J. M. Perz, and E. Fawcett), 611.
Kondorskii, E. I., T. I. Kostina, and V. P. Medvedchikov, 1981, Vestn. Mosk. Univ. Ser. 3, **36**, 22 [Moscow Univ. Phys. Bull. **36**, 25 (1981)].
Kondorskii, E. I., T. I. Kostina, V. P. Medvedchikov, and Yu. P. Kuskova, 1979, Fiz. Met. Metalloved. **48**, 1158 [Phys. Met. Metallogr. (USSR) **48**, 27 (1981)].
Kondorskii, E. I., T. I. Kostina, and N. V. Trubitsina, 1983, Zh. Eksp. Teor. Fiz. **85**, 268 [Sov. Phys. JETP **58**, 155 (1983)].
Kondorskii, E. I., T. I. Kostina, N. V. Trubitsina, and I. V. L'vova, 1983, Fiz. Met. Metalloved. **56**, 396 [Phys. Met. Metallogr. (USSR) **56**, 170 (1983)].
Kontani, M., M. Hayashi, and Y. Masuda, 1983, J. Phys. Soc. Jpn. **52**, 284.
Kontani, M., T. Hioki, and Y. Masuda, 1975, J. Phys. Soc. Jpn. **39**, 672.
Kontani, M., and Y. Masuda, 1979, Solid State Commun. **32**, 1265.
Kontani, M., and Y. Masuda, 1981, J. Phys. Soc. Jpn. **50**, 1126.
Kontani, M., and Y. Masuda, 1983, J. Magn. Magn. Mater. **31–34**, 287.
Kossler, W. J., A. T. Fiory, D. E. Murnick, C. E. Stronach, and W. F. Lankford, 1977, Hyperfine Int. **3**, 287.
Köster, W., E. Wachtel, and K. Gruke, 1963, Z. Metallkd. **54**, 393.
Kostina, T. I., V. N. Men'shov, and V. V. Tugushev, 1985, Fiz. Met. Metalloved. **59**, 9 [Phys. Met. Metallogr. (USSR) **59**, 430 (1985)].
Kotani, A., 1974a, J. Phys. Soc. Jpn. **36**, 103.
Kotani, A., 1974b, J. Phys. Soc. Jpn. **37**, 1493.
Kotani, A., 1975, J. Phys. Soc. Jpn. **38**, 974.
Kotani, A., 1978, J. Phys. Soc. Jpn. **44**, 1455.
Kuentzler, R., and D. E. Moody, 1980, J. Magn. Magn. Mater. **15**, 279.
Kulikov, N. I., and V. V. Tugushev, 1984, Usp. Fiz. Nauk **144**, 643 [Sv. Phys. Usp. **27**, 954 (1984)].
Kuwano, H., and K. Ono, 1977, J. Phys. Soc. Jpn. **42**, 72.
Kuwano, H., and K. Ono, 1979, J. Phys. (Paris) **40**, C2-196.
Kuz'menko, P. P., N. G. Babich, N. I. Zakharenko, and P. A. Suprunenko, 1986, Fiz. Met. Metalloved. **61**, 1212 [Phys. Met. Metallogr. (USSR) **61**, 169 (1986)].
Landolt-Börnstein, 1986, *Numerical Data and Functional Relationships in Science and Technology,* New Series 19a: Magnetic Properties of Metals—3d, 4d, and 5d Elements, Alloys and Compounds, edited by H. P. J. Wijn (Springer, Berlin).
Lebech, B., and K. Mikke, 1972, J. Phys. Chem. Solids **33**, 1651.
Leng, Q., J. A. Wolf, P. Grünberg, and W. Zinn, 1993, Int. J. Mod. Phys. B **7**, 434; *Physics of Transition Metals,* Proceedings of the International Conference, Darmstadt, Germany, July 1992, edited by P. M. Oppeneer and J. Kübler (World Scientific, Singapore), Vol. I, p. 434.
Levy, P. M., K. Ounadjela, S. Zhang, Y. Wang, C. B. Sommers, and A. Fert, 1991, J. Appl. Phys. **67**, 5914.
Lind, M. A., and J. L. Stanford, 1984, J. Phys. Soc. Jpn. **53**, 4029.
Litterst, F. J., and G. M. Kalvius, 1989, Eds., *Proceedings of the International Conference on Nuclear Methods in Magnetism,* Hyperfine Interactions **49**.
Liu, S. H., 1970, Phys. Rev. B **2**, 2664.
Liu, S. H., 1986, private communication.
Lowenhaupt, M., W. Hahn, Y. Y. Huang, G. P. Felcher, and S. S. P. Parkin, 1993, Int. J. Mod. Phys. B **7**, 438; *Physics of Transition Metals,* Proceedings of the International Conference, Darmstadt, Germany, July 1992, edited by P. M. Oppeneer and J. Kübler (World Scientific, Singapore), Vol. I, p. 438.
Lomer, W. M., 1962, Proc. Phys. Soc. London **80**, 489.
Lourens, J. A. J., and H. L. Alberts, 1993, Int. J. Mod. Phys. B **7**, 630; *Physics of Transition Metals,* Proceedings of the International Conference, Darmstadt, Germany, July 1992, edited by P. M. Oppeneer and J. Kübler (World Scientific, Singapore), Vol. II, p. 630.
Loshmanov, A. A., 1964, Kristallografiya **9**, 377 [Sov. Phys. Crystallogr. **9**, 301 (1964)].
Lutgemeier, H., and S. M. Dubiel, 1982, J. Magn. Magn. Mater. **28**, 277.
Lynch, D. W., R. Rosei, and J. H. Weaver, 1975, Phys. Status Solidi A **27**, 515.
Machida, K., 1982, Solid State Commun. **41**, 217.
Machida, K., 1984, Phys. Rev. B **30**, 418.
Machida, K., and M. Fujita, 1984, Phys. Rev. B **30**, 5284.
Machida, K., M. A. Lind, and J. L. Stanford 1984, J. Phys. Soc. Jpn. **53**, 4020.
Mackintosh, A. R., 1985 (unpublished).
Mackintosh, A. R., and H. Bjerrum-Moller, 1968, *Localized Excitations in Solids* (Plenum, New York), p. 721.
Major, J., J. Mundy, M. Schmoltz, A. Seeger, K. P. Döring, K. Fürderer, M. Gladisch, D. Herlach, and G. Majer, 1986, Hyp. Int. **31**, 259.
Maki, K., and M. Sakurai, 1972, Prog. Theor Phys. **47**, 1110.
Maki, S., and K. Adachi, 1979, J. Phys. Soc. Jpn. **46**, 1131.
Mamiya, T., and Y. Masuda, 1976, J. Phys. Soc. Jpn. **40**, 390.
Manosa, Ll., G. A. Saunders, H. Rahdi, U. Kawald, J. Pelzl, and H. Bach, 1992, Phys. Rev. B **45**, 2224.
Marcus, P. M., 1994, private communication.
Mason, T. E., G. Aeppli, and H. A. Mook, 1992, Phys. Rev. Lett. **68**, 1414.
Mathon, J., 1991, J. Magn. Magn. Mater. **100**, 527.
Matsumura, M., and K. Asayama, 1977, J. Phys. Soc. Jpn. **43**, 1207.
Mattson, J. E., M. E. Brubaker, C. H. Sowers, M. Conover, Z. Qiu, and S. D. Bader, 1991, Phys. Rev. B **44**, 9378.
Maystrenko, L. G., and V. M. Polovov, 1977, Fiz. Met. Metalloved. **43**, 991 [Phys. Met. Metallogr. (USSR) **43**, 79 (1977)].
McMullan, G. J., 1993, Int. J. Mod. Phys. **7**, 760; *Physics of Transition Metals,* Proceedings of the International Conference, Darmstadt, Germany, July 1992, edited by P. M. Oppeneer and J. Kübler (World Scientific, Singapore), Vol. II, p. 760.
McWhan, D. B., and T. M. Rice, 1967, Phys. Rev. Lett. **19**, 846.
Meaden, G. T., K. V. Rao, and K. T. Tee, 1970, Phys. Rev. Lett. **25**, 359.
Men'shov, V. N., and V. V. Tugushev, 1989, Zh. Eksp. Teor. Fiz. **96**, 1340 [Sov. Phys. JETP **69**, 761 (1989)].
Michel, R. P., N. E. Israellof, M. B. Weissman, J. A. Dura, and C. P. Flynn, 1993, Phys.. Rev. **47B**, 3442.
Mikke, K., and J. Jankowska, 1978a, Inst. Phys. Conf. Ser. **39** (ed. M. J. G. Lee, J. M. Perz, and E. Fawcett), 595.

Mikke, K., and J. Jankowska, 1978b, Inst. Phys. Conf. Ser. **39**, (ed. M. J. G. Lee, J. M. Perz, and E. Fawcett), 599.
Mikke, K., and J. Jankowska, 1979, J. Magn. Magn. Mater. **14**, 280.
Mikke, K., and J. Jankowska, 1980, J. Phys. F **10**, L159.
Mitchell, M. A., and J. F. Goff, 1972, Phys. Rev. B **5**, 1163.
Mitchell, M. A., and J. F. Goff, 1975, Phys. Rev. B **12**, 1858.
Mitsui, T., and C. T. Tomizuka, 1965, Phys. Rev. **137A**, 564.
Mizuki, J., J. R. D. Copley, Y. Endoh, and Y. Ishikawa, 1986, J. Phys. F **16**, L195.
Mizuki, J., and Y. Endoh, 1982, J. Phys. Soc. Jpn. **51**, 3508.
Mizuki, J., Y. Endoh, and Y. Ishikawa, 1982, J. Phys. Soc. Jpn. **51**, 3497.
Moller, H. B., and A. R. Mackintosh, 1965, Phys. Rev. Lett. **15**, 623.
Moller, H. B., A. L. Trego, and A. R. Mackintosh, 1965, Solid State Commun. **3**, 137.
Mori, N., Y. Furuya, and T. Mitsui, 1970, J. Phys. Soc. Jpn. **28**, 531.
Mori, M., Y. Tsunoda, and N. Kunitomi, 1976, Solid State Commun. **18**, 1103.
Moriya, T., 1981, *Electron Correlation and Magnetism in Narrowband Systems* (Springer, New York).
Moriya, T., and K. Usami, 1980, Solid State Commun. **34**, 95.
Moruzzi, V. L., 1990, Phys. Rev. B **41**, 6939.
Moruzzi, V. L., and P. M. Marcus, 1992, Phys. Rev. B **46**, 3171.
Moyer, C. A., S. Arajs, and A. Eroglu, 1980, Phys. Rev. B **22**, 3277.
Moyer, C. A., S. Arajs, and L. Hedman, 1976, Phys. Rev. B **14**, 1233.
Moyer, C. A., J. R. Kelly, and S. Arajs, 1979, Phys. Status Solidi B **96**, 775.
Moze, O., P. W. Mitchell, S. K. Burke, J. R. Davis, and J. G. Booth, 1988, J. Phys. F **18**, 527.
Muheim, S., and J. Müller, 1964, Phys. Kondens. Mater. **2**, 377.
Muir, W. C., E. Fawcett, and J. M. Perz, 1987a, Phys. Rev. Lett. **59**, 335.
Muir, W. C., J. M. Perz, and E. Fawcett, 1987b, J. Phys. F **17**, 2431.
Mukherjee, G. D., C. Bansal, and E. Fawcett, 1994, "Effect of 0.18 at. % Re impurity on the thermal expansion around the Néel transition in Cr," Proceedings of the Indo-U.S.A. Workshop on Order-Disorder Phenomena, Hyderabad (1992–93), in press.
Münch, R., H. D. Hochheimer, A. Werner, G. Materlik, A. Jayaraman, and K. V. Rao, 1983, Phys. Rev. Lett. **50**, 1619.
Munday, B. C., 1971, Phys. Status Solidi **8a**, K129.
Nakanishi, K., and T. Kasuya, 1977, J. Phys. Soc. Jpn. **42**, 833.
Nakata, Y., and S. Kawarazaki, 1983, J. Magn. Magn. Mater. **31–34**, 291.
Newmann, M. M., and K. W. H. Stevens, 1959, Proc. Phys. Soc. London **74**, 290.
Nikolaev, I. N., and I. Yu. Bezotosnyi, 1979, Zh. Eksp. Teor. Fiz. **77**, 1643 [Sov. Phys. JETP **50**, 824 (1979)].
Nishihara, Y., and Y. Yamaguchi, 1985, Solid State Phys. **20**, 824.
Nishihara, Y., Y. Yamaguchi, M. Tokumoto, K. Takeda, and K. Fukamichi, 1986, Phys. Rev. B **34**, 3446.
Nityananda, R., A. S. Reshamwala, and A. Jayaraman, 1972, Phys. Rev. Lett. **28**, 1136.
Noakes, D. R., E. Fawcett, B. J. Sternlieb, G. Shirane, and J. Jankowska, 1994, in press.
Noakes, D. R., E. Fawcett, E. J. Ansaldo, C. Niedermayer, and C. E. Stronach, 1992, J. Magn. Magn. Mater. **114**, 176.
Noakes, D. R., E. Fawcett, and T. M. Holden, 1993, "Critical scattering in Cr+0.5 at. % V," unpublished.
Noakes, D. R., E. Fawcett, B. J. Sternlieb, G. Shirane, and J. Jankowska, "Critical magnetic neutron scattering above the Néel temperature in Cr+0.18 at. % Re," unpublished.
Noakes, D. R., T. M. Holden, and E. Fawcett, 1990, J. Appl. Phys. **67**, 5262.
Noakes, D. R., T. M. Holden, E. Fawcett, and P. C. de Camargo, 1990, Phys. Rev. Lett. **65**, 369.
Ohno, H., T. Suzuki, and H. Takaki, 1967, J. Phys. Soc. Jpn. **23**, 251.
Okpalugo, D. E., J. G. Booth, M. M. R. Costa, and K. R. A. Ziebeck, 1985, J. Appl. Phys. **57**, 3039.
Ostenburg, D. O., D. J. Lam, H. D. Trapp, and D. E. MacLeod, 1962, Phys. Rev. B **128**, 1550.
Overhauser, A. W., 1960a, Phys. Rev. Lett. **4**, 226.
Overhauser, A. W., 1960b, J. Phys. Chem. Solids **13**, 71.
Overhauser, A. W., 1962, Phys. Rev. **128**, 1437.
Papoular, R., D. Debray, and S. Arajs, 1981, J. Magn. Magn. Mater. **24**, 106.
Pearson, W. W., 1958, Vol. 1, and 1967, Vol. 2, *Handbook of Lattice Spacings and Structures of Metals and Alloys* (Pergamon, London/New York).
Peretto, P., G. Teisseron, and J. Berthier, 1979, Hyp. Int. **7**, 1.
Peretto, P., R. Venegas, and G. N. Rao, 1981, Phys. Rev. B **23**, 6544.
Pessall, N., K. P. Gupta, C. H. Cheng, and P. A. Beck, 1964, J. Phys. Chem. Solids **25**, 993.
Petalas, P., and W. Baltensperger, 1968, Helv. Phys. Acta **41**, 388.
Pop, I., D. Dadârlat, T. Petrisor, and A. Giurgiu, 1981, J. Phys. Chem. Solids **42**, 927.
Pynn, R., W. G. Stirling, and A. Severing, 1992 (ICNS'92).
Rao, G. N., 1985, Hyp. Int. **24–26**, 1119.
Rao, G. N., P. Peretto, R. Venegas, L. Trabut, and S. Choulet, 1980, Phys. Lett. **75A**, 403.
Rapp, Ö., G. Bendiktsson, H. U. Åstrom, S. Arajs, and K. V. Rao, 1978, Phys. Rev. B **18**, 3665.
Rice, T. M., 1970, Phys. Rev. B **2**, 3619.
Rice, T. M., A. S. Barker, Jr., B. I. Halperin, and D. B. McWhan, 1969, J. Appl. Phys. **40**, 1337.
Rice, T. M., A. Jayaraman, and D. B. McWhan, 1969, J. Phys. (Paris) **32**, C1–39.
Roberts, R. B., G. K. White, and E. Fawcett, 1983, Physica B **119**, 63.
Ruvalds, J., G. T. Rieck, J. Zhang, and A. Virosztek, 1992, Science **256**, 1664.
Ruvalds, J., and A. Virosztek, 1991, Phys. Rev. B **43**, 5498.
Salamon, M. B., and F. J. Feigl, 1968, J. Phys. Chem. Solids **29**, 1443.
Sano, T., S. Kawarazaki, S. Iida, and N. Kunitomi, 1981, J. Phys. Soc. Jpn. **50**, 1203.
Sarachik, M. P., E. Corenzwit, and L. D. Longinotti, 1964, Phys. Rev. **135**, A1041.
Sato, H., and K. Maki, 1974, Int. J. Magn. **6**, 183.
Schrieffer, J. R., X. G. Wen, and S. C. Zhang, 1989, Phys. Rev. B **39**, 11 663.
Schröder, K., and N. P. Baum, 1968, Phys. Status Solidi **29**, 107.
Schröder, K., and H. Tomaschke, 1968, Phys. Kondens. Mater. **7**, 318.
Schwartzman, K., J. L. Fry, and Y. Z. Zhao, 1989, Phys. Rev. B **40**, 454.
Shibatani, A., 1971, J. Phys. Soc. Jpn. **31**, 1642.

Shibatani, A., K. Motizuki, and T. Nagamiya, 1969, Phys. Rev. **177**, 984.
Shiga, M., M. Miyake, and Y. Nakamura, 1986, J. Phys. Soc. Jpn. **55**, 2290.
Shiga, M., and Y. Nakamura, 1976, Phys. Status Solidi A **37**, K89.
Shiga, M., and Y. Nakamura, 1980, J. Phys. Soc. Jpn. **49**, 528.
Shinjo, T., K. Okada, T. Takada, and Y. Ishikawa, 1974, J. Phys. Soc. Jpn. **37**, 877.
Sidek, H. A. A., M. Cankurtaran, G. A. Saunders, P. J. Ford, and H. L. Alberts, 1993, Phys. Lett. A **172**, 387.
Sinha, S. K., G. R. Kline, C. Stassis, N. Chesser, and N. Wakabayashi, 1977, Phys. Rev. B **15**, 1415.
Sinha, S. K., S. H. Liu, L. D. Muhlestein, and N. Wakabayashi, 1969, Phys. Rev. Lett. **23**, 311.
Skriver, H. L., 1981, J. Phys. F **11**, 97.
Slichter, C. P., 1978, *Principles of Magnetic Resonance* (Springer, New York).
Smit, P., and H. L. Alberts, 1986, J. Phys. F **16**, L191.
Smit, P., and H. L. Alberts, 1987, J. Phys. Chem. Solids **48**, 887.
Smit, P., and H. L. Alberts, 1989, J. Phys. Condens. Matter **1**, 5731.
Smit, P., and H. L. Alberts, 1990, J. Phys. Condens. Matter **2**, 7635.
Smit, P., and H. L. Alberts, 1993, J. Phys. Condens. Matter **5**, 6433.
Smit, P., and H. L. Alberts, 1994, J. Appl. Phys., in press.
Sousa, J. B., M. M. Amado, R. P. Pinto, M. F. Pinheiro, M. E. Braga, J. M. Moreira, L. E. Hedman, H. U. Åstrom, L. Khlaif, P. Walker, G. Garton, and D. Hukin, 1980, J. Phys. F **10**, 2535.
Sousa, J. B., M. R. Chaves, M. E. Braga, M. M. Reis, M. F. Pinheiro, and M. Crisan, 1975, J. Phys. F **5**, L155.
Sousa, J. B., R. P. Pinto, M. N. Amado, J. M. Moreira, P. Walker, G. Garton, and D. Hukin, 1981, Inst. Phys. Conf. Ser. **55** (ed. P. Rhodes), 491.
Squires, G. L., 1978, *Introduction to the Theory of Thermal Neutron Scattering* (Cambridge University, Cambridge, England).
Srinivasan, T. M., and H. Claus, 1967, J. Phys. Chem. Solids **28**, 711.
Standley, K. J., and R. A. Vaughan, 1969, *Electron Spin Relaxation in Solids* (Hilger, London).
Steinemann, S. G., 1978, J. Magn. Magn. Mater. **7**, 84.
Sternlieb, B. J., E. Lorenzo, G. Shirane, S. A. Werner, and E. Fawcett, 1994, "Neutron scattering studies of the spin-density-wave alloy $Cr_{1-x}Mn_x$: diffraction in Cr+0.7 at.% Mn," unpublished.
Sternlieb, B. J., G. Shirane, S. A. Werner, and E. Fawcett, 1993, Phys. Rev. B **48**, 10217.
Stirling, W. J., R. Pynn, K. A. McEwen, and E. J. Lindley, 1989, Physica B **156–157**, 706.
Street, R., B. C. Munday, B. Window, and I. R. Williams, 1968, J. Appl. Phys. **39**, 1050.
Street, R., and B. Window, 1966, Proc. Phys. Soc. London **89**, 587.
Ström-Olsen, J. O., and D. F. Wilford, 1980, J. Phys. F **10**, 1467.
Ström-Olsen, J. O., D. F. Wilford, S. K. Burke, and B. D. Rainford, 1979, J. Phys. F **9**, L95.
Ström-Olsen, J. O., D. F. Wilford, and A. P. Morris, 1982, J. Phys. F **12**, 1247.
Suzuki, T., 1966, J. Phys. Soc. Jpn. **21**, 442.
Suzuki, T., 1976, J. Phys. Soc. Jpn. **41**, 1187.
Suzuki, T., 1977, J. Phys. Soc. Jpn. **43**, 869.
Suzuki, T., 1978, J. Phys. Soc. Jpn. **45**, 1852.
Suzuki, T., 1979, unpublished.
Suzuki, T., and H. Takaki, 1964, J. Phys. Soc. Jpn. **19**, 1241.
Syono, Y., and Y. Ishikawa, 1967, Phys. Rev. Lett. **19**, 747.
Szuszkiewicz, M., B. Rozenfeld, and J. Chojcan, 1981, Phys. Status Solidi B **108**, 623.
Takahashi, J., S. Yamaguchi, Y. Fujino, K. Ozawa, J. Mizuki, and Y. Endoh, 1980, J. Phys. Soc. Jpn. **49**, 1480.
Takenaka, H., and K. Asayama, 1971, J. Phys. Soc. Jpn. **31**, 299.
Takenaka, H., and K. Asayama, 1973, J. Phys. Soc. Jpn. **35**, 740.
Takeuchi, J., H. Sasakura, and Y. Masuda, 1980, J. Phys. Soc. Jpn. **49**, 508.
Teisseron, G., J. Berthier, P. Peretto, C. Benski, M. Robin, and S. Choulet, 1978, J. Magn. Magn. Mater. **8**, 157.
Teisseron, G., P. Peretto, and J. Berthier, 1979, Hyp. Int. **7**, 211.
Templ, W., M. Hampele, D. Herlach, J. Major, J. Mundy, A. Seeger, and W. Staiger, 1990, Hyp. Int. **64**, 679.
Testardi, L. R., 1975, Phys. Rev. B **12**, 3849.
Trego, A. L., and A. R. Mackintosh, 1968, Phys. Rev. **166**, 495.
Tsunoda, Y., Y. Hamaguchi, and N. Kunitomi, 1972, J. Phys. Soc. Jpn. **32**, 394.
Tugushev, V. V., 1992, in *Modulated and Localized Structures of the Spin-Density Wave in Itinerant Antiferromagnets in Electronic Phase Transitions,* edited by W. Hanke and Yu. V. Kopaev (Elsevier, New York/Amsterdam), p. 237.
Uchida, S., *et al.*, 1991, Phys. Rev. B **43**, 7942.
van Cauteren, J., L. Hermans, M. Rots, and G. N. Rao, 1984, Hyp. Int. **20**, 187.
van Rijn, H. J., and H. L. Alberts, 1986a, J. Phys. Chem. Solids **47**, 937.
van Rijn, H. J., and H. L. Alberts, 1986b, J. Magn. Magn. Mater. **54–57**, 1105.
van Rijn, H. J., H. L. Alberts, and J. A. J. Lourens, 1987, J. Phys. Chem. Solids **48**, 283.
Vedernikov, M. V., 1967, Fiz. Tverd. Tela (Leningrad) **9**, 3018 [Sov. Phys. Solid State **9**, 2381 (1968)].
Venegas, R., P. Peretto, G. N. Rao, and L. Trabut, 1980, Phys. Rev. B **21**, 3851.
Venema, W. J., R. Griessen, and W. Ruesink, 1980, J. Phys. F **10**, 2841.
Venter, A. M., H. L. Alberts, and J. A. J. Lourens, 1986, J. Magn. Magn. Mater. **62**, 269.
Virosztek, A., and J. Ruvalds, 1990, Phys. Rev. B **42**, 4064.
Volkov, B. A., and M. S. Nunuparov, 1980, Zh. Eksp. Teor. Fiz. **78**, 632 [Sov. Phys. JETP **51**, 319 (1980)].
Volkov, B. A., and V. V. Tugushev, 1984, Fiz. Tverd. Tela (Leningrad) **26**, 2428 [Sov. Phys. Solid State **26**, 1471 (1984)].
Weidinger, A., G. Balzer, H. Graf, T. Moslang, E. Recknagel, T. Wichert, J. Bigot, and R. I. Grynszpan, 1981, Hyp. Int. **8**, 543.
Werner, S. A., A. Arrott, and H. Kendrick, 1967, J. Appl. Phys. **38**, 1243.
Werner, S. A., E. Fawcett, M. W. Elmiger, and G. Shirane, 1993, J. Appl. Phys. 6454.
Wertheim, G. K., 1961, J. Appl. Phys. **32**, 1105.
White, G. K., 1961, Philos. Mag. **6**, 815.
White, G. K., Y. Nakamura, M. Shiga, and A. B. Kaiser, 1989, J. Phys. Soc. Jpn. **58**, 3485.
White, G. K., R. B. Roberts, and E. Fawcett, 1986, J. Phys. F **16**, 449.
Window, B., 1970, J. Phys. C Suppl. **2**, 210.
Window, B., 1971a, AIP Conf. Proc. **5**, 522.

Window, B., 1971b, J. Phys. E **4**, 401.
Windsor, C. G., 1972, J. Phys. Chem. Solids **33**, 1993.
Wohlfarth, E. P., 1968, J. Appl. Phys. **39**, 1061.
Wohlfarth, E. P., 1969, J. Phys. C **2**, 68.
Yakhmi, J. V., I. K. Gopalakrishnan, and R. M. Iyer, 1983, J. Less-Common Met. **91**, 327.
Yakhmi, J. V., I. K. Gopalakrishnan, and R. M. Iyer, 1984, J. Phys. F **14**, 923.
Yakhmi, J. V., I. K. Gopalakrishnan, and R. M. Iyer, 1985a, J. Appl. Phys. **57**, 3223.
Yakhmi, J. V., I. K. Gopalakrishnan, and R. M. Iyer, 1985b, J. Less-Common Met. **91**, 327.
Yakhmi, J. V., I. K. Gopalakarishnan, and R. M. Iyer, 1987, J. Appl. Phys. **61**, 3994.
Yakhmi, J. V., and I. K. Gopalakrishnan, R. M. Iyer, and L. C. Gupta, 1985, Indian J. Phys. **59A**, 477.
Yakhmi, J. V., I. K. Gopalakrishnan, R. M. Iyer, and J. L. Stanford, 1987, J. Phys. F **17**, L65.
Yakhmi, J. V., R. Walia, S. N. Bhatia, and R. M. Iyer, 1988, J. Phys. (Paris) **49**, C8-217.
Young, C. Y., and J. B. Sokoloff, 1974, J. Phys. F **4**, 1304.
Zhu, X., and M. B. Walker, 1986, Phys. Rev. B **34**, 8064.
Ziebeck, K. R. A., R. Chagnon, and J. G. Booth, 1977, J. Phys. F **7**, 1583.
Zittartz, J., 1967, Phys. Rev. **164**, 575.